City Research Online

City St George's, University of London

Citation: Lu, W. (2019). Thermo-mechanical damage modelling for collapse assessment of steel buildings under blast and fire loads. (Unpublished Doctoral thesis, City, University of London)

This is the accepted version of the paper.

This version of the publication may differ from the final published version. To cite this item please consult the publisher's version.

Permanent repository link: https://openaccess.city.ac.uk/id/eprint/21816/

Copyright and Reuse: Copyright and Moral Rights remain with the author(s) and/or copyright holders. Copies of full items can be used for personal research or study, educational, or not-for-profit purposes without prior permission or charge, unless otherwise indicated, provided that the authors, title and full bibliographic details are credited, a hyperlink and/or URL is given for the original metadata page and the content is not changed in any way. For full details of reuse please refer to City Research Online policy.

City Research Online: http://openaccess.city.ac.uk/ publications@citystgeorges.ac.uk

Thermo-mechanical damage modelling for collapse assessment of steel buildings under blast and fire loads

Weimiao Lu

Department of Civil Engineering
City, University of London

This dissertation is submitted for the degree of
Doctor of Philosophy

February 2019

Table of contents

List of figures **vii**

List of tables **xv**

Acknowledgement **xviii**

Abstract **xxii**

1 Introduction **1**

1.1 Background 1

1.2 Aims and objectives of research 5

2 Literature Review **9**

2.1 Introduction 9

2.2 Past progressive collapse disasters 10

2.2.1 Ronan Point 10

2.2.2 World Trade Centre 7 11

2.3 Progressive collapse assessment methods and provisions 13

2.4 Behaviour of steel-framed buildings in fire 16

2.4.1 Cardington Fire tests 16

2.4.2 Numerical studies on steel frames that survived fire 20

2.4.3 Numerical studies on progressive collapse of steel frames under fire . . . 23

2.4.4 Numerical studies on fire-induced progressive collapse of post-damage building . . . 27

2.5 Structural steel deterioration . . . 30

2.5.1 Constitutive models of structural steel at elevated temperatures . 30

2.5.2 Damage and fracture theory . . . 34

3 Coupled thermo-mechanical damage model 41

3.1 Introduction . . . 41

3.2 Damage model formulation . . . 42

3.2.1 Mechanical damage component . . . 42

3.2.2 Thermal damage component . . . 44

3.2.3 Coupling between mechanical and thermal damage . . . 47

3.2.4 Comparison with experimental results . . . 49

3.3 Implementation of the damage model . . . 54

3.3.1 Constitutive equations . . . 55

3.3.2 Integration algorithm . . . 57

3.4 Summary . . . 61

4 Calibration and validation of the coupled damage model 63

4.1 Introduction . . . 63

4.2 Calibration and validation with fire tests of steel components and assemblies 64

4.2.1 Steel beam fire test (2007) . . . 65

4.2.2 Steel beam-to-column connection fire test (1997) . . . 69

4.2.3 Steel tubular truss fire test (2010) . . . 81

4.3 Calibration and validation with fire tests and analyses of steel frames . . 85

4.3.1 Scaled steel frame fire test (1986) 86

4.3.2 Three-storey steel frame subjected to explosion and fire (2000, 2004, 2005) 88

4.3.3 Cardington fire test 7 (2003) 101

4.4 Summary 109

5 Studies of low-rise and mid-rise office buildings under blast and fire 113

5.1 Introduction 113

5.2 Structural design 114

5.3 Fire loading and fire protection design 117

5.4 FE model 122

5.5 Material modelling 123

5.6 Fire accident scenario design 125

5.7 Simulation results 127

5.7.1 Fire-only analysis 128

5.7.1.1 Five-storey office building 128

5.7.1.2 Ten-storey office building 140

5.7.2 Post-blast fire analysis 150

5.7.2.1 Five-storey office building 151

5.7.2.2 Ten-storey office building 161

5.7.3 Fire-triggered explosion analysis 168

5.7.3.1 Five-storey office building 169

5.7.3.2 Ten-storey office building 172

5.8 Discussions 174

5.9 Summary 178

6 Conclusions **181**

6.1 Major findings and conclusions 181

6.2 Recommendations for design 183

6.3 Recommendations for future research 185

6.3.1 Recommendations for damage model enhancement 185

6.3.2 Recommendations for analysis scenarios 186

6.3.3 Recommendations for FE modelling techniques 187

References **189**

Appendix A Mathematical function construction in damage model development **197**

List of figures

2.1 Dispropotionate collapse of Ronan Point (Pearson and Delatte, 2005) . . 10

2.2 View of debris spread around WTC 7 and fires developing in WTC 7 (Gilsanz et al., 2002) 12

2.3 Large scale fire tests on a real multi-storey steel framed building at Cardington (British steel, 1999) 17

2.4 Floor layout and location of the fire tests (Foster et al., 2007) 18

2.5 Normalized yield strength of steel reported in literature sources 31

2.6 Normalized elastic modulus of steel reported in literature sources 32

2.7 Graphical presentation of the stress-strain relationships of structural steel at elevated temperatures (EN 1993-1-2, 2005) 33

2.8 Reduction factors for stress-strain relationships allowing for strain-hardening of structural steel at elevated temperatures (EN 1993-1-2, 2005) 34

2.9 Damaged element (Lemaitre, 1985) 36

3.1 Thermal damage variable $h(T)$ determined from literature sources . . . 45

3.2 Plots of thermal damage model with parameters best fit to experimental results. 46

3.3 Comparison between the damage evolution predicted by the proposed damage model with best-fit parameters and test results 53

3.4 Reduction factors for effective yield strength of structural steel at elevated temperatures (EN 1993-1-2, 2005) 56

4.1 Test set-up (Dharma and Tan, 2007) 65

4.2 FE model of the steel beam in ABAQUS 66

4.3 Failure mode comparison of specimen S3-1 67

4.4 Mid-span load–deflection of specimen S3-1 68

4.5 Mid-span load–deflection of specimen S3-2 69

4.6 Mid-span load–deflection of specimen S3-3 70

4.7 Ambient-temperature test arrangement (Leston-Jones, 1997) 71

4.8 Flush end plate connection detail (Leston-Jones, 1997) 71

4.9 Numerical model of flush end plate connection in ABAQUS 72

4.10 Modelling details of flush end plate connection 73

4.11 Comparison of ambient-temperature connection response between numerical cases and test data 73

4.12 Ambient-temperature connection failure mode 74

4.13 Elevated-temperature test arrangement (Leston-Jones, 1997) 75

4.14 Fire exposed region within connection model 76

4.15 Elevated-temperature connection failure mode (BFEP 5) 77

4.16 Comparison of connection response between numerical cases and fire test 1 (BFEP5) 78

4.17 Comparison of connection response between numerical cases and fire test 2 (BFEP10) 79

4.18 Comparison of connection response between numerical cases and fire test 3 (BFEP15) 79

4.19 Comparison of connection response between numerical cases and fire test 4 (BFEP20) 80

4.20 Comparison of connection response between numerical cases and fire test 5 (BFEP25) 80

4.21 Test set-up (Liu et al., 2010) 81

4.22 Numerical model of steel tubular truss in ABAQUS 82

4.23 Temperature–time curves of thermocouples TC1–TC11 for specimen SP1 and SP2 (Liu et al., 2010) 83

4.24 Vertical displacement versus maximum temperature curve of specimen SP1 84

4.25 Vertical displacement versus maximum temperature curve of specimen SP2 85

4.26 Configurations of scaled steel frame tests (Rubert and Schaumann, 1986) 87

4.27 Geometric configuration and loading of three-storey steel frame (Chen and Liew, 2005; Izzuddin et al., 2000; Liew and Chen, 2004) 89

4.28 Load sequences in explosion and fire analysis 90

4.29 Variation of normalized overpressure over time (Chen and Liew, 2005) . 91

4.30 FE beam element model of three-storey steel frame 93

4.31 Responses of steel frame under explosion only 94

4.32 Collapse modes of steel frame under blast loads (displacement scale factor enlarged) 94

4.33 Response of steel frame under explosion and followed by fire 95

4.34 Influence of explosion loads on the fire resistance of steel frame 96

4.35 Connecting techniques employed in the mixed element approach (Chen and Liew, 2005) 96

4.36 FE mixed element model of three-storey steel frame 97

4.37 Responses of steel frame under explosion only 98

4.38 Collapse modes of steel frame under blast loads 98

4.39 Response of steel frame under explosion and followed by fire 99

4.40 Collapse modes of steel frame under blast load 90 kN/m followed by fire 100

4.41 Influence of explosion loads on the fire resistance of steel frame 101

4.42 The location of the fire compartment in Cardington fire test 7 (Lennon, 2003) 102

4.43 The extent of the structure incorporated within the numerical model . . 102

4.44 FE model of Cardington test 7 in ABAQUS 103

4.45 Mixed element modelling approach in Cardington test 7 simulation . . . 103

4.46 Measured temperature distributions of beams (Lennon, 2003) 105

4.47 Measured temperatures of columns (Lennon, 2003) 105

4.48 Temperature variation throughout the depth of slab (Foster et al., 2007) . 106

4.49 Stress-strain relationships of concrete at elevated temperatures (EN 1994-1-2, 2005) 107

4.50 Location of vertical displacements measurements on the fourth floor slab (Lennon, 2003) 107

4.51 Comparison of displacements at nodes 206 between numerical cases and test 108

4.52 Comparison of displacements at nodes 211 between numerical cases and test 109

4.53 Comparison of displacements at nodes 216 between numerical cases and test 110

4.54 Comparison of displacements at nodes 220 between numerical cases and test 110

5.1 Schematic view of the five-storey building structural design 116

5.2 Schematic view of the ten-storey building structural design 117

5.3 Comparison of temperature histories of UKC254×254×73 120

5.4 Temperature histories of steel structural members 121

5.5 Temperature distribution across concrete slab depth 121

5.6 FE mesh of the five-storey building 122

5.7 FE mesh of the ten-storey building 123

5.8 Load sequences in post-blast fire analysis 125

5.9 Schematic view of the occurrence of internal blast loads 126

5.10 Load sequences in fire and gas explosion analysis 127

5.11 Location of the corner compartment fire on the ground floor 129

5.12 Vertical displacement of the heated interior column B2 129

5.13 The deformed shape of the building before column buckling initiates . . 130

5.14 Axial forces in columns during fire event 131

5.15 Damage development in the top of column A2 and column B2 131

5.16 Location of the central compartment fire on the ground floor 132

5.17 Vertical displacement of the heated interior column B2 132

5.18 Axial forces in columns during fire event 133

5.19 Residual capacity of the heated columns upon interior column buckling at 71 minutes of fire 134

5.20 Location of the corner compartment fire at the mid-height of the building 134

5.21 Vertical displacement of the heated interior column B2 135

5.22 Axial forces in columns during fire event 135

5.23 Residual capacity of the heated columns upon buckling of column B2 at 63 minutes of fire 136

5.24 Location of the central compartment fire at the mid-height of the building 136

5.25 Vertical displacement of the heated interior column B2 137

5.26 Axial forces in columns during fire event 138

5.27 Location of the corner compartment fire on the top floor 138

5.28 Vertical displacement of the heated interior column B2 138

5.29 Axial forces in columns during fire event 139

5.30 Location of the central compartment fire on the top floor 140

5.31 Vertical displacement of the heated interior column B2 140

5.32 Axial forces in columns during fire event 141

5.33 Location of the corner compartment fire on the ground floor 141

5.34 Vertical displacement of the heated interior column B2 142

5.35 The deformed shape of the building before column buckling initiates . . 142

5.36 Axial forces in columns during fire event 143

5.37 Damage development in the top of heated columns 143

5.38 Location of the central compartment fire on the ground floor 144

5.39 Vertical displacement of the heated interior column B2 144

5.40 Axial forces in columns during fire event 145

5.41 Location of the corner compartment fire at the mid-height of the building 145

5.42 Vertical displacement of the heated interior column B2 146

5.43 Axial forces in columns during fire event 146

5.44 Location of the central compartment fire at the mid-height of the building 147

5.45 Vertical displacement of the heated interior column B2 147

5.46 Axial forces in columns during fire event 147

5.47 Location of the corner compartment fire on the top floor 148

5.48 Vertical displacement of the heated interior column B2 149

5.49 Axial forces in columns during fire event 149

5.50 Location of the central compartment fire on the top floor 149

5.51 Vertical displacement of the heated interior column B2 150

5.52 Axial forces in columns during fire event 150

5.53 Blast induced deformation after the blast analysis in the corner compartment on the ground floor 151

5.54 Vertical displacement of the heated interior column B2 152

5.55 Axial forces in columns during fire event 152

5.56 Damage development in the top of columns subjected to blast and fire . 153

5.57 Blast induced deformation after the blast analysis in the central compartment on the ground floor 153

5.58 Vertical displacement of the heated interior column B2 154

5.59 Axial forces in columns during fire event 154

5.60 Blast induced deformation after the blast analysis in the corner compartment on the third floor 155

5.61 Vertical displacement of the heated interior column B2 156

5.62 Axial forces in columns during fire event 156

5.63 Damage development in the top of blast-damaged columns 156

5.64 Blast induced deformation after the blast analysis in the central compartment on the third floor 157

5.65 Vertical displacement of the heated interior column B2 158

5.66 Axial forces in columns during fire event 158

5.67 Blast induced deformation after the blast analysis in the corner compartment on the top floor 159

5.68 Vertical displacement of the heated interior column B2 159

5.69 Axial forces in columns during fire event 159

5.70 Blast induced deformation after the blast analysis in the central compartment on the top floor 160

5.71 Vertical displacement of the heated interior column 161

5.72 Axial forces in columns during fire event 161

5.73 Blast induced deformation after the blast analysis in the corner compartment on the ground floor 162

5.74 Blast-induced deformation after the blast analysis in the corner compartment on the fifth floor 163

5.75 Vertical displacement of the heated interior column B2 163

5.76 Axial forces in columns during fire event 164

5.77 Damage development in the top of columns subjected to blast and fire . 164

5.78 Blast induced deformation after the blast analysis in the central compartment on the fifth floor 165

5.79 Vertical displacement of the heated interior column B2 165

5.80 Axial forces in columns during fire event 165

5.81 Blast induced deformation after the blast analysis in the corner compartment on the top floor 166

5.82 Vertical displacement of the heated interior column B2 167

5.83 Axial forces in columns during fire event 167

5.84 Blast induced deformation after the blast analysis in the central compartment on the top floor 168

5.85 Vertical displacement of the heated interior column B2 168

5.86 Axial forces in columns during fire event 169

5.87 Deformation before and after fire-triggered explosion occurence 169

5.88 Vertical displacement of the heated interior column B2 170

5.89 Axial forces in columns during fire event 171

5.90 Damage development in the top of blast-damaged columns 171

5.91 Deformation before and after fire-triggered explosion occurence 172

5.92 Vertical displacement of the heated interior column B2 173

5.93 Axial forces in columns during fire event 173

5.94 Damage development in the top of blast-damaged columns 173

List of tables

2.1 Summary of Cardington fire tests 19

3.1 Temperature-dependent elastic modulus at various strain levels determined from tensile coupon test conducted by Pauli et al. (2012) 51

3.2 Damage parameters best fit to tensile coupon test results 52

4.1 Mechanical material properties at room temperature (Dharma and Tan, 2007) 66

4.2 Damage parameters best fit to tensile coupon test results 67

4.3 Damage parameters best fit to steel beam fire test results 69

4.4 Flush end-plate connection experimental programme (Leston-Jones, 1997) 70

4.5 Relative temperature profiles for flush end-plate connection (Leston-Jones, 1997) 76

4.6 Material properties obtained from coupon test at room temperature (Liu et al., 2010) 82

4.7 Damage parameters best fit to steel tubular truss fire test results 83

4.8 Calibrated damage parameters 86

4.9 Damage parameters input for fire analysis of plane steel frame 88

4.10 Test parameters and results of the frame tests 88

4.11 Damage parameters input for explosion and fire analysis of three-storey steel frame 92

4.12 Ambient-temperature material properties (Lennon, 2003) 106

4.13 Damage parameters input for analysis of Cardington fire test 7 106

5.1 Summary of section sizes in the five-storey building 118

5.2 Column sizes of the ten-storey building 118

5.3 Summary of section sizes in the ten-storey building 118

5.4 Ambient-temperature material properties 124

5.5 Damage parameters input for building analysis 124

5.6 Summary of the collapse initiation time in all analysed cases 175

A.1 Summary of the performances of the constructed mathematical functions in fitting to experimental data 199

I would like to dedicate this thesis to my loving parents ...

Acknowledgements

First and foremost, I would like to express most sincere gratitude to my supervisors, Professor D'Mello and Professor Ayoub. Their bright insight and broad knowledge has always inspired me to look at my work from a different perspective. Had it not been for their gracious guidance, this work would not have been here.

Furthermore, I would like to express appreciation to my dear parents. It is their unconditional love and support that have given me enormous strength. I would also like to thank all the precious friends I have met during my Ph.D. study. They are the best friends one could ever imagine and I have learnt tremendous great qualities from them.

Last but not least, I would like to acknowledge the financial support provided by City, University of London for conducting this research.

Declaration

I declare that except where specific reference is made to the work of others, the contents of this dissertation are original and have not been submitted in whole or in part for consideration for any other degree or qualification in this, or any other university. I hereby grant powers of discretion to the University Librarian to allow this thesis to be copied in whole or in part without further reference to the author. This permission covers only single copies made for study purposes, subject to normal conditions of acknowledgement.

Weimiao Lu
February 2019

Abstract

The aim of this research is to develop a coupled thermo-mechanical damage model for implementation in finite element software in support of fire-induced collapse assessment of steel structures. The need for properly modelling steel deterioration behaviour remains a challenging task in structural fire engineering because of the complexity inherent in the damage states of steel at large strains and high temperatures. A fully three-dimensional damage-coupled constitutive model is developed based on the hypothesis of effective space elastoplasticity and isotropic damage theory. The coupled damage is simulated by a coupling formulation between a mechanical damage component and a thermal damage component in attempt to capture the coupled damage growth under combined actions of mechanical loading and fire loading. The proposed damage model comprises a limited number of parameters that could be identified at unloading slopes of stress-strain relationships through tensile coupon tests. Alternatively, an inverse analysis type of calibration procedure could be adopted when coupon test data is unavailable. The proposed damage model is successfully implemented in the finite element software ABAQUS and calibrated with a comprehensive range of experimental results and established numerical results. The damage-affected structural response is accurately reproduced under various loading conditions and a wide temperature range, demonstrating that the proposed damage model is a useful tool in giving a realistic representation of steel deterioration behaviour under combined actions of fire and mechanical loads.

Three-dimensional FE models of a five-storey and a ten-storey steel-framed office building are developed in ABAQUS and the proposed damage model is adopted in assessing their susceptibility to progressive collapse. Three types of accidental scenarios are investigated : (i) fire only scenario, (ii) post-blast fire scenario, and (iii) fire-triggered explosion scenario. The location of the compartment where triggering loads occur is varied and the most vulnerable location is at the mid-height of both building systems. Estimation of ultimate failure time by incorporating damage model with the suggested damage parameter set has the potential to be utilized as a useful tool in helping designers to determine how much time is realistically available for evacuation before progressive collapse occurs in this type of buildings. Results show that the proposed damage model significantly affects the limit state of steel buildings under fire, and especially under combined actions of blast and fire. Compared to conventional numerical approaches, the consideration of coupled thermo-mechanical damage accumulation results in an $8.25\% \sim 23.47\%$ decrease of collapse resisting time. A key finding from this study is that the alternative load path, which is a crucial factor in deciding the survival of buildings upon local column failure, may be severely compromised due to the coupled thermo-mechanical damage propagation in surrounding columns. Based on the identified

collapse mechanisms, effective strategies are suggested to improve the survivability of buildings under blast and fire.

Chapter 1

Introduction

1.1 Background

Fire disasters cause many thousands of deaths and huge economic losses each year. Steel structures are especially known for their susceptibility to fire. To a large extent, the safety of occupants depends on buildings' capability to resist disproportionate collapse in fire.

The term progressive collapse stands for a chain reaction of failures that propagates throughout the structure as a result of local elastic or inelastic instabilities, which often leads to disproportionate collapse. It is defined as "a situation where local failure of a primary structural component leads to the collapse of adjoining members, which, in turn, leads to additional collapse. Hence, the total damage is disproportionate to the original cause." (GSA (General Services Administration), 2003) The original causes include accidental events such as fire, explosion, impact or local failure.

Several steel structure buildings around the world have experienced partial or total collapse triggered by fire. The terrorist attack and catastrophic collapse of World Trade Centre buildings in 2001 led to increasing concern about structural robustness worldwide. After the hijacked aircraft struck World Trade Centre 1 (WTC1), World Trade Centre 7 (WTC 7) suffered structural damage by falling debris of WTC1. But the main cause of WTC 7 collapse was clearly due to observed fire on several floors rather than the impact damage, given that the collapse occurred about six hours after WTC1 collapsed. Prior to this disaster, structural fire engineering has mainly focused on behaviour of individual members and connections. The catastrophic consequence of WTC7 collapse heightens the need for understanding steel structural performance as a system in fire.

Very few full-scale fire tests have been performed on steel frames. Among these, the BRE Cardington fire tests play a significant role in today's understandings of actual structural

system behaviour in real fire. Between 1994 and 2003, a series of seven full-scale fire tests have been carried out on an eight-storey steel frame at Cardington in order to investigate the real building behaviour in fire events (British steel, 1999; Lennon, 2003). Results suggested that structural elements acted as part of a continuous assembly and the structural system should be considered as a whole in assessing structural behaviour subjected to fire. The interactions between structural members, boundary loads and deformation conditions have significant influences on both the responses of individual members and the performances of the whole structure. If such interactions are to be taken into account, fire engineering cannot be practically based on large-scale testing due to the extremely high costs. Thus, research on this subject inevitably relies on careful numerical modelling. By using the test findings as benchmarks for developing and calibrating numerical models, researchers could extend the investigation to predict structural performance of generic steel frames under various fire scenarios.

Thus far, a number of numerical studies have been conducted based on Cardington fire tests, including work of Bailey and Moore (2000a,b), Elghazouli et al. (2000), Sanad et al. (2000), Wang (2000), O'Connor (2003), Lamont et al. (2007, 2004) and Foster et al. (2007). The move to numerical studies as a supplement of Cardington fire tests has been shown to be capable of modelling beneficial or detrimental interactions between structural components with a high degree of accuracy. The success in the modelling attempts has thrown light on extending the available results database by generating further data with carefully calibrated numerical models. A key finding of the numerical studies is that two-dimensional frame analysis is only capable of capturing the load-transfer mechanism of skeletal frames under fire. This type of analyses are obviously not sufficiently representative of the actual behaviour of composite frames, in which three-dimensional flexural bridging, catenary action in slabs and beams, and tensile membrane action in slabs play a crucial role in providing enhanced fire resistance. Therefore, three-dimensional models need to be adopted if real behaviour of structures is to be established.

Though comprehensive and insightful, the Cardington fire tests and the subsequent numerical investigations did not provide a check on the ultimate failure of the structural system. On the other hand, designers are utterly concerned with assessing the fire-induced disproportionate collapse potential of buildings because achieving required fire resistance for buildings is crucial for safe evacuation and firefighting. As a result, there is a growing body of literature that recognizes the importance of collapse assessment of steel frames in various fire scenarios. Ali et al. (2004) studied the collapse mode of single-storey steel frame in different fire scenarios and suggested possible measures that could be taken to change collapse mode in order to maintain integrity of fire wall. Takagi (2007) identified the governing factors in fire-induced structural system collapse using structural sub-assembly models and carried out a probabilistic assessment to determine the most

significant factor. Sun (2012) investigated the progressive collapse mechanisms of a two-dimensional moment resisting frame with different bracing systems under edge bay fire scenario and central bay fire scenario. Results suggested that the pull-in of columns caused by catenary force could lead to progressive collapse and the bracing systems could provide extra redundancy of the structure and alternate load paths after local damage occurred. Lange et al. (2012) examined two possible failure mechanisms for tall buildings subjected to multiple floor fires. The obtained collapse mechanisms were then compared with WTC tower collapse. This framework was based on two-dimensional steel frames and was intended to provide a simple assessment method for tall buildings. Agarwal and Varma (2014) assessed structural robustness of two types of ten-storey steel buildings under fire, one with gravity frame and rigid core in the form of concrete shear wall, and one with gravity frame and perimeter moment resisting frame. Results indicated that gravity columns were most likely to reach critical temperatures first due to the highest utilization ratios. This failure was considered to be the trigger of progressive collapse of whole building. Jiang and Li (2016, 2017) performed progressive collapse analysis of eight-storey moment resisting steel-framed buildings. The severity of various fire locations is investigated and the influences of different load ratios and fire protection levels are also examined. Results provided new insights to our understanding of the collapse mechanisms of three-dimensional steel structures under fire. Building on their numerical findings, further research is required to provide a comprehensive review of progressive collapse mechanisms under various fire scenarios.

The response of structures under the combined actions of explosion and fire is also a major concern in advanced structural fire engineering. Though this field has received increasing attention after the September 11^{th} incident, limited studies have been done on steel structures subjected to blast loads and subsequent fire. As one of the pioneers in this relatively new field, Izzuddin et al. (2000) carried out integrated fire and explosion analysis of a three-storey planar frame. Results showed that the fire resistance of the blast-damaged frame could be reduced by 40%, illustrating that the damage induced by moderate blast load had a considerable impact on the structural fire resistance. Liew and Chen (2004) and Chen and Liew (2005) also proposed an inelastic transient approach to investigate the influence of blast loads on the fire resistance of steel frame. The difference in collapse mode resulting from the blast damage was highlighted. Liew (2008) then carried out a combined fire and explosion analysis on a three-dimensional five-storey building. Results showed that the failure temperature of the frame decreased by 7.2% compared to that of the frame subjected to fire only. Quiel and Marjanishvili (2011) also evaluated the performance of a five-storey office building subjected to fire following blast load or impact load. The damage induced by blast load or impact load was not directly modelled but simulated by removing a column from the perimeter of a steel building. Results indicated a correlation between the amount of passive fire protection and the

collapse time. Ding et al. (2016) evaluated the resistance to progressive collapse of a ten-storey office building under a confined explosion and post-explosion fire. Results showed that the most vulnerable compartment exposed to threat was the peripheral compartment in fire only scenarios and the corner compartment for the combined hazard cases, implying that the blast induced damage had a bigger impact on the fire resistance of a corner compartment. The disproportionate collapse of WTC 7 was also a typical example of fire-induced collapse of post-damage building. McAllister et al. (2011) addressed the collapse phases of WTC 7 with very sophisticated numerical model, giving insights on understanding the sequence of structural failures of WTC 7. The drawback was that modelling techniques were extremely time-consuming. In addition to the accidental events discussed above, another catastrophic phenomenon in fire incidents would be that gas explosion occurs after a period of fire growth. Surprisingly, the effects of this type of blast and fire interaction have not been closely examined in literature.

Having summarized the numerical studies on fire-induced progressive collapse of steel frames, it is important to note that the reliability of modelling attempts heavily depends on the accurate representation of the material behaviour and therefore the choice of constitutive models. Lying at the heart of numerical modelling, constitutive models establish the relation of stress and strain at the material level, and determine the force-displacement relationship at the structural level. Therefore, the choice of constitutive models is crucial in progressive collapse analysis of structures. While it is common practice for researchers to base their numerical work on simplified experimental approximation curves of temperature-dependent stress-strain relationships given in EN 1993-1-2 (2005), far too little attention has been paid to damage and fracture induced by large deformations in steel. There remains a lack of research in careful modelling of steel property deterioration as the structures experience severe fire and undergo large structural deformation in accidental events. Due to the neglect of considering damage induced by plastic deformation, the design codes might turn out to be non-conservative under extreme loads.

As one of the typical damage, the ductile damage accompanying plastic deformation is a result of the growth and coalescence of microdefects. The fracture and breakage of bonds leads to loss of material load-carrying capability and eventual complete failure. A proper modelling of this damage mechanism in the scope of continuum damage mechanics is essential in predicting material failure in steel members and structures. An important aspect of continuum damage mechanics is the concept of effective stress which means mapping stress into the damaged surface. Kachanov (1958) first came up with a definition of a scalar variable which represents loss of effective resisting area. This has been the starting point for development of damage mechanics models including Lemaitre (1985), and Chaboche (1988, 1997). In these works, damage was considered as a thermodynamics state variable representative of the progressive loss of load carrying

capacity due to void formation, growth and coalescence under large plastic deformation. Lemaitre's damage model has fostered wide applications in fields such as metal forming. However, there are only a few instances in the literature where the damage model has been incorporated in structural analysis. For instance, several researchers have successfully incorporated Lemaitre's damage models to track the evolution of damage from onset to failure at the element level and structural level in earthquake engineering (Huang, 2009; Li et al., 2012). In structural fire engineering, there remains a lack of research which accurately simulates steel deterioration behaviour in fire events by considering the combining effects of mechanical and thermal damage. Given that structural members are expected to undergo excessive deformations at the initiation of progressive collapse, it is unconservative to ignore the mechanical damage evolution induced by plastic strains. Furthermore, there is an urgent need to address the precedent damage level in the context of continuum damage mechanics in blast-damaged structures subjected to fire.

1.2 Aims and objectives of research

Based on the literature reviewed and presented, it is evident that there is a lack of study in progressive collapse analysis of steel buildings under fire loading or under sequential blast and fire loading with sophisticated steel deterioration model. Set against this background, this research aims to propose a new methodology for evaluating steel buildings' vulnerability subjected to fire, or combination of blast and fire loads. This study seeks to develop a coupled damage model, which accounts for both mechanical damage and thermal degradation, to predict structural deterioration behaviour in fire with improved accuracy. This methodology is then used to assess the performance of a three-dimensional low-rise five-storey building and mid-rise ten-storey building with office occupancy under fire as well as under combined hazards of blast and fire. This study intends to provide new insight into mitigating disproportionate collapse with an acceptance of local damage.

Specific objectives are:

- Develop a coupled thermo-mechanical damage model for adequately describing the deterioration behaviour of steel under combined mechanical and fire loads.
- Calibrate and validate the proposed model with existing test data and established numerical work.
- Design a five-storey and a ten-storey steel-framed building with office occupancy in accordance with the current building codes, respectively.

- Evaluate the performance of the buildings using the proposed damage model under three types of accidental scenarios: (i) fire only scenario, (ii) post-blast fire scenario, and (iii) fire-triggered gas explosion scenario. The location of the compartment where triggering loads occur is also varied in order to determine the most vulnerable location for the building system.
- Provide a check of the collapse initiation time and assess the role of damage accumulation in eventual structural collapse.
- Identify possible collapse mechanisms under different accidental scenarios and determine the most detrimental fire scenario as well as the weakest link in structural system.
- Suggest effective strategies to prevent progressive collapse in blast and fire incidents.

Thesis outline

An overview of this thesis is given as follows:

Chapter 2 An overview of progressive collapse cases and structural fire engineering.

This chapter first discusses progressive collapse types of catastrophes that have occurred in the past decades. This is followed by reviewing existing progressive collapse assessment methods and provisions in current guidelines and codes. Previous studies on the structural behaviour of steel framed buildings subjected to fire or combined hazards of blast and fire are then summarized. The review of the literature works indicates that there is a gap in assessing structural robustness against progressive collapse in fire with sophisticated material deterioration modelling. A review of constitutive models of structural steel and continuum damage mechanics models is provided in order to facilitate development of coupled thermo-mechanical damage model for steel in the next chapter.

Chapter 3 Development of coupled thermo-mechanical damage model.

This chapter proposes a coupled thermo-mechanical damage model for structural steel and provides a framework for incorporating coupled damage model in FE analysis with available tensile coupon data. The proposed model is calibrated and validated with experimental data at the material level, which verifies its capability in capturing the coupled damage growth under combined mechanical and thermal loads using a limited number of parameters. A numerical implementation

procedure is developed to incorporate the damage-coupled constitutive equations into FE software ABAQUS/Explicit using user developed subroutine VUMAT. This allows the damage mechanism to be treated predominantly locally at material points or component levels, which in turn influences the global structural behaviour and possibly leads to progressive collapse.

Chapter 4 Calibration and validation of coupled damage model.

The proposed damage model is calibrated and validated against a comprehensive set of experimental results and established numerical results ranging from single member test to multi-storey steel frames subjected to severe fire. An inverse analysis type of calibration procedure is adopted which provides a data collection of damage parameters in support of collapse assessment of steel structural systems. Numerical analyses, performed with the calibrated damage model, demonstrate the consistent and accurate predictive capabilities of the damage model. The calibrated damage model is shown to provide excellent predictions of the load-displacement behaviour, ultimate failure temperature and failure initiation locations.

Chapter 5 Studies of steel buildings under blast and fire.

This chapter studies the susceptibility of a five-storey and a ten-storey steel-framed office building against progressive collapse. Sophisticated three-dimensional FE models of the multi-storey steel-framed buildings with concrete slab system are developed in ABAQUS. Three types of accidental scenarios are investigated : (i) fire only scenario, (ii) post-blast fire scenario, and (iii) fire-triggered explosion scenarios. The location of the compartment where triggering loads occur, which is a factor in determining the most vulnerable location for the building system. is also varied. To emphasize the role of damage modelling in collapse assessment, numerical simulations are performed to analyse the behaviour of the office buildings with and without considering damage. This chapter provides a check of commercial buildings for satisfying robustness requirements under accidental loading. Compared with conventional numerical models, the proposed damage modelling framework provides a more conservative prediction of the failure probability of the structure during fire event or under combined hazards of blast and fire, and has the potential to be utilized as a useful tool in helping designers to determine how much time is realistically available for evacuation before progressive collapse occurs in this type of building. The assessment provides important insight into which type of hazard scenarios are likely to result in an unacceptable level of damage. Based on the identified collapse mechanisms, discussions are given regarding the performance of steel structures and effective strategies are suggested to improve the survivability of buildings under blast and fire.

Chapter 6 Conclusions.

This chapter concludes the research, highlights the key findings, makes recommendations to designers and gives suggestions for future research.

Chapter 2

Literature Review

2.1 Introduction

This chapter first discusses progressive collapse types of catastrophes that have occurred in the past decades. This is followed by reviewing existing progressive collapse assessment methods and provisions in current guidelines and codes. Given that the trigger of progressive collapse can be fire, explosion, impact or local failure, this study deals with fire-induced progressive collapse of steel buildings. Previous studies on the structural behaviour of steel members and steel/composite frames subjected to fire or post-blast fire are then summarized. Earlier research in structural fire engineering mainly focuses on the behaviour of single members or the frame behaviour in stable states and has provided important information on the factors which affect structural performance in fire. Among the factors, the degradation of steel properties at elevated temperature is a main contributor in the loss of structural resistance in fire. The characteristic of behaviour of steel at elevated temperatures in test findings are then evaluated. These are compared with the simplified constitutive models of structural steel provided in EN 1993-1-2.

The review of the literature works indicates that there is a gap in assessing structural robustness against progressive collapse in fire with sophisticated material deterioration modelling. Proper modelling of material damage and fracture in the context of continuum damage mechanics is essential in predicting material failure in steel members and structures. A review of continuum damage mechanics models indicates that though a few thermo-mechanical damage models for concrete are currently available in literature, the existing damage models for metal have been limited to ambient temperature or calibrated towards a specific temperature attained in metal forming on a case-by-case basis. Existing work that have dealt with thermo-mechanical damage coupling include studies on metalworking (Lestriez et al., 2004; Saanouni et al., 2011) and thermal-

mechanical fatigue (Egner and Egner, 2016; Razmi, 2012; Velay et al., 2006). There remains a lack of research which accurately simulates steel deterioration behaviour in fire events by considering the combining effects of mechanical and thermal damage. Therefore, this study attempts to address the gap by developing a thermo-mechanical damage model for steel and applying it to progressive collapse analysis of steel buildings under fire as well as combined hazards of blast and fire.

2.2 Past progressive collapse disasters

Partial or total collapse of real buildings in the past offers valuable insights into structural behaviour on the global level. This section presents cases studies of past progressive collapse disasters. The collapse mechanisms are examined in depth and the relevant observations and implications are discussed.

2.2.1 Ronan Point

On 16th May 1989, Ronan point, a 22-storey tower block in East London, suffered progressive collapse due to a gas explosion in the 18th floor flat. The entire south-east corner of the tower block collapsed, resulting in 4 deaths and 17 injuries. This incident has been the motivator for introducing disproportionate collapse provisions in the UK.

Fig. 2.1 Dispropotionate collapse of Ronan Point (Pearson and Delatte, 2005)

Being 64 *m* tall and containing 110 flats, the tower block was constructed by bolting together large concrete prefabricated sections which were cast off-site. Post-disaster investigations found that despite the fact that the design has complied with the building regulations, the structural stability against small explosion, wind loads or fire exposure was not adequate. Moreover, construction defects were discovered, including fire separation not achieved, support of wall panels not evenly spread, strengthening brackets incorrectly attached and joints not properly filled with concrete. These factors resulted in a lack of alternate load paths to redistributed forces in the event of local damage in Ronan Point. After the explosion, the tower was partially rebuilt but eventually demolished due to safety concern.

This catastrophe raised public concern about high-rise buildings and reflected a lack of provisions for structural robustness in building design. Thereafter in the wake of Ronan Point collapse, 'dispropotionate collapse' has now been covered in Approved Document A (2004), which requires that 'the building shall be constructed so that in the event of an accident, the building will not suffer collapse to an extent disproportionate to the cause.' One of the major changes was brought out by the 'fifth amendment' to the UK building regulations in 1970 to ensure structural robustness in the event of an explosion. Buildings of more than five storeys constructed after November 1968 were required to be capable of resisting an explosive force of 34 *kPa*. Existing buildings must be able to resist an explosive force of 17 *kPa*, provided that the gas supply was replaced with electric cooking and heating (Hendry, 1979). Tests performed by the Building Research Station and Imperial College showed that Ronan Point didn't meet this criteria. The investigation concluded that the kitchen and living room walls would fail at an explosive force of 11.7 *kPa* and the exterior wall would fail at an explosive force of 20.7 *kPa*.

The changes in the UK building regulations initiated by Ronan Point collapse are believed to have led to prevention of the collapse of the 24-storey Grenfell Tower (built in 1974) in a disastrous fire in June, 2017. The lessons from Ronan Point collapse have also led to inclusion of provisions on structural robustness into building codes in other countries around the world (Longinow and Ellingwood, 1998; Pearson and Delatte, 2005). In the United States, ASCE (2005) provided general structural integerity provisions, and the most comprehensive guidelines can be found in GSA (General Services Administration) (2003, 2013) and DoD (United States Department of Defense) (2009).

2.2.2 World Trade Centre 7

On September 11, 2001, American Airlines Flight 11 and United Airlines Flight 175 crashed into World Trade Centre twin towers at 8.46 a.m. and at 9.59 a.m. in a coordinated act of terrorism. World Trade Centre 7 (WTC 7) was not hit by a plane but spontaneously

collapsed in 6.5 seconds at 5.20 p.m., about eight hours after the first hijacked aircraft struck WTC 1. It was reported that WTC 7 was structurally damaged by the falling debris during the collapse of WTC 1. Fires were also observed to be burning out of control on several floors of WTC 7 over the course of the day, which were initiated by the flaming debris of WTC 1. The collapse of WTC 7 was the first known instance of a tall building brought down primarily by uncontrolled fires, which raised pressing questions to be answered.

WTC 7 was a 47-storey steel-framed office building and had a considerably large floor plan (4,400 m^2). Both active and passive fire protection systems were in place, specifying a 3-hour fire resistant rating for the columns and a 2-hour fire resistant rating for the beams and steel deck.

(a) General review of WTC 7

(b) Fires on the 11th and 12th floors of the east face of WTC 7

Fig. 2.2 View of debris spread around WTC 7 and fires developing in WTC 7 (Gilsanz et al., 2002)

In November 2008, National Institute of Standards and Technology (NIST) investigated the causes of the collapse of WTC 7 in its final report. According to the fire observations based on views of the exterior façades, the fires broke out in WTC 7 at about 10.28 a.m. and spread to at least 10 floors between Floors 7 and 30. Fires were extremely severe on Floors 7 to 9 and 11 to 13. The heat from uncontrolled fires gave rise to the thermal expansion which pushed the steel girder off its support at Column 79, triggering floor system failures. Due to the loss of lateral support, Column 79 soon buckled and the downward movement of the buckled column pulled the east penthouse and nearby columns down with it. This was followed by progressive collapse of east-to-west across the core due to floor system failures, impact from falling debris and load redistribution

from the buckled columns. Subsequently, the global collapse occurred as the entire building above the buckled region moved downward as a single unit.

The uncontrolled fire spread in WTC 7 reassembled past fire disasters in tall buildings where the automatic sprinklers were out of function. As the first known fire-induced total collapse which progressed from several buckled columns, the collapse of WTC 7 has been thought of as a key event in the history of structural engineering which led to broad re-examination of how buildings will respond to terrorist attacks and natural hazards. It is worthy of note that the design of WTC 7 did not engage specific analyses to look at how the building might perform in real fires (NIST, 2008). As typical of practice, design engineers were not required to explicitly evaluate the fire performance of structural system as a whole. The importance of considering the interactions between structural components has been recognised by researchers in recent years. A comprehensive review of experimental and numerical examinations done on the structural interactions and system behaviour is provided in Section 2.4.

2.3 Progressive collapse assessment methods and provisions

The aforementioned progressive collapse disasters have brought about revisions in existing design provisions and development in new design guidelines, particularly in Europe and in the USA. Had the most recent standards and practices been adopted in the design of Ronan Point tower and WTC 7, the catastrophes would have been avoided. The prevention of progressive collapse relies heavily on the development and adoption of building standards and provisions. This section provides a review of current practices which can effectively reduce the likelihood of progressive collapse of buildings.

Design strategy to prevent progressive collapse is different from traditional structural design approaches. The general framework consists of defining the performance requirements, identifying the threat, assessing the probability and risks of failing to meet the performance requirements. Within this framework, the threat events can be specific as well as non-specific hazard scenarios.

The specific abnormal load hazards may be grouped into (Somes, 1973):

- Pressure loads (e.g. gas explosion, bomb denotation)
- Impact loads (e.g. aircraft or missile impact, vehicular collision, debris)
- Deformation related loads (e.g. steel softening in fire, foundation subsidence)

- Faulty practices

In the event of these identified hazards, the design techniques to mitigate potential progressive collapse include (EN 1991-1-7, 2006):

- Event control, i.e. preventing the occurrence of the accidental events.
- Protect the structure against the postulated events.
- Enhance structural robustness by adopting the following strategies:
  - strengthen certain structural components as key elements.
  - enhance the capacity of structural members by selecting ductile material and adopting ductile member design.
  - ensuing global frame redundancy to provide alternative load paths in the event of local damage.

Alternatively, design can be carried out with regard to non threat-specific scenarios. This covers a wide range of potential hazards. The design goal would be to limit the extent of damage initiated by localised failure. This approach is more general oriented given that potential abnormal loads might remain unidentified during the service life of buildings. Strategies targeted on unidentified accidental actions were outlined as (EN 1991-1-7, 2006):

- Apply prescriptive rules, e.g. tying.
- Design key elements to resist notional accidental action.
- Enhance redundancy so that the structural stability would not be endangered in the event of a local failure.

Similar to EN 1991-1-7 (2006), two general approaches are currently employed in the USA for enhancing the resistance of buildings to progressive collapse (DoD (United States Department of Defense), 2009). The approaches include the indirect approach and the direct approach:

- The indirect approach

  It is a prescriptive approach specifying a minimum level of strength, continuity and ductility to enhance the robustness of the structure. Little additional structural analysis is required to determine the adequacy of structural resistance to progressive collapse.

- The direct approach
  - Specific loading resistance method

    Specific loading resistance method is to design the strength of critical load carrying elements to withstand specific abnormal loads, thus structural collapse is prevented. It is closely related to current structural design provisions.
  - Alternate load path method

    Unlike the specific loading resistance method which is threat specific, the alternate load path method requires the structure to bridge over the local failure zone where one or more primary vertical support members are removed. This method relies on numerical analysis and provides a check for the capability of redistributing loads of remaining structure on removal of specific elements, such as columns.

For the majority of structures, the indirect method will suffice. This prescribed design requirement enhances the structural robustness with greater capacity to resist abnormal loading. For structures of which the potential to progressive collapse is a concern, the direct approach should be adopted to ensure that the structure has sufficient robustness. Once the appropriate design approaches are established, the next critical step is to select measurable performance criteria.

Ellingwood et al. (2007) categorized the performance of buildings into two levels, namely, high performance and acceptable performance.

- High performance

  If the initial damage has been totally absorbed by structural system and the collapse does not initiate.
- Acceptable performance
  - If the initial damage is localised to the bay and does not extend more than one floor above or below, or
  - If the ultimate deformation is limited to a safe value (e.g. limited to a fraction of the storey height), and life safety of occupants outside the initial damage location is not endangered.

In terms of damage extent, it is not always straightforward to determine a quantifiable measure of the permissible amount of damage. The basic concept is that the damage should not be disproportionate to the original cause. It is suggested that for the notional removal of one column, a proportionate damage is within 70 m^2 or 15 % of the floor

area (whichever is less) in Approved Document A (2004), and within 100 m^2 or 15 % of the floor area (whichever is less) in EN 1991-1-7 (2006). However, the total collapse of a building may not be deemed disproportionate, given that the size of the original accidental action is large enough. DoD (United States Department of Defense) (2009) recommended different limits of damage extents for removal of external and internal vertical load-bearing members. When an external column or load-bearing wall is removed, the allowed collapsed area of the floor directly above the removed member must be the lesser of 70 m^2 or 15% of the total floor area. For the removal of an internal column or load-bearing wall, the permissible collapsed area of the floor directly above the removed element should be the smaller of 140 m^2 or 30% of the total area of that floor. In both cases, the floor directly beneath the occurrence of member removal should not fail. In addition, damage must not extend beyond the structure tributary to the exterior removal or beyond the bays adjacent to interior removal.

In summary, it has been shown from this review that modern building codes and design guidelines have recognized the need for prescribing standardized provisions in the field of progressive collapse assessment and mitigation. The prescriptive tying force requirements and the member removal approach provide an acceptable level of structural continuity and redundancy, yet they cannot always guarantee structural resistance to progressive collapse for particular buildings. The explicit consideration of the likelihood of progressive collapse in specific abnormal load events and damage scenarios has to be made on a case-by-case basis. There is a pressing need for researchers to select appropriate analysis techniques for specific projects and identify the best practices for building design to meet the performance requirements.

2.4 Behaviour of steel-framed buildings in fire

2.4.1 Cardington Fire tests

Very few full-scale fire tests have been conducted on steel frames. Among these, Cardington fire tests play a significant role in today's understanding of actual structural behaviour in real fire. British Steel and Building Research Establishment (BRE) conducted a series of full-scale fire tests on an eight-storey typical braced steel office building at Cardington in UK between 1994 and 2003. The building spanned 21 m by 45 m in area and reached 33 m in height. There were three bays spaced 6 m, 9 m, 6 m along the width and five bays spaced 9 m along the length of the building. The building was designed as braced frame with a central lift core and two end stairwells. The structure was designed for a dead load of 3.65 kN/m^2 and an imposed load of 3.5 kN/m^2. The connections consisted of flexible

end-plates for the beam-to-column connections and fin plates for the beam-to-beam connections. The composite floor system consisted of steel deck, lightweight concrete and reinforcing mesh, and design load was simulated by placing sand bags over the specified area. A total of seven fire tests were carried out at different locations and floors.

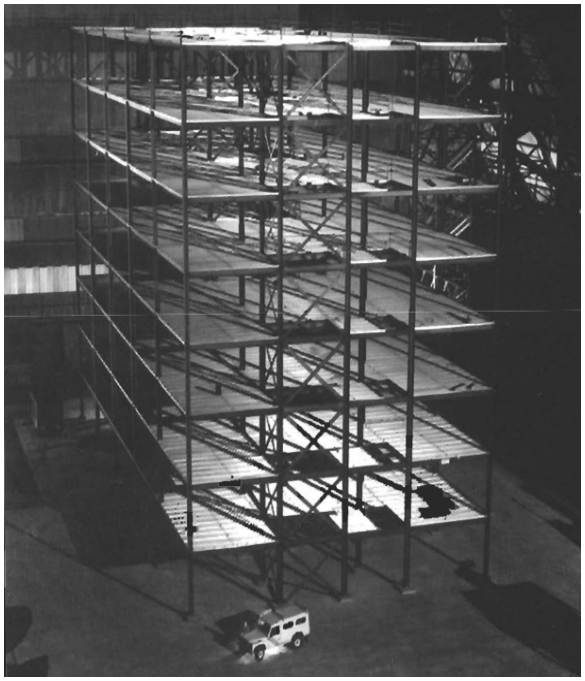

(a) General review of the eight-storey test structure

(b) Fire test in progress

Fig. 2.3 Large scale fire tests on a real multi-storey steel framed building at Cardington (British steel, 1999)

Test 1 was the restrained beam test. It was designed to obtain a direct comparison with the standard fire tests. An unprotected 9 *m* long internal beam and the supported slab were heated by a gas fired furnace on the 6th floor until the temperature got to 800°C - 900°C through the section profile while the connections were still at ambient temperature. The maximum sagging that occurred was 232 *mm* ($span/35$), but the mid-span vertical displacement reduced to 113 *mm* once the beam returned to ambient temperature. Yielding and local buckling at both ends of the test beam were also observed during the experiment. Lower flange at the ends of the beam was distorted as restraining forces occurred due to thermal expansion against the web of the column section. Fractures of end-plate connections at both ends of the beam were inspected visually after the test. It should be noted that the failure deflection occurred at over 1000°C in the test, whereas it would have happened at 700°C if tested in isolation.

Test 2 was to investigate primary beams and columns along grid line B (see Figure 2.4)which supported the 4th floor. The primary, secondary beams and top 800 *mm* of columns were left unprotected. The exposed parts of the columns squashed at approximately 670°C, causing the rate of vertical displacement of central primary beam to

increase rapidly. The test was terminated when the central primary beam reached a vertical deflection of 293 *mm* ($span/31$). As test observations indicated that squashing of columns may lead to the floors above the fire compartment turning unstable, it was concluded that the columns should be fully protected along the entire length to limit damage to fire compartment area only.

Test 3 was carried out in a corner compartment on the first floor. The objective was to investigate the behaviour of a complete floor system in fire, especially the membrane action which provided alternative load paths for load redistribution. All structural members were left unprotected apart from columns, column-to-beam connections and external perimeter beams. The maximum recorded steel temperature was 935°C. Large sagging was recorded to be 428 *mm* ($span/21$) of the secondary beam and the displacement reduced to 296 *mm* after cooling. Extensive buckling was noticed at beam-to-column connections. Worthy of note was that the end of an internal secondary beam which was connected to a primary beam buckled locally due to axial restraints from adjacent members. However, no local buckling occurred at the other end of the beam which was connected to an external beam. This could be attributed to the thermal expansion of the secondary beam, which caused the external beam to twist and resulted in insufficient restraint to induce local buckling.

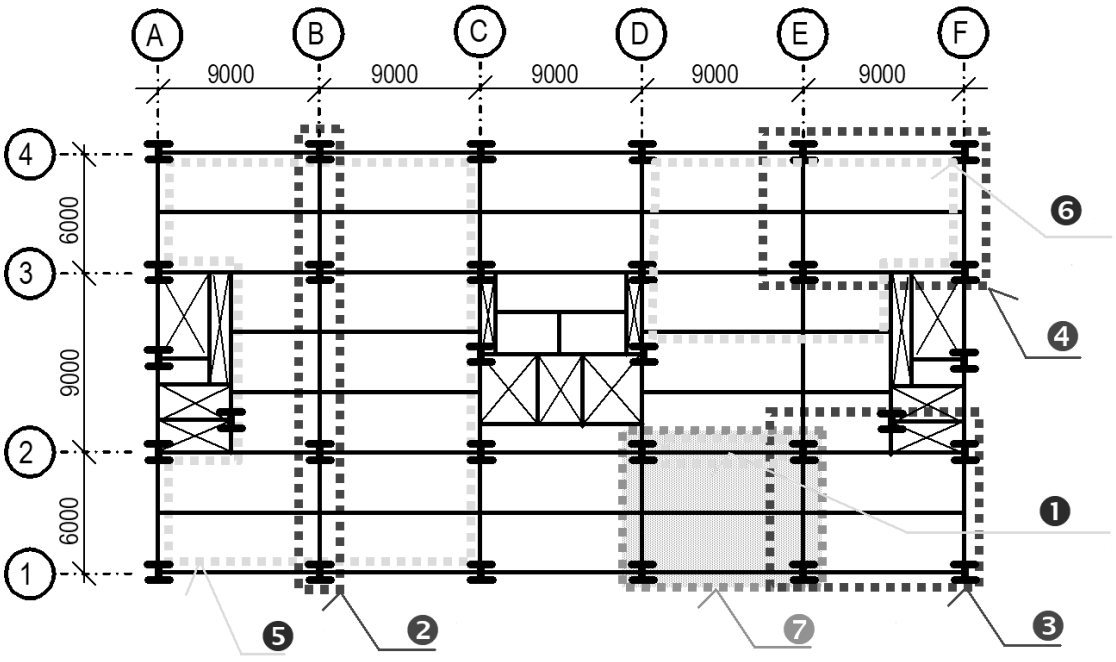

Fig. 2.4 Floor layout and location of the fire tests (Foster et al., 2007)

In Test 4, a corner compartment was subjected to fire from the upper floor. Only columns were protected. The development of the fire being restricted by low level of oxygen as a result of closed windows and doors. The temperature of the fire dropped after the initial rise and the fire continued to smoulder. Flashover did not occur until two windows were removed. It was recorded that the maximum steel temperature was 903°C and

Table 2.1 Summary of Cardington fire tests

Test	Description	Fire area(m^2)	Location	Duration (minutes)	Temperature(°C) Atmos	Steel	Maximum deflection(mm)
1	Restrained beam	24	Level 7	170	913	875	232
2	Plane frame	53	Level 4	125	820	800	445
3	1^{st} Corner	70	Level 2	75	1020	950	325
4	2^{nd} Corner	54	Level 3	114	1000	903	269
5	Large compartment	342	Level 3	70	746	691	557
6	Office	136	Level 2	40	1150	1060	610
7	Integrity	77	Level 4	55	1108	1088	1200

the maximum deflection of the slab was 269 mm ($span/33$). The compartment wall was found to affect the behaviour of unprotected beams. When the wall was removed, distortional buckling occurred along most of the beam length. This was due to high thermal gradient through the section profile of the beam caused by the placement of the wall.

Test 5 was conducted in a large (340 m^2) compartment between the second and third floor. A fire resistance wall was constructed along the full width of the building. Unlike Test 4, enough ventilation was allowed for the fire to develop. All the steel beams were left unprotected. The maximum recorded atmosphere temperature and steel temperature were 746°C and 691°C, respectively. The fire was not very severe because it lasted longer with lower temperatures. The maximum deflection reached 557 mm ($span/16$) and recovered to 481 mm after cooling. A number of beam-to-beam connections were found to have locally buckled and fractures were observed in many end-plate connections after cooling.

In Test 6, a more realistic open plan office fire scenario was simulated using office furniture as consuming fuel in a compartment area of 135 m^2. Only columns and beam-to-column connections were protected. Within 10 minutes of ignition, the maximum temperature attained in the compartment was over 900°C. The maximum steel temperature recorded during the test was 1150°C and the maximum vertical displacement reached 600 mm ($span/15$). No signs of failure were observed, but there was extensive cracking forming in the concrete slab during the latter phase of cooling.

Test 7 was conducted in a $11m \times 7m$ fire compartment on the third floor of the building. The imposed load (3.19 KN/m^2) gave a higher load ratio than in the previous six fire tests. Only columns and a short length of the primary edge beams were protected with cementitious spray. The maximum recorded temperature was 1072°C for beams and 420°C for columns. The maximum slab displacement recorded was about 1000 mm ($span/9$) in the central zone of the compartment.

A summary of the test conditions and results of the aforementioned Cardington fire tests is presented in Table 2.1. In conclusion, the Cardington fire tests play a significant role in today's understandings of actual structural behaviour in real fire. The superior performance of composite floor systems that cannot be evaluated from isolated member fire tests is regarded as one of the most important findings. It should be noted that though no structural collapse took place, the excessive deflections observed in tests could cause integrity failure which may result in extensive damage in realistic situations. The understanding gained from Cardington test observations forms the basis of calibration for FE modelling and benefits the design of composite construction, which is introduced in the following section.

2.4.2 Numerical studies on steel frames that survived fire

Due to the high costs of fire tests on structures, a number of researchers attempted to employ numerical models to simulate structural behaviour in fire. Till this day, Cardington fire tests have acted as well-documented benchmarks for researchers to calibrate and validate numerical models. On this basis researchers have extended the investigation to predict structural performance of generic steel frames under various fire scenarios.

Wang (2000) presented the numerical findings on Cardington fire test 4 (the corner compartment test) and test 5 (the large compartment test) . Simulation results indicated that the large deflections experienced by floor systems during fire tests cannot be modelled by pure flexural bending. Tensile membrane action need to be included to capture the inherent good performance of slab system. It was also suggested that large moments may be induced in columns as a result of being pushed by thermal expansion of heated beams. Conclusions were still tentative at this stage.

Bailey and Moore (2000a) developed a new method for predicting steel frame behaviour in fire by taking into account the tensile membrane action of the composite floor system. This approach was validated against six of Cardington fire test and gave accurate predictions for five out of six tests. Bailey and Moore (2000b) then applied this method to practical composite floor system and compared with traditional design approaches. Results suggested that by considering membrane action it was not necessary to protect secondary beams and thus provided a cost-effective solution compared to traditional design practice. The membrane action achieved in the slab system was limited by a conservative estimation of the maximum allowable vertical displacement. However, this failure limit state could not yet be verified because the failure by structural collapse was never reached during the series of Cardington fire tests. Based on Bailey's method (2000a; 2000b), the recommendation of allowing the secondary beams in composite steel

structures to be left unprotected has become an established design approach published by the steel construction institution of the UK (Newman et al., 2006).

Elghazouli et al. (2000) performed numerical analyses of Cardington fire test 1 (restrained beam test) and test 3 (corner compartment test) and closely examined the response of composite floor under fire conditions. The obtained vertical deflections of floor systems at elevated temperatures were in general agreement with test data. The importance of the restraint to thermal expansion by cool surrounding bays was highlighted in this study. In the restrained beam test, the restraint from surrounding stiff structure induced high level of compressive force in the heated floor and caused early buckling of the floor system. This buckling combined with material degradation led to rapid increase in the vertical deformation. Compared with the restrained beam test, the heated area in the corner test was larger and therefore the level of axial restraint to heated floor was lower. Therefore, the early buckling of floor system was less noticeable than in the restrained beam test. Instead the deflection was more gradual as a result of substantial loss of stiffness and strength at elevated temperatures. The author also examined the effect of gravity loading magnitudes on the structural performance. Results showed that by doubling the load level in corner test, the vertical deflection increased by 40%. The author suggested that further study are required to establish suitable failure criteria, which can be related to limiting mechanical strains in the reinforcement.

O'Connor (2003) presented the key findings from Cardington fire tests and discussed the implications of the new understandings on fire engineering design. Traditional design practice usually neglected the inherent redundancy in structures and related to deformation limit as failure criteria. Contradictory to traditional understanding, increasing beam section size might not be always beneficial in fire engineering because this would lead to an increase in forces imposed on the surrounding structure and the cooler slab. Another distinction from traditional design was that the rapidly increasing displacement was not considered as imminent failure in fire but rather a sign of tensile membrane action development. Given the inherent fire resistance of steel composite structures, it was recommended by the author that part of the beams may remain unprotected on careful examination.

Foster et al. (2007) carried out numerical investigation and extended sensitivity studies of Cardington fire test 7. The author confirmed again that the tensile membrane action was the main load-carrying mechanism at high deflections. The author also suggested designers to pay attention to concrete cracks at high deflection of slab when making use of tensile membrane action. It was noted that at excessive deflections localised crack might occur due to the brittle nature of concrete. As a result, the two-dimensional load-carrying capacity of concrete may be compromised.

Based on the understanding gained from Cardington fire tests, Lamont et al. (2004) extended the investigation of structural behaviour in fire to a generic steel composite frame. This was done by comparing the structural behaviour of a small (5 storey) generic composite steel and light weight concrete frame during two different single floor compartment fires ("short-hot" fire and "long-cool" fire). The structure performed in distinct way in these two fire scenarios. In the "short-hot" fire, though high temperatures were achieved in steel beams, only the exposed face of the concrete responded to heating while the other portions of slab depth remained cool. Thus the structure experienced greater thermal bowing than in the "long-cool" fire. It was concluded that the "short-hot" fire (equivalent to 60 min of standard exposure) resulted in worse consequences on the structure than the "long-cool" fire (approximately 120 min of standard exposure). Lamont et al. (2007) then extended this study to examine the effects of removing the fire protection of the edge beams. Results showed that the deformation of the slab was much larger when the edge beam was unprotected. This was because the unprotected beam can not provide perimeter support for the slab to develop two-dimensional tensile membrane action. A weaker one-way load carrying mechanism similar to beam's catenary action was developed instead. This one-way load carrying mechanism and excessive deformation led to pull-in of column at the end of the fire. While applying fire protection to edge beams generally enhanced structural fire resistance, it should be noted that average mechanical strains in reinforcement were higher and earlier instability in the primary beams was observed when edge beams were protected.

The response of structural performance in fire is also highly dependent on the connection behaviour. Connections in a heated steel-framed building are subjected to complex loading conditions that are very different from those at the ambient temperature, and could be potentially a vulnerable link in structural systems (Burgess et al., 2012). As detailed FE modelling of connections at structural scale will be extremely computationally expensive and complicated, there is a growing body of research in developing simplified analytical models for accurately evaluating the connection behaviour under fire. Recent developments in high-temperature component-based models for different types of connections have allowed for full representation of connection performance including fracture of individual components in Vulcan software at University of Sheffield (Block et al., 2007; Dong et al., 2011; Hu et al., 2009; Sarraj, 2007; Yu et al., 2010).

The move to numerical studies as a supplement of Cardington fire tests has been shown to be capable of modelling beneficial or detrimental interactions between structural components with a high degree of accuracy. The success in the modelling attempts has thrown light on extending the available results database by generating further data with carefully calibrated numerical models.

2.4.3 Numerical studies on progressive collapse of steel frames under fire

Though comprehensive and insightful, the Cardington fire tests and the subsequent numerical investigations did not provide a check on the ultimate failure of the structural system. On the other hand, designers are utterly concerned with preventing fire-induced disproportionate collapse of buildings. This is because achieving required fire resistance for buildings is crucial for safe evacuation and firefighting. As a result, there is a growing body of literature that recognizes the importance of collapse assessment of steel frames in various fire scenarios. The following paragraphs introduce the recent development in fire-induce progressive collapse analysis of steel structures.

Two-dimensional numerical models

Ali et al. (2004) presented two collapse modes of single-storey steel frame depending on the fire scenarios, being toward the firewall or away from the fire wall. When fire was placed close to the wall, the collapse mode was toward the firewall as a result of catenary action of the heated beam. As the frame deformed and collapsed toward the firewall, the impact of the frame was considered to be detrimental to the integrity of fire wall. Thus the more desirable collapse mode was away from the wall as a result of thermal expansion of the heated beam.

Takagi (2007) conducted a collapse assessment of a 10-storey steel-framed building under fire using structural sub-assembly models. The restraints effect from surrounding framing was simulated using three types of sub-assemblies, namely an interior gravity column, a composite floor beam, and an exterior column-beam assembly. Results indicated that the rotational restraints from the columns above and below the fire floor had considerable impact on the stability of fire affected columns. The governing factors in structural system collapse were identified, and a probabilistic assessment was carried out to evaluate these parameters. It was concluded that the variability of steel yield strength at high temperatures was the most significant factor in the collapse probability assessment.

Lange et al. (2012) examined two possible failure mechanisms for tall buildings subjected to multiple floor fires. Fire occurred at floor 6, 7, 8 of a 12-storey composite steel frame. For simplification it was assumed that no connection failure occurred and steel members were unprotected. Two collapse mechanisms were identified, i.e. a weak floor mechanism and a strong floor mechanism. The weak floor collapse mechanism was initiated by the failure of the floor below the fire floor. Upon the failure the loads on the floor below increased, triggering a progressive collapse. In the strong floor collapse mechanism

(assuming floor beam axial stiffness 3.2 times greater than that in the weak floor model), failure was initiated by the formation of three plastic hinges in the column. At elevated temperatures, the floor system transitioned from a flexural load-carrying mechanism to a catenary mechanism due to the loss of the flexural capacity. The floor pulled the column inward and rapidly induced large moments in the column until three hinges formed, leading to progressive collapse. The identified collapse mechanisms were then compared with WTC tower collapse. This framework was based on two-dimensional steel frames and was intended to provide a simple stability assessment method for tall buildings under multiple floor fires without complicated numerical modelling. The author provided valuable insight into possible collapse mechanisms of tall building in fire but the time to failure was not predicted in this study.

Sun et al. (2012b) studied the progressive collapse mechanisms of a two-dimensional moment resisting frame using a static-dynamic procedure developed by the author. All beam to column connections were assumed to be fixed. Parametric studies were carried out to investigate the influence of load ratios, beam section sizes and bracing system on the collapse mechanisms under fire conditions. Results suggested that for unbraced frames the high load levels and small beam sizes generally resulted in localised collapse, whereas low load levels and large beam sizes led to higher failure temperature and therefore global collapse. The beneficial effect of bracing system was highlighted. The lateral stiffness from bracing system was effective in reducing the vertical displacement of columns at failure.

Sun et al. (2012a) used the same procedure to study the progressive collapse mechanisms of a two-dimensional moment resisting frame with different bracing systems under edge bay fire scenario and central bay fire scenario. Results suggested that the pull-in of columns caused by catenary force was a main factor in triggering progressive collapse. The bracing systems were capable of providing extra redundancy of the structure and alternate load paths after local damage occurred. Horizontal "hat truss" bracing facilitated loads transfer from buckled columns to adjacent members but could hardly reduce the pull-in of columns due to catenary force in largely deflected beams. On the other hand, vertical bracing systems not only enhanced the lateral restraint of the frame which restricted the pull-in of the columns, but also effectively prevented the collapse propagation. A combination of "hat truss" and vertical bracing system was considered to be most effective in reducing the likelihood of progressive collapse in the event of a column buckling.

Jiang et al. (2014) studied the progressive mechanisms of steel frames under single-compartment fire, horizontal multiple-compartment fire and vertical multiple-compartment fire, respectively. The single-compartment fire scenario was simulated by locating the fire at central bay and edge bay on the ground floor and third floor. For the central bay

fires, the collapse mode was local downward collapse for both the ground floor and the third floor due to the buckling of the heated column. In contrast, for the edge bay fires, the collapse mode was of global lateral drift for the ground floor and local downward collapse for the third floor. It was observed that the edge bay fire on the ground floor was more severe compared to other locations, in which the whole frame swayed and all ground floor columns buckled. Comparing the results of multiple-compartment fires with single-compartment fire, it was concluded that the collapse mechanism of vertical multi-compartment fire was similar to single-compartment fire, while the horizontal multi-compartment fire was more prone to global downward collapse.

Although capable of demonstrating key issues in collapse mechanisms, two-dimensional frame analyses focused on the load-transfer mechanism of skeletal frames and neglected the structural out-of plane stiffness and strength. These analyses are obviously not sufficiently representative of the actual behaviour of composite frames, which concerns load-transfer through interaction with slabs and transverse frame bays. To this end, a number of numerical studies have been recently performed on three-dimensional frame models.

Three-dimensional numerical models

Agarwal and Varma (2014) assessed the robustness of two types of ten-storey steel buildings under fire, one with gravity frame and rigid core in the form of concrete shear wall, and one with gravity frame and perimeter moment resisting frame. Results indicated that gravity columns were most likely to reach critical temperatures first due to the highest utilization ratios. This failure was recognized as the initiation of progressive collapse of the whole building. When local failure of column occurred, the tensile capacity of adequate steel reinforcement was found to be very effective in facilitating load redistribution paths and therefore maintaining the overall structural stability. This study offered some important insights into the progressive collapse mechnisms of tall building. However, the selected fire scenarios were limited to fire compartments on the fifth floor which might not be the most detrimental fire scenario for considering progressive collapse probability of steel frames. A more comprehensive study would be to include simulation of fire compartments on various floors of the building.

Jiang and Li (2016) carried out a numerical study on assessing the progressive collapse potential of an eight-storey moment-resisting steel-framed building subjected to localised fire. The selected fire scenarios included heating a single column on the ground floor and simultaneously heating four columns in the fire compartment. Numerical results indicated that the collapse did not occur at a loading ratio of 0.25 for columns in the event of a single column heated at the corner, internal or perimeter of the ground floor.

Load redistribution mechanism came into effect after buckling and the loads shed by the buckled column were sustained by the adjacent columns. The impact of load ratios was investigated by increasing the load ratio to 0.5. The internal columns buckled first regardless of the location of the heated column, initiating global structural collapse. This was followed by investigation of a compartment fire scenario in which four columns were heated simultaneously. The frame collapsed in the corner bay and the long edge bay fire scenario but survived the internal bay and the short edge bay fire scenario. In the internal bay fire scenario, the loads originally carried by the failed columns were redistributed evenly to the surrounding columns. As a result, the stability of frame system was maintained. The difference of the structure performances between the long edge bay fire and the short edge bay fire can be explained by the uneven load redistributions in the longitudinal and transverse directions. Higher magnitudes of redistributed loads were transferred along the short span than the long span. The author also suggested that the critical temperature at which the global collapse occurred was about 50-100°C higher than that of individually heated column.

Jiang and Li (2017) then performed progressive collapse analysis of another eight-storey moment resisting steel frame with different levels of fire protection, namely low, medium and high, respectively. The severity of various fire locations (corner bay, internal bay, edge bay) was investigated. It was found that the global collapse occurred 1 hour later than the local failure of the heated column. The indicator of global collapse was defined as the first buckling of cool columns which would likely induce sequential buckling of other columns. Results showed that for steel frame with a low fire protection level (1-hour fire rating for columns and beams), the corner and edge fire scenarios were more detrimental than internal fire scenarios. It was thus recommended to enhance the fire protection for perimeter columns. For steel frame with a medium level of fire protection (2-hour and 1.5-hour fire rating for columns and beams, respectively), the structure withstood the fire in all three scenarios. Simulation results also indicated that the buckling of the cool columns was caused by the lateral displacements of column ends rather than the axial loads. Increasing the fire protection of beams would be beneficial for structural stability as the slab deflection would be reduced and in turn the lateral displacements experienced by columns would be limited. But it should be noted that excessive fire protection of beams might lead to run-away failure of floor system.

As discussed above, Jiang and Li (2016, 2017) have provided new insights to advance our knowledge of the collapse mechanisms of three-dimensional steel structures under fire. On the basis of their numerical findings, further research need to be carried out on steel frames to provide a comprehensive review of progressive collapse mechanisms under various fire scenarios.

2.4.4 Numerical studies on fire-induced progressive collapse of post-damage building

The above subsection has dealt with numerical investigations on progressive collapse of steel structures under fire. The response of structures under the combined actions of explosion and fire is also a major concern in advanced structural fire engineering. Though this field has received increasing attention after September 11th incident, limited studies have been done on structural robustness under blast and subsequent fire. This subsection presents fire-induced progressive collapse analyses of steel frames with initial structural damage which demonstrate the influences of structural damage level on the collapse initiation time.

As one of the pioneers in this relatively new field, Izzuddin et al. (2000) carried out integrated fire and explosion analyses of a three-storey planar frame. Both rate dependency and temperature dependency of steel properties were accounted for in the analysis. Results showed that the fire resistance of the blast-damaged frame could be reduced by 40%, illustrating that the damage induced by moderate blast load had a considerable impact on the structural fire resistance. Liew and Chen (2005; 2004) also proposed an inelastic transient approach to investigate the influence of blast loads on the fire resistance of steel frame. It was assumed that connections did not fail under blast and fire. The rate-dependent model proposed by Perzyna (1966) was incorporated and then deactivated when the accidental loads transitioned from blast to fire. The difference in collapse modes resulting from the precedent blast damage was highlighted. Depending on the magnitudes of the explosion load, the frame might suffer more than a 10% loss in the fire resistance. These pioneering works were limited to simple steel frames. Instead of realistic blast and fire loading, simplified blast load profiles and a monotonic temperature increase history were applied to the members. Therefore, the results might not represent the real building behaviour.

Quiel and Marjanishvili (2011) evaluated the performance of a five-storey office building subjected to fire following blast load or impact load. The numerical model only considered the 2D portion of the perimeter MRF. The damage induced by blast load or impact load was not directly modelled but simulated by removing a column from the perimeter of a steel building. Results indicated a correlation between the amount of passive fire protection and the collapse time. This study was still restricted to two-dimensional structural model and the author did not model the damage induced by realistic blast loads in detail but rather simplified the damage extent as a column removal.

To capture the behaviour of a more realistic structure under fire and explosion, Liew (2008) carried out a combined fire and explosion analysis on a three-dimensional five-storey building. A 1000 kg equivalent of explosive was assumed to be detonated at 5

m from the front surface of the building. When the perimeter columns at the building front were subjected to the blast wave, they underwent lateral deformation and caused some loads to be transferred to the internal columns. The increased axial force led to internal columns buckling first after a period of heating. The perimeter columns buckled afterwards as a result of loads redistributed from internal columns, the blast-induced permanent deformation as well as material degradation at elevated temperatures. Progressive collapse occurred when there was no alternate path in the structural system to redistribute the loads. Results showed that the failure temperature of the frame decreased by 7.2% compared to that of the frame subjected to fire only. This study examined the interaction between explosion load and fire resistance of a three-dimensional steel frame assuming that the blast load acted on the building front. Hence, the vulnerability of steel frames subjected to internal blast and subsequent fire needs to be investigated to determine the detrimental effects of internal blast loads in further study.

Ding et al. (2016) evaluated the resistance to progressive collapse of a ten-storey office building under a confined explosion and post-explosion fire. The internal explosive load was modelled by placing the charge weight varying from 64 *kg* to 250 *kg* at 1.2 *m* above the ground. Simulations indicated that slab elements were seriously distorted under high blast loads, causing numerical inconvergence. For simplicity, slab elements were directly deleted from the model in the blast analysis, which resulted in non-continuity in floor system. Results showed that the most vulnerable compartment was the peripheral compartment in fire only scenarios and the corner compartment for the combined hazard cases, implying that the blast induced damage had a bigger impact on the fire resistance of a corner compartment. After the failures of gravity columns and shear tab connections, the tensile membrane action of the slab became the dominant load-carrying mechanism. It was observed from the simulation results that the membrane action was compromised in some cases when the restraints of the floor weakened or the continuity of the floor was lost. Design recommendations were proposed by the author that the reinforcement ratios should be increased and the columns in the corner compartment should be encased in concrete or fabricated from fire-resistant steel. As the conclusions were based on the analysis on the ground floor, the examination of the progressive collapse risks when the triggering loads occurred in the upper floors was beyond the scope of this study.

The disproportionate collapse of WTC 7 was also a typical example of fire-induced collapse of post-damage building. McAllister et al. (2011) addressed the collapse phases of WTC 7 with very sophisticated numerical model. In the first phase, a 16-storey pseudo static finite-element model was studied in ANSYS to simulate the collapse initiation - 4 hours leading up to the collapse. In the second phase, a 47-storey dynamic finite-element model was built in LS-DYNA to study the sequential failures and collapse process (approximately 15 seconds). Criteria for connections failure, shear studs failure, buckling instability of beams and girders, and cracking and crushing of concrete slab was

developed on the basis of experiments and mechanics in the pseudostatic model. Based on the local plastic strain of each element, the element was immediately removed as long as the criterion was exceeded and therefore not contributing to the strength or stiffness of the structure anymore. Thus sequential failures leading to global collapse were simulated and extreme impedance of analysis convergence was avoided. Three different temperatures were used for the fire, with the first temperature from FDS simulations, the second and third temperatures increasing and decreasing by 10%, respectively. It was found that the failures occurred in similar places in the building across three temperatures. The only difference was that the highest temperature caused failure to occur in a shorter time period than the cooler temperatures. The analysis took approximately 6 months for the pseudo static model and 8 weeks for the dynamic model. This study threw light on understanding the sequence of structural failures of WTC 7, but the computational efficiency was a major drawback.

In addition to the accidental situations discussed above, another catastrophic phenomenon in fire incidents is that the high temperatures reached in fire might be the trigger of explosions. Surprisingly, few studies have investigated the blast effects on structural members in fire. Among these, Forni et al. (2017) presented a study on the load carrying capacity of steel columns under fire and followed by an explosion. Xi (2016) compared the responses of restrained steel beams subjected to fire followed by an explosion, and subjected to an explosion followed by fire. Results indicated that the beam subjected to fire followed by an explosion was more vulnerable. This study illustrated that the disastrous consequences of such load sequences should receive more attention. However, the effects of this type of blast and fire interaction on steel frames have not been closely examined in literature.

It should also be noted that extensive studies have been conducted on progressive collapse of steel buildings subjected to impact or blast alone, mostly by column removal (Byfield et al., 2014). A brief summary of some of the key works is provided here. Izzuddin et al. (2008) investigated the progressive collapse of multi-storey composite buildings under sudden column removal scenario using a novel design-oriented framework. Results indicated that the investigated structures are susceptible to progressive collapse, mainly due to the inability of the internal secondary beam support joints to safely transfer the vertical loads to the adjacent members. Kim and Kim (2009) studied the progressive collapse resistance of steel moment frames using the analysis procedures recommended in the guideline published by GSA (General Services Administration) (2003) and DoD (United States Department of Defense) (2009). The effects of the location of column loss and the number of stories on the progressive collapse potential were identified. Li and El-Tawil (2013) assessed the collapse potential of a seismically designed steel-framed moment resisting building subjected to column removal using 3-D nonlinear computational models. Results suggested that column loss on the upper floors is more

detrimental compared to that of the lower floors, and this type of building is particularly vulnerable under removal of internal gravity columns. Fu et al. (2017) studied a 3-D composite floor system under both static and sudden removal of internal column using verified macro-based models, and conclusions were found about the load-transfer mechanisms and the dynamic increase factors.

2.5 Structural steel deterioration

2.5.1 Constitutive models of structural steel at elevated temperatures

The previous section has summarized the numerical studies on fire-induced progressive collapse of steel frames. The reliability of modelling attempts heavily depends on the accurate representation of the material behaviour and therefore the choice of constitutive models. Lying at the heart of numerical modelling, constitutive models establish the relation of stress and strain at the material level, and determine the force-displacement relationship at the structural level. Therefore, the choice of constitutive models is crucial in progressive collapse analysis of structures.

Much of the knowledge about steel properties at elevated temperatures is gained from material tests, which are usually carried out by transient-state or steady-state methods. In the steady-state regime, the specimen is heated to a pre-determined temperature before applying mechanical loads. The temperatures are kept constant during the test. On the other hand, the test specimen is subjected to constant mechanical loads and heated until failure in the transient-state regime. The heating rate is usually $5-50^{\circ}C/min$ in transient-state testing. Though steady-state tests are usually easier to conduct, transient-state regime is the preferred method because it represents the realistic situations of structures in fire. Generally the transient-state tests yield more conservative results than steady-state tests at small strains, but the difference in the obtained material properties is negligible between two methods when test specimens approach limit of deflection (Kirby and Preston, 1988).

The variations in test conditions inevitably led to variations in the reported mechanical properties at high temperatures. A comprehensive review of the high-temperature test data and constitutive models available can be found in Kodur et al. (2010). The severe deteriorating effects of high temperatures have also been well recognized by design codes, and the simplified representations of temperature-dependent degradation behaviour of steel provided in ASCE (1992) and Eurocode 3 (2005) have been widely adopted for

structural fire safety design. In the following pages, a summary of the experimental results as well as Eurocode 3 model are presented to provide an overview of steel characteristics in fire.

Yield strength and Young's modulus

The majority of the experimental research on high-temperature properties of steel reports the normalized yield strength and Young's modulus instead of the full stress-strain behaviour. Figure 2.5 and Figure 2.6 show a rich set of yield strength and Young's modulus data reported by reputable testing laboratories, along with the recommended values in the Eurocode 3 stress-strain model and those proposed by Poh (2001). Normalized by the reported room-temperature value, yield strength and Young's modulus are plotted as a function of temperature. A review of the data set shows significant variations in test data on yield strength and Young's modulus. This can be attributed to many factors, including the differences in steel grades, steady-state or transient-state testing regimes, various heating and loading rates. A careful comparison of the reported data provides general understanding of steel characteristics at high temperatures.

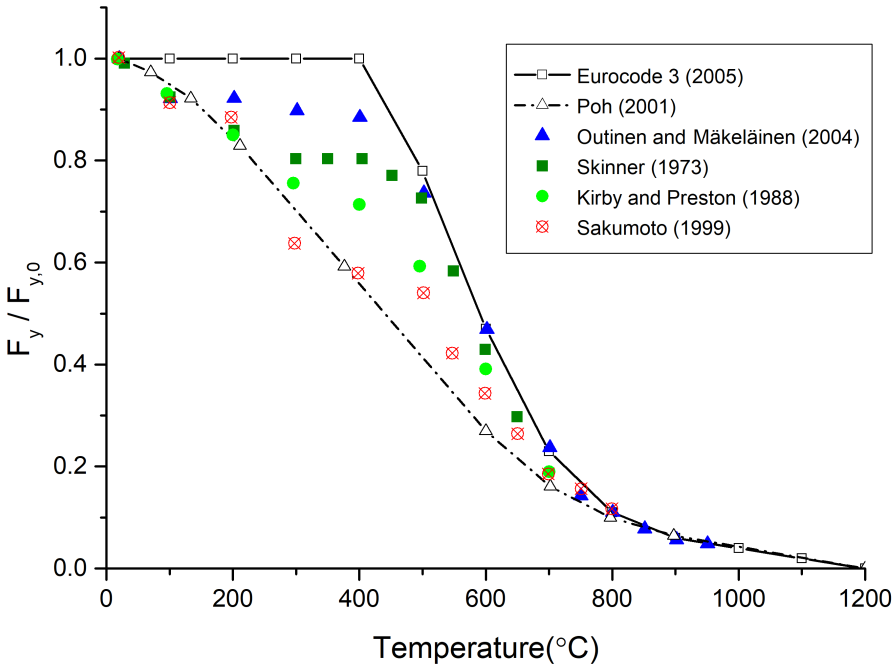

Fig. 2.5 Normalized yield strength of steel reported in literature sources

As the most commonly reported parameter, the reduction factors for the steel yield strength at varying temperatures were determined with respect to the initial yield strength at ambient temperature. It can be seen from Figure 2.5 that a significant drop in strength

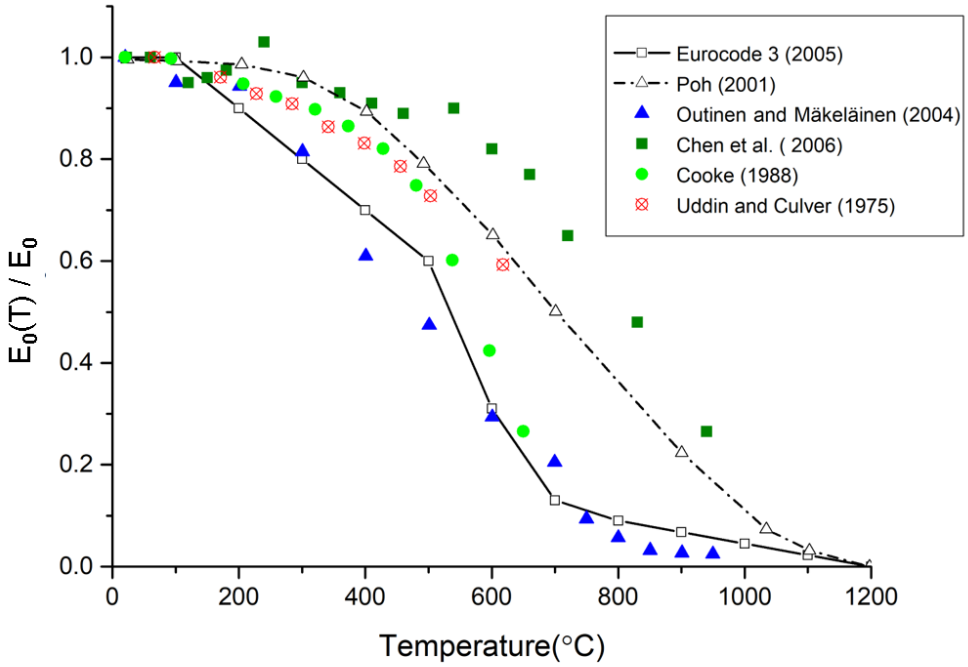

Fig. 2.6 Normalized elastic modulus of steel reported in literature sources

is observed in all sources for the temperatures between 400°C and 700°C. When steel is heated up to 800°C, it is only at 11% of its initial strength. A comparison of the plots indicates that Eurocode 3 model is unconservative for temperatures below 800°C.

On the other hand, as can be seen from Figure 2.6, the reduction factors of the initial elastic modulus show large variations above 300°C. These variations perhaps reflect the difficulty in eliminating the influences of test conditions on determining elastic modulus. All but a few data points lie above the Eurocode 3 line. This indicates that Eurocode 3 model predicts a higher reduction in Young's modulus than most of other sources.

The variations in high-temperature steel properties can lead to significantly different predictions of fire resistance. This poses challenges to design engineers when selecting reliable mechanical properties in predicting the performance of steel structures in fire.

Stress-strain curves

The stress-strain curves of steel at elevated temperatures differ from those at room temperature. Under fire conditions, the clearly defined yield point vanishes and the stress-strain history becomes nonlinear. Relatively few literature sources have reported full stress-strain relationships for structural steel at elevated temperatures that have simple mathematical forms and practical application range. Of these, the constitutive model

proposed by Eurocode 3 (2005) has been well accepted and widely used because of its consistency with existing test data and simple mathematical model (Twilt, 1991). Determined from the experimental data obtained by Kirby (1983), the Eurocode 3 model uses a multi-parameter model at fixed temperature points to describe the stress-strain curve.

The stress-strain curve comprises a linear elastic region up to the proportional limit, an ellipse that connects the end of the linear part to 2% strain, a yield plateau (possibly with strain hardening for up to $400^{\circ}C$), and a descending branch where the stress decreases from the maximum to zero. Figure 2.7 provides a graphical illustration for the constitutive model.

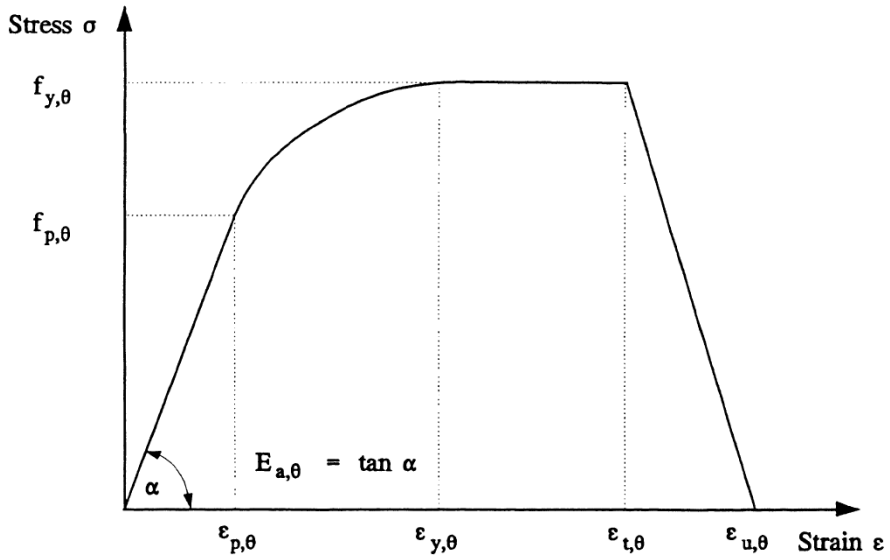

Fig. 2.7 Graphical presentation of the stress-strain relationships of structural steel at elevated temperatures (EN 1993-1-2, 2005)

The mathematical description is given by the following equations:

$$\sigma = \begin{cases} E_{a,\theta}\varepsilon, & \varepsilon \leq \varepsilon_{p,\theta} \\ f_{p,\theta} - c + (b/a)\sqrt{a^2 - (\varepsilon_{y,\theta} - \varepsilon)^2}, & \varepsilon_{p,\theta} < \varepsilon < \varepsilon_{y,\theta} \\ f_{y,\theta}, & \varepsilon_{y,\theta} < \varepsilon < \varepsilon_{t,\theta} \\ f_{y,\theta}[1 - (\varepsilon - \varepsilon_{t,\theta})/(\varepsilon_{u,\theta} - \varepsilon_{t,\theta})], & \varepsilon_{t,\theta} < \varepsilon < \varepsilon_{u,\theta} \end{cases} \tag{2.1}$$

The parameters used in this model are:

$$a = \sqrt{(\varepsilon_{y,\theta} - \varepsilon_{p,\theta})(\varepsilon_{y,\theta} - \varepsilon_{p,\theta} + c/E_{a,\theta})},$$

$$b = \sqrt{c(\varepsilon_{y,\theta} - \varepsilon_{p,\theta})E_{a,\theta} + c^2},$$

$$c = \frac{(f_{y,\theta} - f_{p,\theta})^2}{(\varepsilon_{y,\theta} - \varepsilon_{p,\theta})E_{a,\theta}) - 2(f_{y,\theta} - f_{p,\theta})},$$

and $\varepsilon_{p,\theta} = f_{p,\theta}/E_{a,\theta}$, $\varepsilon_{y,\theta} = 0.02$, $\varepsilon_{t,\theta} = 0.15$, $\varepsilon_{u,\theta} = 0.20$.

The reduced strength and modulus at elevated temperatures are required as input for this constitutive model. The temperature dependence of these terms are expressed as ratios of the value at elevated temperature to that at room temperature as shown in Figure 2.8.

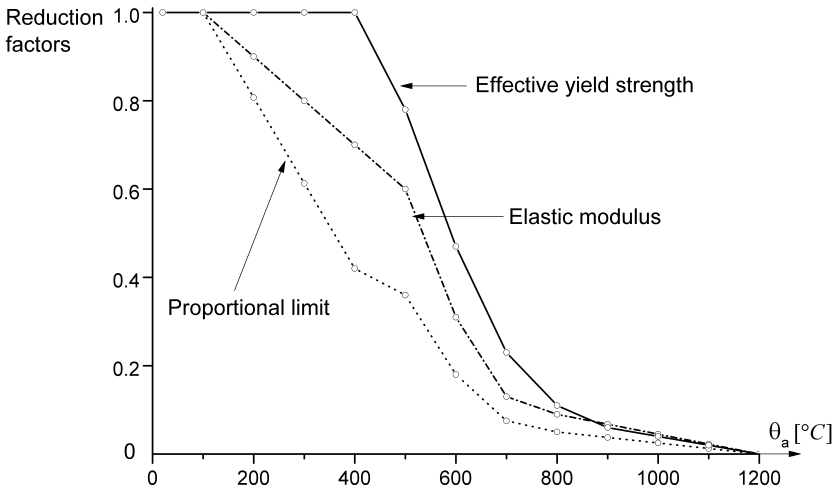

Fig. 2.8 Reduction factors for stress-strain relationships of structural steel at elevated temperatures (EN 1993-1-2, 2005)

To summarize, this subsection has reviewed high-temperature mechanical properties of structural steel reported by several notable experimental studies as well as Eurocode 3 model formulation. Despite the fact that large variations exist in the reported steel properties at elevated temperatures, Eurocode 3 model has been widely used in fire safety design of steel structures of common steel grades. Further studies need to be carried out to assess the adequacy of the Eurocode material model for performance-based structural fire safety design.

2.5.2 Damage and fracture theory

As discussed above, the research to date has addressed the degradation of steel properties due to fire exposure. It is common practice for researchers to base their numerical work on simplified experimental approximation curves of stress-strain relationships given in EN 1993-1-2 (2005). This simplified constitutive model is generally considered to be conservative in fire safety design. However, far too little attention has been

paid to damage and fracture induced by large deformations in steel. As the theory of damage concerns all materials at both low and high temperatures under any kind of load (Lemaitre and Chaboche, 1994), there remains a lack of research in modelling steel property deterioration as the structures experience severe fire as well as large structural deformation in accidental events. Due to the neglect of considering damage induced by plastic deformation, the design codes might turn out to be non-conservative under extreme loads.

The ductile damage accompanying plastic deformation is a result of the growth and coalescence of microdefects. The fracture and breakage of bonds leads to loss of material load-carrying capability and eventual complete failure. A proper modelling of this damage mechanism in the scope of continuum damage mechanics is essential in predicting material failure in steel members and structures. The fundamental aspect of continuum damage mechanics is the concept of effective stress which maps stress into the damaged surface. Kachanov (1958) first came up with a definition of a scalar variable which represents loss of effective resisting area. This has been the starting point for development of damage mechanics models including Lemaitre (1985), Chaboche (1988, 1997), Simo and Ju (1987), Chow and Wang (1987), Chandrakanth and Pandey (1993), Bonora (1997) and Bonora et al. (2004). Among these, the ductile damage model proposed by Lemaitre (1985) is most widely used and has been successfully implemented in structural analysis (Huang, 2009; Li et al., 2012). The following is a brief description of the continuum damage mechanics framework for ductile damage proposed by Lemaitre (1985).

Ductile damage model of Lemaitre

In the following pages, the principle features of the isotropic ductile plastic damage model proposed by Lemaitre (1985) are explained. The damage development in ductile materials together with the resulting deterioration in their mechanical properties are given in the framework of thermodynamics.

Damage variable Damage may be interpreted as a state variable that represents the effects of microvoids on a volume element. Consider a damaged body in a Representative Volume Element (RVE), let A be the total section area of the RVE defined by its normal n and let A_D be the total area of the microvoids in that section (see Figure 2.9), the isotropic damage variable D associated with the normal n can be defined as the effective surface density of microdefects:

$$D = \frac{A_D}{A} \tag{2.2}$$

where D is bound by 0 and 1, with 0 corresponding to undamaged RVE and 1 representing rupture of RVE.

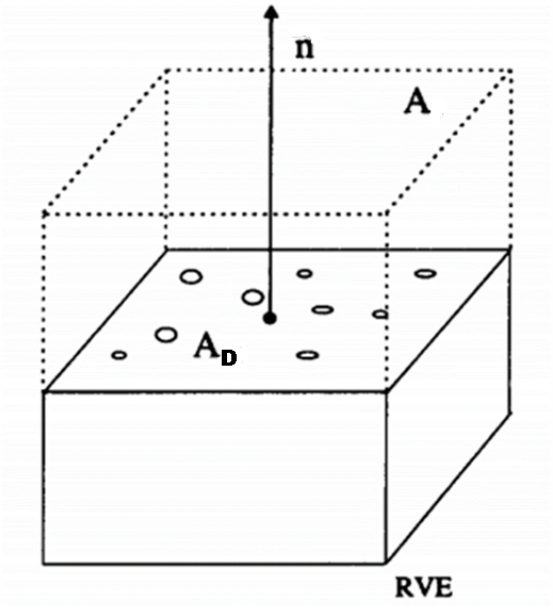

Fig. 2.9 Damaged element (Lemaitre, 1985)

Effective stress concept Consider the section A of the damaged RVE is loaded by a force F, the effective stress $\widetilde{\sigma}$ relates to the effective load resisting section area:

$$\widetilde{\sigma} = \frac{F}{A - A_D} = \frac{\sigma}{1 - D} \tag{2.3}$$

where $\sigma = F/A$.

The concept of effective stress overcomes the difficulty of describing the states of discontinuous damaged solid and enables effective physical properties to be defined in the current damage state.

Strain equivalence hypothesis The hypothesis of strain equivalence allows for mapping physical properties into the damaged surface so that any strain constitutive equation may be derived in the same way except that the effective stress replaces the stress in the undamaged material. The strain behaviour of a damaged material is modified only through the effective stress:

$$\varepsilon_e = \frac{\widetilde{\sigma}}{E} = \frac{\sigma}{(1 - D)E} \tag{2.4}$$

where ε_e is the elastic strain and E is Young's modulus.

Coupling between strains and damage The effective stress concept associated with the strain equivalence hypothesis allows one to write the state potential Ψ in the framework of thermodynamics, from which coupled strain damage constitutive equations are derived.

Taking the Helmhotz free energy Ψ as a convex function of state variables and assuming that the elasticity and the plasticity behaviours are uncoupled gives:

$$\Psi\left(\varepsilon^e, R, X, D\right) = \Psi^E\left(\varepsilon^e, D\right) + \Psi^{IN}\left(R, X\right) \tag{2.5}$$

The elastic part can be written as

$$\Psi^E\left(\varepsilon^e, D\right) = \frac{1}{2}\varepsilon^e : (1-D)C : \varepsilon^e \tag{2.6}$$

where ε^e is the elastic strain tensor, C is the standard elasticity tensor, R and D are the scalar internal variables associated respectively with isotropic hardening and isotropic damage, and the second-order tensor X is the internal variable for kinematic hardening.

Based on the hypothesis of strain equivalence, the damaged elasticity law derived from the elastic potential is:

$$\sigma = \frac{\partial \Psi}{\partial \varepsilon^e} = (1-D)\, C : \varepsilon^e \tag{2.7}$$

The variable associated with D is damage strain energy release rate Y, constituting the power dissipated $(-Y\dot{D})$ in the damage process. Y is defined by:

$$Y = -\frac{\partial \Psi}{\partial D} = \frac{1}{2}\varepsilon^e : C : \varepsilon^e \tag{2.8}$$

Ductile damage evolution In order to derive constitutive equations for damage variable D, the existence of a dissipation potential as a scalar convex function of state variables $\Psi^*\left(Y, \dot{p}\right)$ is assumed. Write the dissipation potential as a power function of Y for convenience and linear in $\dot{p}$ to ensure the non-explicit dependency of D with time:

$$\Psi^*\left(Y, \dot{p}\right) = \frac{S}{(s+1)}\left(\frac{Y}{S}\right)^{s+1}\dot{p} \tag{2.9}$$

where S is the damage strength and s is the damage exponent (sometimes s=1), which can be determined through experimental data, and $\dot{p}$ is the equivalent plastic strain rate.

Damage growth rate $\dot{D}$ is given by the normality property of the potential:

$$\dot{D} = -\frac{\partial \Psi^*}{\partial Y} = \begin{cases} 0, & p \leq p_D \\ (\frac{Y}{S})^s \dot{p}, & p > p_D \end{cases} \tag{2.10}$$

where p is the equivalent plastic strain measure, p_D is the damage strain threshold, the critical point at which the damage growth starts.

In the one-dimension case of loading in terms of stress σ, the damage strain energy release rate Y is written as,

$$Y = -\frac{\partial \Psi}{\partial D} = \frac{1}{2}\varepsilon^e : C : \varepsilon^e = \frac{\sigma^2}{2E(1-D)^2} \tag{2.11}$$

which gives,

$$\dot{D} = -\frac{\partial \Psi^*}{\partial Y} = \begin{cases} 0, & p \leq p_D \\ \left(\frac{\sigma^2}{2ES(1-D)^2}\right)^s \dot{p}, & p > p_D \end{cases} \tag{2.12}$$

Generalize to the multiaxial isotropic case, the expression for Y is:

$$\begin{aligned} Y &= \frac{1}{2E(1-D)^2}[(1+\nu)\ \sigma' : \sigma' + 3(1-2\nu)\ {\sigma_H}^2] \\ &= \frac{{\sigma_{eq}}^2}{2E(1-D)^2}[\frac{2}{3}(1+\nu) + 3(1-2\nu)(\frac{\sigma_H}{\sigma_{eq}})^2] \\ &= \frac{{\sigma_{eq}}^2 R_v}{2E(1-D)^2} \end{aligned} \tag{2.13}$$

where σ' is the stress deviator, σ_H is the hydrostatic stress, σ_{eq} is the von Mises equivalent stress for plasticity $\sigma_{eq} = (\frac{3}{2}\sigma' : \sigma')^{1/2}$, ν is Poisson's ratio, R_v is the triaxiality function, and $R_v = \frac{2}{3}(1+\nu) + 3(1-2\nu)(\frac{\sigma_H}{\sigma_{eq}})^2$.

Substituting the expression of Y into Equation (2.12), the damage evolution equation can be written as:

$$\dot{D} = -\frac{\partial \Psi^*}{\partial Y} = \begin{cases} 0, & p \leq p_D \\ \left(\frac{{\sigma_{eq}}^2 R_v}{2ES(1-D)^2}\right)^s \dot{p}, & p > p_D \end{cases} \tag{2.14}$$

Rupture criterion Discussions above indicate that the critical value of fracture D_c should be equal to 1. But experimental observations suggested that materials may become suddenly incapable of carrying the load because of void growth and as a result the failure occurs sooner than $D = 1$.

Measurement of damage Returning to the damage variable definition $D = S_D/S$, evaluation of damage can be determined from the crack surface area. On the other hand, a non-direct measure of damage through characterizing the variation in elastic modulus has been widely adopted because the reduction in stiffness represents the development of microdefects.

Write again the damaged elasticity law (Equation 2.4):

$$\varepsilon_e = \frac{\widetilde{\sigma}}{E} = \frac{\sigma}{(1-D)E}$$

Take $\widetilde{E}$ as the elastic modulus of the damaged material,

$$\widetilde{E} = (1-D)E \tag{2.15}$$

Thus, careful measurement of elastic modulus E (most accurate during unloading) allows us to evaluate the damage state and derive corresponding damage parameters through the following equation:

$$D = 1 - \frac{\widetilde{E}}{E} \tag{2.16}$$

Application of damage model Lemaitre's damage model has fostered wide applications in fields such as metal forming. However, there are only a few instances in the literature where the damage model has been incorporated in structural analysis. For instance, several researchers have successfully incorporated Lemaitre's damage models to track the evolution of damage from onset to failure at the element level and structural level in earthquake engineering (Huang, 2009; Li et al., 2012).

In structural fire engineering, by contrast, there have been few studies that have incorporated mechanical damage evolution in steel structures under fire conditions. Given that structural members are expected to undergo excessive deformations at the initiation of progressive collapse, it is unconservative to ignore the mechanical damage evolution induced by plastic strains. Furthermore, there is an urgent need to address the precedent damage level in the context of continuum damage mechanics in blast-damaged structures subjected to fire.

One of the main obstacles is that so far the existing damage models for metal have been limited to ambient temperature or calibrated towards a specific temperature attained in metal forming. The major drawback is that such calibration is on a case-by-case basis and the calibrated damage parameters can not be generalised to all temperatures. Not one simple equation can describe the damage evolution for full temperature increase history.

Well known Johnson-Cook ductile failure model (Johnson and Cook, 1985), which was developed based on test data of several metallic materials subjected to various strain rates and temperatures, has been extensively used in failure analyses of metals under high-rate deformation or melting process. The proposed cumulative damage parameter determines the occurrence of ultimate material failure when a value of 1 is exceeded without progressively reducing the yield strength or elastic modulus. In other words, the effect of evolution of fully coupled mechanical damage and thermal softening is not reflected.

On the other hand, some progress has been made in thermo-mechanical damage modelling approach for concrete by introducing two damage variables, one for mechanical damage component d and the other for thermal damage component g. These two damage mechanisms were considered to act in a cumulative but independent way. A thermo-mechanical interaction damage term D, which summarized both the mechanical and thermal effects, was thus given by:

$$D = 1 - (1 - g)(1 - d) \tag{2.17}$$

Based on this coupling approach, a few authors have proposed thermo-mechanical damage models for concrete exposed to high temperatures. Among them, Stabler and Baker (2000) implemented a coupled thermo-damage constitutive model in analysing coupled thermo-elasticity problems with the evolving equations satisfying the first and second laws of thermodynamics. Nechnech et al. (2002) developed a computational damage model allowing for thermo-mechanical analysis of concrete structures at high temperatures. Transient creep interaction with localized mechanical damage was also considered. Simulation of a fire test on a reinforced concrete slab with the computational damage model showed good agreement of experimental observations. Similarly, Luccioni et al. (2003) presented a thermo-mechanical model by extending a coupled plastic-damage model to account for damage induced by high temperatures. The model was calibrated with experimental data from residual strength tests on concrete specimens, and then applied to assessing the damage of a concrete wall of the Channel Tunnel under fire loading.

Despite this, far too little attention has been paid to addressing material damage and fracture of steel in fire events. There is little published data for steel deterioration accompanying large structural deformation at elevated temperatures apart from the linear descending branch of yield strength between 15% and 20% strain given in the Eurocode model. A search of the literature reveals that the impact of coupled thermo-mechanical damage development on structural steel is understudied. There is a lack of frameworks for addressing the combining effects of mechanical damage and thermal damage on steel behaviour in fire scenarios, especially for structures prone to progressive collapse.

Chapter 3

Coupled thermo-mechanical damage model

3.1 Introduction

The review of the material models in the previous chapter has highlighted the need for sophisticated modelling of steel deterioration under thermo-mechanical loading. This chapter will develop a coupled thermo-mechanical damage model and provide a framework for incorporating damage modelling in structural fire analysis performed with FE software. As continuum damage mechanics has proved to be a versatile tool in predicting damage of ductile material, the proposed damage model chooses an enhanced Lemaitre damage model (Bouchard et al., 2011) as the description of a mechanical damage component and extends it to incorporate thermal damage evolution as well as thermo-mechanical interaction at elevated temperatures. At the macroscopic level, the phenomenological damage growth in steel is represented by damage-coupled constitutive equations.

The proposed damage model provides a new approach to define and evaluate the damage evolution and progressive failure in structural steels under a combination of elevated temperatures and mechanical loads. A numerical implementation procedure is developed to introduce the damage-coupled constitutive equations into structural fire analysis performed with the FE software ABAQUS. The implementation allows the damage mechanism to be treated predominantly locally at material points or component levels, which in turn influences the global structural behaviour and possibly leads to progressive collapse. This framework aims to provide a better means of assessing structural fire resistance in the presence of damage.

3.2 Damage model formulation

This section addresses the formulation of a coupled thermo-mechanical damage model for steel subjected to a combination of elevated temperatures and mechanical loads. A thermo-mechanical scalar damage model is proposed, which is an extension of an enhanced Lemaitre damage model (Bouchard et al., 2011) by taking into account the high-temperature effects. Two damage component variables d and $h(T)$, associated with mechanical damage and thermal damage processes, respectively, are introduced first. The mechanical damage parameter d describes the stiffness degradation caused by the micro-fracturing that develops under loading, while the thermal damage parameter $h(T)$ accounts for the thermally induced degradation of stiffness. Assuming that the two damage mechanisms act in an interactive way, it is therefore possible to define one non-decreasing scalar damage variable D, which is interpreted as the total density of material defects. The damage variable is considered as a non-decreasing parameter defined within the framework of irreversible processes of thermodynamics. In order to describe the interactive development of thermo-mechanical damage, new variables that feature an accelerated damage growth pattern are introduced. This new damage model is able to reproduce the damage development due to simultaneous high temperatures and large strains.

3.2.1 Mechanical damage component

As introduced in Chapter 2, Lemaitre's damage model (Lemaitre, 1985) has been widely used for describing ductile damage of steel, in which the damage rate equation is given by the partial derivative of damage dissipation potential Ψ^*:

$$\dot{d} = -\frac{\partial \Psi^*}{\partial Y} = \begin{cases} 0, & p \leq p_D \\ (\frac{Y}{S})^s \dot{p}, & p > p_D \end{cases} \tag{3.1}$$

where Y is the damage strain energy release rate, S is the damage strength, s is the damage exponent, and $\dot{p}$ is the equivalent plastic strain rate.

It is clear that damage evolution depends on the choice of damage potential. While the form of potential introduced by Lemaitre (1985) has been generally accepted, in some cases it results in difficulties in identifying Lemaitre damage parameters in order to fit experimental data. To tackle this problem, Bouchard et al. (2011) proposed an enhanced Lemaitre's damage model through modifying the damage potential by adding a term of equivalent plastic strain:

$$\dot{d} = -\frac{\partial \Psi^*}{\partial Y} = \begin{cases} 0, & p \leq p_D \\ (\frac{Y}{S})^s \frac{\dot{p}}{p^r}, & p > p_D \end{cases} \tag{3.2}$$

Note that when $r = 0$, Equation (3.2) is identical to Lemaitre's damage model.

A value of 1 has been suggested by Lemaitre and Chaboche (1994) for damage exponent s which gives best results when compared to the cavity growth models of McClintock (1968) as well as Rice and Tracey (1969). Substitute the expression of Y (Equation 3.3)into the damage rate equation (Equation 3.2),

$$Y = \frac{{\sigma_{eq}}^2 R_v}{2E(1-d)^2} \tag{3.3}$$

We obtain

$$\dot{d} = -\frac{\partial \Psi^*}{\partial Y} = \begin{cases} 0, & p \leq p_D \\ \frac{{\sigma_{eq}}^2 R_v}{2ES(1-d)^2} \frac{\dot{p}}{p^r}, & p > p_D \end{cases} \tag{3.4}$$

where R_v is the triaxiality function, $R_v = \frac{2}{3}(1+v) + 3(1-2v)(\frac{\sigma_H}{\sigma_{eq}})^2$, v is Poisson's ratio, σ' is the stress deviator, σ_H is the hydrostatic stress, σ_{eq} is the von Mises equivalent stress for plasticity, and $\sigma_{eq} = (\frac{3}{2}\sigma' : \sigma')^{1/2}$.

The ductile damage only occurs when the equivalent plastic strain p reaches the threshold p_D and the strain hardening has saturated. Referring to the effective stress concept introduced in Chapter 2, it is assumed that the damage-coupled plastic flow occurs in the undamaged material by means of effective quantities. Note that the von Mises yield criterion is expressed as $\sigma_{eq}/(1-d) - \sigma_y - R = 0$, where σ_y is the initial yield stress and R stands for strain hardening. Denote the saturated yield stress as σ_s, we have

$$\sigma_{eq}/(1-d) = \sigma_s = constant$$

The damage accumulation caused by mechanical work, which is taken as the mechanical damage component in this chapter, can be obtained by integration of Equation (3.4). With the simplifying assumption that the triaxiality function R_v is constant during loading process, the mechanical damage component introduced in this thesis is obtained as:

$$d = \begin{cases} 0, & p \leq p_D \\ \frac{{\sigma_s}^2}{2ES} R_v (p - p_D)^{1-r}, & p > p_D \end{cases} \tag{3.5}$$

In the special case of uniaxial loading where $R_v = 1$, the mechanical damage component is written as:

$$d = \begin{cases} 0, & p \leq p_D \\ \frac{{\sigma_s}^2}{2ES} (p - p_D)^{1-r}, & p > p_D \end{cases} \tag{3.6}$$

3.2.2 Thermal damage component

On the material level, high temperature induces loss of material stiffness and strength. The thermal damage component of steel is described in terms of experimentally determined Young's modulus of mechanically undamaged steel at high temperatures, given the fact that Young's modulus is most sensitive to elevated temperatures. Assuming the thermal damage component is proportional to the relation between reduction of the elastic modulus and the initial one, one can write:

$$h(T) = 1 - \frac{E_0(T)}{E_0} \tag{3.7}$$

The thermal damage variable $h(T)$ can be experimentally determined through known data of tensile tests conducted on specimens that are heated at different temperatures. Often measured at very low strains and defined as the initial slope of the stress-strain curve, temperature-dependent elastic modulus $E_0(T)$ reported in previous tensile tests can be considered as thermal degradation in mechanically undamaged steel. Therefore, thermal damage variable $h(T)$ can be plotted as a function of temperature based on experimentally determined reduction factors (measured at early unloading slopes at very low strains) as shown in Figure 3.1. It can be seen from the graph that the thermal damage values derived from different literature sources show some variations but have a common characteristic of exponential growth. The variations can be attributed to a number of factors, including the differences in steel grades, test regimes and heating methods. Despite these differences, an exponential function of temperature is considered to be capable of capturing the key aspects of thermal damage patterns.

Therefore, the thermal damage evolution equation developed in this study is written as an exponential form of the maximum attained temperature governing the thermally activated damage process and the shape of the softening curve:

$$h(T) = ae^{\frac{b}{T+c}} \tag{3.8}$$

where a, b and c are material inputs which can be identified by plotting experimentally determined degradation of Young's modulus versus temperatures.

In line with the concept of the irreversibility of damage, the thermal damage growth rate $h(\dot{T})$ is controlled by the following condition:

$$h(\dot{T}) = 0, \;\; if\ \dot{T} \leq 0; \;\; h(\dot{T}) > 0, \;\; if\ \dot{T} > 0 \tag{3.9}$$

The thermal damage model proposed here describes phenomenological thermally-induced degradation in a similar manner to Arrhenius equation $k = Ae^{\frac{-E_a}{RT}}$, in which T is the

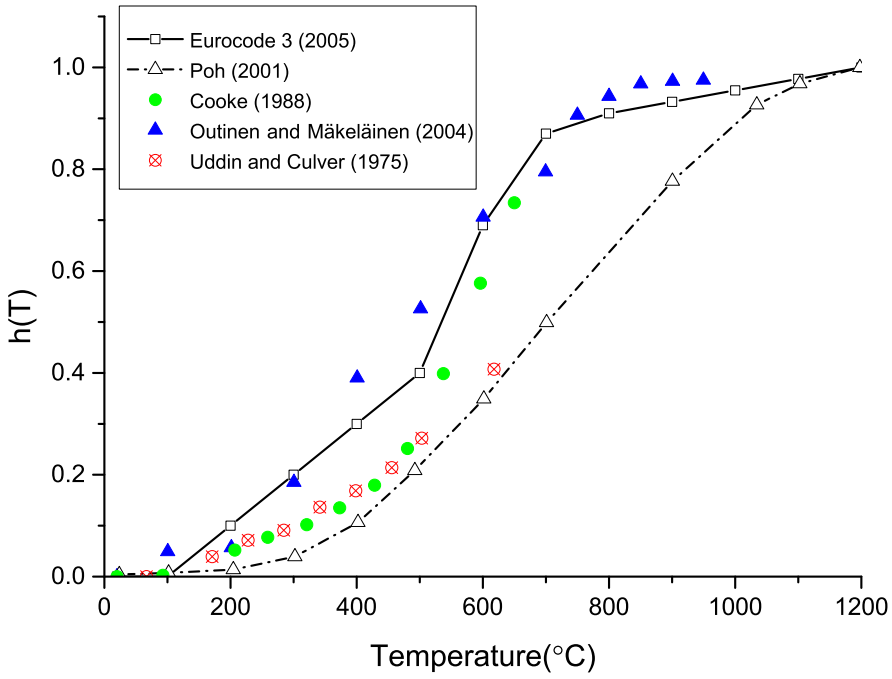

Fig. 3.1 Thermal damage variable $h(T)$ determined from literature sources

absolute temperature, A, E_a and R are constants. Arrhenius equation (Arrhenius, 1889) is an empirical relationship which can be used to model the effect of temperature on vacancy diffusion and many other thermally-induced processes/reactions. By analogy with Arrhenius equation one may postulate that the proposed thermal damage model characterizes a similar temperature-driven degradation process governed by the exponential law.

In order to confirm the validity of the proposed model, the thermal damage model developed in this study is fitted to experimental data presented in Figure 3.1. The parameters a, b, and c are determined as best-fit values with the method of least squares and the damage evolution predicted by the thermal damage model is plotted in Figure 3.2. It can be seen from all five subsets of Figure 3.2 that the proposed model with best-fit parameters is capable of simulating the damage development which is in good agreement with steel degradation at various temperature levels. The good correlation confirms that the exponential form of thermal damage description allows an accurate prediction of the degradation in elastic modulus at elevated temperatures with the ease in fitting to the data. The proposed thermal damage formulation by means of an exponential equation is therefore a versatile tool to predict the thermal damage development of steel under fire loading.

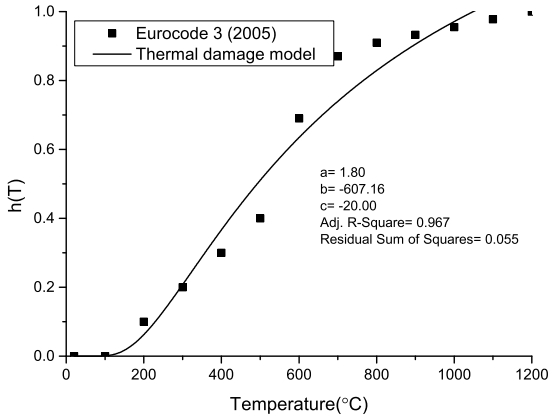

(a) Eurocode3 (2005)

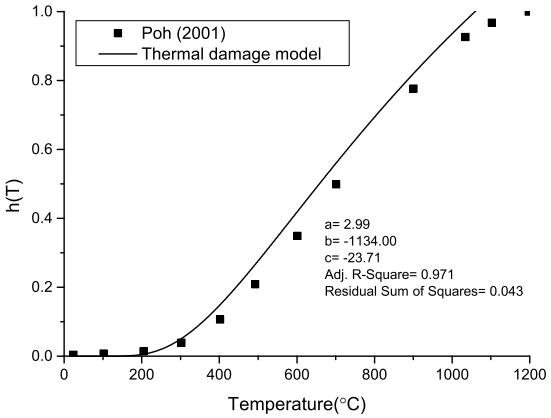

(b) Poh (2001)

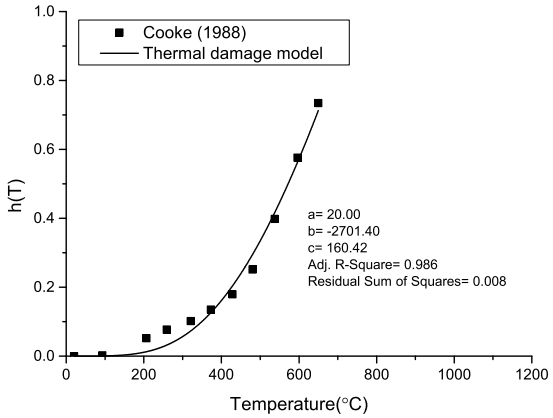

(c) Cooke (1988)

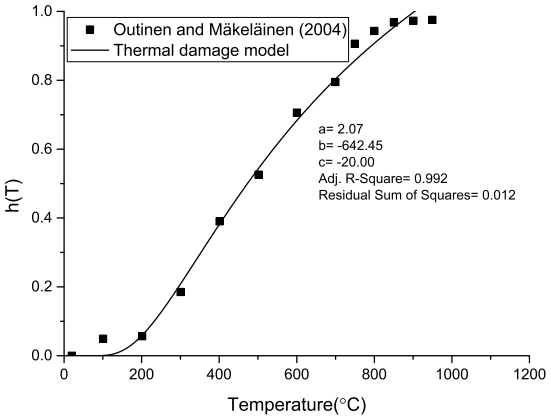

(d) Outinen and Mäkeläinen (2004)

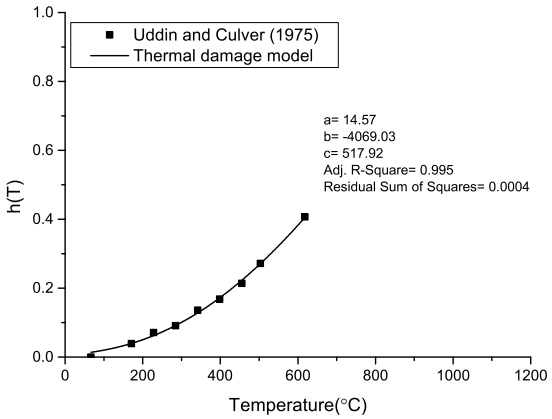

(e) Uddin and Culver (1975)

Fig. 3.2 Plots of thermal damage model with parameters best fit to experimental results.

3.2.3 Coupling between mechanical and thermal damage

The previous subsections have dealt with individual mechanical damage component and thermal damage component, respectively. While mechanical damage is determined by the breaking and re-establishing of atomic bonds (Skrzypek and Ganczarski, 2013), thermal degradation can be attributed to decreased bond strength as a result of the nucleus of the iron atoms in steel moving apart at elevated temperatures (Kodur et al., 2010). In both cases, the damage process is the result of several different modes of microstructural kinetics, such as movement of dislocations, diffusion of vacancy, microcracking propagation, etc. It is generally accepted that atomic bond rupture is a thermally activated process, suggesting that a rise in temperature would provoke an accelerated damage processes (Cottrell, 1981). For a given material internal state, it is not known what percentage of damage is caused by mechanical or thermal action and what is their mutual effect. By assuming the distribution of the interatomic bonds, dislocations and vacancies are smeared out and homogenized, a total damage variable can be defined. The overall damage is considered as the reduction of the load-resisting elementary area as the number of bonds decreases, which is interpreted as the total density of material defects. In choosing an appropriate form for representing the damage, the proposed coupling model should be a macroscopically homogeneous, phenomenological damage model which reflects the irreversible changes in the material internal state induced by an external supply of work and heat.

Therefore, a unified damage function is proposed in this study which meets the requirements and couples both the mechanical and thermal damage processes. It should be noted that the proposed coupled damage formulation is chosen from a number of alternative forms of coupling functions. The coupling functions have been derived mainly on the basis of the premise that proper modelling of coupled damage growth should not only represent the damage state governed independently by mechanical damage process or thermal damage process, but also include the damage development brought about by the interaction of mutual mechanical and thermal effects. The quantification of accumulative damage can thus be described by combining the functions of Equation (3.6) and Equation (3.8), and including a set of coefficients as the controlling parameters to account for the overall material deterioration. The number of parameters necessary to capture the whole behaviour should be minimized for simplicity while maintaining the accuracy in representing the data. The type of coupled damage growth is highly dependent on the choice of the added terms of deformation/temperature dependency. Depending on placing the introduced coefficients on different power position or multiplier position, the damage increase will be higher or lower with respect to deformation or temperature. By the use of appropriate damage onset criteria, the specific forms of the postulated functions have a common characteristic of being reducible to damage development due to the plastic

deformation, that due to thermal softening and that due to combined mechanical-thermal loading. In some cases it is not possible to match experimental results using certain forms of formulations, and the function that has the best performance in predicting the coupled thermo-mechanical damage development is chosen. A review of the performances of mathematical functions that have been developed in this study is provided in Appendix A.

The coupled thermo-mechanical damage model proposed in this thesis is:

$$D = \frac{{\sigma_s}^2}{2ES}(p-p_D)^{(1-r-T_1^m)}H(p-p_D) + ae^{\frac{b}{T+c}}e^{k(p-p_D)H(p-p_D)} \tag{3.10}$$

$H(p-p_D)$ is Heaviside function, controlling the onset of mechanical damage,

$$H(p-p_D) = \begin{cases} 0, & p \leq p_D \\ 1, & p > p_D \end{cases}$$

where σ_s is the saturated yield stress at ambient temperature, S is material constant, p is plastic strain, p_D is the damage threshold in strain measure, m and k are additional variables introduced to account for thermo-mechanical interaction, T_1 is a non-dimensional temperature which enables the maximum attained temperature T of a material to be described as a fraction of its melt point:

$$T_1 = \frac{T - T_{room}}{T_{mp} - T_{room}}$$

T_{room} is room temperature 20°C and T_{mp} is the melting temperature of structural steel, normally taken as 1500°C.

Key factors influencing the initiation of damage process are the temperature T and plastic strain p. The proposed coupling model can be reduced to mechanical damage equation at room temperature, or thermal degradation equation when the plastic strain is below the damage threshold. This means that the coupled thermo-mechanical damage model developed in this study can be broken down into the strain and temperature spaces where mechanical or thermal damage are special cases with governing equations defined for each regime as below:

$$D = \begin{cases} 0 & p \leq p_D, T \leq 20°C \\ \frac{{\sigma_s}^2}{2ES}(p-p_D)^{(1-r)} & p > p_D, T \leq 20°C \\ ae^{\frac{b}{T+c}} & p \leq p_D, T > 20°C \\ \frac{{\sigma_s}^2}{2ES}(p-p_D)^{(1-r-T_1^m)} + ae^{\frac{b}{T+c}}e^{k(p-p_D)} & p > p_D, T > 20°C \end{cases} \tag{3.11}$$

The proposed damage model has the valuable feature of incorporating mutual mechanical and thermal effects by introducing coefficients that account for the accelerated growth of

damage. Aspects of thermo-mechanical damage interaction are described by including temperature dependency in the power function of plastic strain which characterizes the influence of temperature on mechanical damage development, and by adding exponential dependency of plastic strain in the thermal degradation term which produces the marked acceleration of thermal damage growth at large plastic strains. The coupling effect remains inactivated until the damage threshold is exceeded in both plastic strain measure and temperature measure. These parameters allow a shift from descriptions of mechanical damage at ambient temperatures or thermal damage at small strains to coupled thermo-mechanical damage under combined loading as one can easily see in structural states in abnormal events. In this way, the interaction between mechanical and thermal damage processes is incorporated into modelling of material deterioration in a smoothed manner without the complexity that normally characterises a micromechanics-based theory. The evolution of damage is non-decreasing since the reduction of effective resisting area of section will continuously increase until material failure. This gives a realistic description of the material response by limiting the scope of the present study to the heating phase. If not experimentally measured, fracture is generally considered to occur when the accumulated damage variable reaches a value of unity.

As discussed above, the proposed damage model in this study is a convenient, phenomenological formulation which features mutual strain and temperature effects on microcracks growth with few parameters. This characteristics makes it advantageous in the identification of model parameters and easy to introduce in structural calculation. In the next subsection, the effectiveness of the proposed model is ascertained by describing material degradation behaviour exhibited in published experimental studies.

3.2.4 Comparison with experimental results

In order to evaluate the performance of the proposed damage model, it is important to compare the predicted damage evolution with experimental data. In this subsection, the experimental identification procedure is discussed and the damage parameter set for the steel under investigation is identified.

To determine the global deterioration produced by simultaneous high temperatures and large strains, damage measurements need to be performed by tracking the elastic slope changes through loading-unloading cycles at increasing levels of strains and temperatures. A search of the published data shows that Pauli et al. (2012) has performed high-temperature tensile coupon tests with loading-unloading cycles on steel at high deformation levels. At the Institute of Structural Engineering at ETH Zürich, Pauli et al. (2012) carried out steady-state tensile material tests on coupons taken from column sections SHS 160×160×5, RHS 120×60×3.6 and HEA 100 at temperatures of 20°C,

400°C, 550°C, and 700°C. The heating rate was $10K/min$ during the first heating stage and then decreased to $2K/min$ until reaching the target temperature. After that, the specimens were loaded in uniaxial tension with a strain rate of $0.1\%/min$ while the temperature was held constant. The temperature-dependent elastic modulus E was determined at small strains as well as at the reloading branches at engineering strain levels of 2%, 5% and 10%, while the initial elastic modulus E_0 was taken as the slope of initial elastic branch at ambient temperature. The changes in measured elastic modulus allow for evaluating the damage evolution which reflects the global deterioration induced by both temperature rise and increasing levels of plastic deformation. The damage variable D can be computed for each unloading-reloading cycle as:

$$D = 1 - \frac{E}{E_0}$$

A summary of the tensile coupon test results (Pauli et al., 2012) and derived damage values is given in Table 3.1. It is clear that the coupled effects of mechanical damage and thermal damage in test series M7, M8 and M9 are evident. At each temperature level the degradation in elastic modulus becomes more pronounced as the strain increases, which justifies the marked acceleration of damage growth brought about by thermo-mechanical damage interaction as featured in the proposed damage model. Note that there is some deviation in the reduction of elastic modulus observed in test series M7, M8 and M9 within a reasonable margin of error. This may be explained by the slight variations in material properties of different batches of steel and the inconsistency existing in test conditions and measurements in each test.

The proposed damage model is fitted to the experimentally determined damage values in Table 3.1, from which the following material constants are deduced:

- the damage threshold strain. The ductile damage growth starts only at a critical value of accumulative plastic strain (Lemaitre, 1985). Due to the difficulty in determining the starting point at which the mechanical damage is activated, the damage threshold strain usually need to be extrapolated. Here the damage threshold in a plastic strain measure of 0.004 is found to be very close to the elastic limit, indicating that the initiation of mechanical damage occurs soon after yielding.
- the exponent $1 - r$ in mechanical damage term is dependent on the type of the nonlinear dependency of the plastic strain observed.
- the damage strength S is determined by plotting the damage D versus the accumulated plastic strain at room temperature, $S = ({\sigma_s}^2/2E)(\delta p/\delta D)^{(1-r)}$, where σ_s is taken as the effective yield stress at ambient temperature.

Table 3.1 Temperature-dependent elastic modulus at various strain levels determined from tensile coupon test conducted by Pauli et al. (2012)

Test series	Coupon	Temperature(°C)	True strain	$E_0(N/mm^2)$	$E(N/mm^2)$	Damage
M7 (SHS 160×160×5)						
	M7-T02	20	0.000	1.88E+11	1.88E+11	0.000
	M7-T02	20	0.009	1.88E+11	1.66E+11	0.117
	M7-T02	20	0.021	1.88E+11	1.51E+11	0.197
	M7-T02	20	0.041	1.88E+11	1.36E+11	0.277
	M7-T07	400	0.000	2.18E+11	1.77E+11	0.188
	M7-T07	400	0.009	2.18E+11	1.75E+11	0.197
	M7-T07	400	0.021	2.18E+11	1.62E+11	0.257
	M7-T07	400	0.041	2.18E+11	1.47E+11	0.326
	M7-T11	550	0.009	2.17E+11	1.23E+11	0.433
	M7-T11	550	0.021	2.17E+11	1.12E+11	0.484
	M7-T11	550	0.041	2.17E+11	1.00E+11	0.539
	M7-T05	700	0.009	2.24E+11	5.87E+10	0.738
	M7-T05	700	0.021	2.24E+11	6.09E+10	0.728
	M7-T05	700	0.041	2.24E+11	5.13E+10	0.771
M8 (RHS 120×60×3.6)						
	M8-T02	20	0.000	2.11E+11	2.11E+11	0.000
	M8-T02	20	0.009	2.11E+11	1.74E+11	0.175
	M8-T02	20	0.021	2.11E+11	1.59E+11	0.246
	M8-T02	20	0.041	2.11E+11	1.42E+11	0.327
	M8-T05	400	0.009	2.06E+11	1.68E+11	0.184
	M8-T05	400	0.021	2.06E+11	1.56E+11	0.243
	M8-T05	400	0.041	2.06E+11	1.41E+11	0.316
	M8-T10	550	0.009	2.11E+11	1.16E+11	0.450
	M8-T10	550	0.021	2.11E+11	1.08E+11	0.488
	M8-T10	550	0.041	2.11E+11	9.70E+10	0.540
	M8-T11	700	0.009	2.00E+11	8.17E+10	0.592
	M8-T11	700	0.021	2.00E+11	7.29E+10	0.636
	M8-T11	700	0.041	2.00E+11	6.42E+10	0.679
M9 (HEA 100)						
	M9-T03	20	0.000	2.02E+11	2.02E+11	0.000
	M9-T03	20	0.009	2.02E+11	1.83E+11	0.094
	M9-T03	20	0.021	2.02E+11	1.65E+11	0.183
	M9-T03	20	0.041	2.02E+11	1.46E+11	0.277
	M9-T08	400	0.009	2.14E+11	1.71E+11	0.201
	M9-T08	400	0.021	2.14E+11	1.60E+11	0.252
	M9-T08	400	0.041	2.14E+11	1.46E+11	0.318
	M9-T15	550	0.009	2.10E+11	1.21E+11	0.424
	M9-T15	550	0.021	2.10E+11	1.14E+11	0.457
	M9-T15	550	0.041	2.10E+11	1.02E+11	0.514
	M9-T20	700	0.009	2.14E+11	9.42E+10	0.560
	M9-T20	700	0.021	2.14E+11	7.00E+10	0.673
	M9-T20	700	0.041	2.14E+11	5.66E+10	0.736

- the coefficients of thermal damage term a, b, and c are determined by plotting thermal degradation of Young's modulus versus temperatures at small strains.
- the coupling parameters m and k are calibrated last using the method of least squares, with the intention of matching the overall damage evolution with the experimental dataset.

The best fit of parameters for each test series are given in Table 3.2. The calibrated damage coefficients show slight differences across three test series due to the scatter of test data. A comparison between the damage evolution predicted by the proposed damage model and experimental results is presented in Figure 3.3. It can be seen from the graph that the damage model closely matches the experimental dataset for each case. Some deviations from experimental values have been expected considering the simplicity of the model and the limited data points for calibration. The good correlation suggests that it is possible to identify the whole damage parameter set even with limited data available. The obtained material parameters will be considered as basic data in the damage coupled numerical simulations performed afterwards.

Table 3.2 Damage parameters best fit to tensile coupon test results

Test series	Best-fit damage parameters							
	S	P_d	a	b	c	r	m	k
M7	4.98E+05	0.004	4.375	-1213.75	-20	0.695	1.864	0.064
M8	5.66E+05	0.004	2.334	-915.7	-20	0.786	4.99	0.125
M9	4.75E+05	0.004	1.952	-837.323	-20	0.613	3.01	0.248

The proposed damage model in this study can be generalised to the multiaxial isotropic case based on the assumption that damage is uniformly distributed in the volume,

$$D = \frac{{\sigma_s}^2}{2ES}(p-p_D)^{(1-r-T_1^m)}H(p-p_D) + ae^{\frac{b}{T+c}}e^{k(p-p_D)H(p-p_D)} \tag{3.12}$$

where $H(p-p_D)$ is Heaviside function which controls the onset of mechanical damage, σ_s is saturated yield stress, S, m and k are material constants, p is the equivalent plastic strain, p_D is the damage threshold in strain measure, T_1 is a non-dimensional temperature.

For cases in which material triaxiality differs from that of tensile tests, calibration against experimental data at different levels of triaxiality are generally required. However, there does not exist sufficient data to enable calibration of such triaxiality-dependent models at elevated temperatures. As a result, it is not possible to inlucde the effects of triaxial stress fields on damage growth in the damage model with confidence. This simplification can be justified given the fact that severe thermal degradation will be dominant at high temperatures and thus, the effects of triaxiality can be assumed insignificant. The consideration of traxiality dependency will likely result in an over-complicated model in

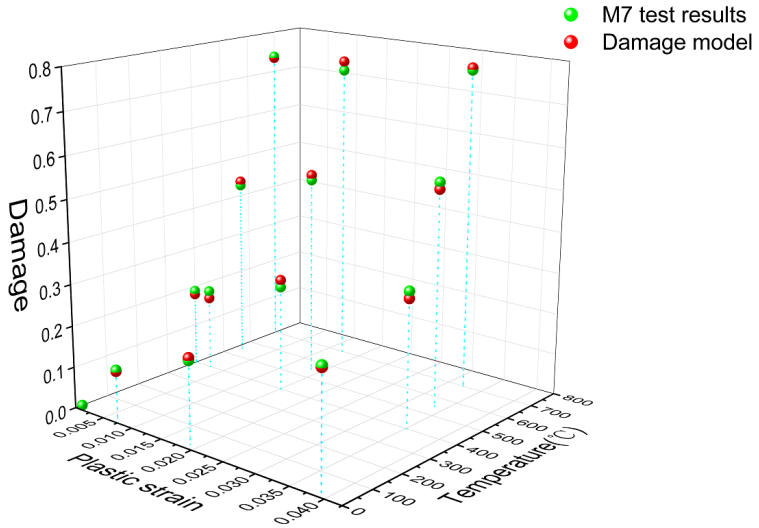

(a) M7

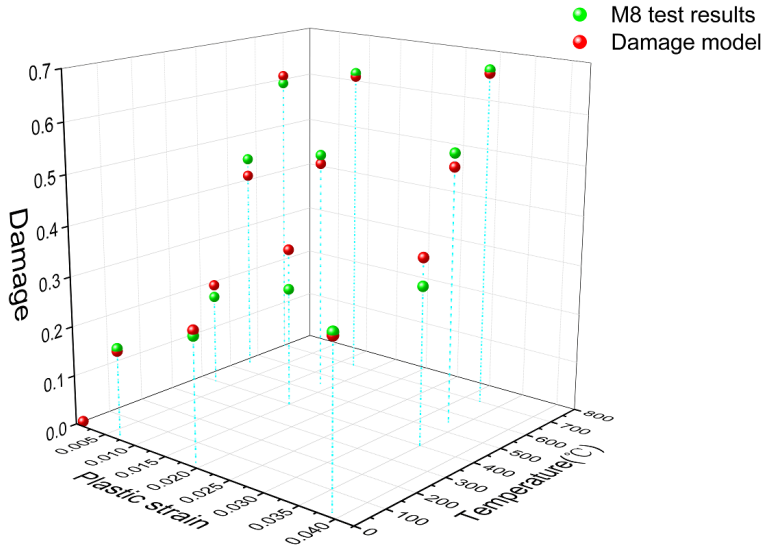

(b) M8

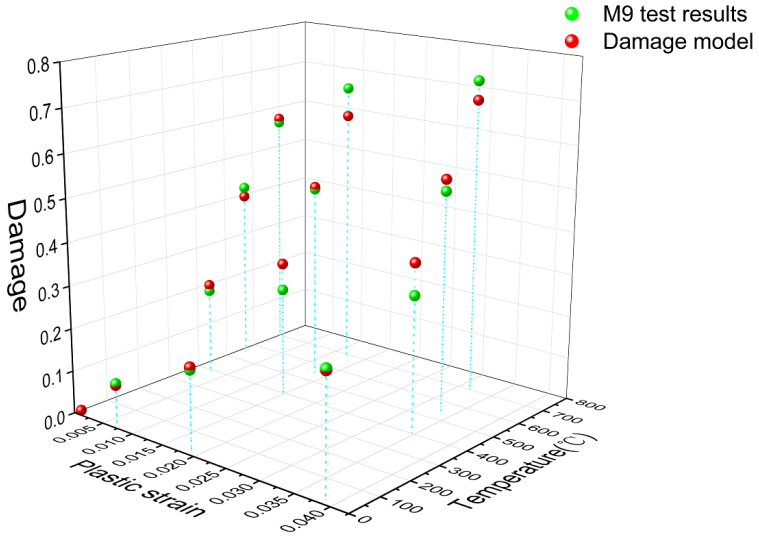

(c) M9

Fig. 3.3 Comparison between the damage evolution predicted by the proposed damage model with best-fit parameters and test results

terms of parameters identification and computation with little or no improvement in the predicative capability of the model. Despite this limitation, the use of a coupling model adapted from classic Lemaitre's ductile damage equation and taking into account high-temperature thermal degradation is a phenomenological approach where the underlying mechanisms that govern the damage processes have been retained. Therefore, the proposed damage model is considered to exhibit conservative behaviour outside the range of the data it is based on and is sufficiently accurate for representing the coupled thermo-mechanical damage growth in steel.

To summarize, a coupled thermo-mechanical damage model is proposed in this section. This newly developed model is able to reproduce the damage behaviour of steel induced by simultaneous mechanical loads and fire exposure. Such a damage modelling approach is needed to enable evaluation of steel deterioration behaviour and its impacts on performance of steel components and structures. Coupled thermo-mechanical analysis of steel structures can be performed with the damage model incorporated in a FE software. The procedure of numerical implementation will be introduced in the next section.

3.3 Implementation of the damage model

This section introduces the numerical aspects and the implementation of the proposed damage model in FE software ABAQUS. Owing to the fact that the implicit scheme is prone to convergence problems upon the occurrence of local failures, ABAQUS/Explicit solver is chosen for the resolution of the global equilibrium equations. To enable simulation of successive failures of elements and the subsequent redistribution of loads, the proposed damage model is incorporated into user subroutine VUMAT which defines user's own, complex constitutive relationships of materials that are not included in the material library of ABAQUS/Explicit.

As previously stated, damage development interferes with the mechanical constitutive behaviour of material. This requires the yielding and damage equations to be integrated simultaneously. Components of the damage-coupled governing constitutive equations, including yield criterion, isotropic hardening behaviour, and damage evolution, are presented in this section. The constitutive equations are integrated by incrementally updating solution-dependent state variables such as stress, strain and the damage indicator at each Gauss point using return mapping algorithms. The computational model has an "element-kill" option, that is when the damage indicator reaches its critical value, the element is considered to have failed. Corresponding discretization and update procedure of the computational model is explained in detail in this section.

3.3.1 Constitutive equations

To derive the governing equations of coupled thermo-elasticity and thermo-plasticity in the presence of damage, we write the Helmholtz free energy density function Ψ in the sum of elastic part Ψ^E and inelastic part Ψ^{IN} in the fictitious undamaged configuration.

$$\Psi\left(\varepsilon^e, R, T, D\right) = \Psi^E\left(\varepsilon^e, D, T\right) + \Psi^{IN}\left(R, T\right) \tag{3.13}$$

where ε^e is the elastic strain tensor, R and D are the scalar internal variables associated with isotropic hardening and isotropic damage, T is a measure of temperature. Note that the effect of kinematic hardening is omitted here because it is considered to have little influence on the plastic flow of steel in structural analysis under blast and fire loads (de Souza Neto et al., 2011). The plasticity model is therefore characterised with isotropic hardening only and a kinematic hardening parameter can be added if necessary.

The expression for the thermo-elastic free energy density Ψ^E proposed by Stabler and Baker (2000) for high temperature increments is used here:

$$\Psi^E\left(\varepsilon^e, D\right) = \frac{1}{2}\varepsilon^e : (1-D)C : \varepsilon^e - (T-T_0)\beta : \varepsilon^e + c_v[T - T_0 - Tln(\frac{T}{T_0})] \tag{3.14}$$

where C is the elastic modulus tensor, ε^e is the elastic strain tensor, T_0 is the initial temperature, T is a measure of temperature, β is the thermo-elastic coupling tensor that represents stress induced by thermal expansion, and c_v is the specific heat.

The constitutive stress-strain equation is obtained from the free energy density as:

$$\sigma = \frac{\partial \Psi}{\partial \varepsilon^e} = (1-D)\, C : \varepsilon^e - (T-T_0)\beta \tag{3.15}$$

The plastic flow in the presence of damage is formulated in the effective stress space. In the von Mises yield criterion, the homogenized von Mises equivalent stress σ_{eq} is replaced by the effective equivalent stress $\widetilde{\sigma}_{eq} = \frac{\sigma_{eq}}{1-D}$. The yield criterion is given as a function of the stress, damage and temperature,

$$f^p(\sigma, R, D, T) = \frac{\sigma_{eq}}{1-D} - \sigma_y(R,T) = 0 \tag{3.16}$$

where $\sigma_y(R,T)$ defines the yield surface evolution under thermal and mechanical loading, σ_{eq} is the von Mises equivalent stress for plasticity, $\sigma_{eq} = \left(\frac{3}{2}\sigma' : \sigma'\right)^{1/2}$, σ' is the stress deviator.

As discussed in Chapter 2, the decrease of yield strength in steel is evident with temperature rise. The reduction of effective yield strength given in Eurocode 3 (2005) has been generally accepted as a fairly good representation of the contraction of yield surface with

increasing temperature. However, it should be noted that if the temperature-dependent effective yield strength (Eurocode 3, 2005) is taken as $\sigma_y(R,T)$ here in the fictitious undamaged configuration, the yield surface inevitably undergoes a further isotropic contraction induced by elevated temperature owing to the fact that the total damage variable D has already taken into account the effects of thermal degradation. Undoubtedly this will lead to an erroneous and over-conservative prediction.

Therefore, a modified yield surface is adjusted by precluding the effects of thermal degradation $h(T)$ brought about by the total damage D while keeping the reduction factors of yield strength $k_{y,T}$ as specified in Eurocode 3 (2005):

$$\sigma_y(R,T) = \frac{\sigma_y(R)}{1-h(T)} k_{y,T} \tag{3.17}$$

where $\sigma_y(R)$ is the yield strength measured in a tensile test at ambient temperature, $h(T)$ is the thermal damage component, and $k_{y,T}$ is the temperature-dependent reduction factor of effective yield strength specified in Eurocode 3 (2005) as shown in Figure 3.4. The characterization of plastic response is hence formulated by extrapolating the yield surface in three-dimensional principle stress space, with the effects of damage reflected in the accompanying degradation in stiffness and yield strength.

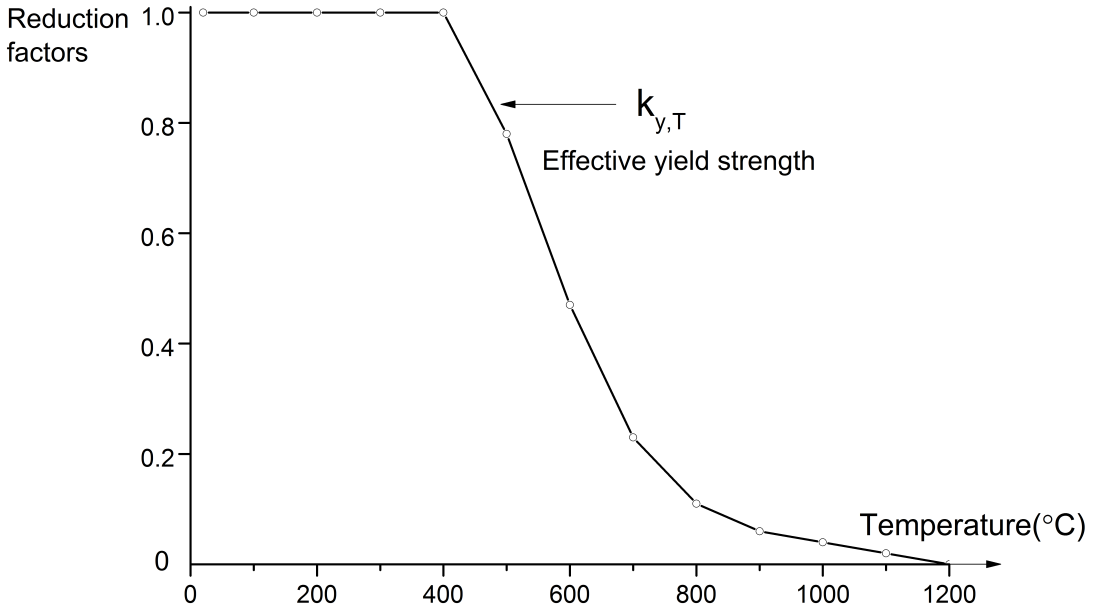

Fig. 3.4 Reduction factors for effective yield strength of structural steel at elevated temperatures (EN 1993-1-2, 2005)

3.3.2 Integration algorithm

The constitutive equations presented above are discretized within the framework of FE method based on the numerical approach presented by Benallal et al. (1988) and de Souza Neto et al. (2011). A stable radial return algorithm is used for the integration of damage evolution equation coupled with isotropic hardening plasticity model. The calculations of the stresses and strains are performed by an elastic predictor assuming the first increment to be purely elastic and a plastic corrector to return the stress state to the yield surface which ensures the plastic criterion and kinetic laws are satisfied.

Implementation of the user defined material law requires transforming the constitutive equations to incremental equations within the architecture of subroutine VUMAT. During the solution process, ABAQUS performs an incremental loading and passes the strain increment to the VUMAT subroutine which is stored in "old" arrays. The subroutine performs calculations of new stress components and state variables such as the equivalent plastic strain and the damage indicator. The updated variables are stored in "new" arrays at the end of the current increment, and provided to the beginning of the next increment designated as "old" arrays. The corresponding integration algorithm is explained in detail in the following pages.

The radial return algorithm consists of elastic predictor phase and plastic corrector phase. In the first phase, the total strain increment is assumed to be elastic. The elastic trial stress σ_{new}^{trial} is given by,

$$\sigma_{new}^{trial} = \sigma_{old} + \lambda(1-D_{old})trace(\Delta\varepsilon)I + 2G(1-D_{old})\Delta\varepsilon^{el} \tag{3.18}$$

where σ_{new}^{trial} is the trial stress tensor at the end of the increment, σ_{old} is the stress tensor at the beginning of the increment, $\Delta\varepsilon^{el}$ is the elastic strain increment, $\Delta\varepsilon^{el} = \Delta\varepsilon - \Delta\varepsilon_T$, $\Delta\varepsilon_T$ is the thermal strain, $trace(\Delta\varepsilon)$ is the volume strain increment, I is the identity matrix, λ and G are the Lames constants, and D_{old} is the damage variable calculated at the beginning of the increment,

$$D_{old} = \frac{{\sigma_s}^2}{2ES}(p_{old}-p_D)^{(1-r-T_1^m)}H(p_{old}-p_D) + ae^{\frac{b}{T_{old}+c}}e^{k(p_{old}-p_D)H(p_{old}-p_D)} \tag{3.19}$$

$$T_1 = \frac{T_{old}-T_{room}}{T_{mp}-T_{room}} \tag{3.20}$$

where σ_s is the saturated yield stress measured at ambient temperature, p_{old} is the equivalent plastic strain at the beginning of the increment, T_{old} is the maximum attained temperature passed into user subroutine by ABAQUS at the beginning of the increment and kept constant during the current increment.

The elastic predictor, the von Mises equivalent stress based on purely elastic behaviour, is calculated as,

$$q_{new}^{trial} = \sqrt{\frac{3}{2} s_{new}^{trial} : s_{new}^{trial}} \tag{3.21}$$

where s_{new}^{trial} is the deviatoric trial stress, $s_{new}^{trial} = \sigma_{new}^{trial} - \sigma_m^{trial}$, σ_m^{trial} is the mean trial stress.

Call the yield function

$$f^p(\sigma, R, D, T) = \frac{q_{new}^{trial}}{1 - D_{old}} - \sigma_y(R_{old}, T_{old}) \leq 0 \tag{3.22}$$

If the elastic predictor satisfies the yield criterion, the new stress is set equal to the trial stress. Otherwise, the material point goes beyond the yield surface and the plastic correction is required in which the stress state is returned to the yield surface along the direction of plastic flow. This process is called return mapping, given by:

$$\sigma_{new} = \sigma_{new}^{trial} - 2G(1 - D_{new})\Delta\varepsilon_p \tag{3.23}$$

where $\Delta\varepsilon_p$ is the plastic strain increment.

The evolution of the plastic strain is governed by the plastic flow rule (also referred to as the normality rule),

$$\Delta\varepsilon_p = \Delta\gamma N_{new} \tag{3.24}$$

where $\Delta\gamma$ is the plastic multiplier, N_{new} is the normal vector to the yield surface at the end of the increment, given by

$$N_{new} = \frac{3}{2} \frac{s_{new}}{(1 - D_{new}) q_{new}} \tag{3.25}$$

where s_{new} is the deviatoric stress, q_{new} is the von Mises equivalent stress.

The equivalent plastic strain increment is calculated by,

$$\Delta p = \sqrt{\frac{2}{3}\Delta\varepsilon_p : \Delta\varepsilon_p} = \sqrt{\frac{2}{3}\left(\frac{3}{2}\frac{\Delta\gamma s_{new}}{(1 - D_{new}) q_{new}}\right) : \left(\frac{3}{2}\frac{\Delta\gamma s_{new}}{(1 - D_{new}) q_{new}}\right)} = \frac{\Delta\gamma}{1 - D_{new}} \tag{3.26}$$

The plastic multiplier can be obtained by ensuring that the yield condition must be satisfied at the end of the increment,

$$\widetilde{q}_{new}^{trial} = \frac{q_{new}}{1 - D_{new}} + \frac{3\Delta\gamma G}{1 - D_{new}} \tag{3.27}$$

where $\widetilde{q}_{new}^{trial}$ is the effective elastic predictor.

Rearranging the above equation gives the plastic multiplier,

$$\Delta\gamma = \frac{(1-D_{new})\tilde{q}_{new}^{trial} - q_{new}}{3G} \tag{3.28}$$

The hardening state variable is altered by plastic deformation, indicating that the radius of the yield surface increases with equivalent plastic strain,

$$R_{new} = R_{old} + \Delta\gamma \tag{3.29}$$

The elastic strain at the end of the increment is obtained as,

$$\varepsilon_{new}^{e} = \varepsilon_{new}^{trial} - \Delta\gamma N_{new} - \varepsilon_T \tag{3.30}$$

where ε_T is thermal strain, $\varepsilon_T = (T_{old} - T_0)\alpha$, α is thermal expansion coefficient.

The stress tensor is brought back onto the yield surface at the end of the increment using radial return method,

$$\sigma_{new} = \sigma_{new}^{trial} - 2G(1-D_{new})\Delta\gamma N_{new} \tag{3.31}$$

The equivalent plastic strain at the end of the increment is given as,

$$p_{new} = p_{old} + \Delta p \tag{3.32}$$

The updated damage variable can now be written as,

$$D_{new} = \frac{{\sigma_s}^2}{2ES}(p_{new} - p_D)^{(1-r-T_1^m)} H(p_{new} - p_D) + ae^{\frac{b}{T_{old}+c}} e^{k(p_{new}-p_D)H(p_{new}-p_D)} \tag{3.33}$$

When the damage indicator D_{new} reaches the critical value D_{cr} (D_{cr} is usually taken as 1 if not experimentally measured), the material point is deleted from the analysis model by setting the stress components to zero for the rest of the analysis.

To summarize, a damage-plasticity model in terms of effective stresses coupled with isotropic damage is implemented in user subroutine VUMAT of ABAQUS/Explicit. The yielding and damage equations are integrated simultaneously using an elastic predictor, radial return algorithm, as summarised in Box 3.1. It should be noted that the numerical integration algorithm is applicable for solid elements in 3D principal stress space and can easily be reduced to 1D beam element and 2D plane stress shell element.

Box 3.1 Integration algorithm for multiaxial isotropic hardening plasticity coupled with thermo-mechanical damage model (modified from de Souza Neto et al. (2011))

1. Elastic predictor.

Given strain increment and state variables at t_n, calculate the elastic trial stress

$$\varepsilon_{n+1}^{e\ trial} = \varepsilon_n^e + \Delta\varepsilon$$

$$D_n = \frac{{\sigma_s}^2}{2ES}(p_n - p_D)^{(1-r-T_1^m)} H(p_n - p_D) + ae^{\frac{b}{T_n+c}} e^{k(p_n-p_D)H(p_n-p_D)}$$

$$\sigma_{n+1}^{trial} = (1-D_n)C :\ \varepsilon_{n+1}^{e\ trial}$$

$$q_{n+1}^{trial} = \sqrt{\frac{3}{2} s_{n+1}^{trial} : s_{n+1}^{trial}}$$

2. Check the plastic consistency.

IF $\Phi^{trial} = \frac{q_{n+1}^{trial}}{(1-D_n)} - \sigma_y(R_n, T) \leq 0$ THEN

$Set(.)_{n+1} = (.)_{n+1}^{trial}$ (elastic step) and RETURN

ELSE go to (3)

3. Return mapping (plastic step).

Plastic corrector

$$q_{n+1} - (1-D_{n+1})\widetilde{q}_{n+1}^{trial} + 3G\Delta\gamma = 0$$

$$N_{n+1} = \frac{3}{2}\frac{s_{n+1}}{(1-D_{n+1})q_{n+1}}$$

Plastic flow and evolution

$$R_{n+1} = R_n + \Delta\gamma$$

$$p_{n+1} = p_n + \frac{\Delta\gamma}{1-D_{n+1}}$$

$$\varepsilon_{n+1}^e = \varepsilon_{n+1}^{trial} - \Delta\gamma N_{n+1} - (T_n - T_0)\alpha$$

Update the damage indicator

$$D_{n+1} = \frac{{\sigma_s}^2}{2ES}(p_{n+1} - p_D)^{(1-r-T_1^m)} H(p_{n+1} - p_D) + ae^{\frac{b}{T_n+c}} e^{k(p_{n+1}-p_D)H(p_{n+1}-p_D)}$$

Check failure criterion

IF $D_{n+1} < D_c$ THEN

$$\sigma_{n+1} = (1-D_{n+1})C : (\varepsilon_{n+1}^{trial} - \Delta\gamma N_{n+1})$$

ELSE $\sigma_{n+1} = 0$

All stress components are set to zero and remain zero for the rest of the analysis.

4. EXIT

3.4 Summary

A new damage model for describing the deterioration behaviour of steel under coupled mechanical loads and elevated temperature has been developed in this chapter. Considering the deterioration behaviour is a combination of mechanical damage and thermal damage and the contribution of each depends on the external supply of heat and work, a coupled damage model is formulated comprising a mechanical damage component, a thermal damage component and thermo-mechanical interaction terms. The proposed coupled damage formulation is chosen from a number of alternative forms of coupling functions and a review of the performances of mathematical functions that have been constructed in this study is provided in Appendix A. This proposed model is capable of representing individual damage process in the strain or temperature space as well as capturing the global deterioration brought about by the combination of both phenomena. The proposed damage model is calibrated with the tensile coupon test (Pauli et al., 2012). Calibration results show that the damage parameters presented manage to reproduce the damage development induced by the complicated phenomena that take place when steel is subjected to both mechanical loads and elevated temperatures.

The simple and convenient formulation has made the proposed damage model advantageous for implementation in FE software. The numerical implementation scheme of the present model in ABAQUS/Explicit has been introduced. Damage equation is fully coupled into constitutive equations at each Gauss point and dynamic equilibrium solution is determined by incrementally advancing the kinematic states. The updated stress tensors and the overall state variables hence reflect the degradation effects of damage on material constitutive behaviour. The computational model is applicable for beam element as well as shell and solid elements for numerical analysis in ABAQUS/Explicit.

Developed on the thermodynamic and effective stress concept basis, the validity of the proposed model is limited by the hypothesis of multiaxial isotropic damage and multiaxial isotropic plasticity which is representative of structural steel. For cases in which material triaxiality differs from that of tensile tests, calibration against experimental data at different levels of triaxiality are generally required. Unfortunately, experimental data on steel deterioration at elevated temperatures are insufficient to support the inclusion of the effects of triaxiality. Notwithstanding these limitations, this chapter provides a framework for incorporating thermo-mechanical damage modelling of structural steel in FE analysis with currently available tensile coupon data. Numerical analyses will be performed with ABAQUS/Explicit in the next chapter in order to further verify the the predictive capabilities of the proposed damage model and its suitability for use in structural fire engineering simulations.

Chapter 4

Calibration and validation of the coupled damage model

4.1 Introduction

A coupled thermo-mechanical damage model for predicting steel deterioration behaviour under simultaneous mechanical loads and elevated temperatures has been presented in the previous chapter. The model has been calibrated and validated with experimental data at the material level, which verifies its capability in capturing the coupled damage growth under combined mechanical and thermal loads using a limited number of parameters. This chapter will continue to verify the applicability and effectiveness of the proposed damage model at the component and structure level.

The damage model has been implemented in FE software ABAQUS/Explicit using user developed subroutine VUMAT, which can be used with all elements in ABAQUS/Explicit that include mechanical behaviour with particularization to the corresponding stress states. This allows an extensive choice of elements used for numerical simulations. In order to support validation and calibration of the proposed damage model, it is essential to test it against a comprehensive set of experimental results or other established results ranging from single member test to multi-storey steel frames subjected to severe fire. In particular, it is of interest to verify the coupling effects of the proposed damage model against research work in which different levels of loads and temperatures are considered. Thus, a broad array of research studies have been selected for calibration and validation of the proposed damage model.

As mentioned in the previous chapter, the damage model parameters need to be calibrated from material coupon tests by tracking the elastic slope changes through loading-

unloading cycles where possible. However, such information is not always available for the tested steels. Therefore, the damage parameters obtained from the material tests conducted by Pauli et al. (2012) in Chapter 3 are used as the default input data for numerical simulations. Validations of the damage parameters are done through comparison with experimental results. When the simulation results overestimate or underestimate the extent of deterioration, corrections are made to adjust the damage parameters until the predicted force-displacement curves match experimental results. Despite the original lack of coupon test data that enables straightforward damage model calibration, this inverse analysis type of calibration procedure manages to provide a data collection of damage parameters in support of collapse assessment of steel structural systems. The calibrated
different types of structural components and frames, suggesting the robustness of this damage model outside the calibrated range.

It is important to examine if using the damage model with the calibrated parameters will yield a more accurate and better prediction of the structural response than using conventional numerical approaches. Numerical analyses, performed with the proposed damage model, demonstrate the capabilities of the damage model to reproduce strength deterioration and the resulting force-displacement history under fire with improved accuracy. The proposed damage model succeeds in capturing material deterioration behaviour in a series of experimental studies which are often used as reference for computational simulations.

Overall, the model's ability of predicting large structural deformation and progressive failure of structures under fire is verified here. This chapter concludes by summarizing the capability, applicability and effectiveness of the proposed damage model and discussing recommendations for its use.

4.2 Calibration and validation with fire tests of steel components and assemblies

In this section, the calibration and validation of the damage model are performed using a broad array of tests results at the component and assembly level, ranging in complexity from single beam test to beam-to-column connections. The studies include an initial comparison with room temperature tests, as well as comparison with fire tests under various load levels and temperature levels. The EC3 (Eurocode 3) material model is chosen as the reference model to carry out parallel analyses in numerical validations for the purpose of highlighting the effects of damage on the structural response. The structural responses obtained by the damage model are compared with those obtained by

EC3 model and test results in order to evaluate the performance of the proposed damage model.

Depending on the type of structural behaviour observed in tests, numerical validations of the coupled damage model are performed using three different kinds of elements, i.e., (1) shell elements, (2) solid elements, and (3) beam elements. The calibration of the damage model parameters is a trial and error procedure repeated until the best fit is achieved between the predicted force-displacement data and test results. Optimum damage model parameters are found which provide consistent and accurate predictions. From the computational point of view, predicting strong damage localization is not a critical issue but the element size needs to be adequate in order to properly account for the strain gradient and damage development. A mesh sensitivity study needs to be carried out for each simulation to ensure that the calculated damage development is not significantly affected by a finer mesh. As a result, the mesh size varies from simulation to simulation but meets the criteria. Time step sensitivities are also studied and the converged solutions are presented.

4.2.1 Steel beam fire test (2007)

For the purpose of damage model calibration and validation, a steel I-beam is first studied comparing with the experimental results by Dharma and Tan (2007). In the experimental study, a series of tests were conducted on steel I-beams to investigate the beam behaviour under fire conditions. As shown in Figure 4.1, the beam was simply supported with web stiffeners placed at supports and mid-span. Specimen S3-1 was tested at room temperature while specimens S3-2 and S3-3 were heated to 415°C and 615°C at a heating rate of 7°C/min, respectively. After the target temperature was achieved in the furnace, the beam specimen was loaded at mid-span until failure. The values of the mechanical properties of steel at room temperature are listed in Table 4.1.

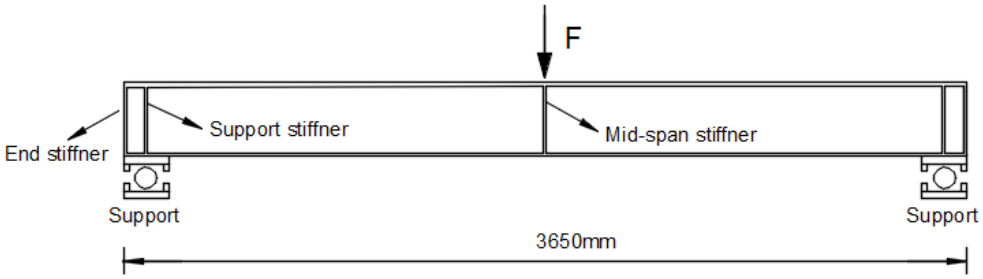

Fig. 4.1 Test set-up (Dharma and Tan, 2007)

Table 4.1 Mechanical material properties at room temperature (Dharma and Tan, 2007)

Coupon	Yield strength (MPa)	Elastic modulus (MPa)	Ultimate strength (MPa)
Flange	224.1	201697	392.1
Web	277.1	206063	452.0

The FE model is constructed using shell elements, as shown in Figure 4.2. Based on a mesh sensitivity study and micromechanical considerations, the mesh of the FE model is refined to have six elements across the flange width and six elements through the depth of the web. The mid-span point load is simulated in displacement control by specifying a displacement history for the top of the mid-span stiffener. The beam is simply supported at both ends and lateral restraints are provided at certain intervals along the beam length to prevent lateral deflection.

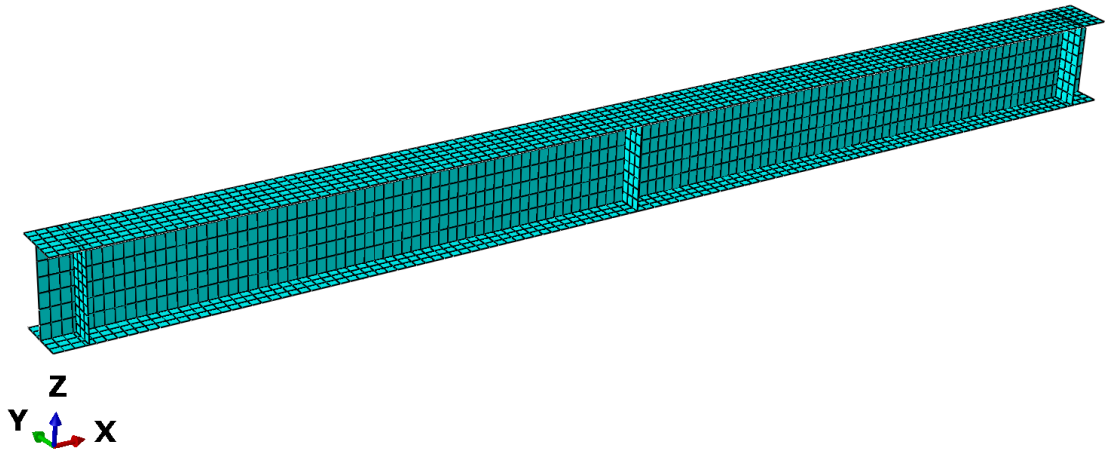

Fig. 4.2 FE model of the steel beam in ABAQUS

The temperature dependency of steel properties is critical to the prediction of load-displacement relationships of the beam. The user defined subroutine VUMAT provides the functionality to perform numerical simulations with the newly developed damage model in ABAQUS/Explicit. Comparison with simulations using conventional material model is also required for the purpose of highlighting the effects of damage on the structural response. Therefore, the EC3 material model, which adopts temperature dependent stress-strain relationships of steel referring to EN 1993-1-2 (2005), is employed in parallel analysis. The EC3 model is converted to a series of true stress and plastic strain data pairs as material input in ABAQUS.

The damage parameter sets presented in Chapter 3 are used as initial estimate in damage analysis due to the fact that the tensile coupon tests in Dharma and Tan (2007) did not provide sufficient information for identifying damage model parameters. Table 4.2 presents the list of damage parameter values, which have been determined from coupon test data in Pauli et al. (2012). By performing simulations with each damage parameter set, the influence of the damage development on the overall structural response is

investigated. Calibration results show that the load versus displacement curves generated by the damage model parameter set M7 and M8 give poor predictions for the beam under consideration, whereas M9 parameter set gives excellent experimental fit.

Table 4.2 Damage parameters best fit to tensile coupon test results

Test series	Calibrated damage parameters							
	S	P_d	a	b	c	r	m	k
M7	4.98E+05	0.004	4.375	-1213.75	-20	0.695	1.864	0.064
M8	5.66E+05	0.004	2.334	-915.7	-20	0.786	4.99	0.125
M9	4.75E+05	0.004	1.952	-837.323	-20	0.613	3.01	0.248

By employing M9 parameter set as damage model input, both the buckling and damage features are well captured by the numerical analysis with the proposed damage model. The local and lateral torsional buckling mode predicted by the proposed damage model is shown in Figure 4.3, which matches the description in Dharma and Tan (2007) well. Using the same damage parameter set, the damage model prediction for each loading case in terms of load versus displacement data are presented in Figure 4.4, 4.5 and 4.6, respectively, along with the test results. Numerical results generated by the EC3 model are also included to illustrate the impact of damage modelling on structural behaviour prediction. Note that the damage propagation behaviour is not included in the EC3 model and the softening in this case is due to geometric nonlinearity.

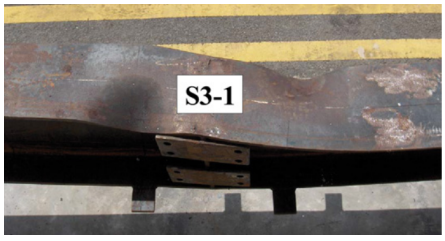

(a) Local and lateral torsional buckling observed in test (Dharma and Tan, 2007)

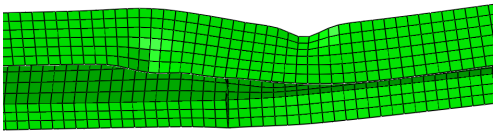

(b) Local and lateral torsional buckling predicted by damage model

Fig. 4.3 Failure mode comparison of specimen S3-1

As can be seen from the load-deflection curves, the damage model predictions and experimental data agree quite well in all cases. The stiffness, strength and deterioration in the overall beam behaviour is well reproduced, which confirms the effects of damage imposed on the behaviour of the steel beam. In particular, the softening branch is simulated with remarkable accuracy, which validates the choice of damage model parameters used in the analysis.

It should be noted that the damage parameters are the governing factors which control the shape of the load-deflection curve in the post-peak softening branch. The evolving damage accounts for the progressive degradation after the damage threshold is exceeded

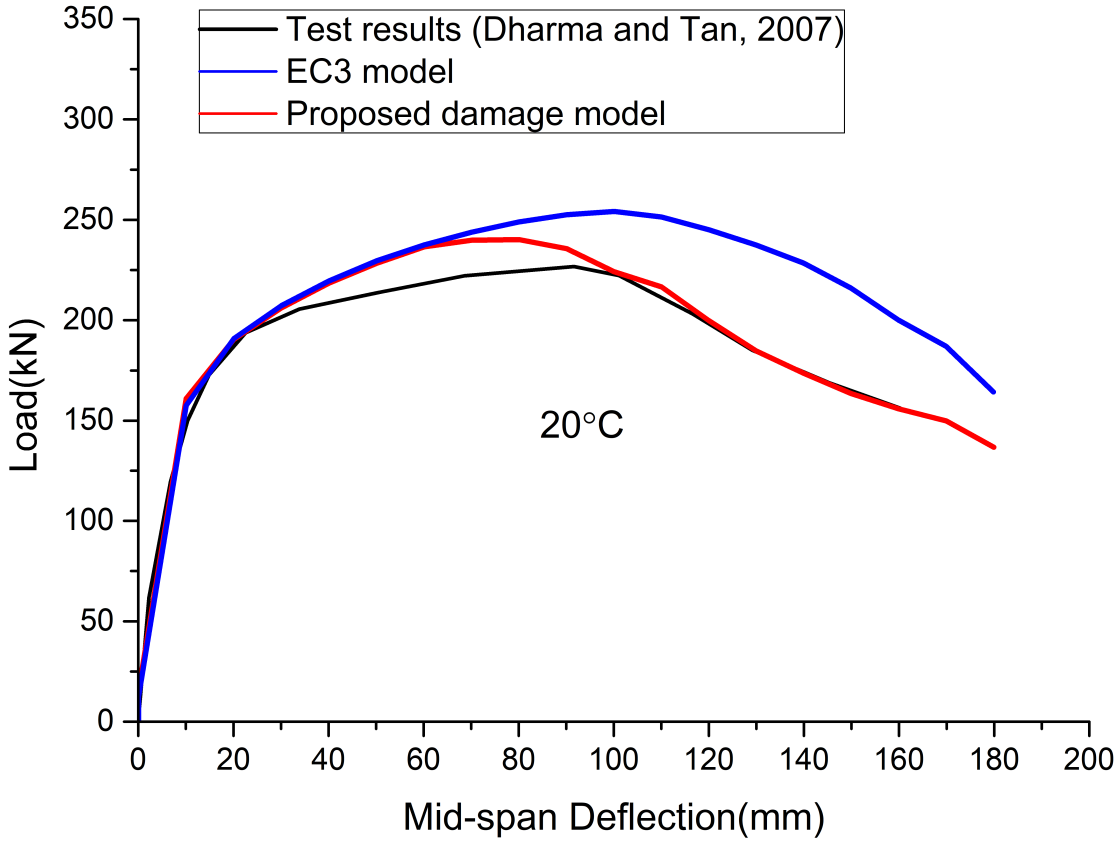

Fig. 4.4 Mid-span load–deflection of specimen S3-1

or the removal of elements once the critical damage value is reached at integration points. This is not the case for the EC3 model, which explains the fact that EC3 model predictions overestimate the capacity of the steel I-beams considerably. It should also be noted here that the EC3 model is not specifically calibrated for this case. This over-estimation does not arise from the unconservativeness of the EC3 model in the reduction factors related to yield strength ($F_y/F_{y,0}$) and Young's modulus (E/E_0). This is because the proposed damage model keeps the same $F_y/F_{y,0}$ as specified in the EC3 model (See Section 3.3.1). Moreover, the initial slopes of the load-deflection relationships generated by the two models follow the same path and the curves only start to diverge at large deflections, suggesting the consistent E/E_0 in the two models before the mechanical damage comes into effect. These results also validate the ability of the damage model to predict the displacement at which the ultimate failure occurs.

Note that there is some discrepancy in the yield strength and hardening branch of specimen S3-2 between the numerical predictions and the experimental data. This is probably due to the differences between the material properties in experiments and FE models and the use of idealised restraints in simulations. Nevertheless, the maximum load is well predicted by the proposed damage model for specimen S3-2. Overall, the results have successfully captured the main trends exhibited in the experimental data and are sufficiently accurate for the current computational exercise. It can be concluded

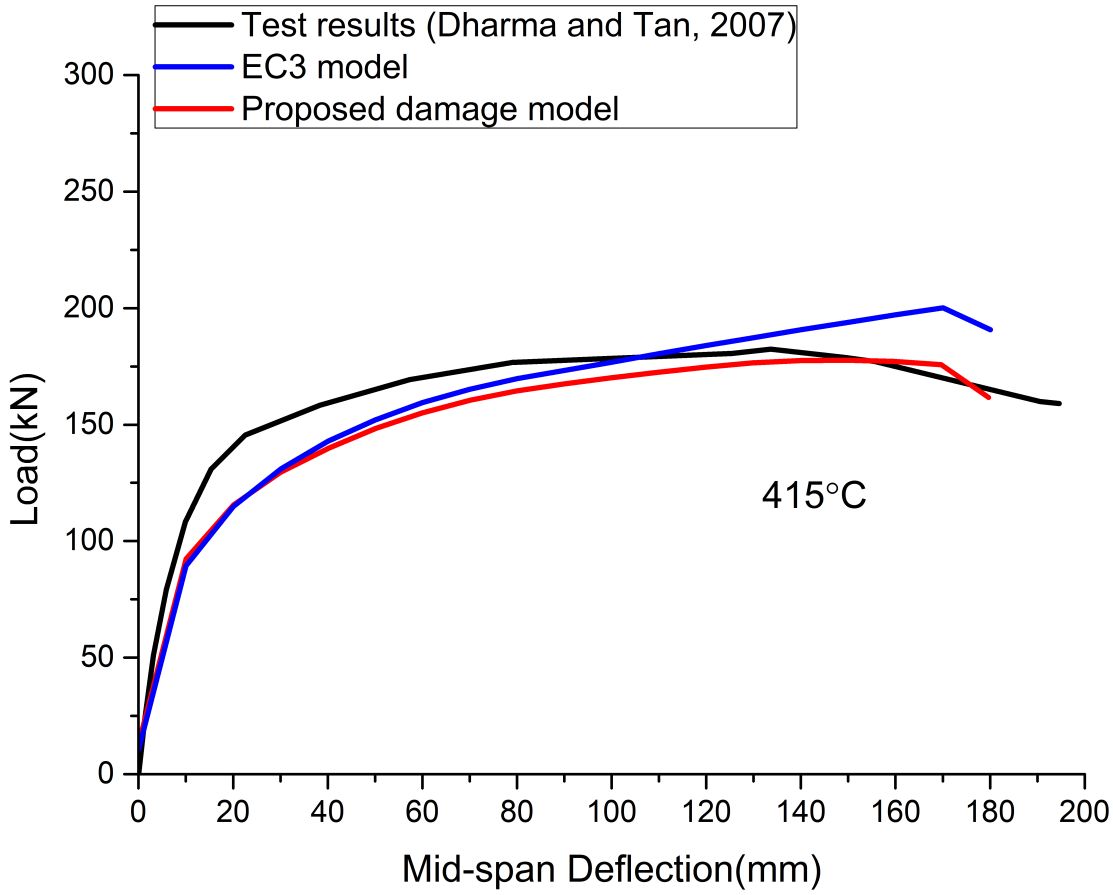

Fig. 4.5 Mid-span load–deflection of specimen S3-2

Table 4.3 Damage parameters best fit to steel beam fire test results

S	P_d	a	b	c	r	m	k
4.75E+05	0.004	1.952	-837.323	-20	0.613	3.01	0.248

that the calibration of the damage model is successful and the coupled effect of damage and plasticity on the predicted behaviour is evident. The predictions match experimental results fairly well in all cases, indicating the adequacy of the damage model in describing phenomena in both low range and high range of temperatures. The calibrated damage model parameters, which have been used consistently for all three loading cases, are summarized in Table 4.3.

4.2.2 Steel beam-to-column connection fire test (1997)

The capability of the damage model approach in simulating damage development, material degradation and subsequent element deletion is also validated through comparison with experimental study of steel beam-to-column connection. The experimental study chosen for validation was performed by Leston-Jones (1997) to investigate the elevated-

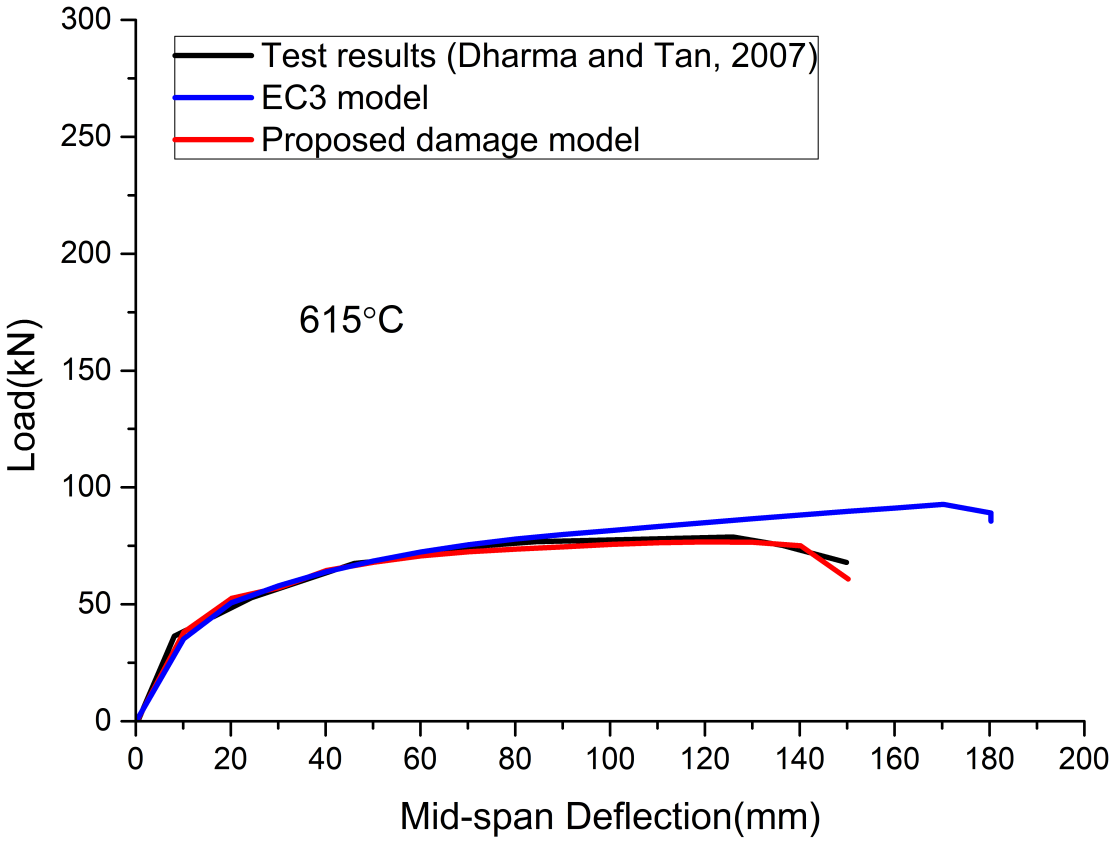

Fig. 4.6 Mid-span load–deflection of specimen S3-3

temperature degradation characteristics of steel flush end-plate connection. The test program consisted of seven full-scale flush end-plate connection assemblies: One loaded at room temperature until failure, one subjected to various heating rates, and five tested under different load levels across a range of temperature. The details of the test program are listed in Table 4.4. Each assembly consisted of a 152×152×23UC Grade 43 column 2700 *mm* in length, two 254×102×22UB Grade 43 beams 1700 *mm* in length and a 12 *mm* thick end-plate with six M16 Grade 8.8 bolts in 18 *mm* diameter clearance holes.

Table 4.4 Flush end-plate connection experimental programme (Leston-Jones, 1997)

Test	Applied Moment	Temperature	Description
BFEP AMB	Full Range	Ambient	Ambient moment-rotation curve
BFEP TEMP	None	Various	Influence of heating rate
BFEP 5	$5kN \cdot m$	10°C/min	Fire test 1
BFEP 10	$10kN \cdot m$	10°C/min	Fire test 2
BFEP 15	$15kN \cdot m$	10°C/min	Fire test 3
BFEP 20	$20kN \cdot m$	10°C/min	Fire test 4
BFEP 25	$25kN \cdot m$	10°C/min	Fire test 5

Ambient-temperature material coupon tests were performed for the test specimens. The recorded yield stress, ultimate stress and elastic modulus of Grade 43 steel is 319

N/mm^2, 465 N/mm^2 and 220 kN/mm^2, respectively. Elevated-temperature material properties were not obtained due to the cost of testing. The newly developed damage model is adopted in numerical simulations and the EC3 material model is employed in parallel analysis for comparison. Due to the fact that no stress-strain data is available for calibrating the damage model, the initial estimate for the damage model parameters is identical to that used in Section 4.2.1.

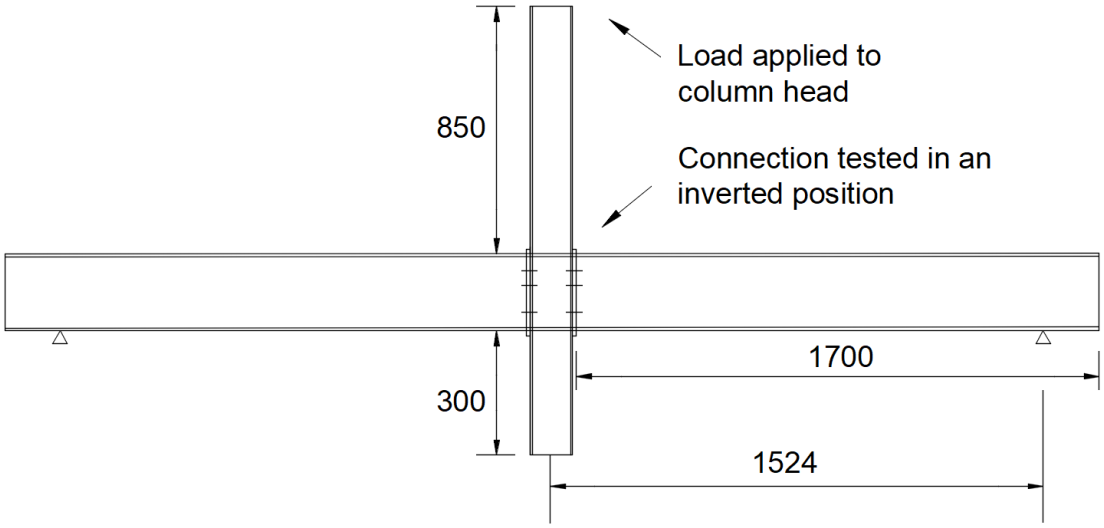

Fig. 4.7 Ambient-temperature test arrangement (Leston-Jones, 1997)

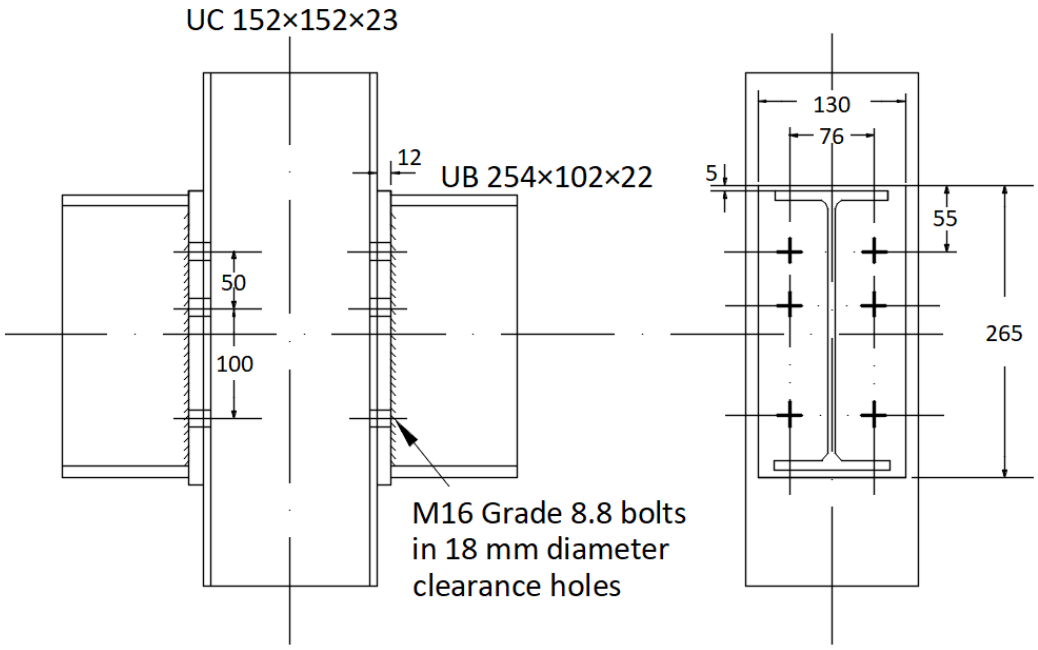

Fig. 4.8 Flush end plate connection detail (Leston-Jones, 1997)

For the ambient-temperature test, the specimen was arranged in an inverted position with a reduced column length of 1400 *mm* due to the restrictions of the test rig employed. An incremental load was applied at the top end of the column while the beams were

restrained at a position of 1524 *mm* away from the column centre-line. The overall layout of the test specimen is depicted in Figure 4.7 and the details of the full-depth end plate connection are presented in Figure 4.8. A detailed FE model is constructed for simulating the connection assembly using three-dimensional solid elements C3D8R, as shown in Figure 4.9. A mesh sensitivity study shows that the appropriate global mesh size for structural components is 10 *mm* to 20 *mm*. Test observations suggest that significant deformation occurred in the column web in compression and in the column flange in tension. In order to capture this failure mode, the mesh of the region near the face of the beam-column connection is further refined with a minimum of three layers of elements specified through the plate thickness.

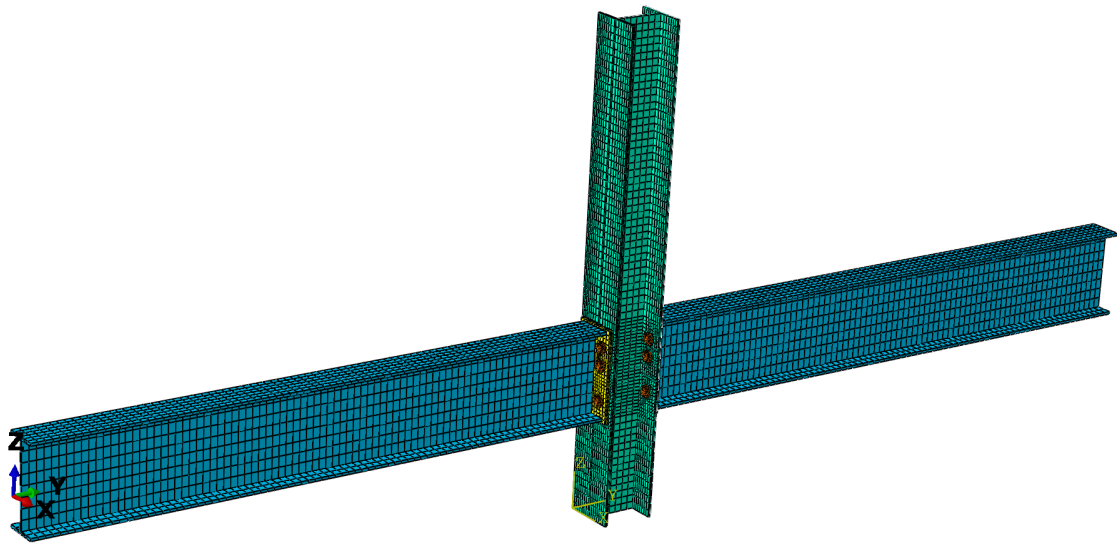

Fig. 4.9 Numerical model of flush end plate connection in ABAQUS

Connection components including the 12 *mm* thick end-plate with 18 *mm* diameter clearance holes and six M16 bolts are modelled in detail, as shown in Figure 4.10. A number of contact pairs exist within the connection, such as between end plate to column, bolt shank to holes, and bolt head to the connected plate. Contact is modelled using ABAQUS surface to surface contact option. "Hard" contact is assumed for the normal behaviour and a friction coefficient of 0.1 is specified for tangential behaviour in contact property definition. Simulation results are found to be insensitive to the value of friction coefficient. The initial gap between the bolt shank and bolt hole is set at 0.1 *mm*. Pre-stress is applied to the bolts given the fact that all bolts were tightened in the test. Weld is not directly modelled but achieved using ABAQUS "tie" option.

Figure 4.11 shows the numerically obtained moment-rotation curves as well as the test results. In the moment versus rotation curve, the moment is directly determined from the point load applied on the beam, and the rotation is assumed relative to the column centre-line. It can be seen from the graph that the EC3 model significantly overpredicts the capacity of the connection while the damage model predicts the moment capacity

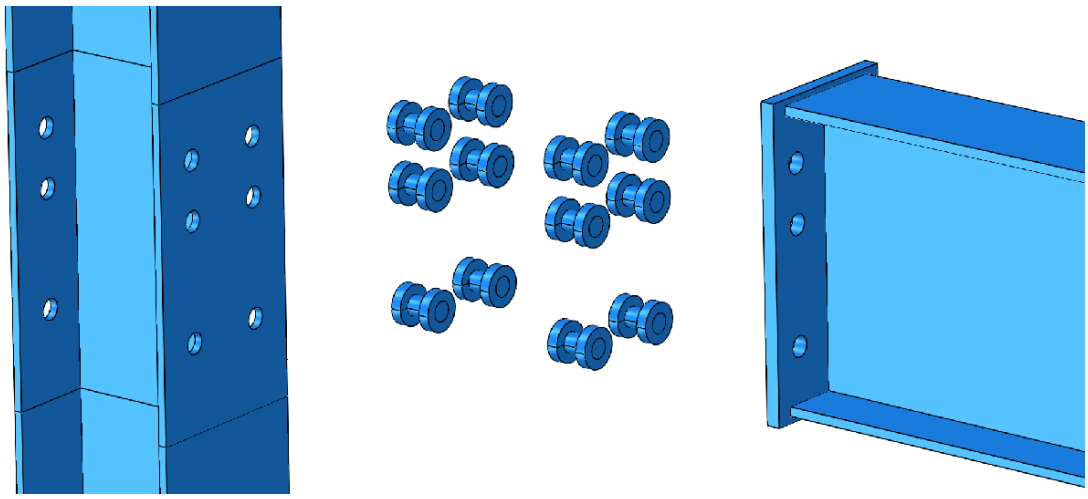

Fig. 4.10 Modelling details of flush end plate connection

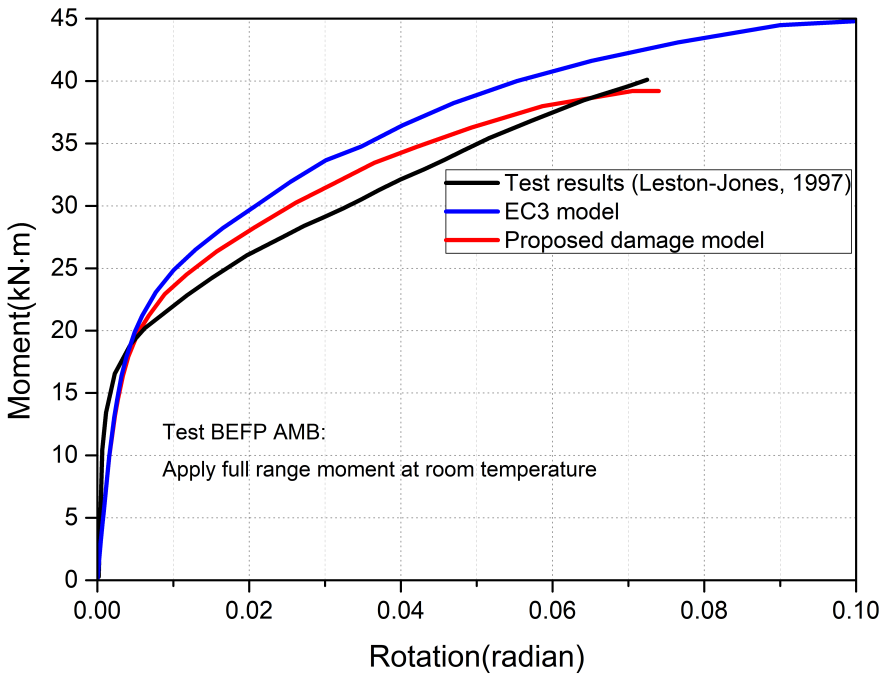

Fig. 4.11 Comparison of ambient-temperature connection response between numerical cases and test data

well and has a close fit for moment-rotation relationships. The good agreement with experimental data therefore validates the input parameters for the damage model.

Comparison of numerical predictions with and without damage model highlights the progressive degradation in the stiffness and strength in the moment-rotation curve after the elements reach the damage threshold. Apart from describing the overall structural response with improved accuracy, the proposed damage model also provides an excellent

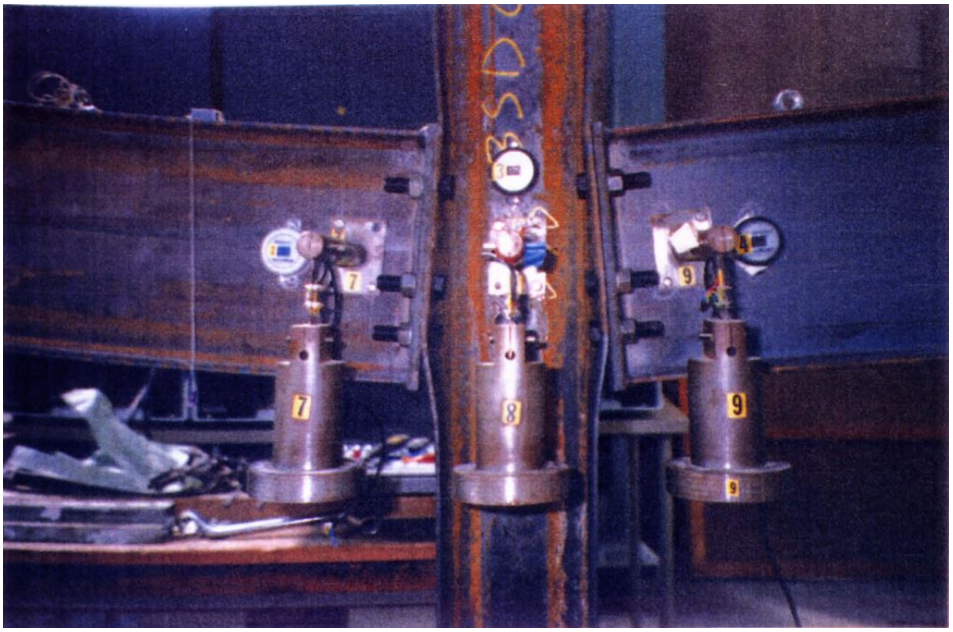

(a) Connection failure mode observed in test BFEP AMB (Leston-Jones, 1997)

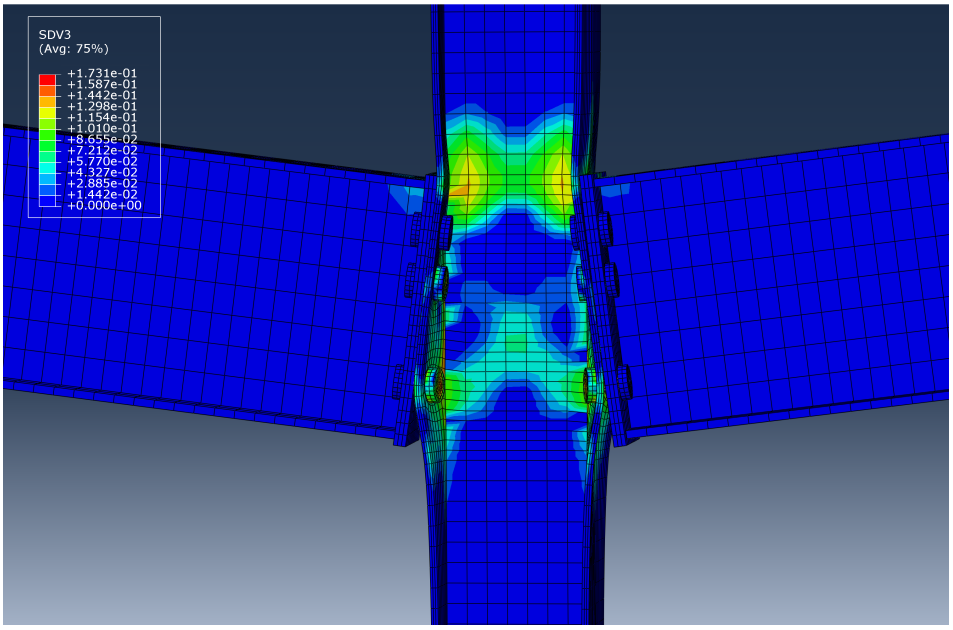

(b) Damage distribution and failure mode in damage model prediction

Fig. 4.12 Ambient-temperature connection failure mode

estimate of the damage locations. In the experimental test, the failure consisted of significant deformation across the column web in the compression zone and within the column flange in the tension zone. Little damage was observed in beams or end-plates due to the relative dimensions of the end-plates and the column flanges. In the damage model prediction, the distribution of damage concentrates in the compression web and tension flange of the column, which coincides with the experimental results. The damage distribution contour as well as the failure mode of the connection are shown in Figure 4.12. The similarities between numerical and experimental failure modes confirm that

the proposed modelling approach captures the key aspects of the steel behaviour. It is evident that it will be non-conservative to ignore the existent damage propagation in the specimen.

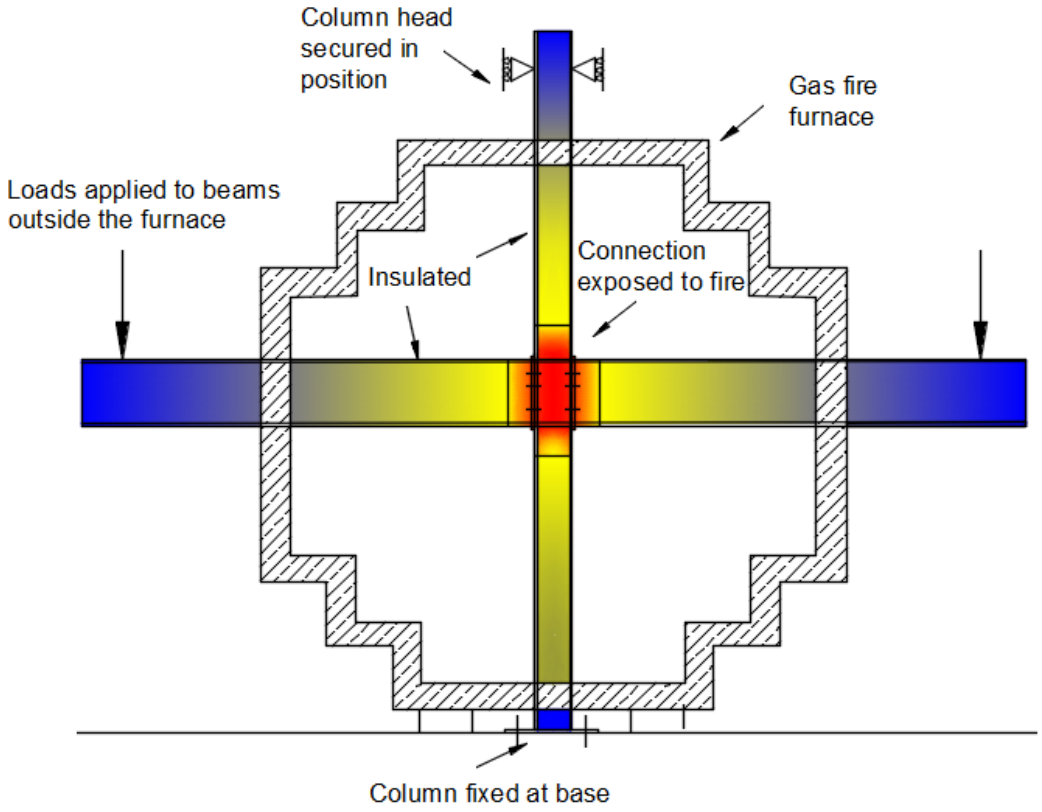

Fig. 4.13 Elevated-temperature test arrangement (Leston-Jones, 1997)

Following the ambient-temperature test, a complete set of fire tests were carried out on the connection assemblies to establish the moment-rotation relationships at elevated temperatures. The elevated-temperature test arrangements were similar to that of the ambient test, as shown in Figure 4.13. Loads were applied to the beams outside the furnace at a distance of 1524 *mm* away from the column centre-line, while the column bottom was fixed and free thermal expansion was allowed at the column head. A large portion of beams and column were insulated using ceramic fibre blocks and ceramic blanket. The region within approximately 100 *mm* from the face of the connection were left unprotected against furnace heating. After conducting a trial fire test (BFEP TEMP) for the purpose of determining an appropriate heating rate (10°C/min) which produces realistic temperature distributions, Leston-Jones (1997) performed a series of five elevated-temperature tests on flush end-plate connections under constant moment.

The FE model of flush end-plate connections tested in fire is illustrated in Figure 4.14 with the fire exposed region highlighted. Two stages of loading are applied to the FE model:

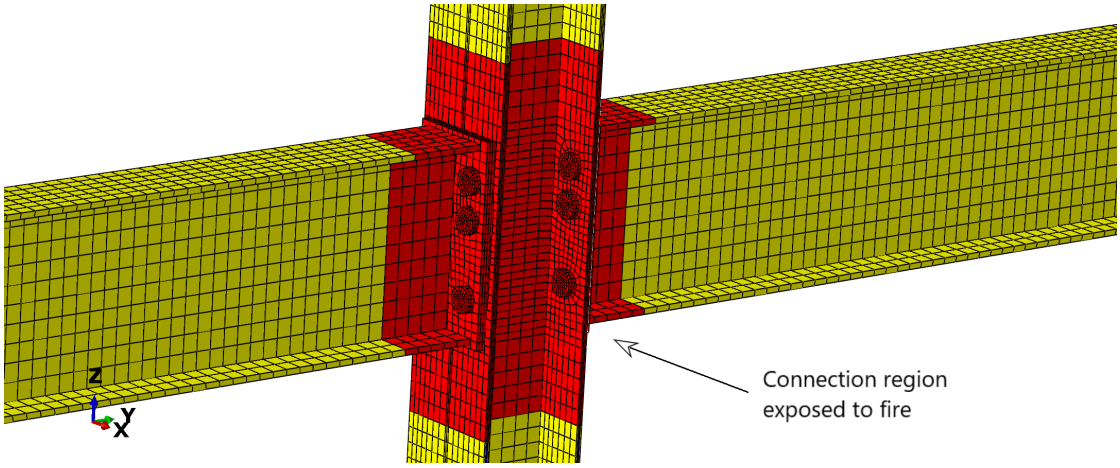

Fig. 4.14 Fire exposed region within connection model

(1) two point loads are applied to the beam; (2) increase temperature while maintaining the structural loads. Temperature variations were monitored at different locations within the connection in the test and given in Table 4.5. The fire action is modelled by assigning the respective temperature profiles for different parts of the connection assembly.

Table 4.5 Relative temperature profiles for flush end-plate connection (Leston-Jones, 1997)

Location:	BFEP 5:	BFEP 10:	BFEP 15:	BFEP 20:	BFEP 25:	Average:
Beam Lower Flange	1.000	1.000	1.000	1.000	1.000	1.000
Beam Centre Web	0.971	1.026	0.973	0.972	0.983	0.985
Beam Top Flange	0.685	0.699	0.685	0.647	0.668	0.677
Beam Lower Flange (insulated)	0.293	0.238	0.242	0.256	0.290	0.264
Beam Top Flange (insulated)	0.291	0.264	0.246	0.280	0.260	0.268
Lower Bolt	0.954	1.037	0.983	0.972	0.988	0.987
Middle Bolt	0.930	1.014	0.974	0.946	0.965	0.966
Top Bolt	0.875	0.967	0.946	0.924	0.926	0.928
Column Web	1.066	1.180	1.150	1.133	1.188	1.143
Column Flange	0.998	1.095	1.022	1.057	1.008	1.036
Column Flange (insulated)	0.305	0.332	0.343	0.339	0.296	0.323
End-plate	0.929	1.023	1.010	0.964	0.986	0.982

Similar to the ambient-temperature test findings, significant deformation was observed in the column compression web and column tension flange, while beams and end-plates experienced little damage. Figure 4.15 shows that the damage analysis is able to identify the zone of damage propagation. There is noticeable damage accumulation in elements within the experimentally observed failure locations. It is worth noting that damage is also observed in the tension web of the column and beam web but less intensified judging from the magnitude of the damage values. This means that these locations are prone to fracture though no associated significant deformation is observed by the end of the

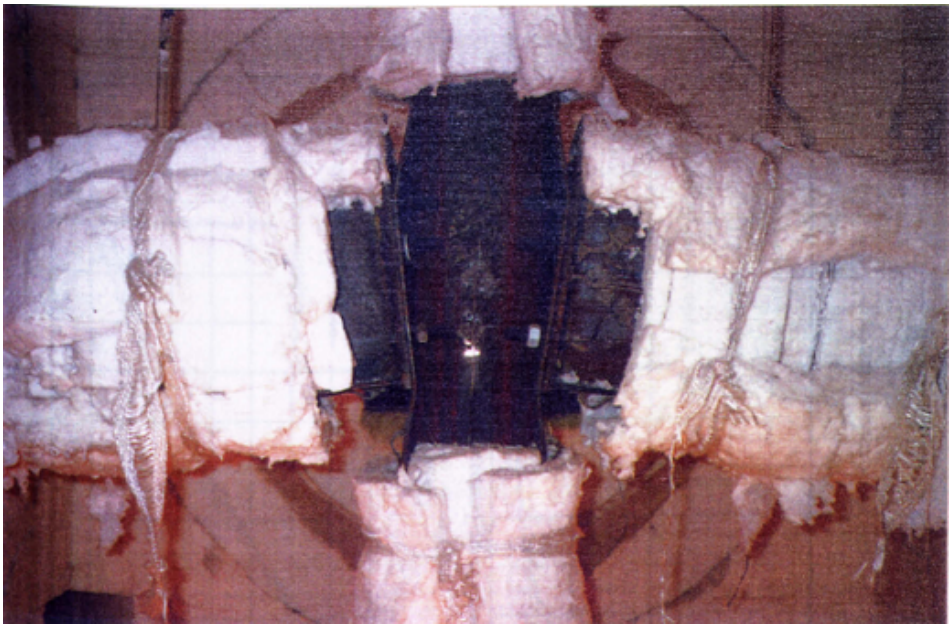

(a) Connection failure mode observed in test BFEP5 (Leston-Jones, 1997)

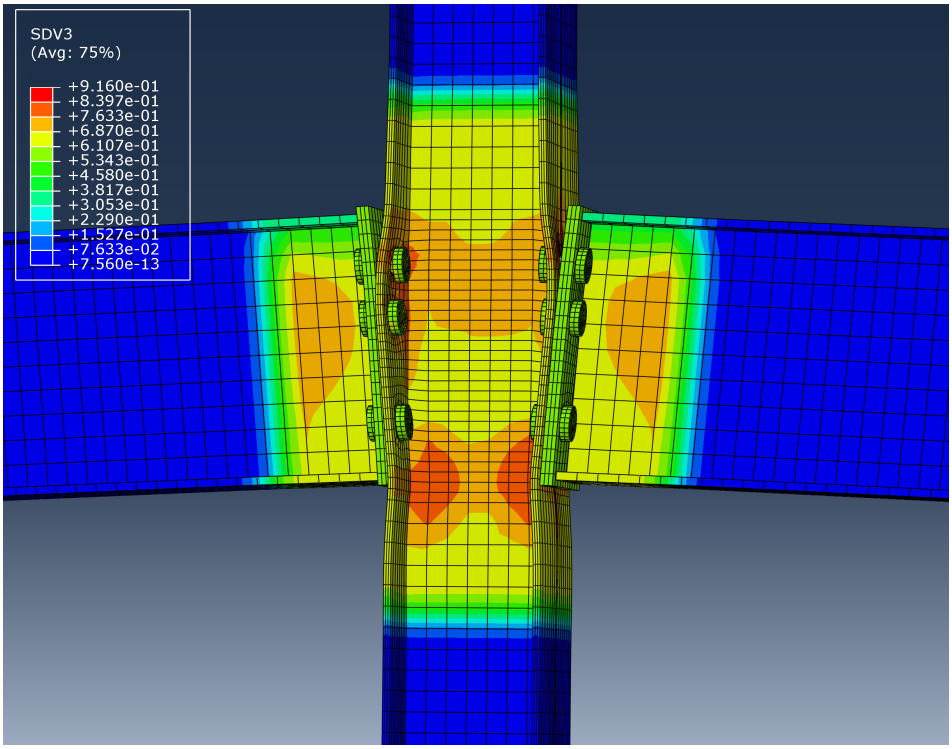

(b) Damage distribution and failure mode in damage model prediction

Fig. 4.15 Elevated-temperature connection failure mode (BFEP 5)

heating regime in the test. It can be concluded that the proposed damage model is able to predict damage concentration fairly well and can be considered as useful tool to evaluate potential fracture locations which might be imperceptible in experimental setting.

The temperature-rotation curves plotted in Figure 4.16 to 4.20 are obtained with both the proposed damage model and EC3 model. Numerical results are found to be in good

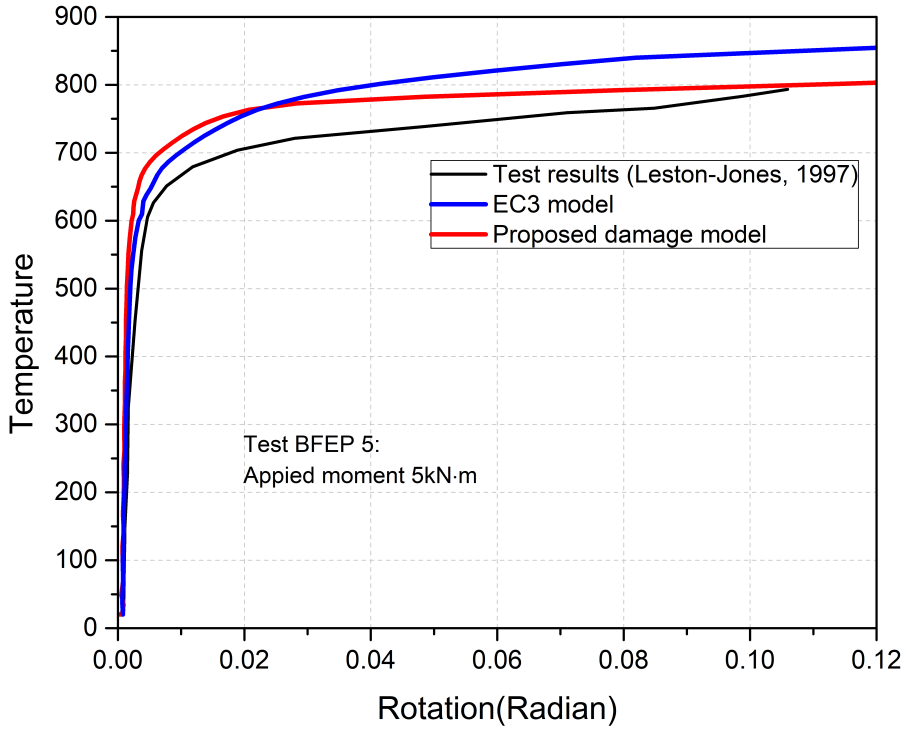

Fig. 4.16 Comparison of connection response between numerical cases and fire test 1 (BFEP5)

agreement with test results. The predictions of the damage model compare favourably with those of the EC3 model for all loading cases, particularly in terms of failure temperature. The first fire test was conducted at a relatively low moment level of $5kN \cdot m$. Both numerical approaches overpredict the temperature corresponding to plastification of the elements within the connection. This may be explained by the fact that the furnace heating might not be as uniform as in numerical simulations. The initial stiffness predicted by the damage model is slightly higher than that of the EC3 model. However, the stiffness and moment capacity of the connection are reduced progressively when the coupled thermo-mechanical damage comes into effect at increasing temperatures and extensive plastification. From the results it can be seen that the proposed damage model is capable of capturing the effects of thermo-mechanical damage development and predicting the ultimate failure temperature of connection assembly with marginal error.

The pattern of structural response at moment level of $10kN \cdot m$ and $15kN \cdot m$ is similar to that observed in the first fire test. On the other hand, the coupled effects of mechanical damage and thermal damage is particularly evident in the case of moment level $20kN \cdot m$ and $25kN \cdot m$. These two cases with high load ratios provide insight closely related to the degradation of connection capacity. Results indicate that the damage model prediction has a nearly perfect fit for the plateau in the connection response upon rapid increase in rotation, whereas the failure of the connection occurs at significantly higher temperature in EC3 model prediction.

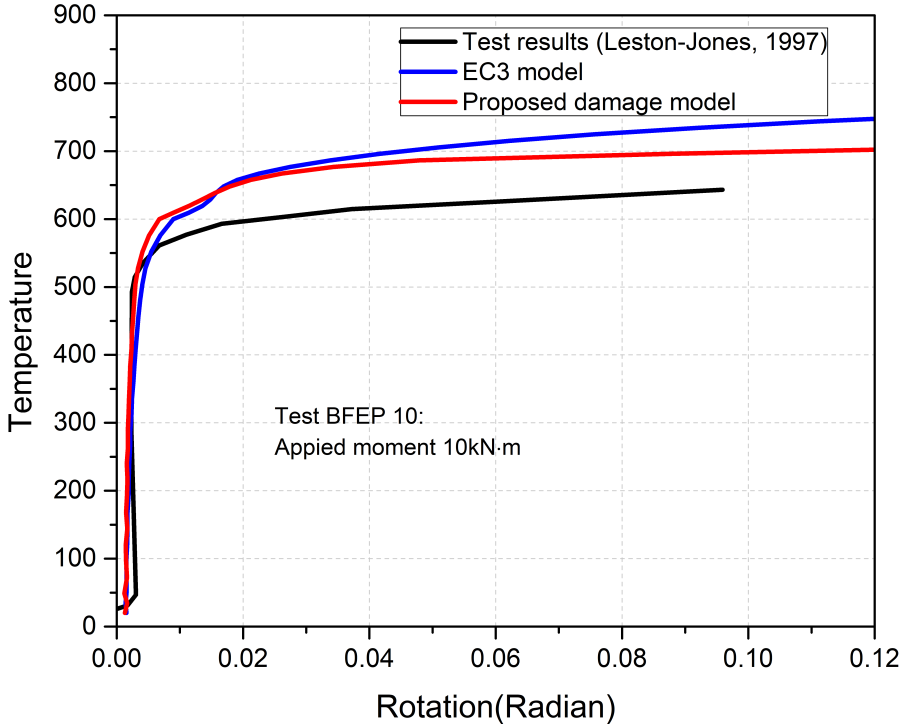

Fig. 4.17 Comparison of connection response between numerical cases and fire test 2 (BFEP10)

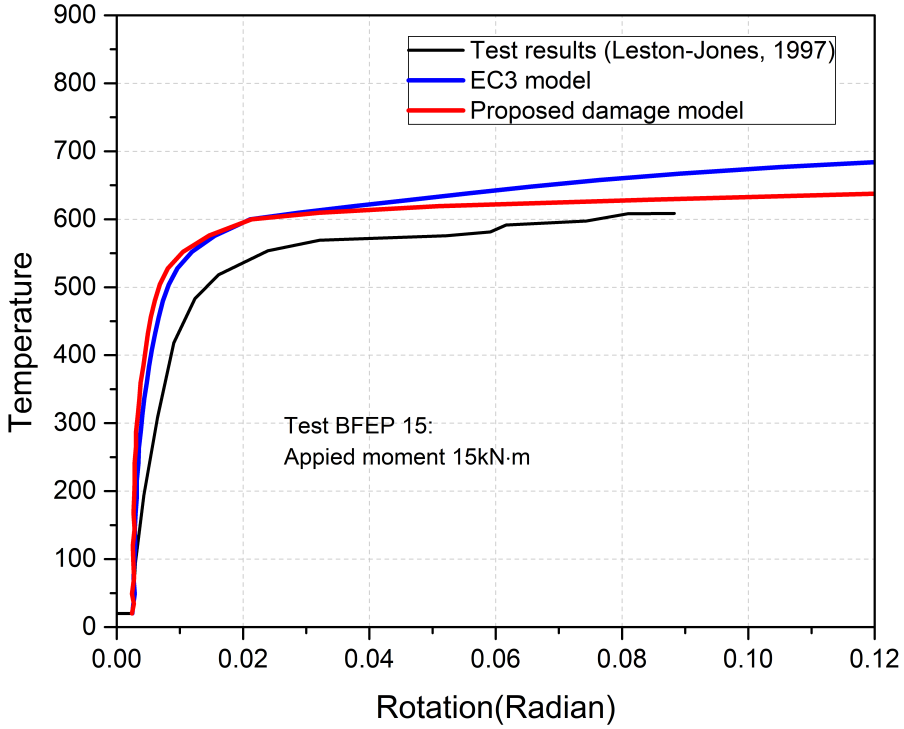

Fig. 4.18 Comparison of connection response between numerical cases and fire test 3 (BFEP15)

Overall, the proposed damage model manages to predict the failure temperatures within a 5% error margin for almost all loading cases except BFEP10. It is important at this

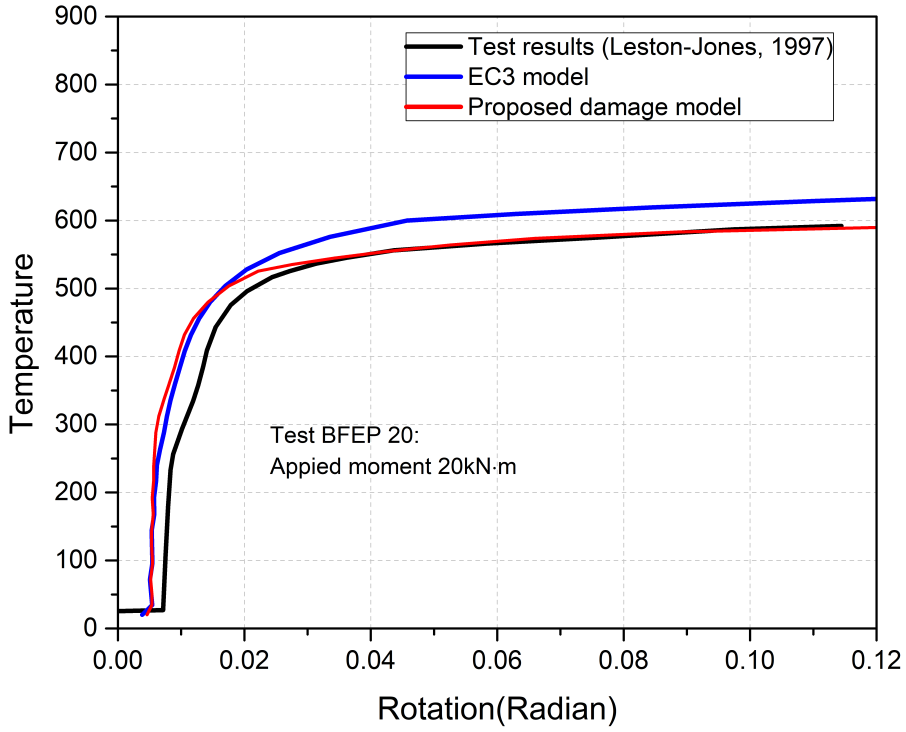

Fig. 4.19 Comparison of connection response between numerical cases and fire test 4 (BFEP20)

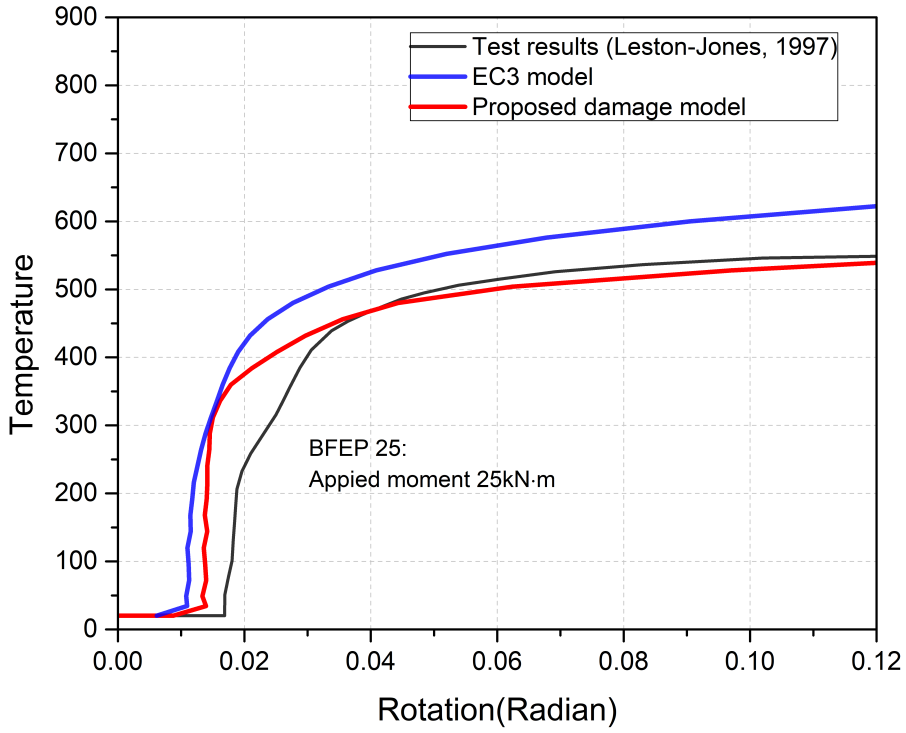

Fig. 4.20 Comparison of connection response between numerical cases and fire test 5 (BFEP25)

stage to keep in mind that by making further adjustments in the magnitudes of the damage model parameters, results of some loading cases might be improved at the

cost of numerical accuracy in other loading cases. Therefore, judging from the overall performance of the damage model, the calibrated parameter input succeeds in adequately describing experimental phenomena. A list of the calibrated parameters is provided in Table 4.3. To summarize, the damage model has a significant contribution in estimating structural behaviour at high load levels during fire events and the damage model should be incorporated into numerical simulations even for low levels of loading.

4.2.3 Steel tubular truss fire test (2010)

In addition to establishing the effectiveness of the damage model approach in modelling connection assembly, the validation attempt also includes studies on steel tubular truss. Liu et al. (2010) conducted fire tests on steel tubular trusses under two different levels of axial loads. As shown in Figure 4.21, the steel tubular truss specimen consisted of two vertical chords, two horizontal braces and two diagonal braces. The testing procedure comprised two steps: (1) an axial load was applied to the upper end of the left chord, (2) fire was ignited inside the furnace while the load was kept constant. Testing of specimen SP1 and SP2 are identical except that the axial load was 400 *kN* for SP1 and 600 *kN* for SP2.

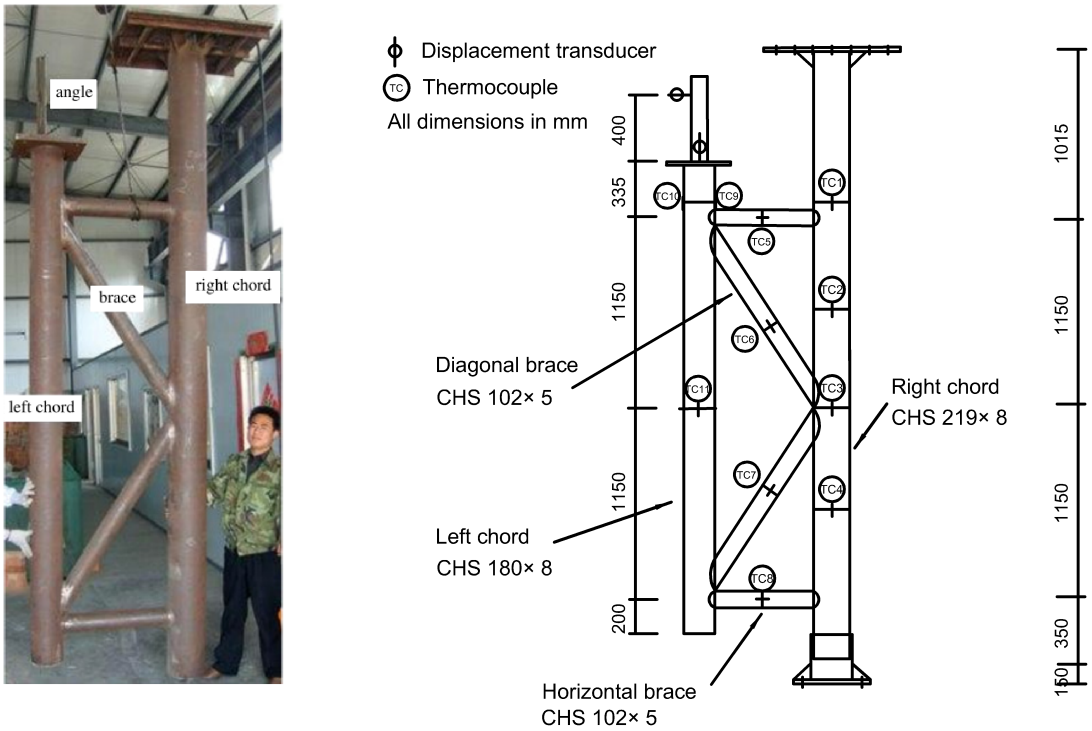

Fig. 4.21 Test set-up (Liu et al., 2010)

The FE simulations are carried out in ABAQUS using beam element B21, in which both the proposed damage model and EC3 model are employed for comparison. The model's

ability to reproduce strength deterioration and the resulting displacement-temperature curve is verified here by comparing with the experimental results of Liu et al. (2010). Figure 4.22 shows the FE model with associated boundary conditions and loading. The temperature histories of individual member recorded in tests are given in Figure 4.23 and used as temperature field input in numerical simulations. Ambient-temperature material properties obtained from tensile coupon tests are listed in Table 4.6.

(a) Beam element model (b) Rendered beam profiles

Fig. 4.22 Numerical model of steel tubular truss in ABAQUS

Table 4.6 Material properties obtained from coupon test at room temperature (Liu et al., 2010)

Member	Young's modulus (GPa)	Yield stress (MPa)	Tensile stress (MPa)
Left chord	193	368	553
Right chord	196	381	565
Braces	202	376	559

The initial estimate for the damage model parameters is identical to that provided in Table 4.3 but is found unable to closely replicate the experimental reported displacement-temperature behaviour. Calibration is thus conducted to find the most appropriate damage model parameters based on achieving the desirable failure temperature prediction through a trial and error procedure. Among the model parameters, parameters a, b and c are calibrated initially to match the displacement behaviour at low range of temperatures. Parameters S and r are adjusted to give a better prediction of mechanical damage growth, with the plastic strain threshold p_d determined as the initiation point of mechanical damage. After this, the coefficients m and k which account for the coupled effects of thermo-mechanical damage growth are manipulated to obtain the desirable accelerated damage rates. It is important to note that the rapid loss of load carrying capacity can be premature or delayed by choosing different combinations of these model parameters. The optimum damage model parameters that provide the closest fit to experimental results are listed in Table 4.7.

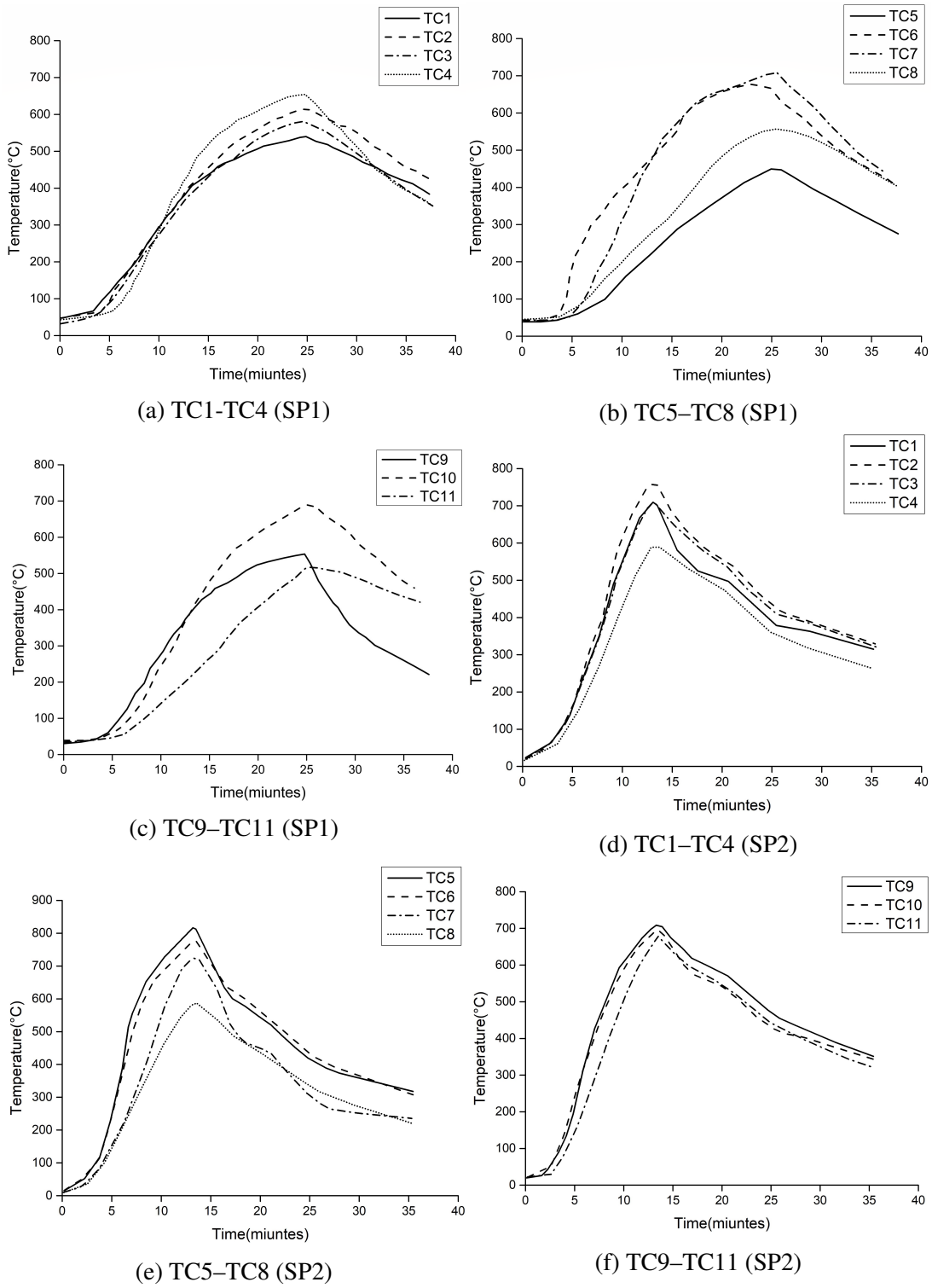

(a) TC1-TC4 (SP1)

(b) TC5–TC8 (SP1)

(c) TC9–TC11 (SP1)

(d) TC1–TC4 (SP2)

(e) TC5–TC8 (SP2)

(f) TC9–TC11 (SP2)

Fig. 4.23 Temperature–time curves of thermocouples TC1–TC11 for specimen SP1 and SP2 (Liu et al., 2010)

Table 4.7 Damage parameters best fit to steel tubular truss fire test results

S	P_d	a	b	c	r	m	k
1.72E+05	0.01	2.81	-1027	-20	0	9.63	4

The vertical displacement versus maximum temperature curve obtained from numerical simulations and test results for specimen SP1 and SP2 are plotted in Figure 4.24 and Figure 4.25, respectively. In both cases the damage model prediction correctly follows the trend of test results, with the quantitative agreeement being particularly good for specimen SP2. It is observed that the buckling of the diagonal brace member in compression initiates the overall failure of the steel truss. The failure temperature is defined as the critical point at which sudden drop occurs in the displacement.

Figure 4.24 shows that the damage model prediction and EC3 model prediction look very similar for specimen SP1. The failure temperature predicted by both numerical approaches is 645 °C, which is slightly lower than 678 °C reported in test. The discrepancies observed may be attributed to possible experimental errors and simplified modelling approximations. The inclusion of damage model does not exhibit a major impact in this case, suggesting that the structural response of specimen SP1 is mainly governed by the material temperature-dependency and to a lesser extent the contribution of mechanical damage component. The damage propagation resulting from the coupled thermo-mechanical damage growth is in relatively small scale compared to the size of the specimen SP1.

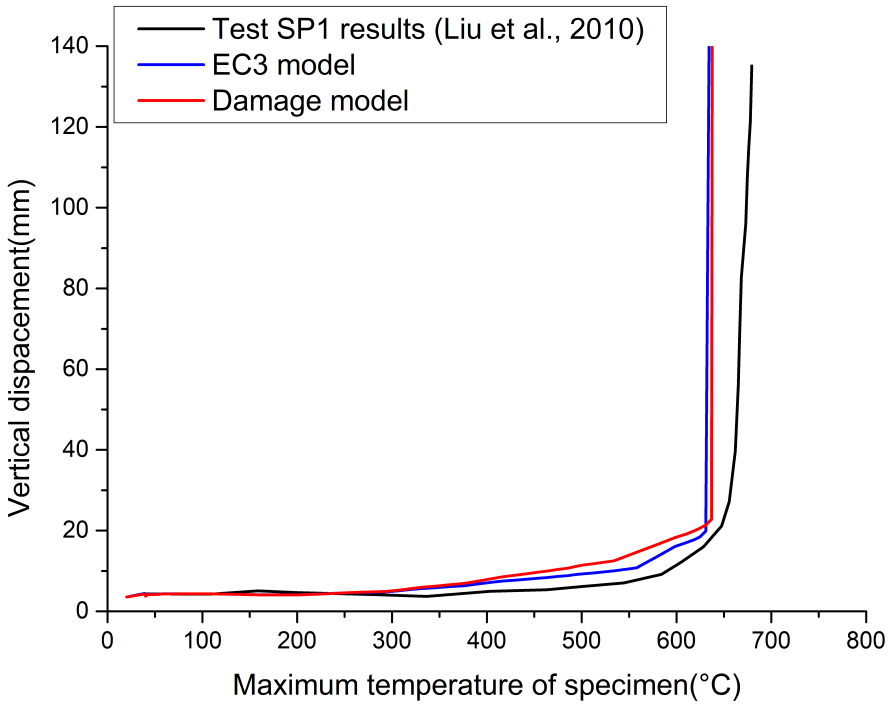

Fig. 4.24 Vertical displacement versus maximum temperature curve of specimen SP1

Figure 4.25 shows a trend similar to that observed in specimen SP1. However, due to a higher level of applied load on specimen SP2, the damage growth and therefore the

deterioration in load-carrying capacity is more pronounced. As a result, the difference between the damage model prediction and EC3 model prediction is more distinguishable in specimen SP2 than in specimen SP1. The proposed damage model provides an excellent prediction of failure temperature which is identical to the test finding and the predicted displacement matches the test results closely up to the failure temperature. On the other hand, the EC3 model overestimates the failure temperature of the steel truss considerably. This again shows that the coupled effects of mechanical damage and thermal damage are more evident under high load levels.

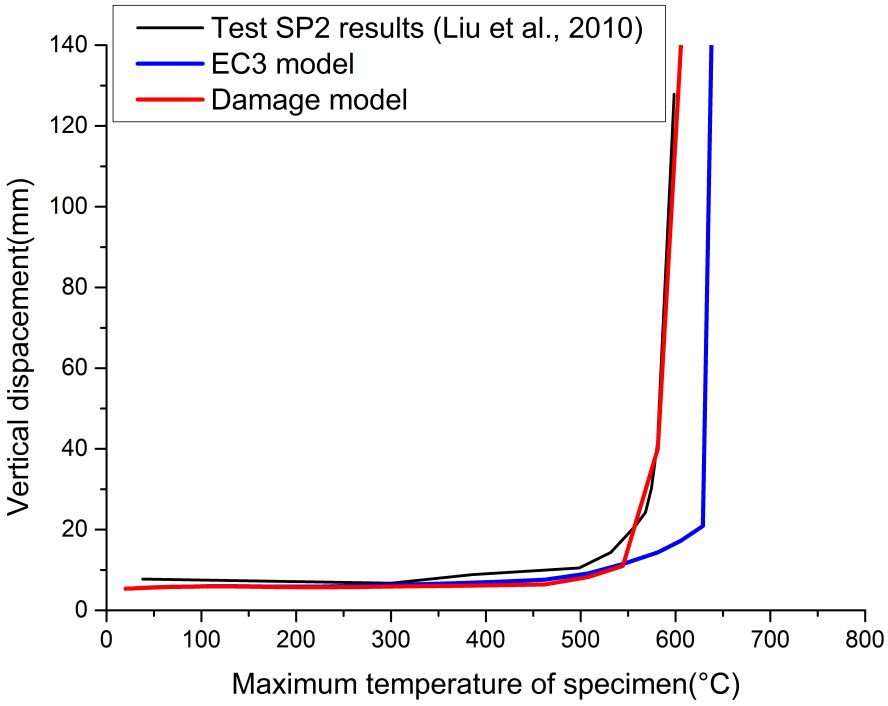

Fig. 4.25 Vertical displacement versus maximum temperature curve of specimen SP2

4.3 Calibration and validation with fire tests and analyses of steel frames

The previous section has dealt with calibration and validation at the component and assembly level. Computational results obtained with the proposed damage model correlate well with experimental results for a wide range of problems, including steel beams, steel beam-to-column connections, and steel tubular trusses. This makes it reasonable to extend the validation study of steel components and assemblies to larger model of steel frames.

It is observed from the previous section that the procedure adopted allows for adequate derivation of damage model parameters despite the lack of coupon test data. An array of values are initially proposed for the parameters across the possible solution range in the identification process. Optimum solution is obtained through updating the magnitude of each parameter in a series of simulations until the closest fit to experimental results is obtained. It is important to note that the choices of coefficient m and k account for the different contributions of mechanical damage process and thermal damage process to the global damage development, and different combinations of these model parameters can be chosen to obtain the desirable type of coupled damage growth. The damage model predictions match the experimental results fairly well, and the calibrated parameter sets are found to depend considerably on the heating rate range. This makes it reasonable to categorize the calibrated damage parameters based on the heating rate (Table 4.8), which permits applying the proposed damage model to different types of structural fire engineering. It is worth mentioning here that the fact that values of coefficient m and k vary considerably between two sets does not affect the model's capability to describe the material deterioration behaviour. This is because it is the combining action rather than the respective value of the parameters that controls the shape of the coupled damage evolution. These two parameter sets are used throughout all the simulations, and the validity of the calibrated damage model is further examined in this section through comparison with experimental results and established numerical studies on steel frames.

Table 4.8 Calibrated damage parameters

Heating rate	Damage parameters							
	S	P_d	a	b	c	r	m	k
>10°C/min	1.72E+05	0.01	2.81	-1027	-20	0	9.63	4
$\leq$ 10°C/min	4.75E+05	0.004	1.952	-837.323	-20	0.613	3.01	0.248

Thus, this section starts with validations of two-dimensional simple frame systems subjected to fire loading. After this, the validation attempt is supplemented by extending the scope to integrated explosion and fire analysis of steel frames. In addition to two-dimensional frame analysis, the validation study is further completed by simulating complex three-dimensional structural system tested in Cardington fire test 7. This series of validation study is anticipated to lay the foundation for carrying out blast and fire analysis on three-dimensional steel buildings in a subsequent case study.

4.3.1 Scaled steel frame fire test (1986)

Rubert and Schaumann (1986) conducted a series of fire tests on 1/6-1/4 scale plane steel frames. All members were made of IPE 80 sections with grade St 37 steel ($\sigma_y = 240N/mm^2$). Three structural configurations were investigated, with EHR standing for

two-bar frames, EGR for simply supported single span frames, and ZSR for two-bay frames. Figure 4.26 shows the schematic test arrangements. Out-of-plane deformations were prevented by adequate bracing. In the first and second test series, all members were heated uniformly except beams were kept cold in EGR7 and EGR8. In the third test series, only the left bay of frame was fully heated with the remaining two members kept at room temperature.

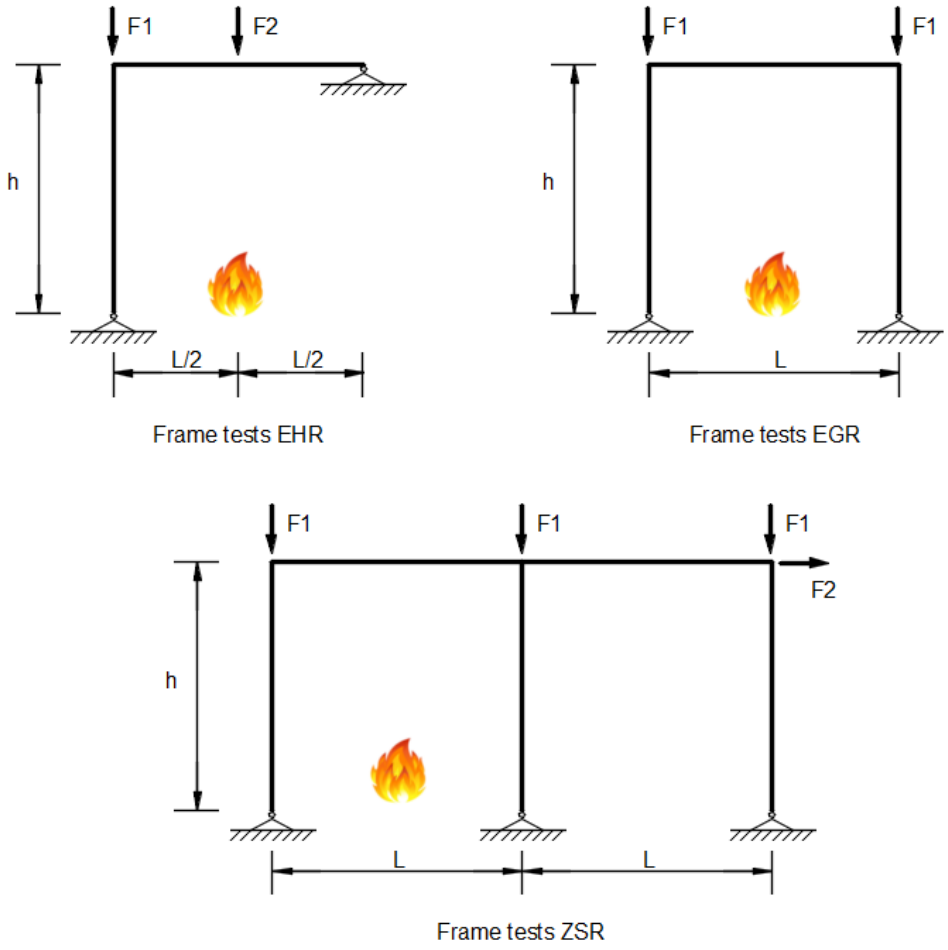

Fig. 4.26 Configurations of scaled steel frame tests (Rubert and Schaumann, 1986)

The dimensions and load magnitudes of the fire tests performed are summarized in Table 4.10. Numerical simulations of the tests are carried out in ABAQUS with the proposed damage model, using 10 beam elements for each structural member. The damage parameter input is presented in Table 4.9. Table 4.10 gives the critical temperatures predicted by the proposed damage model in comparison to test findings in Rubert and Schaumann (1986) as well as ADAPTIC predictions by Izzuddin et al. (2000). The critical temperatures are defined as the temperature at which large structural deflections initiate.

Table 4.9 Damage parameters input for fire analysis of plane steel frame

S	P_d	a	b	c	r	m	k
4.75E+05	0.004	1.952	-837.323	-20	0.613	3.01	0.248

Table 4.10 Test parameters and results of the frame tests

System	l	h	$F1$	$F2$	Critical temperature(°C)			Error	
	(cm)	(cm)	(kN)	(kN)	Test	ADAPTIC	Damage	ADAPTIC	Damage
EHR1	119	117	56	14	600	620	584	3.33%	2.67%
EHR2	124	117	84	21	530	542	519	2.26%	2.08%
EHR3	124	117	112	28	475	452	456	4.84%	4.00%
EHR4	125	150	20	5	562	529	523	5.87%	6.94%
EHR6	125	150	27	6.7	523	417	433	20.27%	17.21%
EGR1	122	117	65	2.5	515	489	472	5.05%	8.35%
EGR2	122	117	40	1.6	612	599	589	2.12%	3.76%
EGR3	122	117	77	3	388	387	360	0.26%	7.22%
EGR4	122	117	77	3	424	417	441	1.65%	4.01%
EGR6	122	117	88	3.4	350	293	315	16.29%	10.00%
EGR7	122	117	68.5	2.6	454	426	442	6.17%	2.64%
EGR8	122	117	77	3	464	423	442	8.84%	4.74%
ZSR1	120	118	74	2.85	547	514	523	6.03%	4.39%
ZSR2	120	118	84.5	3.25	479	464	489	3.13%	2.09%
ZSR3	120	118	68.5	2.64	574	579	565	0.87%	1.57%

The damage model predictions remarkably agree with those obtained from tests for all three configurations. Overall, the damage model parameters give excellent fits to the experimental behaviour. The relatively poor quantitative agreement between the test results and damage model prediction in the case of EHR6 and EGR6 is probably due to less representative input data employed in simulations. It is worth noting that in most of the cases the damage model predictions show smaller discrepancy than ADAPTIC predictions with respect to test results. This indicates that the damage model approach compares favourably with the existing numerical approach in terms of predicting the critical temperature for simple steel frames.

4.3.2 Three-storey steel frame subjected to explosion and fire (2000, 2004, 2005)

Moving on now to consider applying the damage model approach to integrated analysis of steel frame structures subjected to explosion loads followed by fire. This problem has been numerically analyzed by Izzuddin et al. (2000) and Liew and Chen (2004) using beam element approach, as well as by Chen and Liew (2005) using mixed element approach. This subsection attempts to offer a comprehensive comparison of the proposed damage model approach to other established numerical results on the subject of blast and

fire analysis. Figure 4.27 shows the schematic configuration of a three-storey planar frame with the first floor side compartment subjected to explosion and fire loads. The frame is restrained from out-of-plane displacements. Ambient-temperature steel properties are $E = 210,000 N/mm^2$ and $\sigma_y = 399 N/mm^2$.

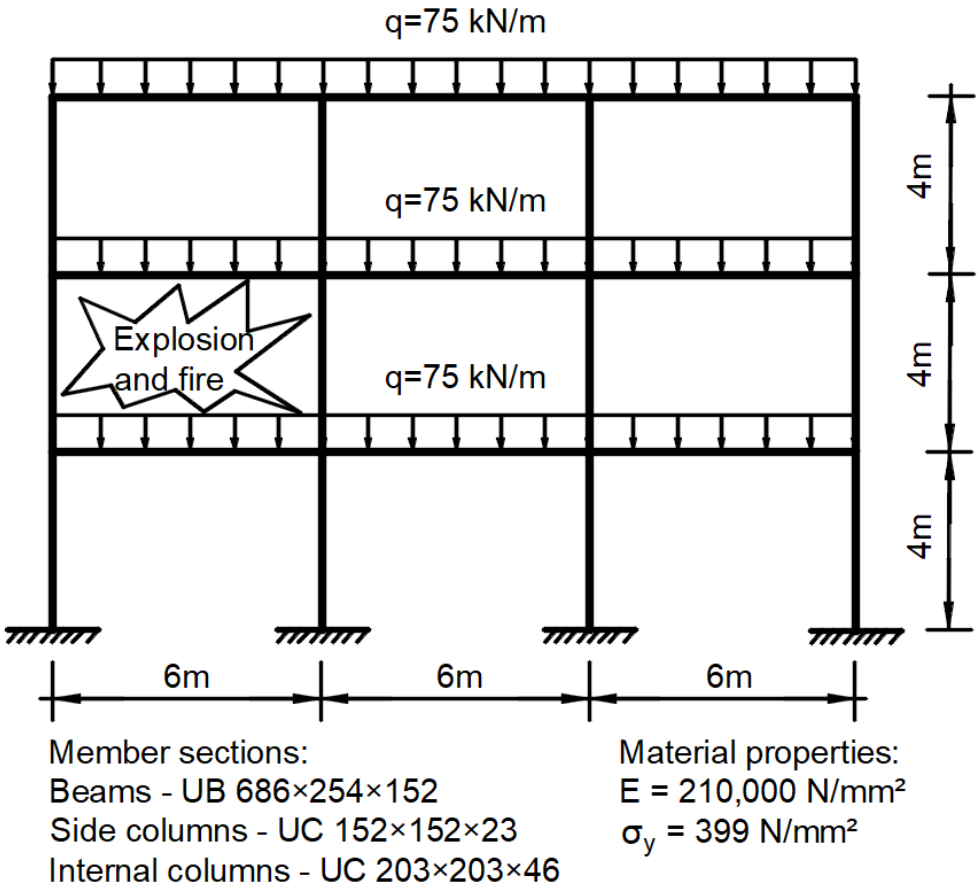

Fig. 4.27 Geometric configuration and loading of three-storey steel frame (Chen and Liew, 2005; Izzuddin et al., 2000; Liew and Chen, 2004)

Loading scenarios and load sequences

In order to investigate the impacts of blast loading on the fire resistance of steel frame, three loading scenarios are considered: (1) frame subjected to blast loads only, (2) frame subjected to fire loads only, and (3) frame subjected to blast loads followed by fire. The integrated explosion and fire analysis of the steel frame consists of three load sequences as illustrated in Figure 4.28.

An initial vertical load of 75 kN/m is applied to the steel frame in the first step. This is followed by applying a uniformly distributed overpressure $P(t) = p_0 p(t)$ to the member surface of the steel columns and beams in the side compartment on the first floor. p_0 is the

peak pressure and $p(t)$ is the predefined overpressure time-history, given by a triangular pulse with a rise time of 120 *ms* and a total duration of 150 *ms* (Figure 4.29) . The effects of the blast loads on the concrete slab and walls are neglected in the two-dimensional analysis on steel plane frames. For the explosion analysis, damping is considered to have minor effects on the fundamental response peak and therefore ignored (Liew and Chen, 2004).

In the third step, the temperature rise T in fire compartment is modelled as monotonic increase from room temperature until failure. Assuming that the side column is fire protected and the lower beam is not affected by the temperature rise, Figure 4.28 shows the temperature variations across the steel sections in the fire compartment in terms of the temperature parameter T. The temperature distribution is assumed to be uniform along the member length and linear across the section depth.

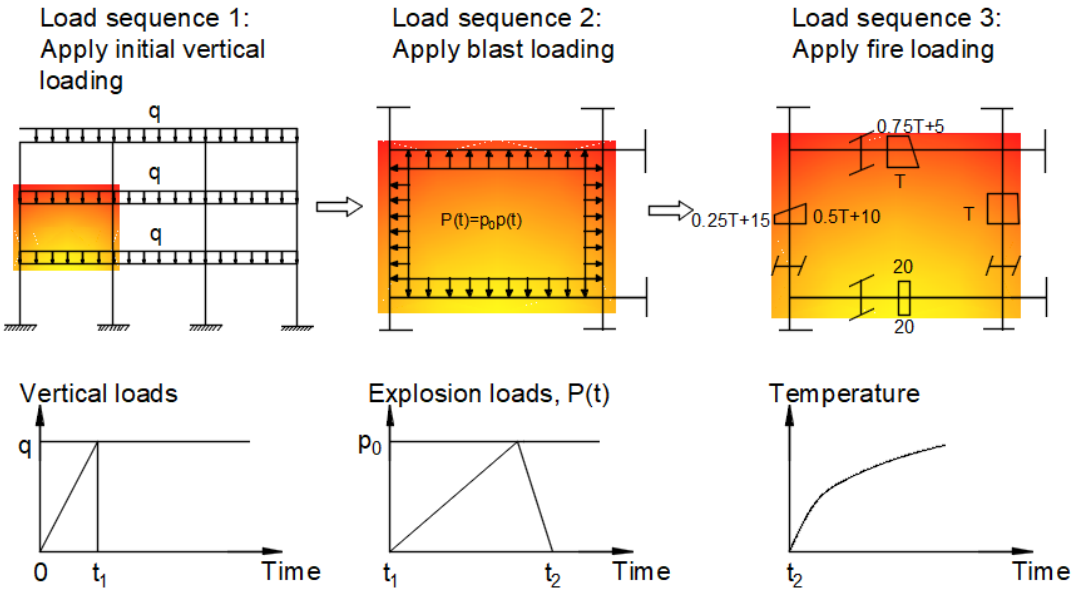

Fig. 4.28 Load sequences in explosion and fire analysis

Introducing rate-dependent material model

It has been widely reported that the mechanical material properties of steel exhibit dependency on the strain rate. The short duration of explosion loads indicates that there is a substantial difference in the material behaviour compared to under static loading. The yield strength of steel can be noticeably increased by high strain rates due to material damping, while the elastic modulus generally remains insensitive to the loading rate (Yandzio and Gough, 1999). To capture the effects of high strain rates that are induced by blast loads, the material constitutive model need to take into account rate dependency

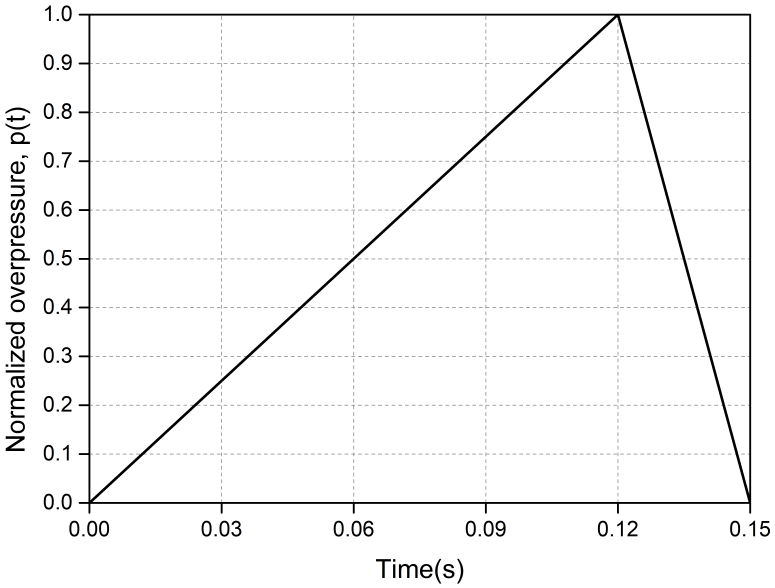

Fig. 4.29 Variation of normalized overpressure over time (Chen and Liew, 2005)

based on the model proposed by Perzyna (1966):

$$\sigma_y^{'} = \left[1 + \left(\frac{\dot{\varepsilon}_{pl}}{\gamma}\right)^{m}\right]\sigma_y \tag{4.1}$$

where $\sigma_y^{'}$ is the dynamic yield stress, $\dot{\varepsilon}_{pl}$ is the equivalent plastic strain rate, m is the strain rate hardening parameter, γ is the viscosity parameter, and σ_y is the static yield stress. The suggested values for the rate-sensitive parameters at room temperature are $\gamma = 40s^{-1}$ and $m = 0.2$ (Bodner and Symonds, 1960; Izzuddin and Fang, 1997). After the explosion load ceases, the rate-dependent effect should be ignored under the subsequent fire loads. This is achieved by assigning $\gamma = 400s^{-1}$ and $m = 1.0$, which leads to a static solution (Chen and Liew, 2005).

This rate-dependent component is integrated into the proposed damage model in an attempt to adequately describe the steel behaviour in the integrated explosion and fire analysis. While a number of studies have investigated the material behaviour under high-rate loading (Børvik et al., 2001; Dowling and Harding, 1967; Lee and Liu, 2006), there is limited research on the combined effect of the high-rate loading and temperature rise on material degradation. Bonora and Milella (2001) presented a non-linear damage model by incorporating strain rate and temperature effect, supported by the experimental data obtained at low strain rates. Mirmomeni et al. (2015) performed tensile tests on mild steel under high strain rate loading and various temperature conditions. Results indicated that it is necessary to develop material models that accurately reflect the material damage induced by high strain rate loading and subsequent temperature rise. Well known rate-dependent material models such as the Johnson-Cook model (Johnson

and Cook, 1985) used in FE packages considers material dependence of strain rates while the effect of elevated temperature on the constitutive relationships is accounted for through recommendations by design codes (EN 1993-1-2, 2005). In this study, the representation of blast-induced damage is simplified through association with the irreversible plastic deformation induced by high strain rate loading. The damage growth is assumed to remain inactive during the blast analysis. At the end of the blast load step, the damage formulation calculates the accumulated mechanical damage based on the permanent structural deformation induced by blast loads. The computed damage at the Gauss point for each finite element is thereby passed into the subsequent fire analysis as initial damage, which is a crucial component of the subsequent coupled thermo-mechanical damage growth.

It is anticipated that the modified damage model is capable of reproducing blast induced damage and at the same time refraining from the complexity and uncertainty of addressing stages of dynamic damage development. Postulating that the heating rate is higher than 10°C/min, the damage model data input is described in Table 4.11.

Table 4.11 Damage parameters input for explosion and fire analysis of three-storey steel frame

S	P_d	a	b	c	r	m	k
1.72E+05	0.01	2.81	-1027	-20	0	9.63	4

FE analysis using beam element approach

First, and for validation purpose, numerical simulations are undertaken for the three aforementioned loading scenarios using beam element approach. Figure 4.30 shows the FE mesh of the steel frame in which 13 elements are used for column members and 20 elements are used for beam members. It is concluded from the mesh sensitivity study that this is a reasonable choice regarding both numerical accuracy and computational efficiency.

Frame subjected to blast loads only The explosion analysis is carried out with the proposed damage model in order to validate its predictive capabilities in terms of steel mechanical behaviour under blast loads. Figure 4.31 presents and compares the responses of the steel frame subjected to different intensities p_0 of blast loads. The displacements predicted by the damage model are very similar to the published results of Liew and Chen (2004), suggesting that the proposed damage model is perfectly capable of simulating the structural responses in explosion analysis. It can be seen from the graph that when $p_0 > 310\ kN/m$, the vertical displacement at the top left corner of the frame increases

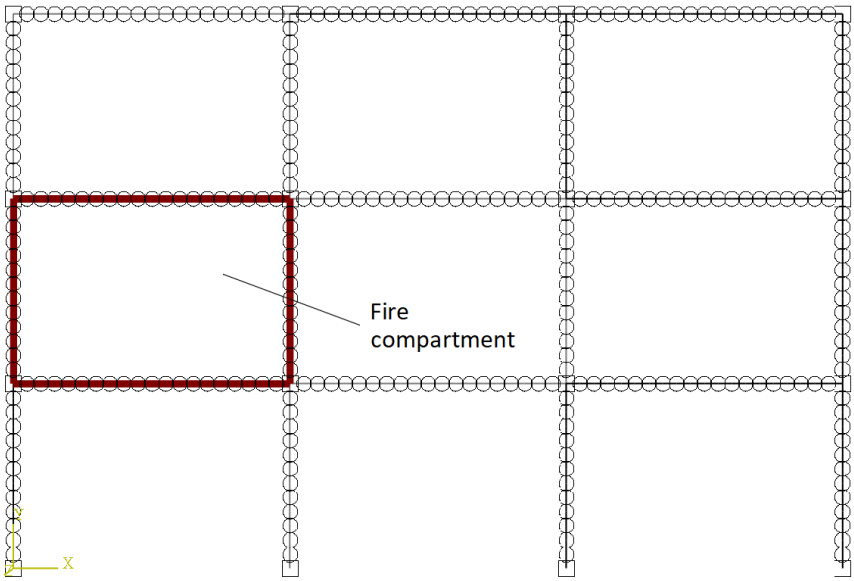

Fig. 4.30 FE beam element model of three-storey steel frame

uncontrollably, signifying the initiation of the structural collapse. Therefore, the blast resistance of the steel frame in terms of the peak overpressure is taken as 310 kN/m. The overall structural failure is found to be triggered by the instability of the side column, which is the most vulnerable member in the frame system under blast loads due to its smaller section stiffness and weaker rotational end restraints. Figure 4.32(b) shows the collapse mode of the steel frame, with the dash lines representing the undeformed shape of the frame. The similarity to the final deflected shape of steel frame reported in Liew and Chen (2004) further confirms that the proposed damage model replicates the structural behaviour under blast loads well and is suitable for use in explosion analysis.

Frame subjected to fire loads only A separate fire analysis is carried out on the steel frame to determine the fire resistance of the frame under fire action alone. Figure 4.33 shows the vertical displacement-temperature history at the top left corner of the frame. In the absence of the explosion loading, the internal column buckles earlier than the side column as a result of higher temperatures experienced. The fire resistance is established in terms of the maximum temperature at which overall structural failure initiates. The critical temperature T_{max} of the frame predicted by the proposed damage model is 810°C. Compared to $T_{max} = 858$°C predicted by Liew and Chen (2004), the damage model approach provides more conservative results. This is attributed to the effects of coupled damage accumulation throughout the fire duration which again demonstrates the capability of the damage model.

Frame subjected to blast loads followed by fire A series of integrated analyses are carried out on the steel frame subjected to various intensities of blast loads and subsequent

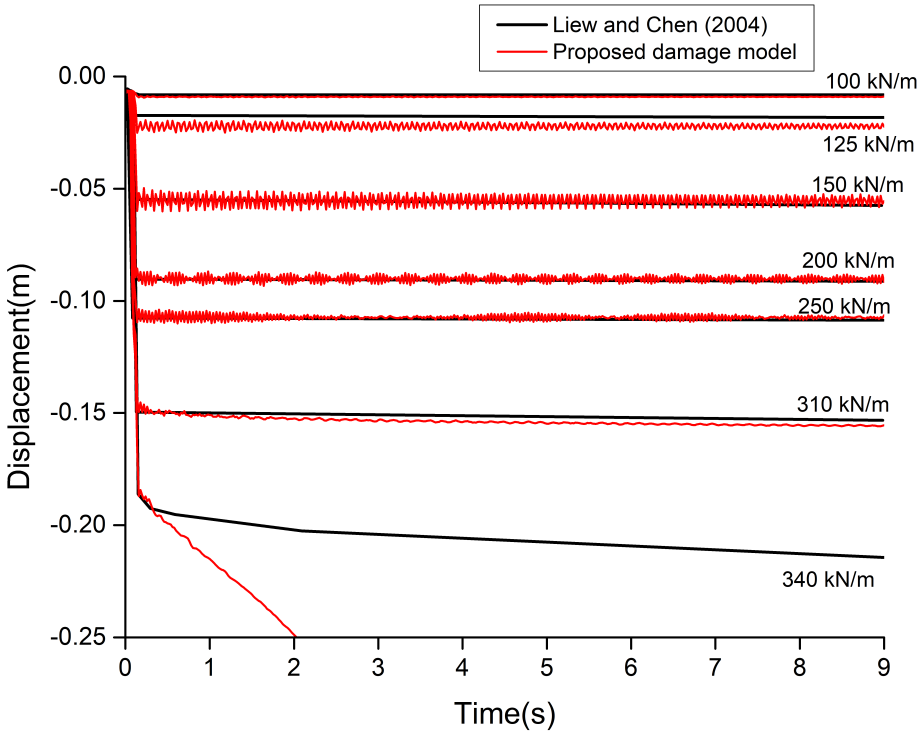

Fig. 4.31 Responses of steel frame under explosion only

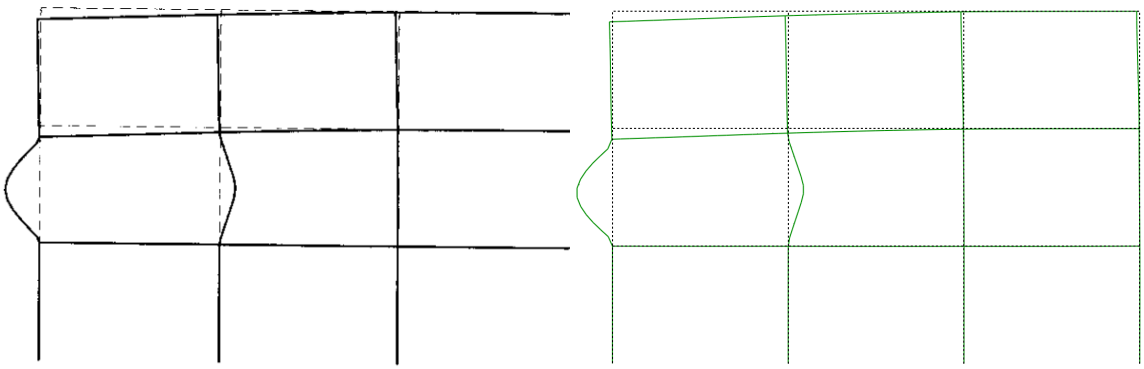

(a) Liew and Chen (2004) (b) Proposed damage model approach

Fig. 4.32 Collapse modes of steel frame under blast loads (displacement scale factor enlarged)

temperature rise. For a given blast intensity (varying from 0 to p_{max}), the corresponding fire resistance is obtained in terms of the critical temperature. The displacement versus temperature curves of the steel frame are plotted in Figure 4.33. The influence of the blast loads are illustrated through obtaining the interaction curve between the normalized fire resistance and explosion loads, as presented in Figure 4.34. It can be seen from the interaction curve that the fire resistance is considerably affected by explosion loading. This is because when the magnitude of blast load increases, the side column experiences intensified damage. As a result, the vertical loads originally carried by the side column

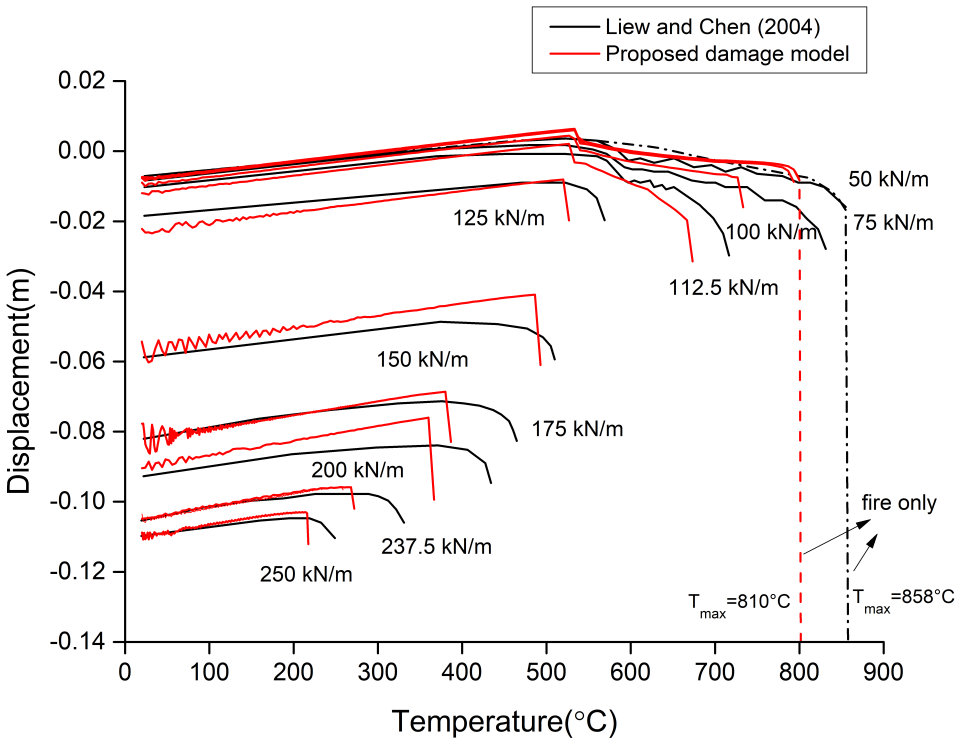

Fig. 4.33 Response of steel frame under explosion and followed by fire

redistribute to the adjacent internal column, leading to earlier failure of the frame system. The overall interaction curve predicted by the damage model is in good agreement with Liew and Chen (2004), except that more severe reduction in the fire resistance is predicted for blast intensities range [$0.5p_{max}$, $0.8p_{max}$]. This illustrates that even when the extent of structural deformation is not severe, the proposed damage model is capable of capturing the initial damage induced by permanent deformation under blast loads and the subsequent thermo-mechanical coupled damage growth as temperature rises. To conclude, the superiority of the proposed damage model is reflected in providing a more conservative prediction of deteriorated fire resistance induced by blast load levels that were considered as not severe in conventional numerical approaches.

FE analysis using mixed element approach

Though computationaly efficient and reasonably accurate, the FE model built using beam elements can not capture local buckling and distortion of the members in structural analysis. Under high blast load level, it is anticipated that local buckling and member instability would occur in the columns of the fire compartment. Therefore, the mixed element approach proposed by Chen and Liew (2005) is adopted in the following analyses.

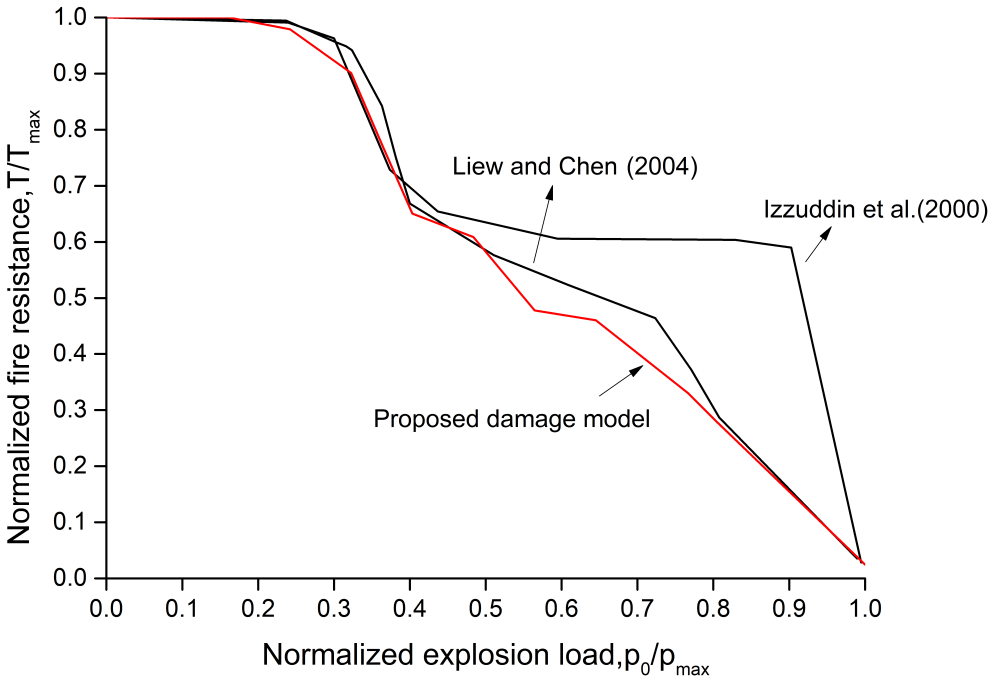

Fig. 4.34 Influence of explosion loads on the fire resistance of steel frame

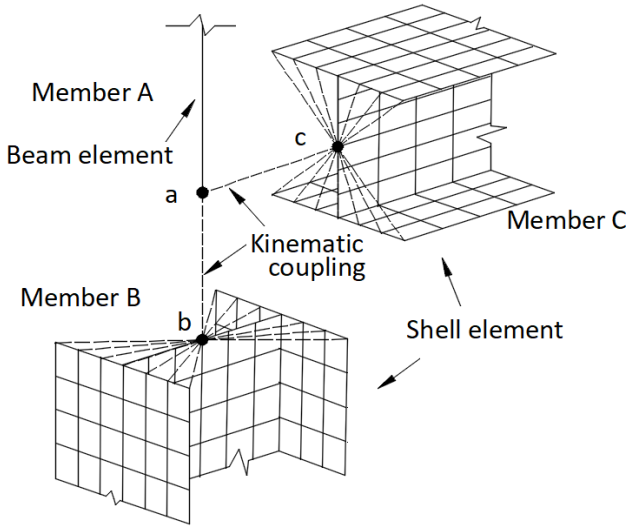

Fig. 4.35 Connecting techniques employed in the mixed element approach (Chen and Liew, 2005)

The structural members in the fire compartment affected by the actions of blast and fire are modelled with refined shell elements S4R. The non-critical members that are not directly subjected to blast and fire are modelled using beam elements B31. Kinematic coupling techniques are used to link these two types of elements. As shown in Figure 4.35, member B and C under direct actions of blast and fire are modelled with refined shell elements, while non-critical member A is modelled with beam element. The end

node a and centroid nodes b and c should in reality be intersected but they are offset at a small distance in simulations for the convenience of assigning different temperature profiles for each member. Centroid nodes b and c act as controlling nodes which kinematically control the displacements and rotations of the end sections of member B and C, respectively. By establishing kinematic coupling between node a, b and c using *MPC type BEAM option in ABAQUS, the degrees-of-freedom of shell element member end sections are rigidly connected to beam element member A. It is presumed that the connections do not fail under blast and fire loads, which is consistent with the assumption made in Chen and Liew (2005).

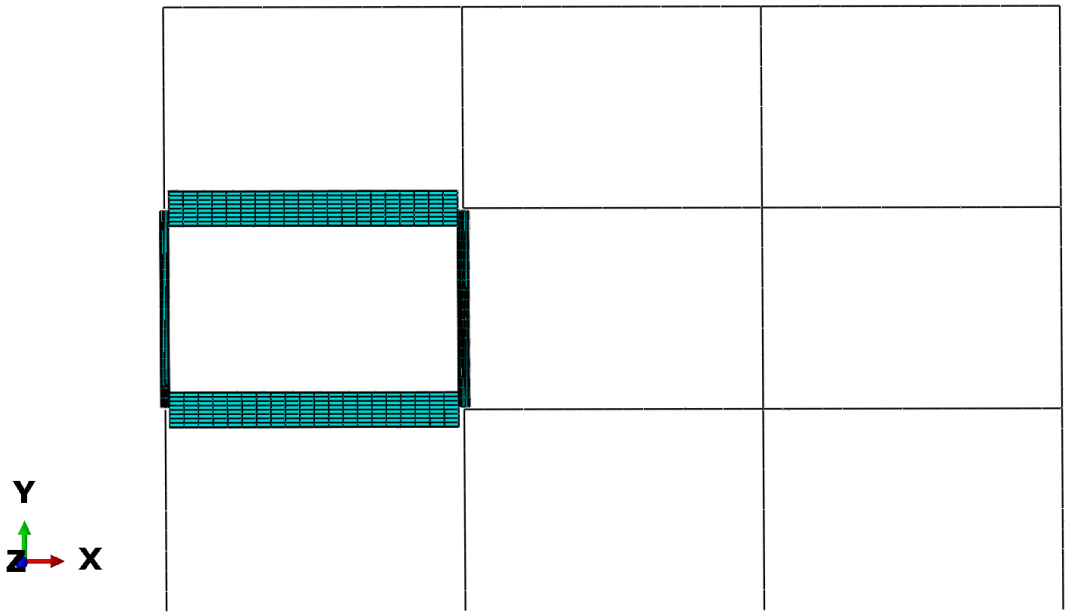

Fig. 4.36 FE mixed element model of three-storey steel frame

Hence this mixed element modelling technique is used for constructing the FE model of the steel frame, as shown in Figure 4.36. Six elements are used across the flange width and through the slab depth of steel sections based on mesh sensitivity study. Along the member length, the critical regions of the members with higher stresses, such as middle and end parts of the columns, are modelled using refined meshes with aspect ratios close to 1.0. On the other hand, coarser mesh sizes are used in the regions with smaller stresses. Again the steel frame is considered under three loading scenarios, as discussed in the following pages.

Frame subjected to blast loads only The explosion analysis is repeated on the FE mixed element model. Figure 4.37 shows the vertical displacements of the top left corner of the frame corresponding to different levels of blast loads. Good agreement is observed between results obtained by the damage model and by Chen and Liew (2005), which demonstrates the capability of the proposed damage model in simulating explosion

analysis using shell elements with an excellent level of accuracy. The blast resistance is obtained as 120 kN/m, which is lower than the previous predictions with beam element model. This observation is in agreement with the findings in Chen and Liew (2005). The final deflected shape of the frame under explosion loads is depicted in Figure 4.38(b). Damage induced by blast is observed to concentrate in the side column. Note that the local buckling in the side column and the collapse mode reported in Chen and Liew (2005) are well reproduced by the damage model, which again confirms its applicability in blast analysis.

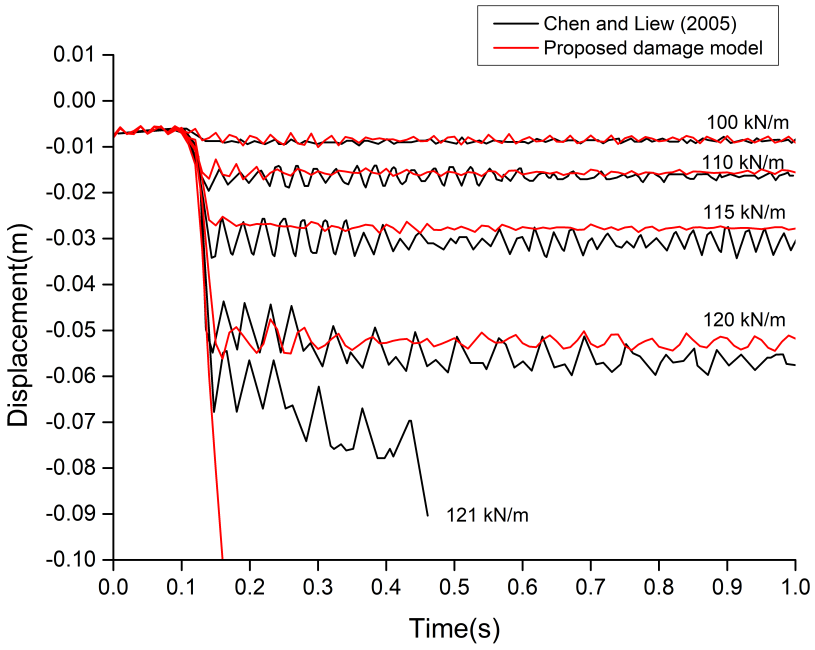

Fig. 4.37 Responses of steel frame under explosion only

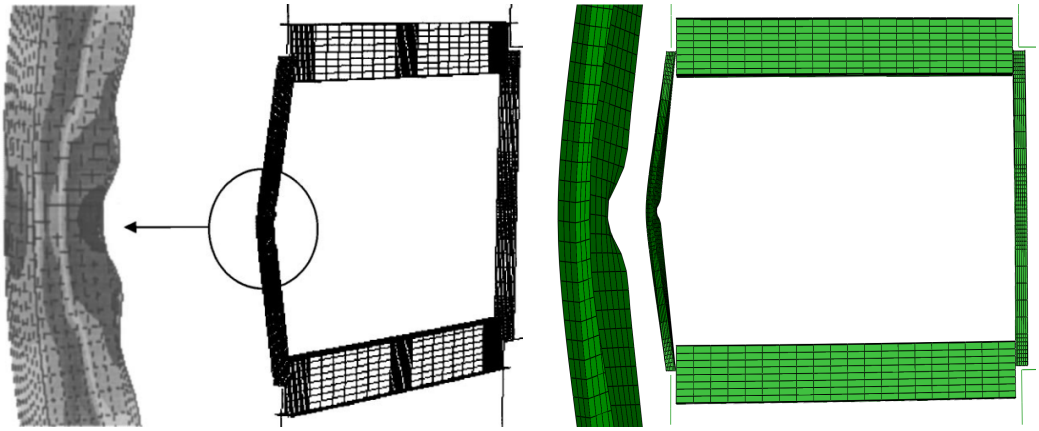

(a) Chen and Liew (2005) (b) Proposed damage model approach

Fig. 4.38 Collapse modes of steel frame under blast loads

Frame subjected to fire loads only Using the mixed element approach, the fire resistance of the frame predicted by the damage model under fire alone is $T_{max} = 574$ °C, which is 29% less than the damage model prediction using the beam element approach. This observation is similar to the 27% difference found by Chen and Liew (2005) between two different types of element approach, which is attributed to the inability of the beam element approach to model local buckling and lateral-torsonal buckling of members. Figure 4.39 compares the displacement-temperature plots obtained by the damage model approach and by Chen and Liew (2005). The overall failure of the frame is assumed to occur when the displacement increases abruptly. It can be seen from Figure 4.39 that the critical temperature predicted by the damage model is 9.4% less than that predicted by Chen and Liew (2005).

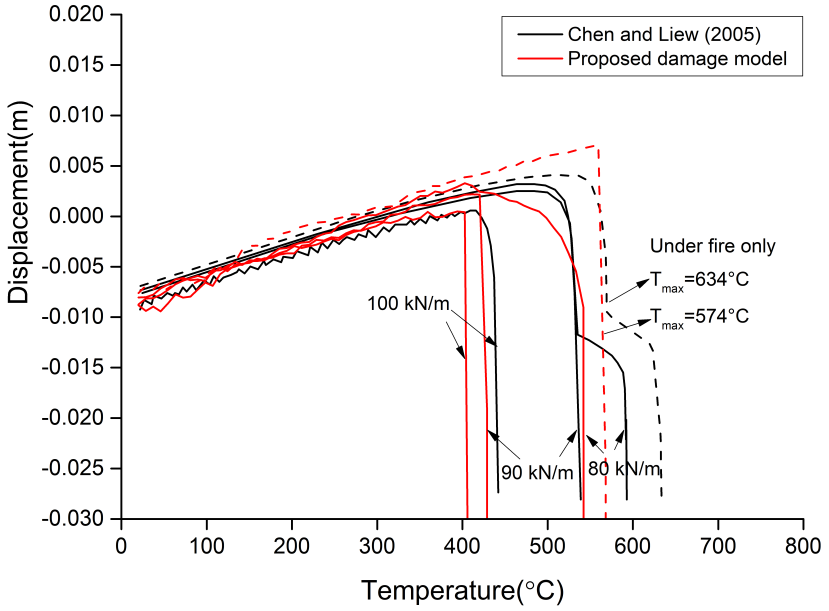

Fig. 4.39 Response of steel frame under explosion and followed by fire

Frame subjected to blast loads followed by fire Moving on now to perform integrated blast and fire analysis on the mixed element model of three-storey steel frame. The blast intensity, or the peak overpressure, is varied over the range [0, p_{max}]. Figure 4.39 shows the responses of the steel frame under different intensities of blast loads and followed by fire. The fire resistance predicted by the damage model at each blast load level is lower compared to Chen and Liew (2005). The extent of the blast induced damage is the main influencial factor in the post-blast fire resistance. The collapse mode of steel frame is presented in Figure 4.40(b), in which both local buckling and lateral-torsional buckling occur in the side column and the internal column. This is consistent with the failure mode reported in Chen and Liew (2005) as depicted in Figure 4.40(a).

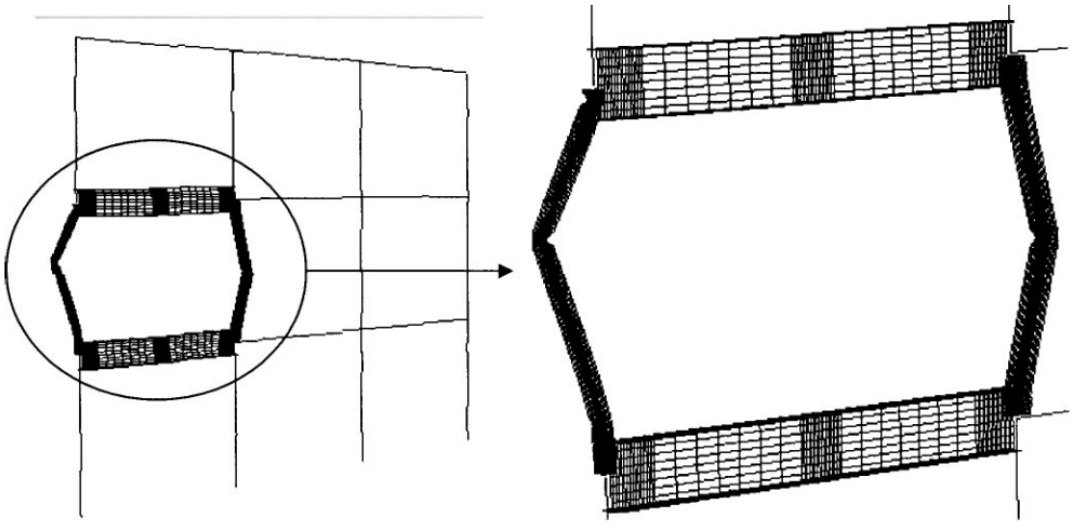

(a) Chen and Liew (2005)

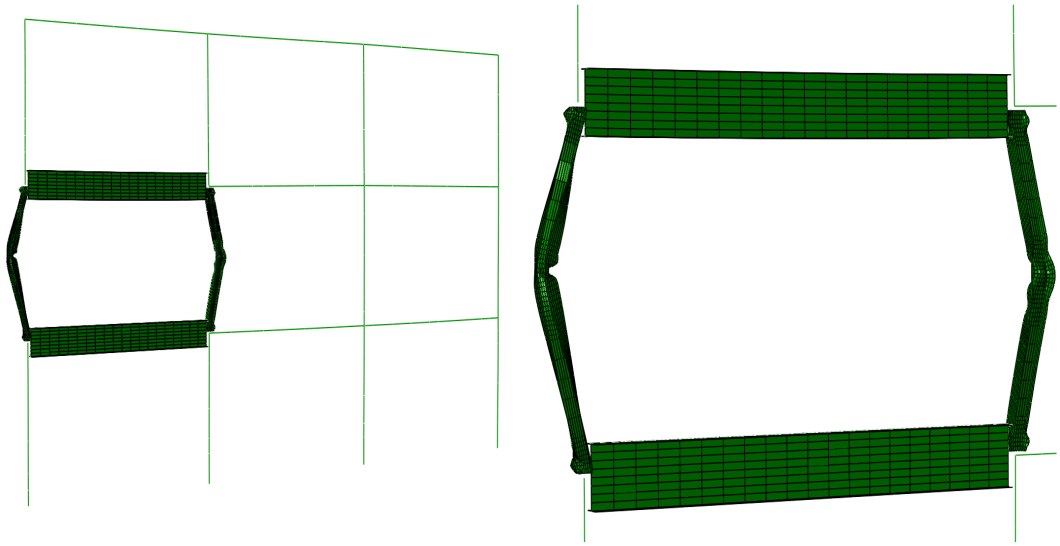

(b) Proposed damage model approach

Fig. 4.40 Collapse modes of steel frame under blast load 90 kN/m followed by fire

The difference in the predicted fire resistance between the damage model and Chen and Liew (2005) is most distinctive at blast load 90 kN/m, with a 15% reduction of the original fire resistance in Chen and Liew (2005) and a 25% reduction in the damage model prediction. The interaction curve between the normalized explosion load and fire resistance is plotted in Figure 4.41. The reduction in fire resistance induced by blast load over the range [$0.7p_{max}$, $0.8p_{max}$] is more severe in the damage model prediction compared to Chen and Liew (2005). This is due to the coupled damage accumulation captured by the proposed damage model as both numerical approaches have taken into account the weakening effect of the post-blast geometry of the damaged frame. This finding illustrates that not only very high overpressure could impose threat to the overall fire resistance. The potential risks of material deterioration that are generally neglected

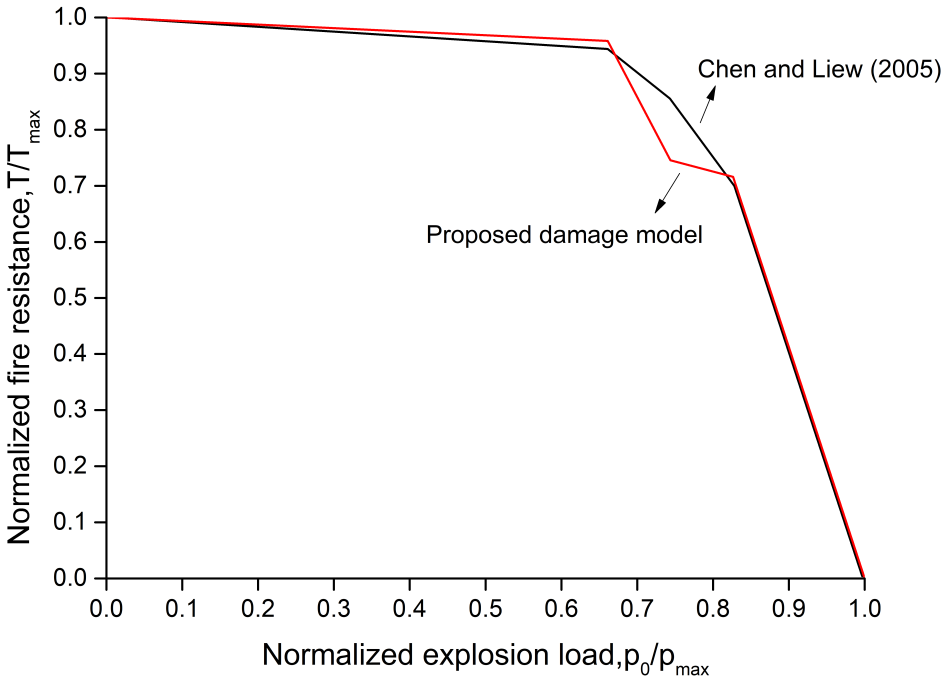

Fig. 4.41 Influence of explosion loads on the fire resistance of steel frame

in conventional numerical approaches can nevertheless be addressed by the proposed damage model.

4.3.3 Cardington fire test 7 (2003)

The previous sections have demonstrated that the proposed damage model can be used with confidence in estimating structural behaviour of two-dimensional steel frames. To further establish the robustness of the damage model approach regarding complex frame systems, the validation study moves to simulating three-dimensional steel frame in Cardington fire test 7. This test has been fully described by Lennon (2003) and also numerically analysed by Foster et al. (2007). The fire test was undertaken on the fourth floor of the eight-storey typical steel office building (fire load on the third floor) in a 11 m by 7 m fire compartment. A schematic plan view of the fire compartment is shown in Figure 4.42. A uniform imposed load of 3.19 kN/m^2 was applied over an area of 18 m by 10.5 m on the fifth floor, which led to a higher load ratio and consequently larger deflections than in the previous six fire tests. The fire load was provided by wooden cribs uniformly distributed within the test area. All columns were protected with CAFCO C300 spray for a 90 minutes standard fire resistance. A short length of the beams in connection to the perimeter columns was also partially spray-protected. The maximum recorded temperature during the fire test was 1072°C for beams and 420°C for columns.

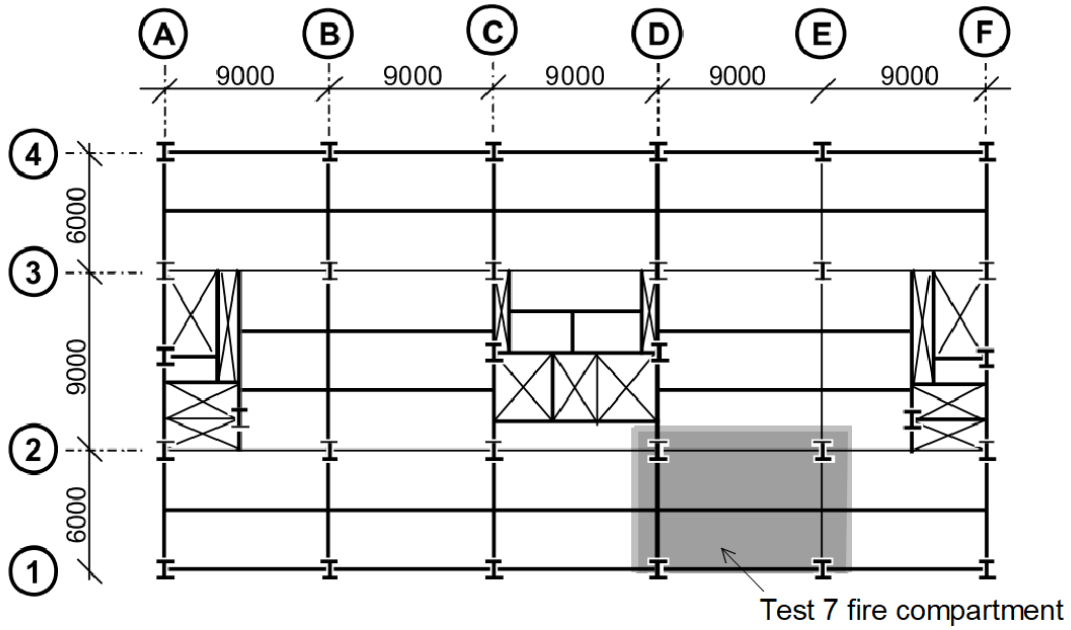

Fig. 4.42 The location of the fire compartment in Cardington fire test 7 (Lennon, 2003)

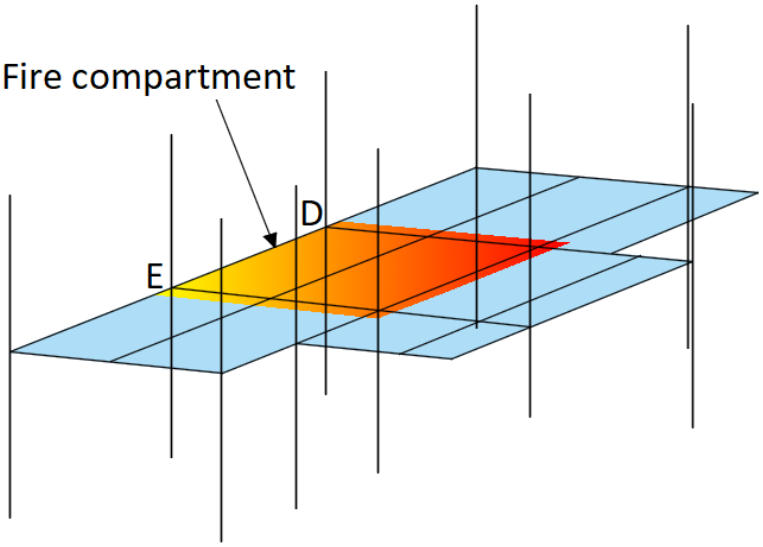

Fig. 4.43 The extent of the structure incorporated within the numerical model

Numerical modelling

Figure 4.43 shows the extent of the structure incorporated within the computational model, which includes the fire floor and the columns of that floor and the floor above. The model encompasses the fire compartment as well as the surrounding cold structure to ensure correct restraint conditions to structural members. Figure 4.44 shows the FE mesh of the fire floor. Fire is assumed to act over the highlighted region from underneath the slab. Appropriate boundary conditions are applied to the FE model based on the test arrangements. The vertical displacement is permitted at the column top while the column base is fixed. The effects of including wind-posts restraints to the edge beam

are discussed by Foster et al. (2007) by differing degrees of restraints at the associated nodes. It is deliberately decided to adopt modelling assumptions close to Foster et al. (2007) in the current study for the purpose of comparing the proposed damage model and the existing numerical approach. Therefore, the effects of wind-posts are modelled by restraining the beam nodes to which the wind-posts are attached against vertical movement, which is consistent with one of the numerical cases in Foster et al. (2007).

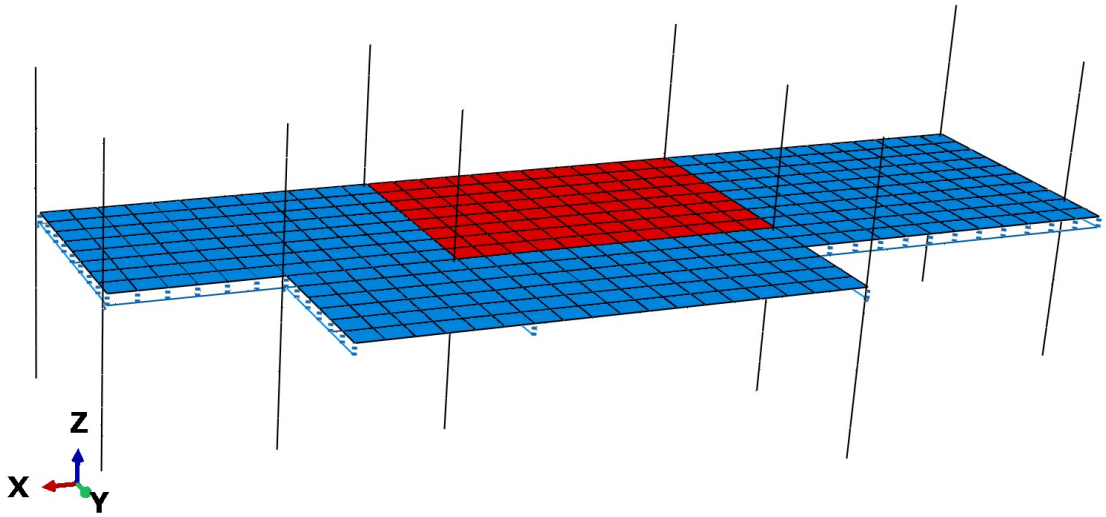

Fig. 4.44 FE model of Cardington test 7 in ABAQUS

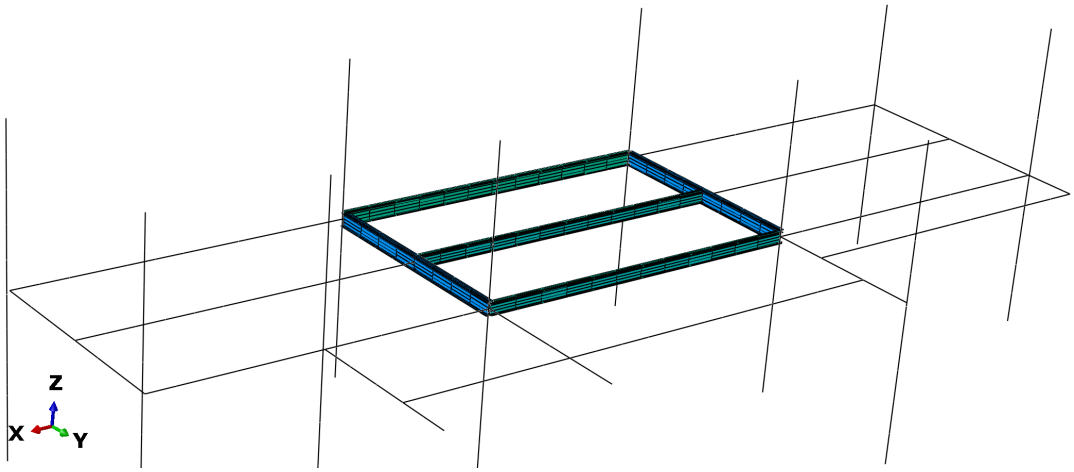

Fig. 4.45 Mixed element modelling approach in Cardington test 7 simulation

The FE model comprises an assembly of beam elements, shell elements, rebar meshes and connector elements. As shown in Figure 4.45, all columns and the ambient-temperature beams are modelled with beam element B31, while the heated steel beams in the fire compartment are modelled with shell element S4R in order to capture local and overall failures. The shell element members are kinematically connected to beam element

members using mixed element connecting techniques described in Section 4.3.2. The 70 *mm* upper continuous portion of slab is modelled using shell element S4R while ignoring the ribs. The slab is offset by a small distance above the top flange of steel beams to ensure that full connection is applied between beams and slab using *MPC type BEAM option in ABAQUS. Beam to column connections and beam to beam connections are modelled by imposing rigid constraints on the displacements and rotations of the associated nodes. Steel reinforcement is modelled as two 0.142 *mm* thick rebar layers embedded in the concrete slab.

Temperature profiles

Each structural member within the fire compartment was heated at a different rate. The fire action is modelled by assigning respective temperature profile for different parts of the heated structure. The recorded temperature histories of the heated beams and columns are presented in Figure 4.46 and 4.47. The structural elements are designated with reference to the grid system. For instance, beam D1D2 spans between gridlines 1 and 2 along gridline D, and beam DE1.5 is the mid-span secondary beam in bay D-E. The slab temperature distribution is approximated by the representation of the temperature gradient divided into 11 layers across the slab depth (Foster et al., 2007), as shown in Figure 4.48. It can be seen that when the bottom layer attains the maximum temperature, the top surface of the slab remains at very low temperature. The temperature of reinforcement, which is located at 55 *mm* below top surface of slab, does not exceed 450°C during the fire. The surrounding cool structure outside the fire compartment is kept at ambient temperature throughout the heating stage.

Material properties

The ambient-temperature material properties for concrete, steel and reinforcement are presented in Table 4.12. The constitutive model of the slab at elevated temperatures adopts stress-strain relationships for concrete from Eurocode 4 (2005), as shown in Figure 4.49. The concrete compressive strength starts decreasing after 300 °C, with the compressive strain and ultimate strain increasing with elevated temperature. Tensile softening behaviour is assumed with zero stresses for full cracking. As for the choice of the damage model parameter input, it can be seen from Figure 4.46 and Figure 4.47 that the heating rate of beams exceeds 10°C/min while the heating rate of columns is considerably lower than 10°C/min in the test. The damage model parameters input is given in Table 4.13.

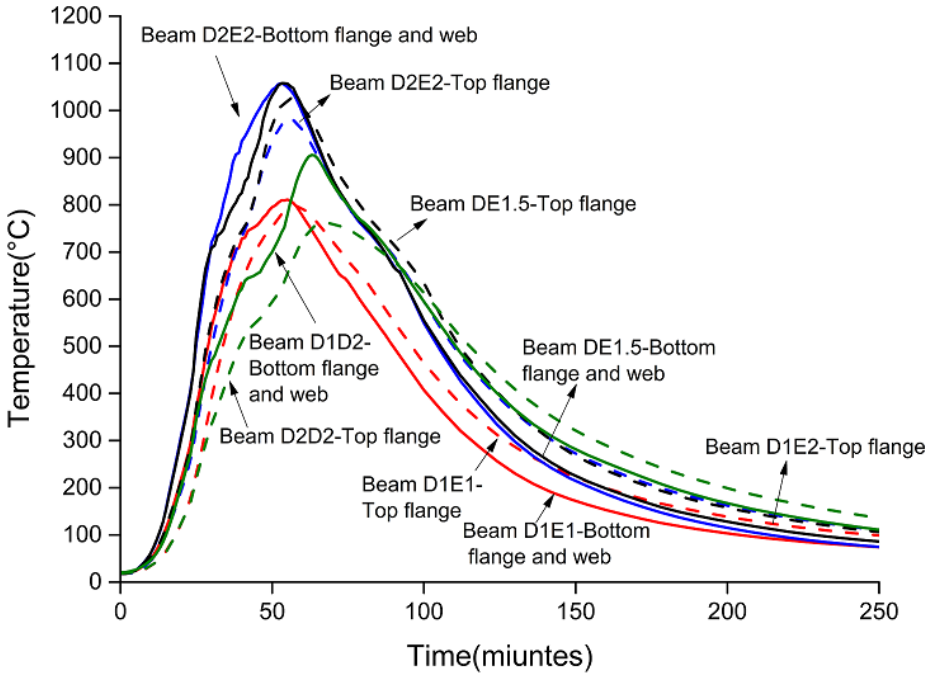

Fig. 4.46 Measured temperature distributions of beams (Lennon, 2003)

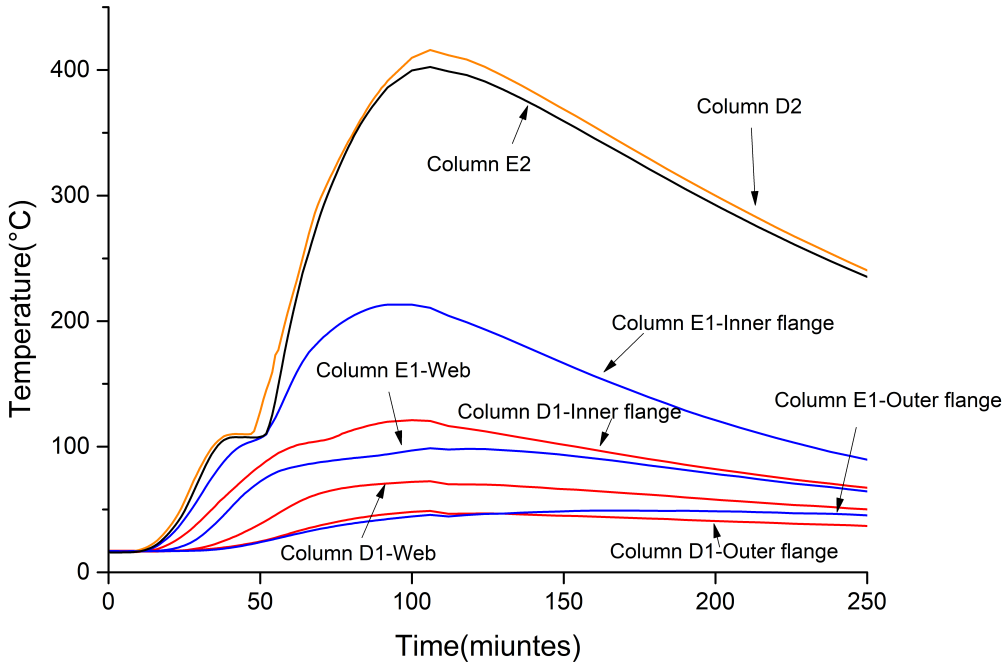

Fig. 4.47 Measured temperatures of columns (Lennon, 2003)

Structural responses

Based on the modelling assumptions and material property representation described above, numerical analysis is carried out on the test frame using the proposed damage

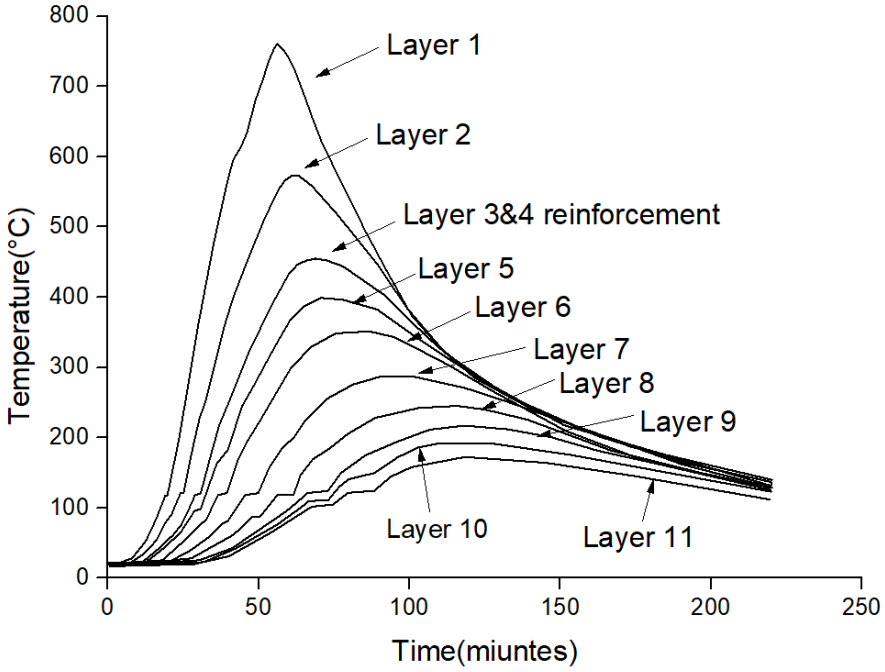

Fig. 4.48 Temperature variation throughout the depth of slab (Foster et al., 2007)

Table 4.12 Ambient-temperature material properties (Lennon, 2003)

Material/Grade	Young's modulus (GPa)	Yield stress (MPa)	Compresive stress (MPa)
Steel/ S275	210	303	
Steel/ S355	210	396	
Reinforcement/ A142 mesh T6@200mm	210	460	
Concrete/ LW35	34		35

Table 4.13 Damage parameters input for analysis of Cardington fire test 7

Structural member	Damage parameters							
	S	P_d	a	b	c	r	m	k
Beams	1.72E+05	0.01	2.81	-1027	-20	0	9.63	4
Columns	4.75E+05	0.004	1.952	-837.323	-20	0.613	3.01	0.248

model. Results are compared with test results reported by Lennon (2003) and numerical predictions by Foster et al. (2007) in order to assess the accuracy of the damage model. The quantities compared are the vertical displacements of slab measured across the centre of the fire compartment from gridline 1 to gridline 2, with the locations of measurements depicted in Figure 4.50. Comparisons of the slab deflection histories between the numerical predictions and test results are plotted in Figure 4.51- 4.54. It should be noted that the loss of the integrity limit state of the concrete slab was recorded by the camera after 54 minutes of fire in the experiment. Such loss of bond between steel and concrete cannot be reproduced in Foster et al. (2007) as well as in the current study. Therefore,

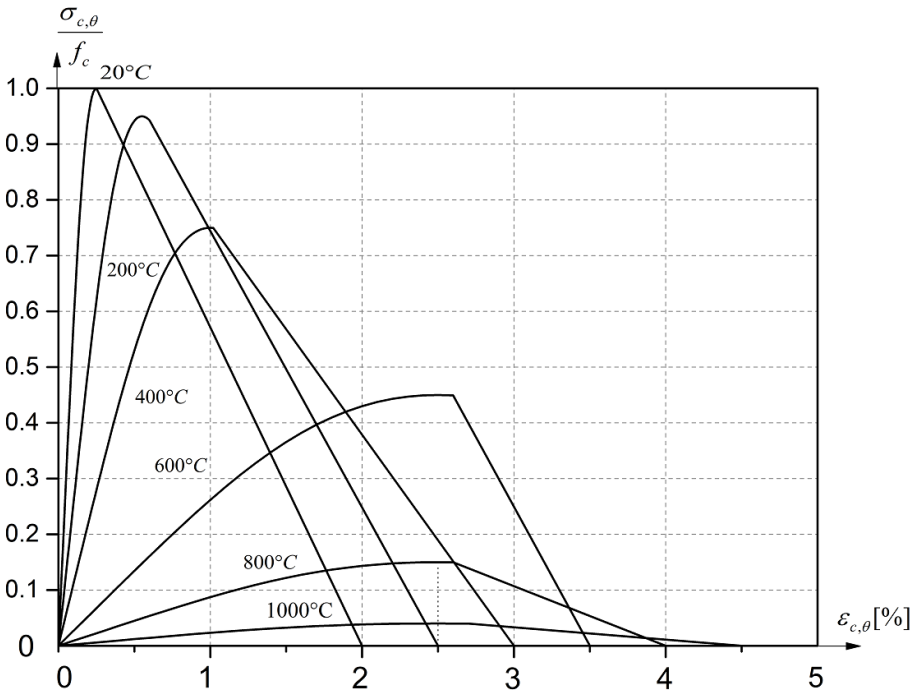

Fig. 4.49 Stress-strain relationships of concrete at elevated temperatures (EN 1994-1-2, 2005)

the comparisons with the experimental measurements are plotted until the last data point at which debonding occurs.

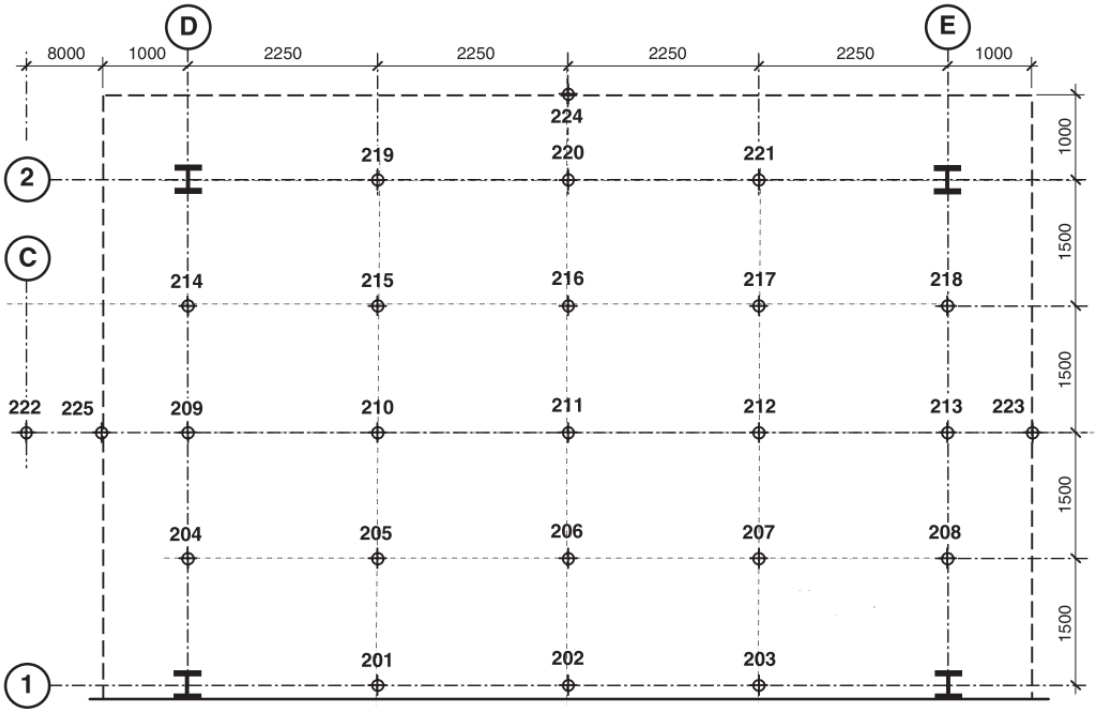

Fig. 4.50 Location of vertical displacements measurements on the fourth floor slab (Lennon, 2003)

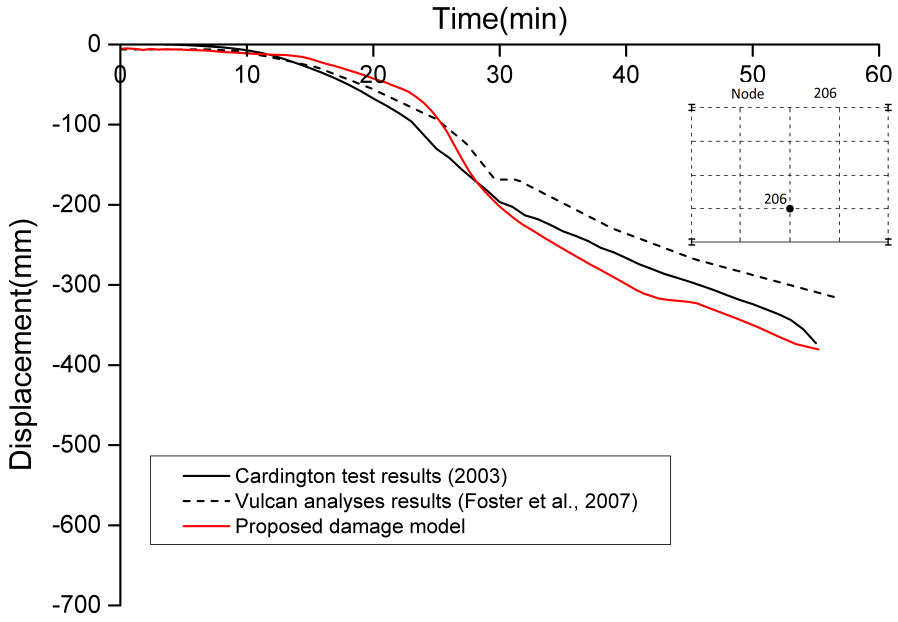

Fig. 4.51 Comparison of displacements at nodes 206 between numerical cases and test

It can be seen that the damage model predictions match the experimental results fairly well over the heating history, suggesting that the damage model has successfully reproduced the complex three-dimensional structural interactions taking place within the frame system. Despite some discrepancies in the early stage of displacement-time history, the predicted displacement pattern in each position is remarkably similar to test results. The discrepancies may be attributed to the inevitable approximation of temperature distribution and boundary conditions adopted in simulations. The results obtained by the damage model also compare favourably with the numerical predictions by Foster et al. (2007). The difference is more pronounced in the later stage as the coupled thermo-mechanical damage accumulates steeply under the combined action of high temperatures and plastic deformation. This highlights the impact that coupled damage accumulation could have on the structural global behaviour.

It is observed that the damage is localised in the fire compartment and the maximum deflection in both numerical predictions and test occurs at node 216. It should be noted that at high temperatures the load carrying capacity of heated beams are severely compromised and the structural response is dominated by tensile membrane action of the composite slab which are at relatively lower temperatures. Hence the structure withstands the severe fire owing to an excellent level of structural redundancy inherent in the composite slab system. The results give confidence that the damage model is capable

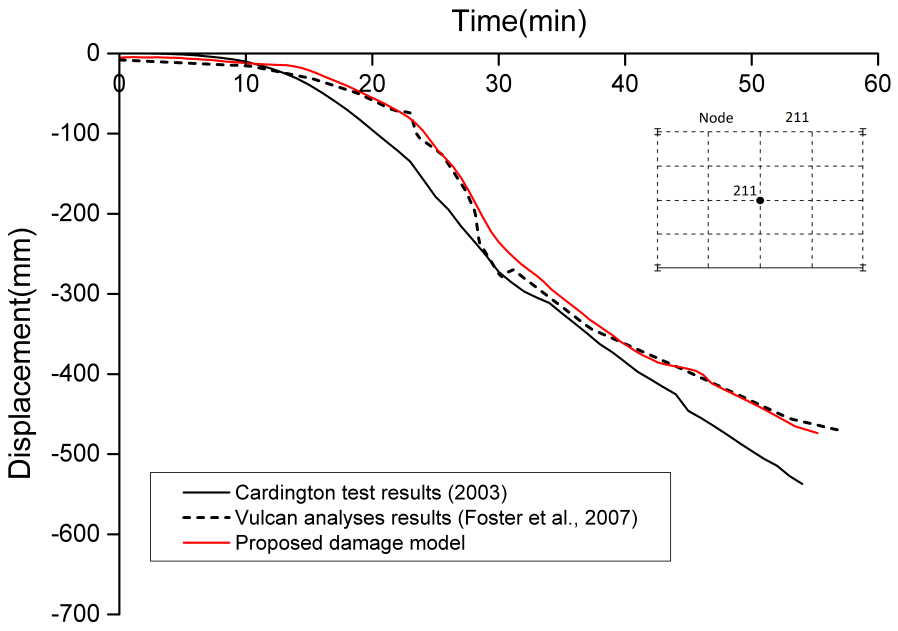

Fig. 4.52 Comparison of displacements at nodes 211 between numerical cases and test

of simulating responses of structural systems subjected to fire where the dynamic load transfer and tensile membrane mechanism are present.

Overall, it can be concluded that the proposed damage model predicts structural response to a satisfying degree and should be incorporated into numerical simulations of steel structures, especially if severe fire and high loads are associated.

4.4 Summary

Thus far, the performance of the proposed damage model is illustrated on several benchmark problems under various states of loading and temperatures. The damage model parameters have been calibrated and verified using an extensive range of analyses on steel structural components and frames. It is observed that the procedure adopted allows for adequate derivation of damage model parameters despite the lack of coupon test data. This inverse analysis type of calibration procedure manages to provide a data collection of damage parameters in support of collapse assessment of steel structural systems. The calibrated data sets are in a consistent format that permits applying the damage model on different types of structural components and frames.

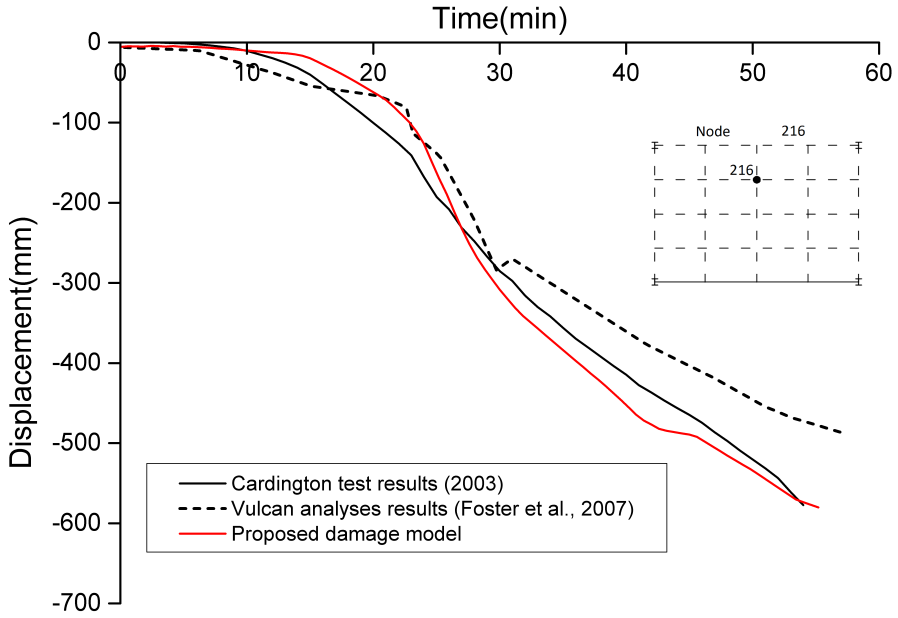

Fig. 4.53 Comparison of displacements at nodes 216 between numerical cases and test

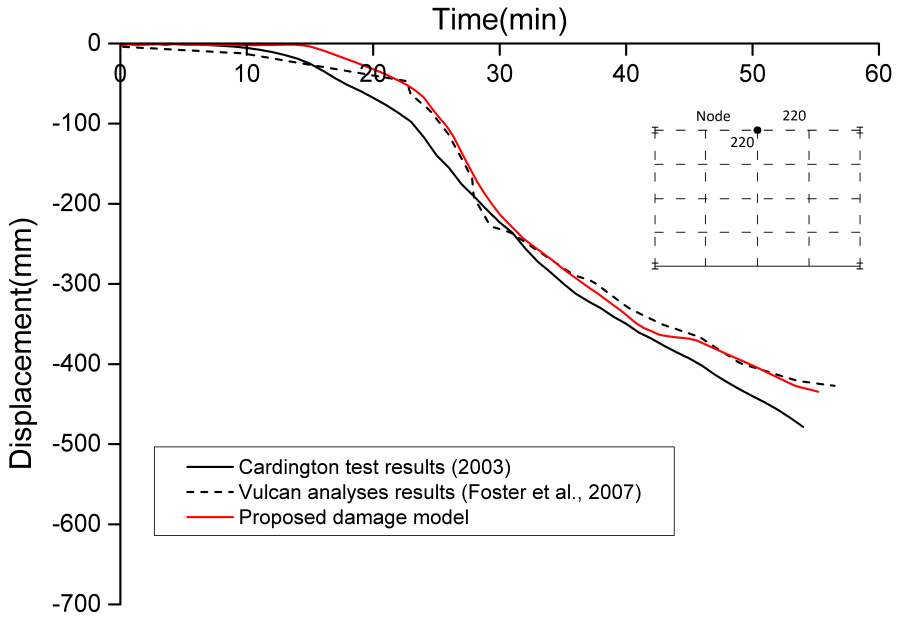

Fig. 4.54 Comparison of displacements at nodes 220 between numerical cases and test

Numerical analyses, performed with the calibrated damage model, demonstrate the consistent and accurate predictive capabilities of the damage model. The calibrated

damage model is shown to provide excellent predictions of the load-displacement behaviour, ultimate failure temperature and failure initiation locations. It can be concluded that the proposed damage model provides an important advancement toward giving a realistic representation of steel deterioration behaviour under combined actions of fire and mechanical loads. Another significant aspect of the damage model is that it proves to be a useful tool to capture the initial damage in structural members induced by blast loads which precede fire analysis. It should be mentioned that this feature is not found in conventional numerical approaches.

One of the advantages with the proposed damage model is that it is fully three-dimensional. Applications of the damage model with a flexible choice of elements, including solid elements, shell elements and beam elements, have been presented in this chapter. It is observed that the damage model's capability to describe stiffness degradation and capacity deterioration is not affected by the choice of elements, so long as mesh sizes are deemed appropriate according to the mesh sensitivity study. It should be noted that the damage model's capability in terms of practical usefulness and numerical robustness has great potential for future works. For instance, practical applications based on solid elements normally include modelling beam-to-column connections. On the other hand, shell elements are superior in simulating buckling behaviour and beam elements are widely used in the analysis of complex structures which might encompass numerous elements.

To summarize, the coupled damage model has been developed, calibrated and validated, which successfully fulfils the purpose of this chapter. It can be concluded that the proposed damage model has a significant contribution in estimating structural behaviour at high load levels and the damage model should be incorporated into numerical simulations even for low levels of loading. Such a model with carefully calibrated parameters could thus be applied with confidence to collapse assessment of large-scale steel buildings in the next chapter. Furthermore, it is recommended that more experimental studies be conducted which will benefit the data collection work of calibrating damage model parameters.

Chapter 5

Studies of low-rise and mid-rise office buildings under blast and fire

5.1 Introduction

A review of the current literature on the subject of fire induced progressive collapse shows that important progress has been made in better understanding the interactive behaviour of structural components in steel frame systems under fire. However, despite this progress, the adequate modelling of the high-temperature material behaviour remains as a significant research need in the field of structural fire engineering. This is due to the inherent complexity and uncertainty concerning steel deterioration, which is hindering reliable numerical evaluations of structural fire resistance (Kodur et al., 2012).

The primary objective of this chapter is to provide assessment of steel buildings under fire loading, or combination of blast and fire loads for the matter of extreme multi-hazards, up to and including collapse. As discussed in Chapter 2, the modelling efforts strongly depend on how well the material behaviour is captured. Therefore, the proposed damage-coupled steel constitutive model is adopted in assessing the susceptibility of steel buildings to progressive collapse in this study. The accurate and conservative predictive capabilities of the damage model approach have been validated in Chapter 4, and therefore it can be used with confidence to predict the vulnerability of steel-framed structures against progressive collapse. It is expected that this study will provide new insight into structural safety under fire, or under combination of blast and fire loads, by taking into account the effects of coupled damage growth in steel.

A five-storey building and a ten-storey building are designed in accordance with the current building codes, representing low-rise and mid-rise office building, respectively.

In order to adequately assess if the robustness requirements are met in the steel building, it is necessary to perform a threat dependent evaluation of the damage extent under accidental loads. Therefore, rather than following notional removal strategy by eliminating individual members, scenario-based fire and explosion analyses are performed in this study. Possible accidental scenarios that might trigger fire induced progressive collapse of the buildings are identified and the case study is divided into three main sections: (i) fire only scenario, (ii) post-blast fire scenario, and (iii) fire-triggered explosion scenario. Apart from the most typical fire hazards, the sequential loading of blast followed by fire as would be seen in some cases of terrorist attacks on buildings (Liew, 2008) is considered. Furthermore, the investigation is extended to post-fire blast analysis, due to the highly likely occurrence of gas explosion in the event of fire. This scenario-dependent assessment intends to provide valuable insight into which type of hazard scenarios are likely to result in an unacceptable level of damage. For each type of scenario, the location of the compartment in which accidental loads occur is also varied, which allows for the assessment of structural responses where collapse is triggered by different locations.

Having identified the possible accidental action scenarios, numerical simulations are carried out in ABAQUS to evaluate the likelihood and consequences of the scenarios. To emphasize the role of damage modelling in collapse assessment, numerical analyses are performed to analyse the behaviour of the office buildings with and without considering damage. Sophisticated three-dimensional FE models of the multi-storey steel-framed buildings with concrete slab system are developed, and the techniques of performing a sequential blast/fire analysis are discussed. In order to understand the performance of the post-attack structures, it is essential to trace the entire response of a steel structure. The extent of damage affected area is assessed and the building's ability to localise the damage is investigated. Failure of a limited part of the structure may be permitted provided that the stability of the whole structure is maintained. Estimation of the ultimate failure time provides a check of the office buildings for satisfying robustness requirements under accidental loading. Based on the identified collapse mechanisms, discussions are given regarding the performance of steel structures and effective strategies are suggested to improve the survivability of buildings under blast and fire.

5.2 Structural design

A low-rise five-storey building and a mid-rise ten-storey building are designed for use as office space. A schematic view of the five-storey building and the ten-storey building is shown in Figure 5.1 and Figure 5.2, respectively. The layout is simpler than Cardington steel frame yet realistic enough to be representative for building behaviour under extreme loadings. The bays are spaced $6m$ along the width and $9m$ along the length of the

building. Each storey is $3.65m$ in height. The building is designed according to EN 1993-1-1 (2005)'s recommended combinations of dead load, live load, wind load and seismic action. The design dead load and live load are $3.65kN/m^2$ and $2.5kN/m^2$, respectively. An additional cladding weight is applied to the perimeter beams, and the design procedure also applies a Eurocode 1 (2005) wind load to the building. The critical fundamental load combination is $1.35G+1.5Q+1.05W$, where G is the dead load, Q is the live load, and W is the wind load. The building is designed to resist earthquake loads with peak ground acceleration of $0.25g$ under the seismic design load combination of $G+0.3Q+E$ (E is the seismic action). In the investigated building, the inter-storey drift sensitivity coefficient is smaller than 0.1 in all storeys in both directions. Therefore, the second-order effects need not be taken into account. The inter-storey drifts are limited to storey height$/300$ for wind loads and storey height$/125$ for seismic loads.

Beams are assumed to act in composite action with the floor system, which consists of an $87.5mm$ concrete slab over a $75mm$ deep ribbed deck. An A142 standard mesh consisting of $6mm$ diameter bars at $200mm$ centres is used for reinforcement. Moment resisting connections are used throughout the structure except that secondary beams are pinned connected to primary beams. The lateral stability requirements are complied with by the use of moment resisting connections. All the columns are oriented with strong axes towards the short span direction to supplement the weak lateral load resistance against earthquake and wind loads in that direction. While the moment connections are modelled as rigid connections in building simulations, it must be noted that care need to be exercised in the actual design of moment connections in which the beams are connected with respect to the minor axis of the column sections. It is expected that the moment resisting connection has appropriate rotational capacity, which enables load redistribution to other parts of structure upon local failures. Therefore, the building is expected to be resilient against accidental loads.

Member section sizes are selected from British Standard W-shaped rolled sections. The steel grade used is S355 which has a characteristic yield strength of $355MPa$. The orientations of the columns are shown in the plan view of buildings. Figure 5.1 shows the member sizes of five-storey building. The section dimensions adopted in the five-storey building design are summarized in Table 5.1, where h, b_f, t_w and t_f represents the height, flange width, web thickness and flange thickness, respectively. The beam sections and column sections of ten-storey building are presented in Figure 5.2 and Table 5.2, respectively, with the section dimensions summarized in Table 5.3.

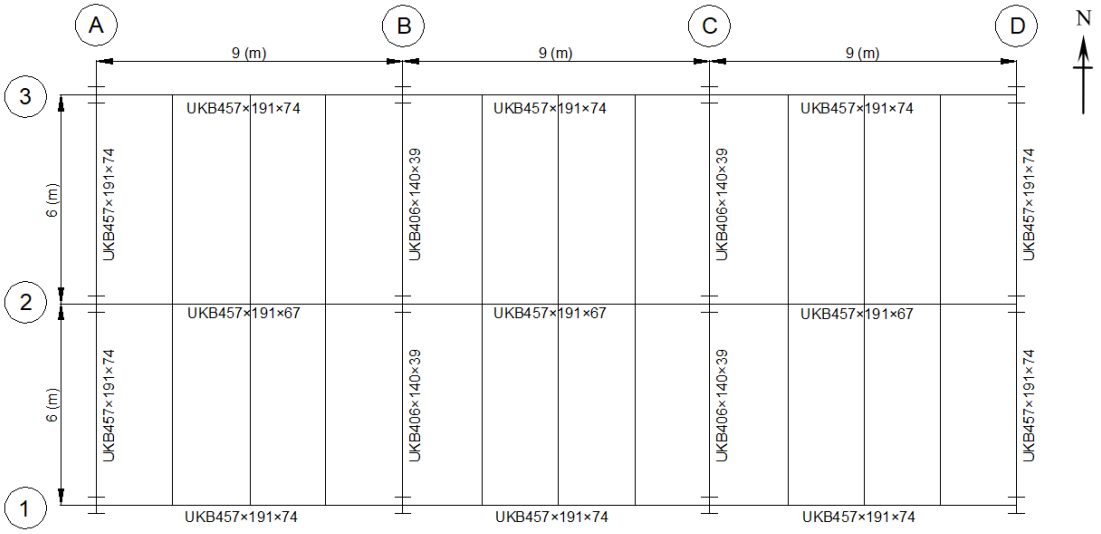

(a) Plan view

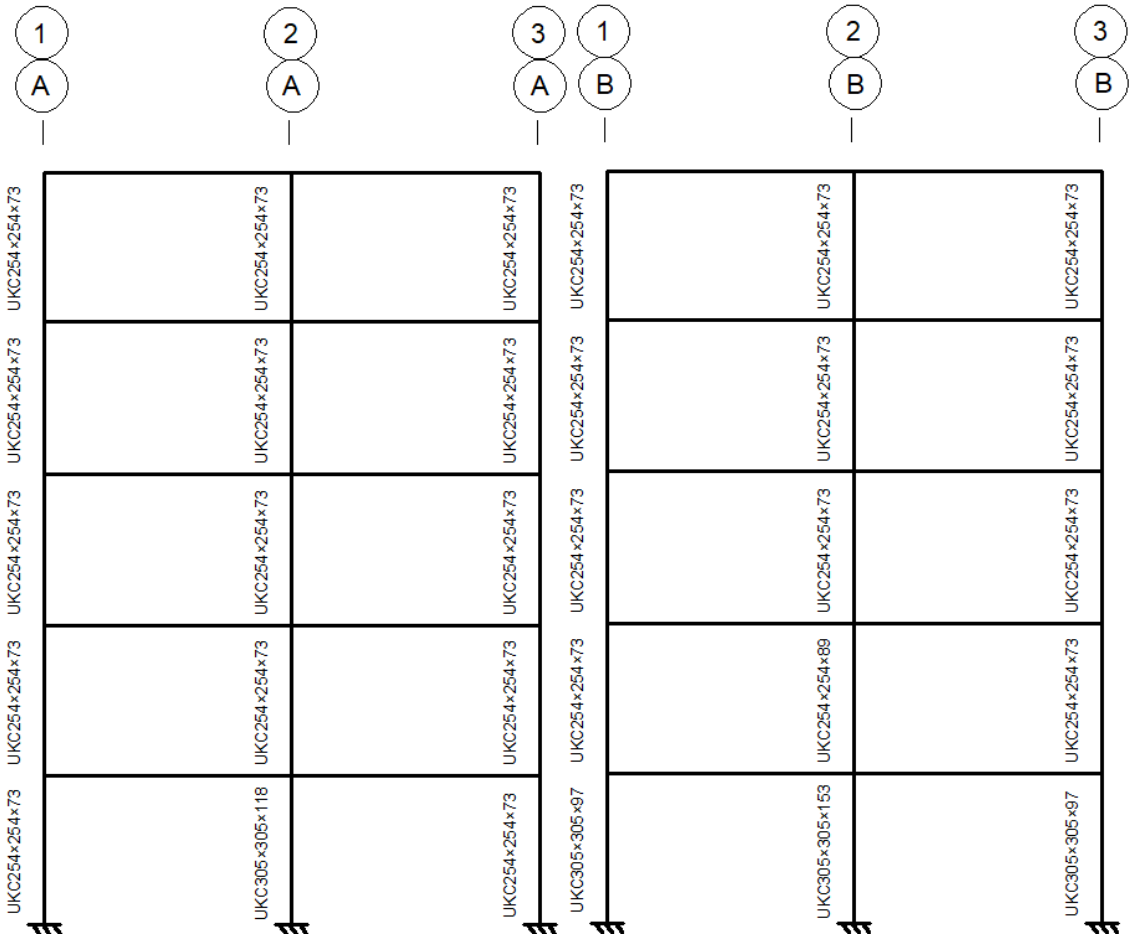

(b) Elevation view of Bay A

(c) Elevation view of Bay B

Fig. 5.1 Schematic view of the five-storey building structural design

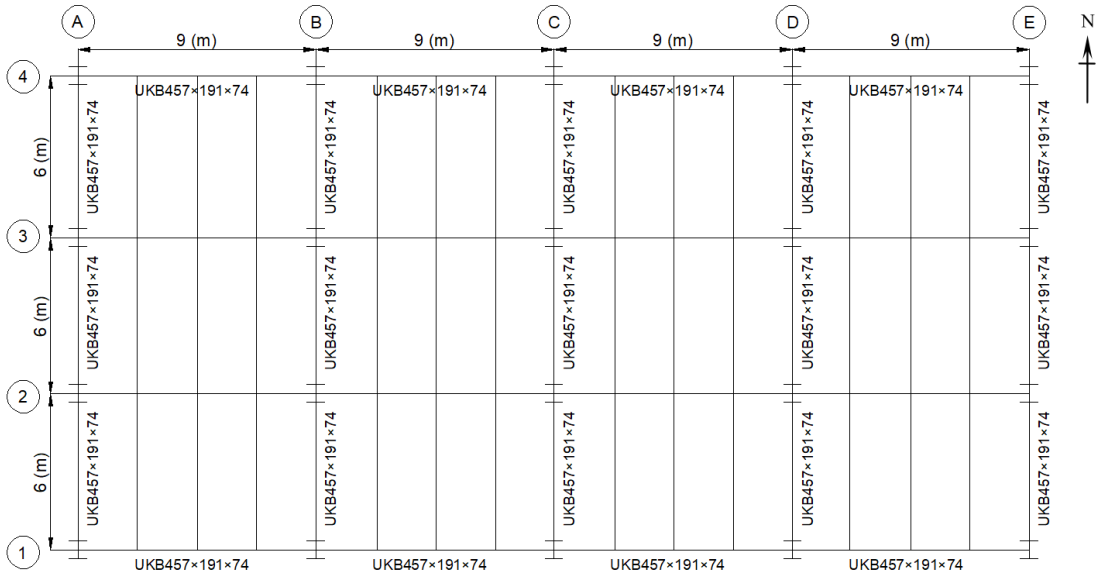

(a) Plan view

(b) Elevation view of Grid 2

Fig. 5.2 Schematic view of the ten-storey building structural design

5.3 Fire loading and fire protection design

It is recognized that columns and primary beams are normally protected in practice. A review of the literature on structural fire safety shows that in the case of adequately

Table 5.1 Summary of section sizes in the five-storey building

Member	Section	$h(m)$	$b_f(m)$	$t_w(m)$	$t_f(m)$
Column	UKC254×254×73	0.2541	0.2546	0.0086	0.0142
	UKC254×254×89	0.2603	0.2563	0.0103	0.0173
	UKC305×305×97	0.3079	0.3053	0.0099	0.0154
	UKC305×305×118	0.3145	0.3074	0.0120	0.0187
	UKC356×368×153	0.3620	0.3705	0.0123	0.0207
Secondary beam	UKB254×102×22	0.2540	0.1016	0.0057	0.0068
Primary beam	UKB406×140×39	0.3980	0.1418	0.0064	0.0086
	UKB457×191×67	0.4534	0.1899	0.0085	0.0127
	UKB457×191×74	0.4570	0.1904	0.0090	0.0145

Table 5.2 Column sizes of the ten-storey building

Floor level	Corner column	Perimeter column (except corner column)		Interior column	
		N-S frames	E-W frames	Bay C	Bay B, D
1	UKC356×368×153	UKC356×368×202		UKC356×406×287	
2	UKC254×254×89	UKC305×305×118		UKC356×368×153	UKC356×368×177
3				UKC305×305×137	UKC356×368×153
4	UKC254×254×73	UKC254×254×107		UKC305×305×137	
5		UKC254×254×107	UKC254×254×89	UKC254×254×107	UKC305×305×118
6		UKC254×254×89	UKC254×254×73	UKC254×254×89	UKC254×254×107
7-10		UKC254×254×73			

Table 5.3 Summary of section sizes in the ten-storey building

Member	Section	$h(m)$	$b_f(m)$	$t_w(m)$	$t_f(m)$
Column	UKC254×254×73	0.2541	0.2546	0.0086	0.0142
	UKC254×254×89	0.2603	0.2563	0.0103	0.0173
	UKC254×254×107	0.2667	0.2588	0.0128	0.0200
	UKC305×305×118	0.3145	0.3074	0.0120	0.0187
	UKC356×368×153	0.3620	0.3705	0.0123	0.0207
	UKC356×368×202	0.3750	0.3750	0.0165	0.0270
	UKC356×406×287	0.3936	0.3990	0.0226	0.0365
Secondary beam	UKB305×102×25	0.3050	0.1016	0.0058	0.0070
Primary beam	UKB406×140×39	0.3980	0.1418	0.0064	0.0086
	UKB457×191×67	0.4534	0.1899	0.0085	0.0127
	UKB457×191×74	0.4570	0.1904	0.0090	0.0145
	UKB533×210×82	0.5280	0.2090	0.0096	0.0132
	UKB533×210×92	0.5330	0.2090	0.0100	0.0156

protecting steel members to resist fire loading, the structural performance of the office buildings during the specified period of fire resistance is likely to be satisfactory because of the inherent robustness of building systems. In order to gain insight into the limit state that could trigger failure in building systems, it is decided that steel members are

protected for 1-hour fire resistant rating and the building is subjected to a 2-hour fire attack. Because the presence of concrete slab partially shields the top flanges of beams from the heating effect, beams are protected on three sides using a spray applied profile protection CAFCO300. This provides beams with 1-hour fire resistance at a critical steel temperature of 620°C. The insulation thickness required is 12 *mm* for the secondary beams, and 10 *mm* for the main beams (minimum thickness - 10 *mm*). On the other hand, Gyproc Gyplyner Encase board is used as four-side box protection for columns to achieve 1-hour fire resistant rating. The thickness chosen for a critical steel temperature of 570°C is 15 *mm* for column UKC254×254×73 and UKC254×254×89, and 12.5 *mm* for all other columns (minimum thickness - 12.5 *mm*).

As the validity of the proposed damage model is limited to the heating phase of fire events, a 2-hour standard ISO834 fire which assumes constantly increasing temperature is used to represent the temperature-time relationship:

$$\Theta_g = 20 + 345\log_{10}(8t+1) \tag{5.1}$$

where Θ_g is the gas temperature in the fire compartment ($^\circ C$),

t is the time (minutes).

The temperature histories developed in the steel members exposed to fire attack is obtained based on a step-by-step spreadsheet calculation method (Buchanan and Abu, 2017). Assuming a uniform temperature distribution across the member section and along its length, the temperature increase in the protected structural steel member is calculated incrementally as,

$$\Delta T_s = \frac{F}{V}\frac{k_i}{d_i\rho_s c_s}\{\rho_s c_s/(\rho_s c_s + \frac{F}{V}\frac{d_i\rho_i c_i}{2})\}(T_f - T_s)\Delta t \tag{5.2}$$

where ΔT_s is the change in steel temperature in the time step ($^\circ C$), Δt is the time interval (seconds), F is the surface area of unit length of the member (m^2), V is the volume of steel in unit length of the member (m^3), ρ_s is the density of steel (kg/m^3), ρ_i is the density of the insulation (kg/m^3), c_s is the specific heat of steel (J/kgK), c_i is the specific heat of the insulation (J/kgK), k_i is the thermal conductivity of the insulation (W/mK), d_i is the thickness of the insulation (m), T_f is the temperature in the fire environment ($^\circ C$), and T_s is the temperature of the steel ($^\circ C$).

By adopting the standard ISO834 fire curve as input data, a heat transfer analysis is also conducted in ABAQUS and compared with the predicted values obtained from the incremental calculation method. Figure 5.3 shows the steel temperature-time responses of column UKC254×254×73 with box protection subjected to four-side uniform fire exposure. The conductivity and specific heat coefficients of Gyproc Gyplyner Encase

board are $0.24W/mK$ and $1085J/kgK$, respectively, while the heat transfer coefficients of steel are taken from EN 1993-1-2 (2005). It can be seen from Figure 5.3 that the average section temperatures of steel column obtained in the heat transfer analysis are very close to those calculated using the incremental method, which confirms the validity of the spreadsheet calculations.

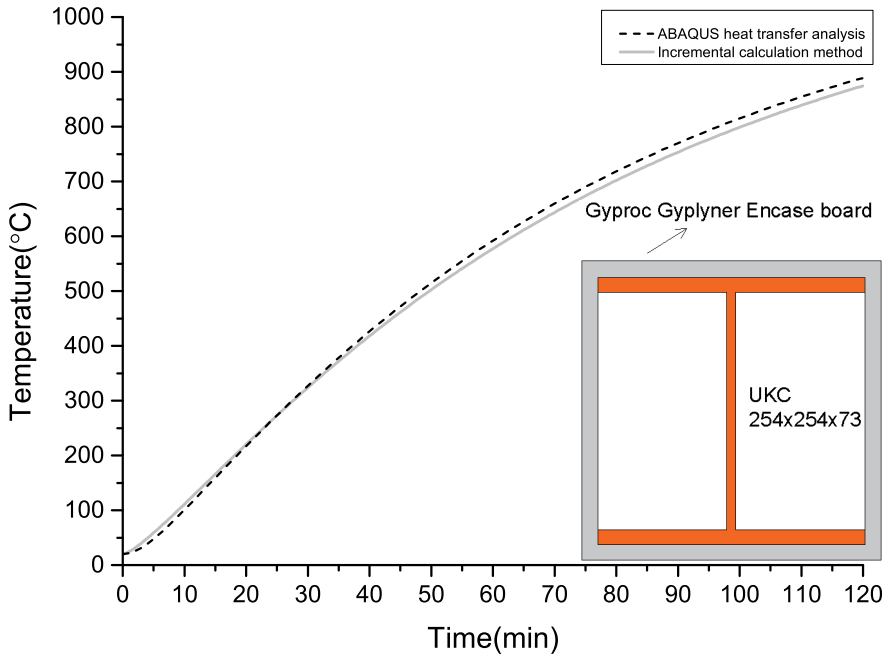

Fig. 5.3 Comparison of temperature histories of UKC254×254×73

Based on the incremental calculation method, the temperature histories of the protected beams and columns are obtained and presented in Figure 5.4. It can be seen from the graph that the standard fire loading translates into a maximum temperature of 620°C in the bottom flanges of protected beams and 577°C in protected columns after 1-hour heating. Due to the shielding effect from the slab on top of the beams, the temperature of the top flanges of the heated beams is assumed 75% of the bottom flange (Jiang and Li, 2017).

Due to the low conductivity of concrete, the concrete slab is characteristic of a non-uniform temperature distribution which is determined by heat transfer analysis in ABAQUS. Considering there is no variation in the applied thermal loading along the slab plane, this approximation allows the use of 2D models in the heat transfer analysis. Temperatures are recorded at five equally spaced layers across the depth of the flat portion of the slab, as shown in Figure 5.5. As expected, significant temperature gradient is observed across the slab thickness. The thermal gradient is passed into the subsequent structural analysis by defining temperature points at five equally spaced locations along the depth of concrete slab.

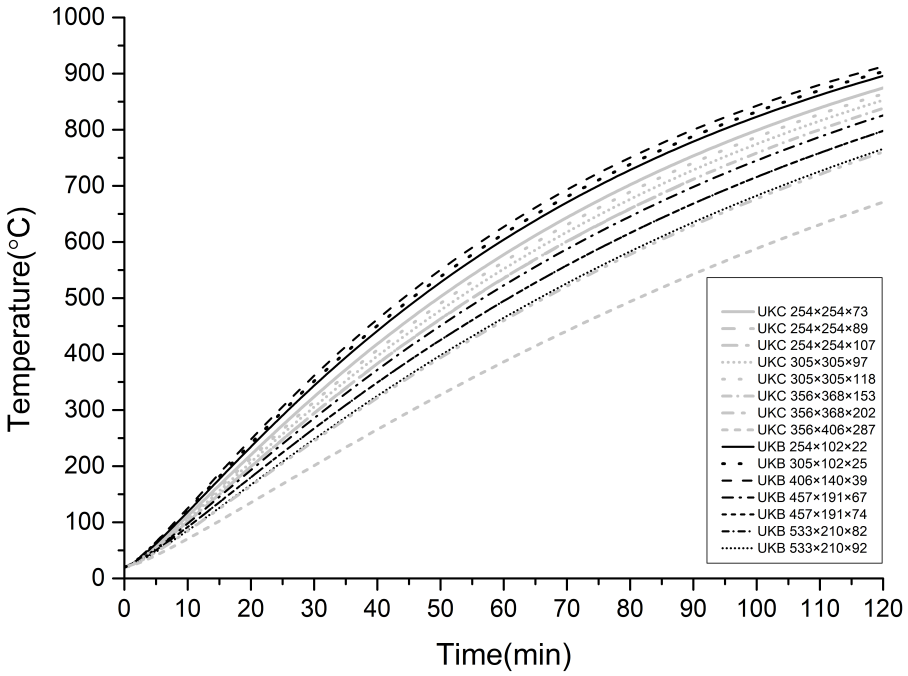

Fig. 5.4 Temperature histories of steel structural members

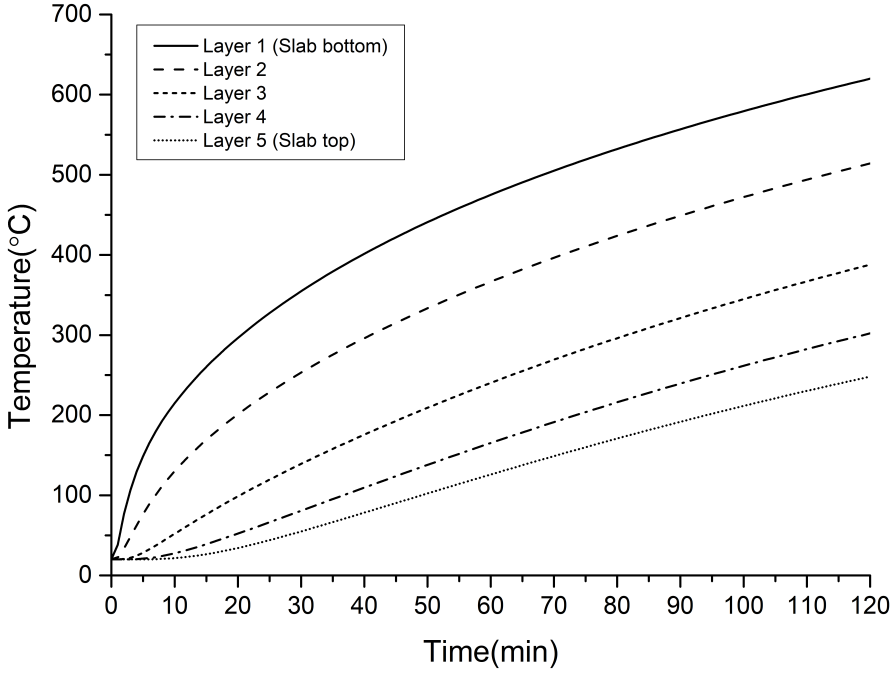

Fig. 5.5 Temperatures across concrete slab depth

5.4 FE model

A three-dimensional numerical model is constructed in ABAQUS for the five-storey and ten-storey steel office buildings, respectively. Considering the computational demands associated with parametric studies of complex building systems, it is decided that beam element will be used for modelling the steel members. Though shell element models will have the advantage of capturing local buckling and lateral torsional buckling of steel members, they have major limitations of requiring longer time in building FE model and consuming intensive computational resources in structural analysis. As the research focus here is the global structural performance of building system, the excessive computational demands generated by shell elements in modelling prolonged fire events is not justified by the benefits of capturing detailed localized effects. Therefore, beam element B31 is judged to be sufficiently accurate and effective for the purpose of the study here.

The FE models of the five-storey steel building and the ten-storey steel building are shown in Figure 5.6 and Figure 5.7, respectively. The concrete slab is assumed to act compositely with the supporting steel beams by imposing rigid connections at regular intervals. The slab is offset by a small distance above the top flange of steel beams to ensure that full connection is applied between beams and slab using *MPC type BEAM option in ABAQUS. The upper continuous portion of slab is modelled using shell element S4R and the contributions of the ribs and steel deck are not included. Moment resisting connections and simple connections are simulated by imposing rigid constraints and pinned constraints on the degrees of freedom of the associated nodes, respectively. The steel reinforcing mesh is modelled as two orthogonal 0.142 *mm* thick rebar layers embedded in the concrete slab.

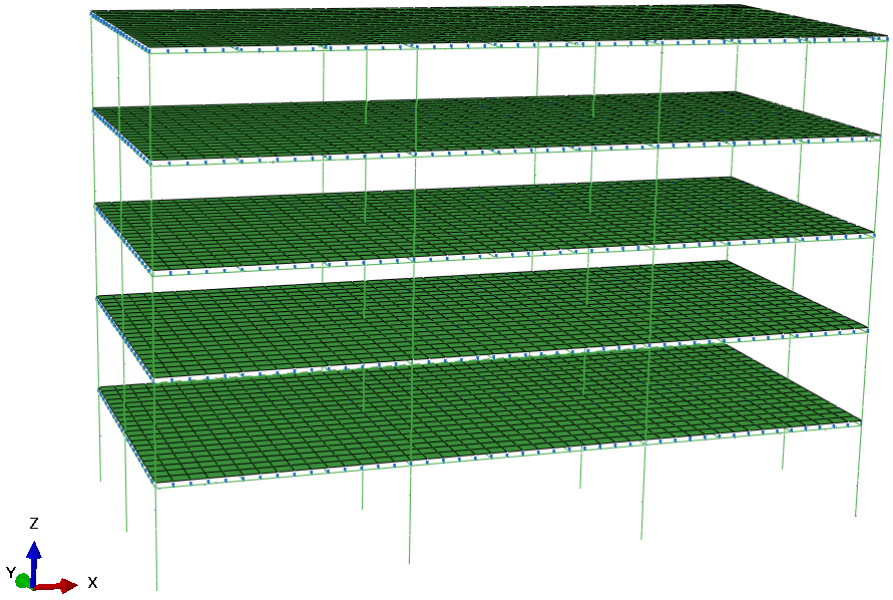

Fig. 5.6 FE mesh of the five-storey building

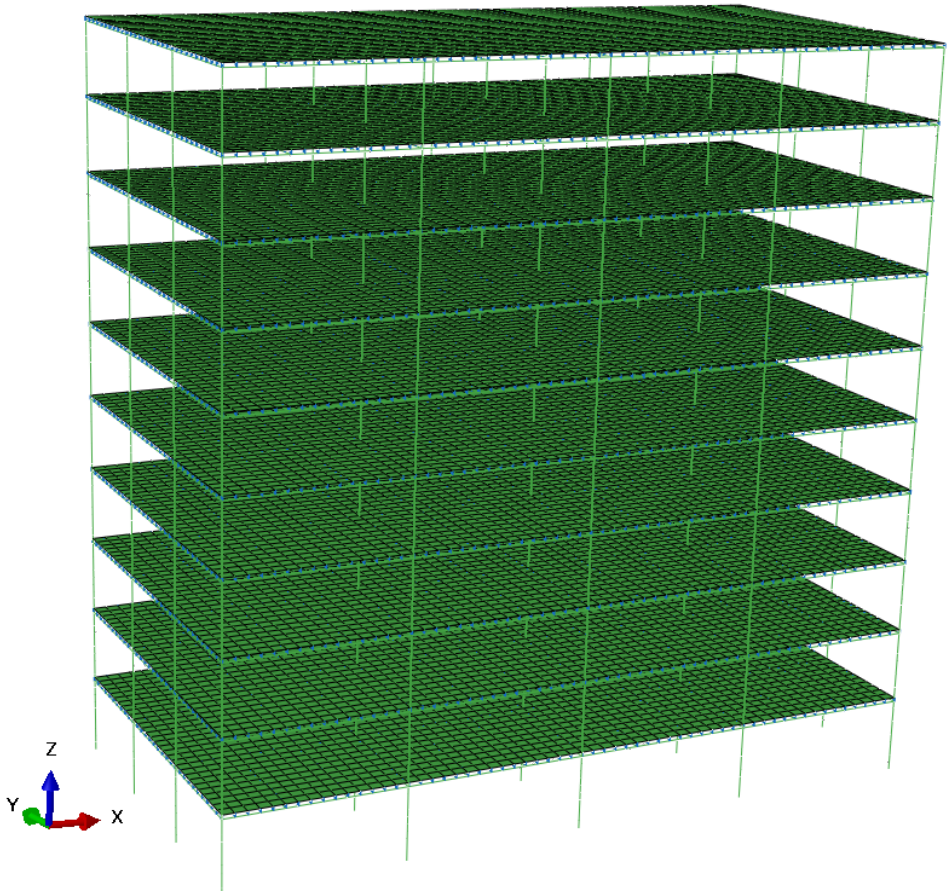

Fig. 5.7 FE mesh of the ten-storey building

Considering both numerical accuracy and computational efficiency, the mesh sensitivity study indicates that the appropriate mesh size is 10 elements along the column length, together with 15 elements for the beams along x-axis and 10 elements for the beams along y-axis. A mesh size of $0.6m \times 0.6m$ is adopted for the concrete slab. This is a reasonable choice which achieves a computational saving model while maintaining sufficient accuracy.

In order to determine the appropriate time scale, a time step sensitivity analysis is also carried out. Preliminary investigations show that a 2-hour standard fire can be scaled to a 120-seconds dynamic explicit analysis in ABAQUS. This time scale not only produces stable structural responses but also achieves significant reduction in CPU demand for the computationally intensive parametric studies conducted in this chapter.

5.5 Material modelling

The ambient-temperature material properties of concrete, steel and reinforcement are listed in Table 5.4. For concrete material input, compressive crushing and tensile cracking

behaviours are required to fully define the constitutive model. The compressive stress-strain relationship for concrete at elevated temperatures is adopted from Eurocode 4 (2005) (as shown in Figure 4.49). The tensile softening behaviour of concrete is assumed with zero stresses for full cracking.

Table 5.4 Ambient-temperature material properties

Material/Grade	Young's modulus (GPa)	Yield stress (MPa)	Compresive stress (MPa)
Steel/ S355	210	355	
Reinforcement/ A142 mesh T6@200mm	210	460	
Concrete/ LW35	34		35

Since the main focus of this study is to properly model the steel deterioration behaviour under combined mechanical loads and fire action, the proposed coupled thermal-mechanical damage model is adopted in numerical simulations. As discussed in Chapter 4, the choice of damage model parameters depends on the heating rate of structural members. Note that the heating rate of the heated steel members is lower than 10°C/min as a result of adequate fire insulation applied, as shown in Figure 5.4. The damage model parameters input chosen based on the heating rate is listed in Table 5.5 and used for all case studies in this chapter. The onset of damage evolution, which allows for element softening, occurs when the damage threshold is exceeded in plastic strain measure or temperature measure. And the element is eventually deleted from FE model when the accumulated damage variable reaches a value of unity.

In the blast analysis, a rate-dependent component in the damage-coupled constitutive model is activated, which captures the rate dependency of the yield strength of steel due to the short duration of blast loads. This rate-dependent component is subsequently deactivated when the blast loads transition to fire loads. It should be noted that the blast-induced damage is calculated based on the permanent structural deformation after the blast loading ceases as a simplified representation of dynamic damage development under high strain rate loading. The computed damage at the Gauss point of each element is thereby passed into the subsequent fire analysis as initial damage, which contributes to the subsequent coupled thermo-mechanical damage growth. The applicability and capability of the proposed damage model in capturing the blast-induced damage in integrated blast and fire analysis has been validated in Chapter 4.

Table 5.5 Damage parameters input for building analysis

Damage parameters							
S	P_d	a	b	c	r	m	k
4.75E+05	0.004	1.952	-837.323	-20	0.613	3.01	0.248

In addition, numerical simulations using conventional material model are also conducted for comparison for the purpose of highlighting the effects of damage on the structural response. The EC3 temperature-dependent constitutive model (EN 1993-1-2, 2005), which is widely used for design purposes, is employed in parallel analysis.

5.6 Fire accident scenario design

The five-storey and ten-storey office buildings are first analysed for the fire only scenario, starting from fire occurrences at lower floor level. The fire compartment covers an area of $9m$ by $6m$ and the location varies in order to determine the most vulnerable location in the building system. The localised fire might occur in corner compartment or central compartment, at three different floor levels (ground floor, mid-height of building and top floor). Compartment fires are simulated by simultaneously heating the four columns, beams and slabs that are enclosed by the compartment. The fire is assumed to be contained in the fire compartment, not spreading horizontally or vertically. This scenario represents one of the most typical fire events that might occur during the service life of office buildings. The severity of potential fire locations is investigated and the threats imposed on structures are studied.

Apart from fire only scenarios, this study moves to examine progressive collapse risks in an extreme multi-hazard scenario where the compartment is subjected to internal explosion loads followed by fire attack. The direct blast pressure acts simultaneously on all member surfaces that the explosive pressure encloses. It is assumed that the applied fire insulation remain intact on the member surfaces. The explosion then triggers a fire occurrence, engulfing all the members within the compartment in fire. The post-blast fire resistance of the steel frame is the focus of this examination. Compared to fire only scenarios, this design scenario represents a situation in which a structure is expected to be more vulnerable to fire induced progressive collapse. This susceptibility is due to blast-induced damages to the structural members.

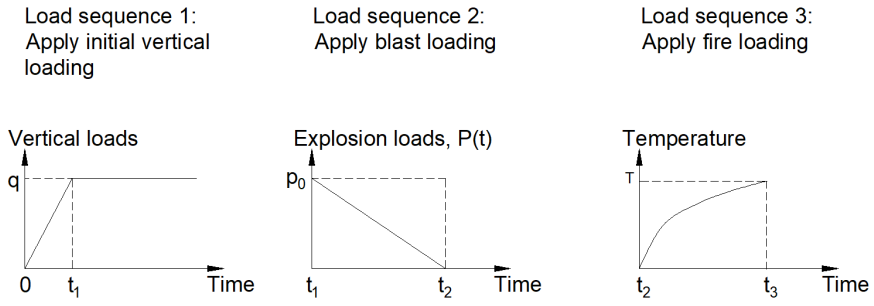

Fig. 5.8 Load sequences in post-blast fire analysis

The load sequence in this multi-hazard scenario would play out as shown in Figure 5.8. Figure 5.9 shows the internal blast loads acting on the compartment, with a 40 *ms* duration triangular pulse assumed for the variation of overpressure. Preliminary investigations indicate that when applying blast loads of the same intensities on structural members, the floor system undergoes excessive deformation while the columns withstand the blast without being affected. Due to the associated vast contact area with the blast pressure and the brittleness of concrete properties, the floor slab will dominate the failure mechanism. However, it should be noted that the focus of this study is to highlight the role of coupled thermo-mechanical damage accumulation played in the collapse of steel frames triggered by potential column failures, which is one of the most typical and critical cases. It is thus decided to position close-distance blast near to the columns, exposing the columns to a blast intensity of 2 *MPa* whereas the floor system is subjected to a blast intensity of 0.08 *MPa*. The blast load levels are chosen such as to induce permanent deflection in structural members but at the same time refrain from failures completely induced by blast. This is followed by subsequent fire analysis and the fire resistance of the damaged structure is re-assessed. This examination is expected to give insight to the structure's capacity for load redistribution when the damaged columns suffer from increased deflections and reduced ability to redistribute loads away to adjacent members. Steel frames in this scenario are likely to have lower failure temperatures.

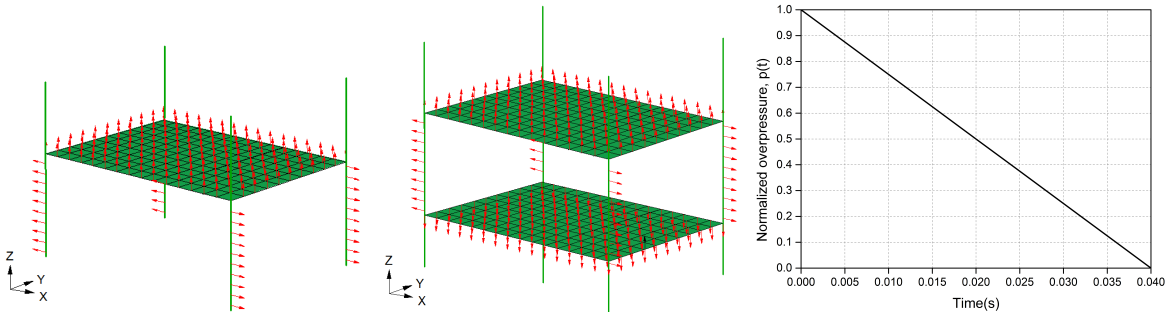

(a) Blast loads occur in ground floor compartment (b) Blast loads occur in upper floor compartment (c) Variation of overpressure over time

Fig. 5.9 Schematic view of the occurrence of internal blast loads

An extension of the above scenarios that we pursue here is that gas explosion is triggered by fire occurrence. This type of scenario is presented as another extreme case to assess the susceptibility of structures to progressive collapse in multi-hazards. Due to the fire-induced deterioration in steel frames, the blast loads are likely to be devastating to the weakened structural system. The focus of this examination is the detrimental impacts of blast loads on heated structures. The applied blast load level is the same as in post-blast fire scenario for comparison. All of this implies that steel buildings following such scenario are likely to have lower ultimate failure temperature as compared to both fire only scenario and post-blast fire scenario. The load sequence is illustrated in Figure 5.10. The damages to fire insulation caused by gas explosion are ignored.

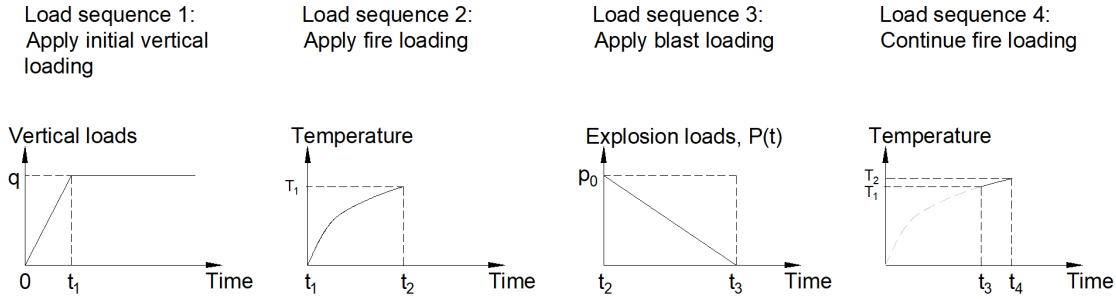

Fig. 5.10 Load sequences in fire and gas explosion analysis

To summarize, the variation of the cases under investigation is listed below.

- Types of scenarios
  - Fire only scenario
  - Post-blast fire scenario
  - Fire-triggered explosion scenario

- Location of accidental events
  - Blast/ fire occurs in the corner compartment on the ground floor.
  - Blast/ fire occurs in the central compartment on the ground floor.
  - Blast/ fire occurs in the corner compartment at the mid-height of building.
  - Blast/ fire occurs in the central compartment at the mid-height of building.
  - Blast/ fire occurs in the corner compartment on the top floor.
  - Blast/ fire occurs in the central compartment on the top floor.

Numerical simulations are then carried out to evaluate the consequences of the design scenarios and the results are provided in the next section.

5.7 Simulation results

In this section, the global system response and the collapse resistance of buildings is evaluated for each scenario. By comparing the fire resistances of structures with and without using the damage model, the effects of incorporating the proposed damage model in structural analysis are demonstrated. In this study, the fire resistance of the structure is quantified in the time domain. It is recognized that it is not always straightforward

to determine a quantifiable measure of performance criteria. Upon the failure of an individual member, the structure does not necessarily suffer from progressive collapse because of the alternate load paths available. The basic concept of acceptable structural performance is that the extent of structural damage should not be disproportionate to the original cause.

In this study, global collapse is assumed to occur when the collapse associated with the initiating event has catastrophic consequences. An indicator of global collapse is defined as the first buckling of adjacent cool columns, which would normally induce sequential buckling of other columns, leading to disproportionate collapse of the whole building. The maximum vertical deflection of the building should also be considered as a global damage indicator because the largely deformed slabs may fall down in reality due to connections fracture and impose dynamic loads on the floors below. This will cause threats to structural integrity, thus triggering progressive collapse as in the case of WTC catastrophe. In order to ensure compartmentation is maintained and the ductility limits of the joints are not exceeded, the maximum displacement is normally limited to a fraction of the storey height or the bay span. The cut-off point defined in this study is that the large deflection becomes unacceptable when the vertical displacement of the slab system exceeds 1/10 of the span. This criterion is similar to that proposed by Alashker and El-Tawil (2011) and is comparable to the maximum beam deflection recorded in the Cardington fire test. By reasonably assuming that no connection failure occurs before the maximum permissible vertical displacement is reached, this would allow the focus to be on the global behaviour of structural frame system. With these failure criteria in mind, the collapse modes and load redistribution scheme of the frames subjected to these fire scenarios are investigated.

5.7.1 Fire-only analysis

Numerical study is first conducted for the most typical scenarios with fire alone occurrences at different locations within the building, starting from lower floor level. The plan locations include a corner compartment and a central compartment. In elevation, fire occurs at the ground floor, mid-height of the building and the top floor. Fire is assumed to act in combination with a vertical load level of 5 kN/m^2. In the following pages, the severity of each potential fire location is investigated and the fire-induced progressive collapse risks are examined.

5.7.1.1 Five-storey office building

1. Corner compartment fire on the ground floor.

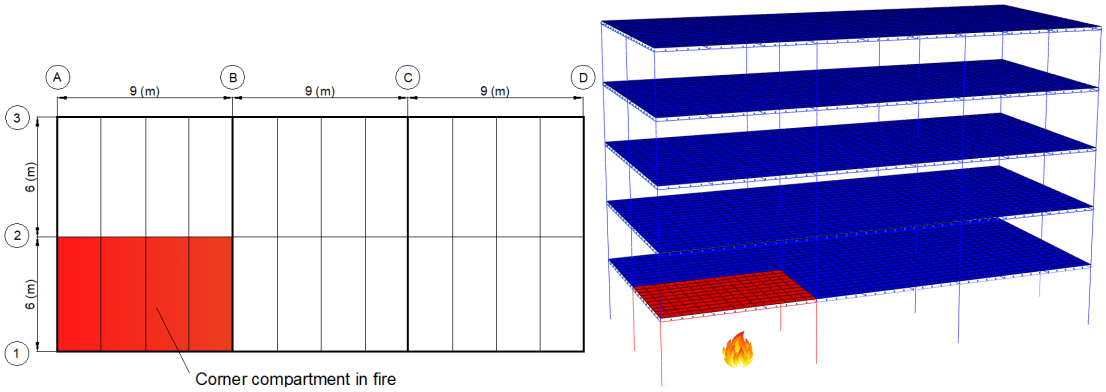

(a) (b)

Fig. 5.11 Location of the corner compartment fire on the ground floor

The corner compartment on the ground floor is heated in this case, as shown in Figure 5.11. The structural elements are designated with reference to the grid system. For instance, the column located at the intersection of gridline B and gridline 2 is designated as column B2. The vertical displacement versus temperature curves in the heated interior column B2 are shown in Figure 5.12. An initial upward movement is observed as a result of thermal expansion with temperature increase in the column. This is followed by an abrupt fall due to the column failing at high temperatures, signifying the catastrophic collapse of the building. The simulation results show that the progressive collapse of the building occurs after 81.5 minutes of fire for the EC3 model and after 71 minutes of fire for the damage model. The critical temperatures of Column B2 are 608 °C and 670 °C with and without considering damage, implying a considerable difference in the predicted failure temperature.

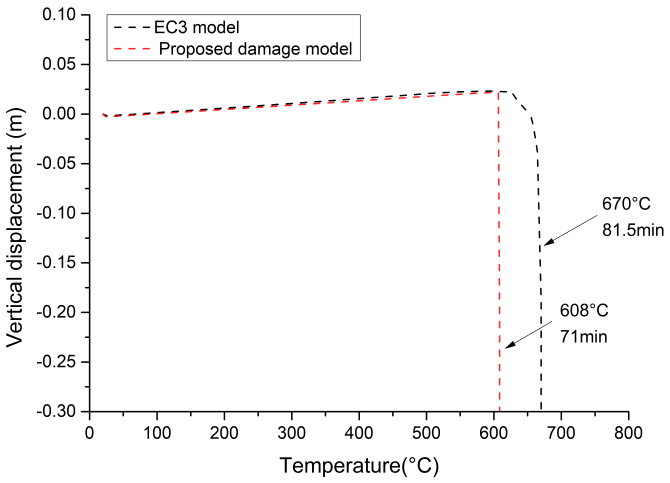

Fig. 5.12 Vertical displacement of the heated interior column B2

The deformed shape of the building prior to column buckling is characterized by mild deflections of the heated beams and slabs, as shown in Figure 5.13. Tensile cracks in the heated slab and some yielding in the heated beams are observed. However, the

deformation experienced by beams is small and as a result no failure occurs in the connections before column buckling. The failure of columns is identified as the trigger of the global collapse in both cases. In order to understand the collapse mechanism and load redistribution, the loads being carried by the heated columns are examined.

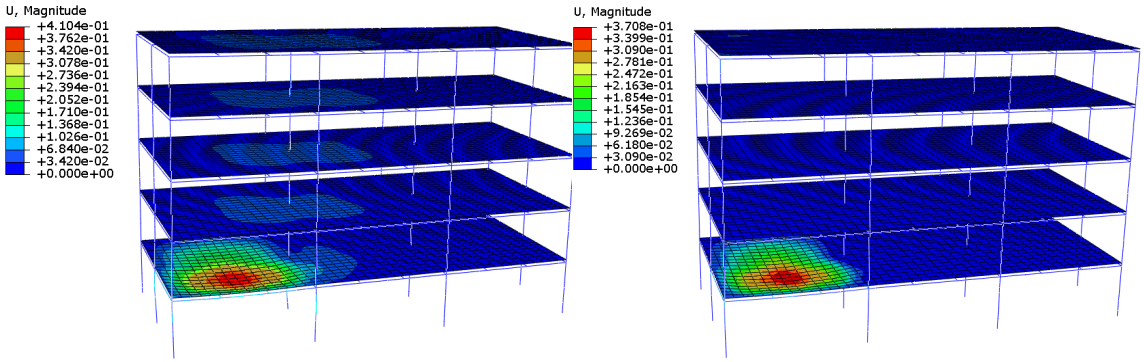

(a) EC3 model (At fire 81 min) (b) Proposed damage model (At fire 70.5 min)

Fig. 5.13 The deformed shape of the building before column buckling initiates

Figure 5.14(a) shows the axial forces of the heated columns obtained with EC3 model. It can be seen from the graph that sequential column buckling that leads to progressive collapse is initiated by buckling of interior column B2. As the temperature rises, additional compression force is developed in column B2 due to thermal expansion and consequent restraint forces. At the same time, the steel properties degrade with elevated temperatures. Due to its highest utilization ratio, column B2 buckles first when the buckling load is exceeded. The loads carried by column B2 are transferred to adjacent columns via flexural action as well as catenary mechanism. Part of the loads are sustained by the heated perimeter columns, which is reflected in their increased magnitudes of axial forces. At fire 81.5 minutes, there is a sudden change in the force values in all the columns, signalling the load redistribution process. The neighbouring columns buckle sequentially as they can no longer support the increased loads. Progressive collapse occurs when there is no alternate path available to redistribute the loads.

In the case of the damage model approach, damage is calculated and the elements degrade during the analysis as damage accumulates. Overall, the axial force development pattern is similar to that in Figure 5.14(a), except that the sequential column buckling is initiated by perimeter column A2 instead due to the damage accumulation and strength deterioration in column A2. As the temperature rises, the compression force in column A2 increases until its high-temperature buckling load is exceeded after 69 minutes of fire. This is immediately followed by buckling of all heated columns and subsequent progressive collapse of the whole building. A close look at the damage accumulation in column A2 would help develop an understanding of how the damage evolution leads to premature column failure.

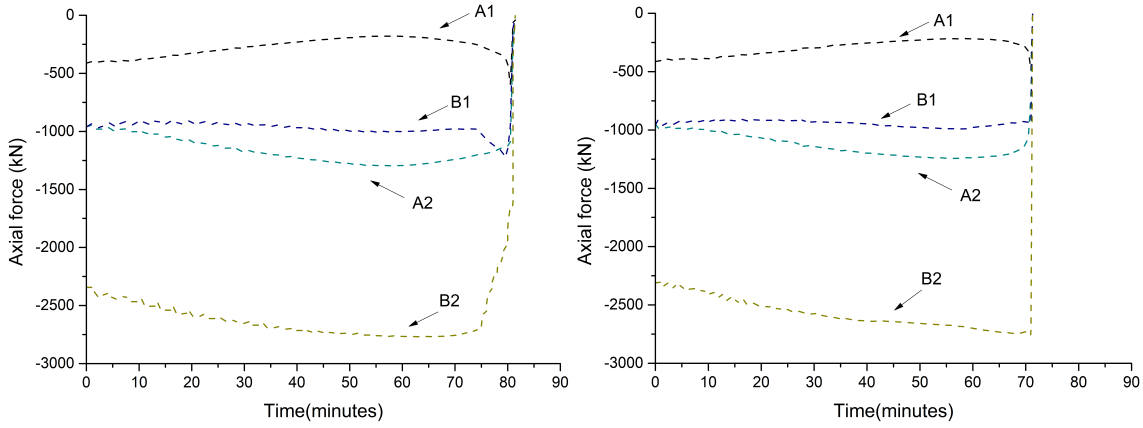

(a) EC3 model (b) Proposed damage model

Fig. 5.14 Axial forces in columns during fire event

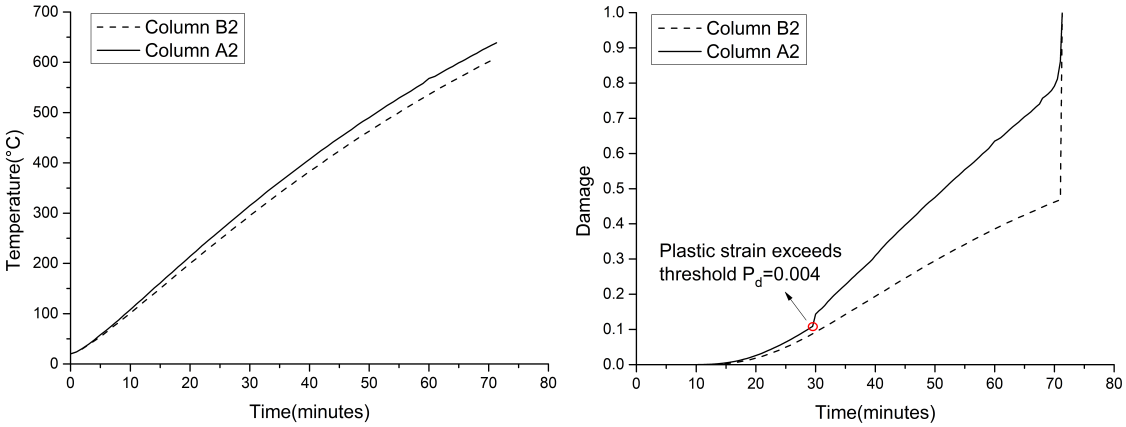

(a) Temperature development (b) Damage development

Fig. 5.15 Damage development in the top of column A2 and column B2

A comparison of the temperature development and evolution of damage between column A2 and column B2 as predicted by the damage model is provided in Figure 5.15. Though the temperature of column A2 is only slightly higher than that of column B2, there is pronounced difference in their damage evolution histories. The damage in column A2 evolves gradually until the plastic threshold strain is exceeded after 30 minutes of fire, which signals the onset of mechanical damage. After this point, the damage growth is significantly accelerated due to the coupled effect of mechanical damage and thermal damage. On the contrary, no yielding occurs in column B2 prior to ultimate failure and as a result no steep accumulation due to coupled damage propagation is observed in column B2. The damage state variable achieves the value of 1.0 after 71 minutes of fire, signifying that the element has lost all of its stiffness and strength and thus deleted from the FE model. The coupled effect of mechanical damage and thermal damage is evident in Figure 5.15(b) and has a significant impact on the global response of the structure and thereby the collapse initiation time. This suggests that it is important to consider damage growth in the collapse assessment of steel buildings as

the conventional numerical approach might not be able to properly capture the material failure and therefore overestimate the collapse resistance.

2. Central compartment fire on the ground floor.

Having analysed the corner compartment fire scenario, it is of interest to examine the central bay fire in which the heated structural members have stronger restraints from the surrounding structure. Figure 5.16 shows the location of the heated central compartment on the ground floor. The maximum vertical displacement of the heated interior column B2 is plotted in Figure 5.17. Simulation results show that the fire resistance is 80 minutes for EC3 model and 71 minutes for the damage model approach.

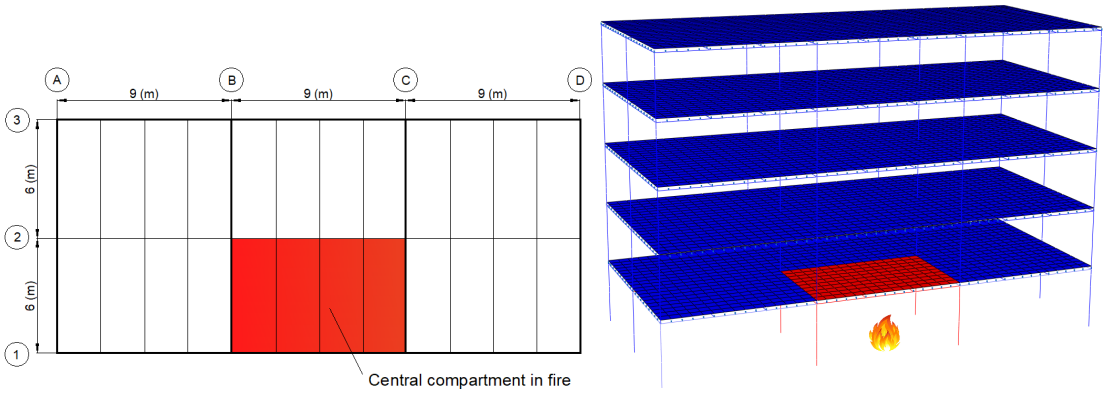

(a) (b)

Fig. 5.16 Location of the central compartment fire on the ground floor

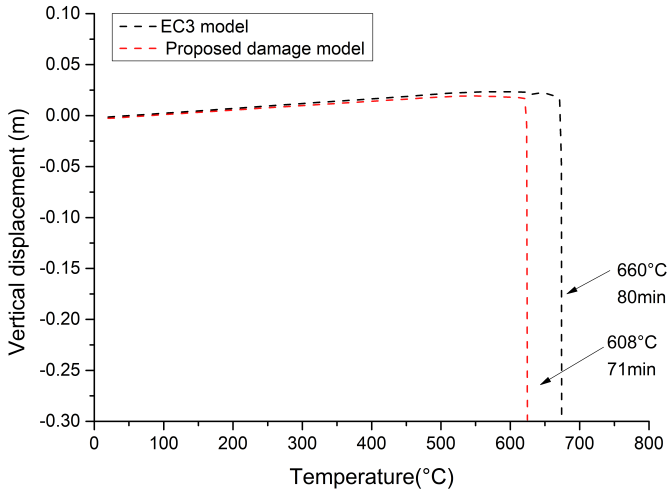

Fig. 5.17 Vertical displacement of the heated interior column B2

Similar to the corner fire scenario, the vertical displacement of slab system is only about 400 *mm* prior to collapse initiation and the global downward collapse is triggered by column buckling for both models. Axial load values in the heated columns of the fire compartment are plotted against time in Figure 5.18. Because of symmetry, the columns in symmetric positions exhibit the same responses. It can be seen from the graph that the

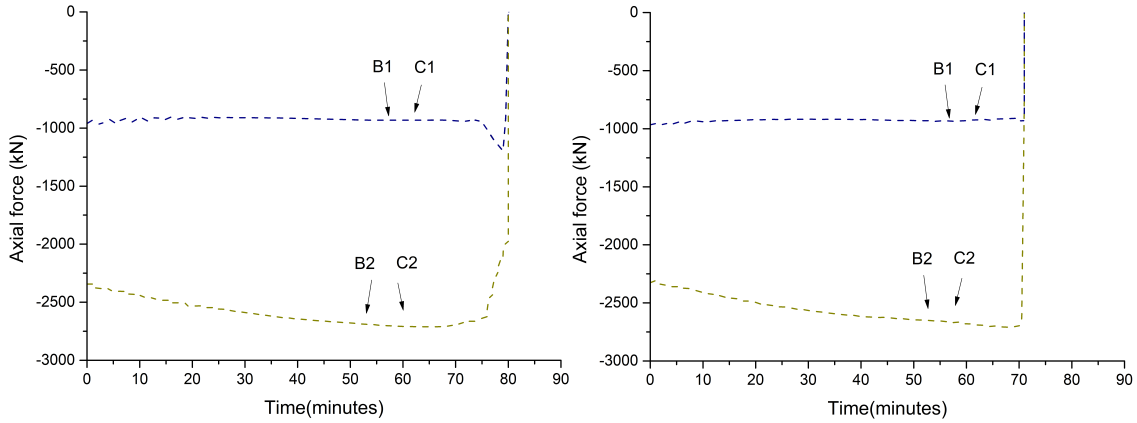

(a) EC3 model (b) Proposed damage model

Fig. 5.18 Axial forces in columns during fire event

failure pattern of the heated columns in the damage model prediction resemble that in EC3 model prediction, with interior column B2 and column C2 buckling first due to the highest load ratios. Yet some differences could be observed between Figure 5.18 (a) and (b).

In the EC3 model prediction, following the failure of column B2 and column C2 at fire 75 minutes, the composite floor is able to redistribute the loads from the failed columns. This could be observed from the suddenly increased magnitudes in the axial forces of column B1 and column C1, as seen in Figure 5.18 (a). Thereby, the occurrence of collapse is delayed until 80 minutes. By contrast, the damage model results indicate that the buckling of interior columns occurs earlier at 71 minutes. It could also be observed from Figure 5.18 (b) that the neighbouring columns fail to support the loads of the failed columns in the damage model prediction. The residual load bearing capacity is a crucial factor in helping understand the compromised load redistribution capability of neighbouring columns, which is presented in Figure 5.19. Owing to the severe deterioration in capacity, perimeter columns buckle immediately afterwards due to the loads shed by interior columns. This is followed by the progressive collapse of the whole building. Thus, the fire resistance of the building in damage model prediction decreases by 11.25% compared to that of EC3 model. It is therefore important to accurately model material behaviour in order to avoid over-predictions of structural robustness against collapse.

3. Corner compartment fire on the third floor.

The above observations are based on fire analysis in which the triggering fire events occur on the ground floor. Compared with ground floor scenario, the axial loads of columns are smaller on the upper floors. On the other hand, the column sizes are smaller on the upper floors as they are in most buildings and thereby the load redistribution capability might not be as robust as ground floor. Therefore, it is of importance to examine progressive

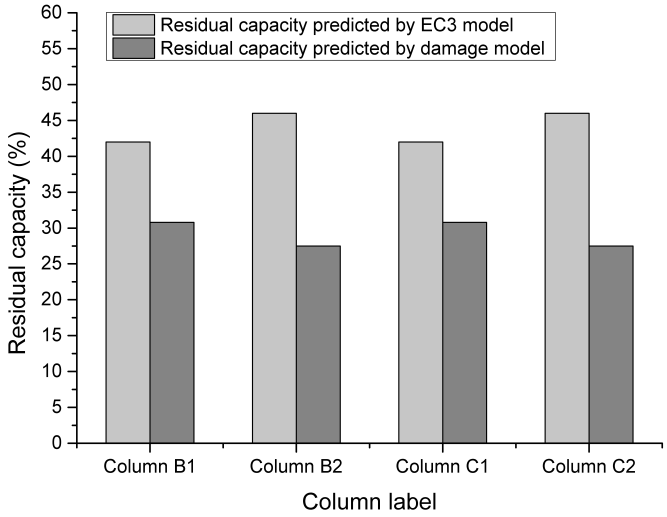

Fig. 5.19 Residual capacity of the heated columns upon interior column buckling at 71 minutes of fire

collapse risks with the triggering loads on the upper floors. The corner compartment on the third floor is heated in this case, as shown in Figure 5.20.

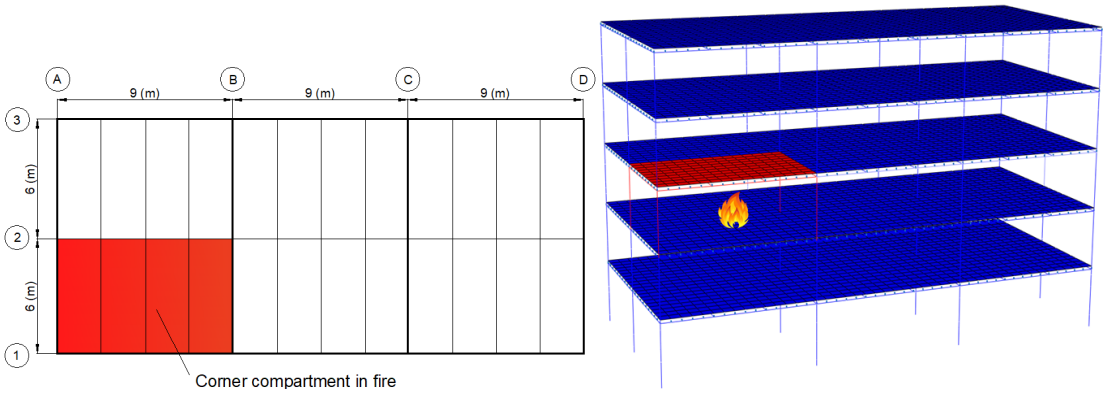

(a) (b)

Fig. 5.20 Location of the corner compartment fire at the mid-height of the building

Fire analysis results indicate that the structural collapse occurs earlier than the ground floor fire scenarios, being 76 minutes in EC3 model prediction and 63 minutes in the damage model prediction, respectively. The vertical displacement of the top of the heated interior column B2 is plotted in Figure 5.21. A sudden downward displacement occurs at column temperature of 600°C in both models. After this point, the fall is arrested in EC3 model prediction and the structure remains stable for another 13 minutes, whereas the vertical displacement cannot be resisted after the column failure and the building suffers from progressive collapse in the damage model prediction.

It is observed that interior heated column B2 buckles first due to the highest utilization ratio in both cases. This column failure then initiates the load redistribution process. The axial load values in the heated columns of the fire compartment are plotted against time

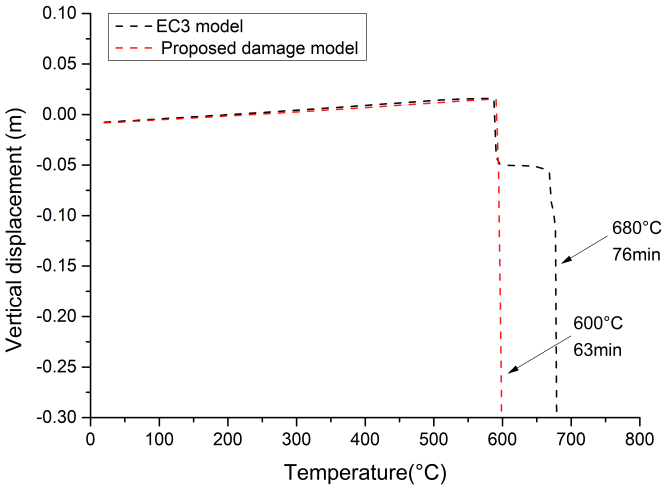

Fig. 5.21 Vertical displacement of the heated interior column B2

in Figure 5.22. It can be seen from Figure 5.22(a) that following the failure of column B2 at fire 63 minutes, the loads originally carried by column B2 are transferred to adjacent columns in EC3 model prediction. The structural system remains stable for another 13 minutes. As the temperature increases further, the adjacent columns could no longer take up the residual forces shed by column B2, leading to progressive collapse of the whole building after 76 minutes of fire.

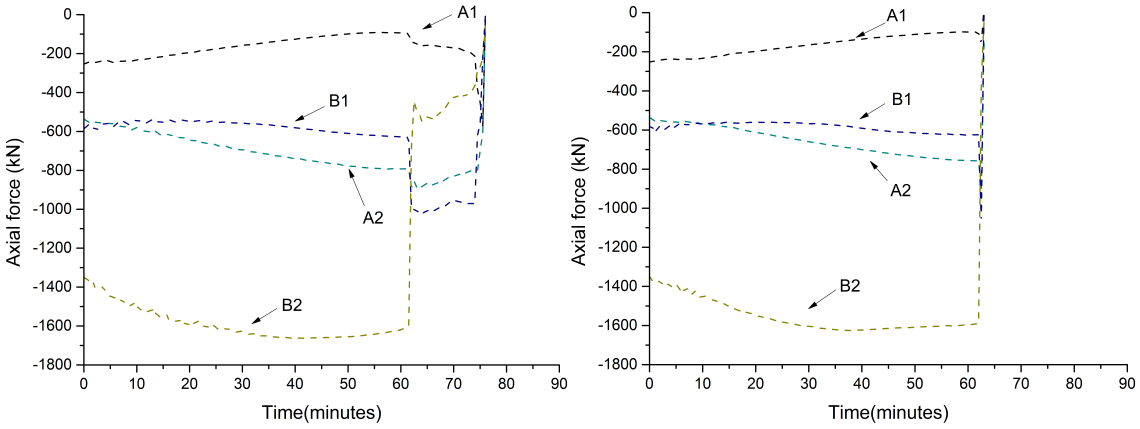

(a) EC3 model (b) Proposed damage model

Fig. 5.22 Axial forces in columns during fire event

On the other hand, the damage model results in Figure 5.22(b) indicate that the axial loads redistributed upon the failure of column B2 at fire 63 minutes lead to a sudden increase in the axial loads carried by adjacent columns and immediately results in their simultaneous buckling. In contrast to EC3 model prediction, the delay achieved in global collapse owing to the load redistribution mechanism is not observed here, which again could be explained by the damage-affected load carrying capacity of adjacent columns as illustrated in Figure 5.23.

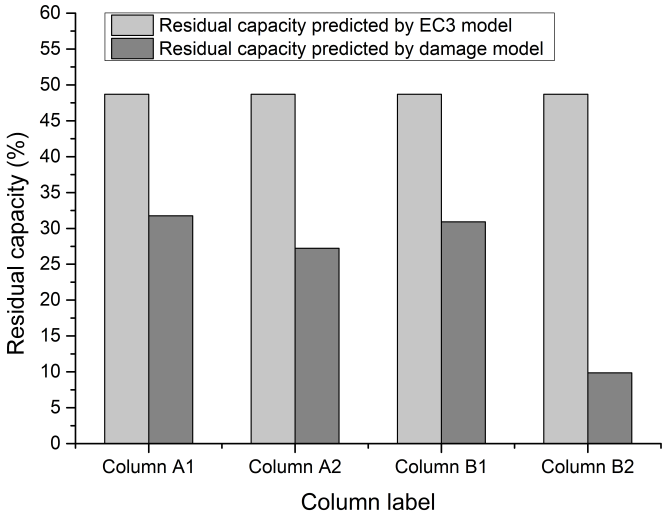

Fig. 5.23 Residual capacity of the heated columns upon column B2 buckling at 63 minutes of fire

Note that upon the buckling of column B2 at 63 minutes of fire, the temperature achieved in all heated columns is 594.5°C. In contrast to a residual capacity of 48.7% at 594.5°C for all heated column as specified in EC3 model, the deterioration in the load carrying capacity predicted by the damage model is more severe as shown in Figure 5.23. As a result, the surrounding columns are unable to sustain the increased loads after the column failure and the load transfer mechanism is compromised. It is the inability of the building to redistribute the loads away from the failed column that propagates the progressive collapse. This kind of abrupt loss in the residual capacity due to coupled thermo-mechanical damage propagation is not captured by EC3 model. Thus, the fire resistance of the building in damage model prediction decreases by 17.11% compared to that of EC3 model.

4. Central compartment fire on the third floor.

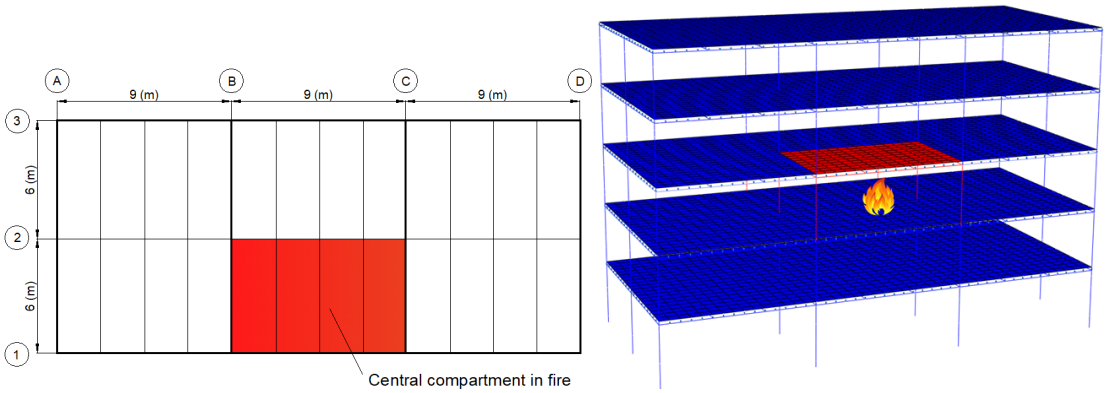

(a) (b)

Fig. 5.24 Location of the central compartment fire at the mid-height of the building

Next a central compartment fire on the third floor is analysed, as shown in Figure 5.24. Simulation results show that the predicted fire resistance is 72 minutes using EC3 model, whereas in the damage model approach the fire resistance is deteriorated by 15.28% as shown in Figure 5.25.

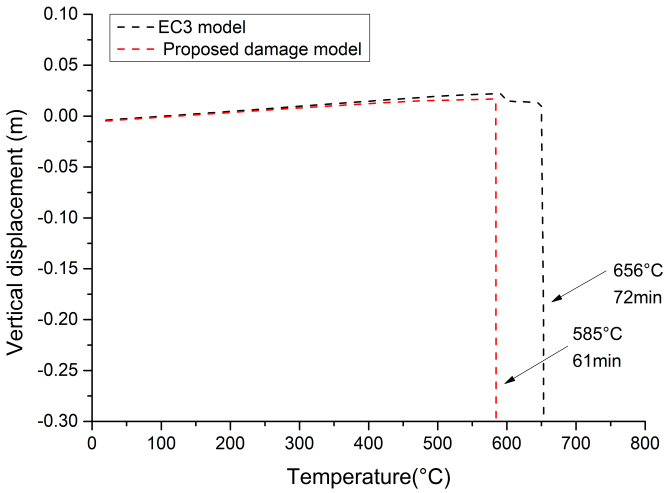

Fig. 5.25 Vertical displacement of the heated interior column B2

Similar to the ground floor central fire scenario, the structure remains stable until a global downward collapse is triggered by simultaneous buckling of internal column B2 and column C2 for both cases. Axial load values in the heated columns are plotted against time in Figure 5.26. Column B2 and column C2 fail around 61 minutes of fire and the additional loads from the redistribution, in combination with the degradation of the material properties at the elevated temperature, result in the failure of all heated columns and eventually lead to the progressive collapse of the steel frame. Again EC3 model results indicate that following the failure of column B2 and column C2 the building remains stable for another 11 minutes, whereas in the damage model prediction the failure of interior columns immediately brings failure to adjacent perimeter columns and the loss of several columns brings down the upper floors in a very short time due to the inability of the surrounding columns to redistribute loads away from the failed columns. It can be concluded from the results that the higher utilization ratio of the interior column could be a deciding factor in structural fire resistance.

5. Corner compartment fire on the fifth floor.

Moving now to applying fire loads to the corner compartment of the fifth floor as shown in Figure 5.27. The structure exhibits a robust performance compared to lower floor fires, with the occurrence of collapse after 97 minutes of fire for EC3 model and 81 minutes of fire for the damage model. The vertical displacement of the heated interior column B2 is shown in Figure 5.28 and the axial load values in the heated columns are plotted in Figure 5.29.

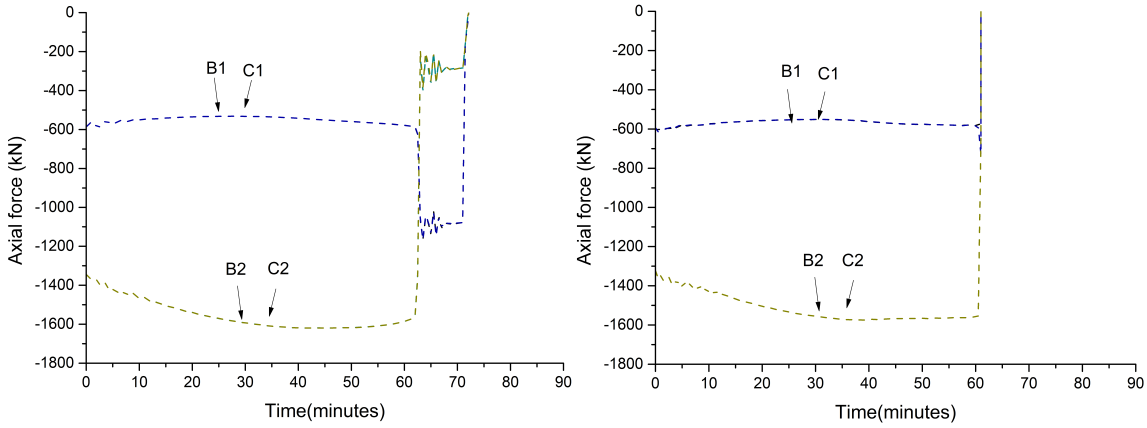

(a) EC3 model (b) Proposed damage model

Fig. 5.26 Axial forces in columns during fire event

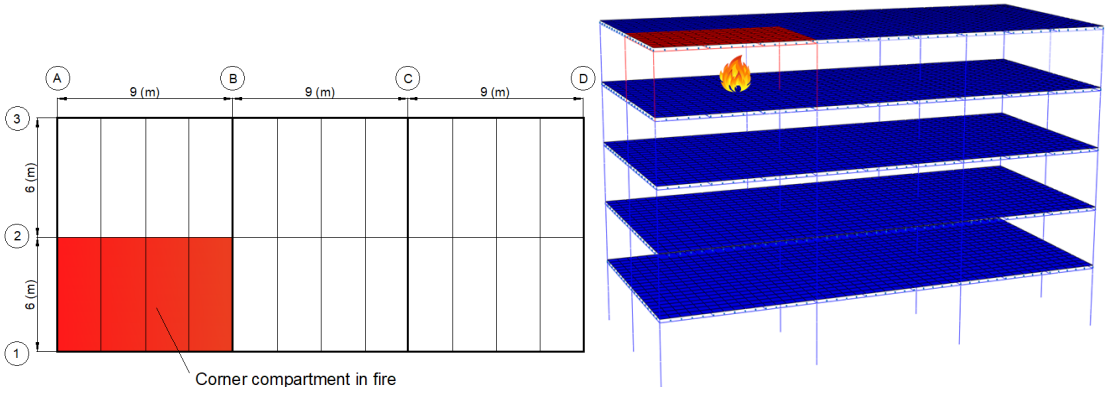

(a) (b)

Fig. 5.27 Location of the corner compartment fire on the top floor

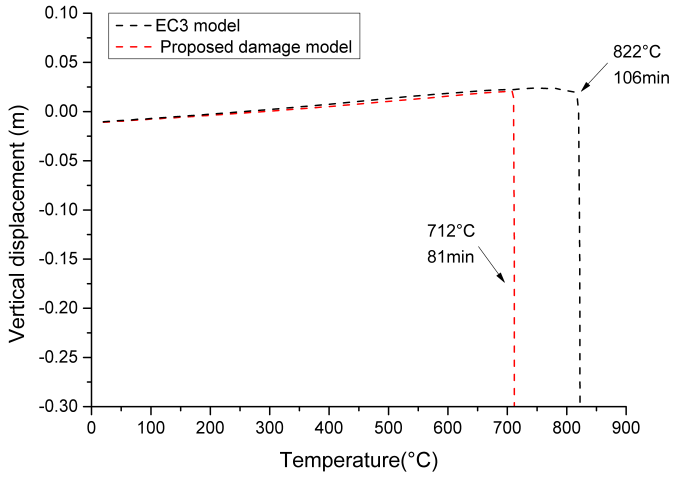

Fig. 5.28 Vertical displacement of the heated interior column B2

Instead of a sudden failure of the interior column B2 as in lower floor scenarios, a gradual decrease in the axial load values of column B2 is observed as the fire progresses due to the lack of restraint conditions from the upper floors. At the same time, the compression

forces in columns A2 and column B1 increase gradually. The results indicate that the restraints of the framing above the heated columns do affect the axial force development pattern. There is a sudden decrease in the axial force of column B2 at the time of column buckling and the redistributed loads are safely carried by the neighbouring columns in EC3 model prediction. The axial load values remain almost constant for another 8 minutes. However, at the time of column B2 buckling, the beams have lost a large portion of their bending capacity and transition to catenary mechanism by deflecting more. Large sagging is observed to exceed 1/10 of the span at 97 minutes of fire. The large deflection of slabs is dangerous to the structural stability, suggesting that the collapse might be imminent.

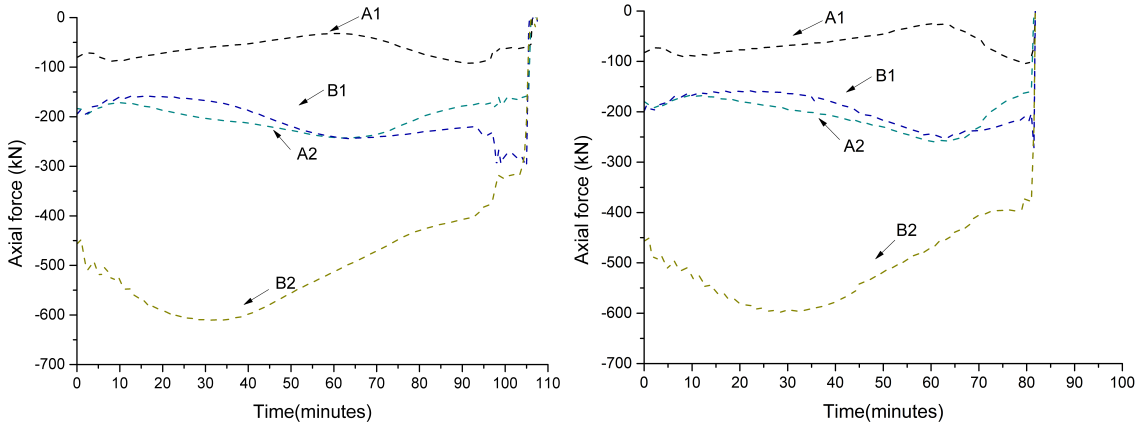

(a) EC3 model

(b) Proposed damage model

Fig. 5.29 Axial forces in columns during fire event

By contrast, the incorporation of damage model shifts the collapse mechanism from deformation dominant to column failure propagation. Upon the failure of column B2 at 81 minutes of fire, the neighbouring columns fail to support this load and lead to further propagation of column failures. Again it is the coupled thermo-mechanical damage accumulation that results in an earlier drastic reduction in column capacity as well as little ability in utilizing alternative load paths as fire progresses. All of this leads to a decrease in the predicted fire resistance by 16.49% compared to EC3 model prediction.

6. Central compartment fire on the fifth floor.

The previous case has witnessed a change of structural response when triggering loads occur on the top floor. In the following scenario, the central compartment on the fifth floor is heated as shown in Figure 5.30. The vertical displacement of the heated interior column B2 is shown in Figure 5.31

Again robust structural performance is observed, with progressive collapse occurring at 97 minutes of fire in EC3 model prediction and at 84 minutes of fire in the damage model prediction. Similar to central compartment fires on lower floors, progressive collapse is

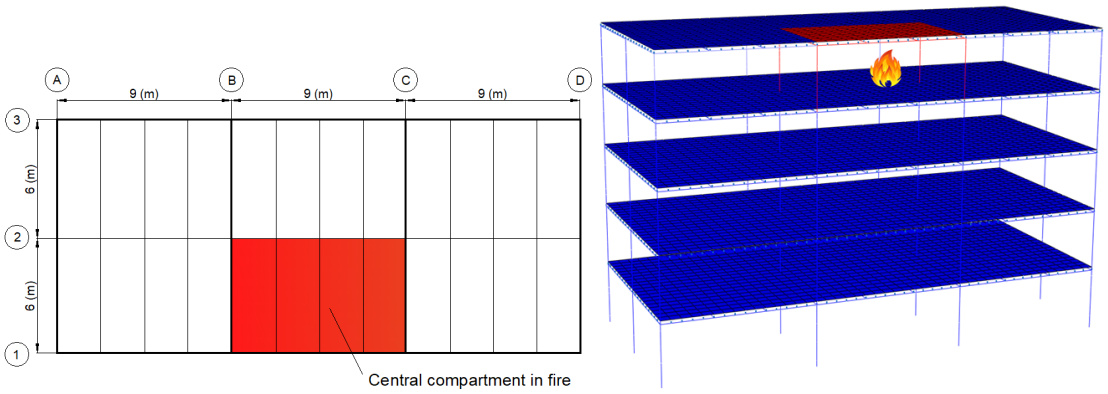

(a) (b)

Fig. 5.30 Location of the central compartment fire on the top floor

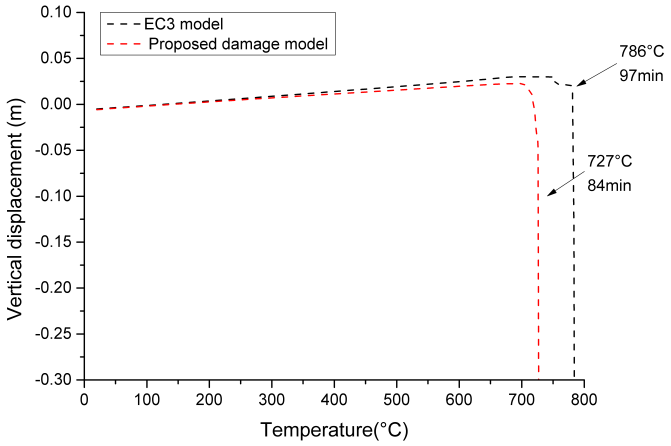

Fig. 5.31 Vertical displacement of the heated interior column B2

triggered by the buckling of interior columns which have highest utilization ratios in both models. The axial load values in the heated columns are plotted in Figure 5.32. A gradual change in axial load values is observed through the fire event with the exception of a sudden increase in axial values upon the column failure. The failure then spreads to the adjacent columns and initiates progressive collapse. A decrease of 13.40% is observed in the fire resistance predicted by the damage model compared to EC3 model prediction.

5.7.1.2 Ten-storey office building

The previous subsection has dealt with evaluation of collapse potential of a low-rise office building. In order to examine whether the same collapse mechanisms will be obtained in a mid-rise office building, the performance of a ten-storey steel building with similar repetitive layout under fire attack is investigated.

1. Corner compartment fire on the ground floor.

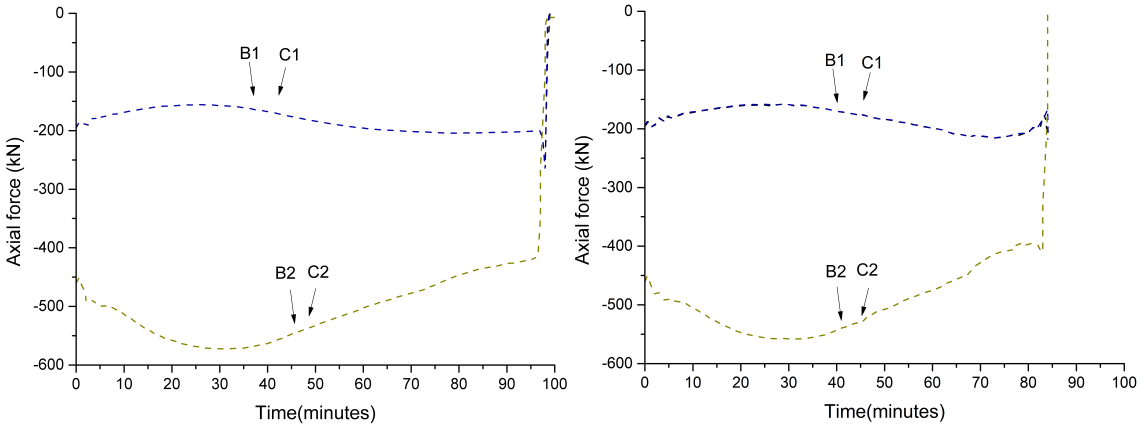

(a) EC3 model (b) Proposed damage model

Fig. 5.32 Axial forces in columns during fire event

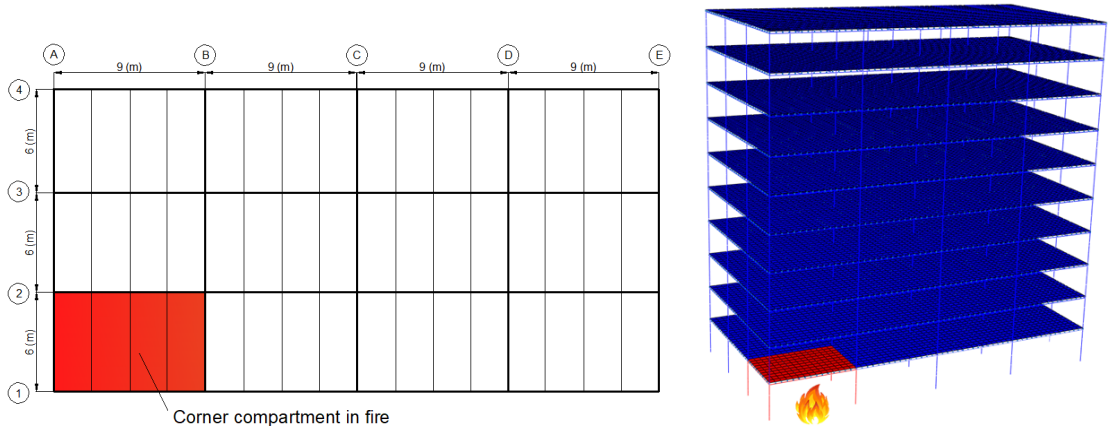

(a) (b)

Fig. 5.33 Location of the corner compartment fire on the ground floor

This study also starts with fire occurrences on the ground floor. Figure 5.33 shows the location of the compartment in fire within the building. A more robust performance is expected compared to fire occurrence at the same location in the 5-storey building as steel member section sizes are larger while the load values are the same as earlier case.

Results indicate that the building withstands the fire for 108.5 minutes in EC3 model prediction and 89.5 minutes in the damage model prediction, as shown in Figure 5.34. The temperature achieved in column B2 at the time of column failure is 550°C and 625°C with and without considering damage, respectively. The long stable period of the building is mainly attributed to the slow temperature development in ground floor columns due to their large section factors. This demonstrates the superior fire resistance of this type of building subjected to this scenario.

As in the case of five-storey building, the failure of columns is identified as the trigger of the global collapse and the deformed shape of the building prior to column buckling is characterized by moderate deflections of the heated beams and slabs as shown in Figure

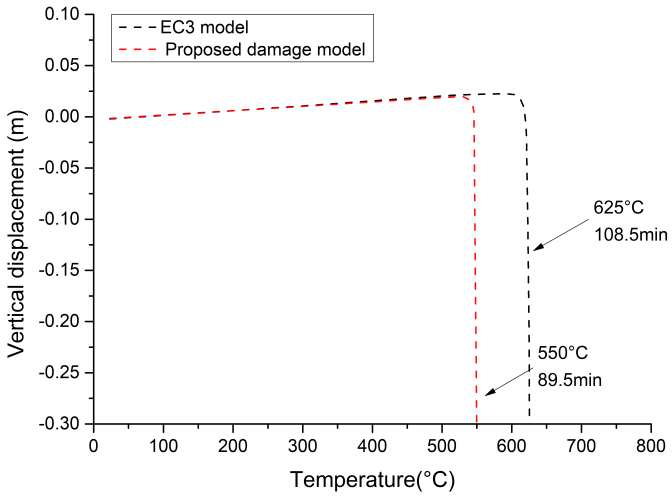

Fig. 5.34 Vertical displacement of the heated interior column B2

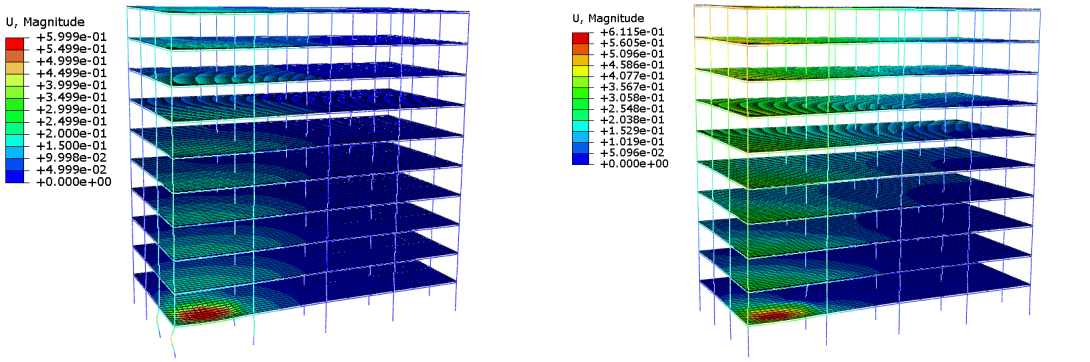

(a) EC3 model (At fire 108 minutes) (b) Proposed damage model (At fire 89 minutes)

Fig. 5.35 The deformed shape of the building before column buckling initiates

5.35. Axial load values in the heated columns of the fire compartment are plotted against time in Figure 5.36. A global downward collapse is triggered by buckling of internal column B2 in the EC3 model prediction, whereas the sequential buckling initiates from the heated perimeter columns in the damage model prediction. Again this change in the sequence of column failure could be explained by the damage accumulation in the members.

A comparison of the temperature development and damage evolution of the heated columns as predicted by the damage model are provided in Figure 5.37. The damage, which is initially thermal degradation dominant, evolves gradually until the plastic strain threshold is exceeded (denoted by the red circles). This is followed by the stage of abrupt acceleration of damage growth governed by coupled effects of thermo-mechanical damage. The damage accumulation results in a progressive erosion of elements and consequently an abrupt drop in the load carrying capacity. These effects, if not accounted for, lead to a significant over-estimation of structural fire resistance by 19 minutes as predicted in EC3 model.

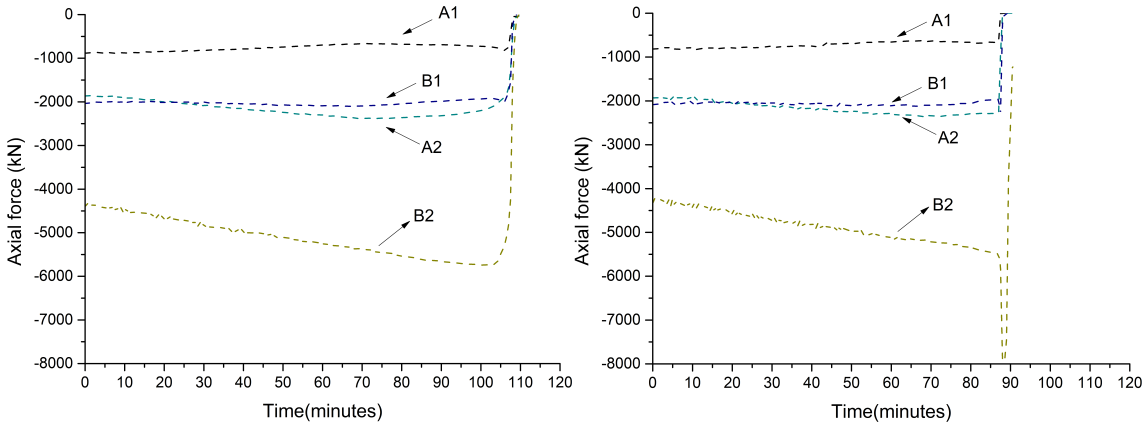

(a) EC3 model (b) Proposed damage model

Fig. 5.36 Axial forces in columns during fire event

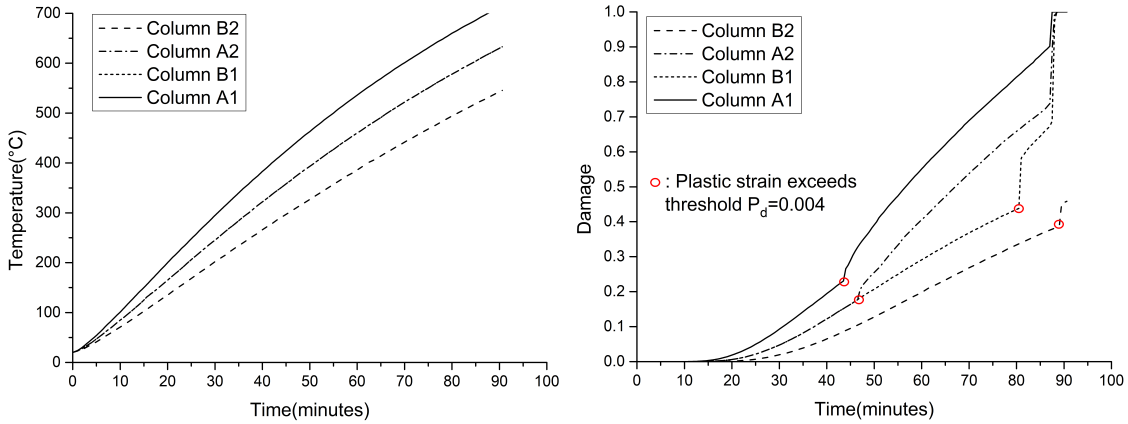

(a) Temperature development (b) Damage development

Fig. 5.37 Damage development in the top of heated columns

2. Central compartment fire on the ground floor.

Figure 5.38 shows a central compartment fire occurrence on the ground floor. It should be noted that due to the different plan layout compared to the five-storey building, the central fire is the internal fire compartment of the ten-storey building and has restraints on all sides from the surrounding structure, whereas the central fire is actually the peripheral compartment in the five-storey building. Therefore, the ten-storey building subjected to an internal fire is expected to show superior collapse resistance owing to a more uniform load redistribution and stronger restraints from the surrounding cool structure.

Figure 5.39 shows a sudden drop in the vertical displacement of column B2 at 103.5 minutes of fire and 108 minutes of fire with and without considering damage, respectively. This drop corresponds to simultaneous buckling of all heated columns, which can be observed in the axial load value development in Figure 5.40. After this point, the fall is arrested and the collapse potential is stopped, signalling that the load transfer mechanism comes into effect and the loads shed by the buckled columns are sustained

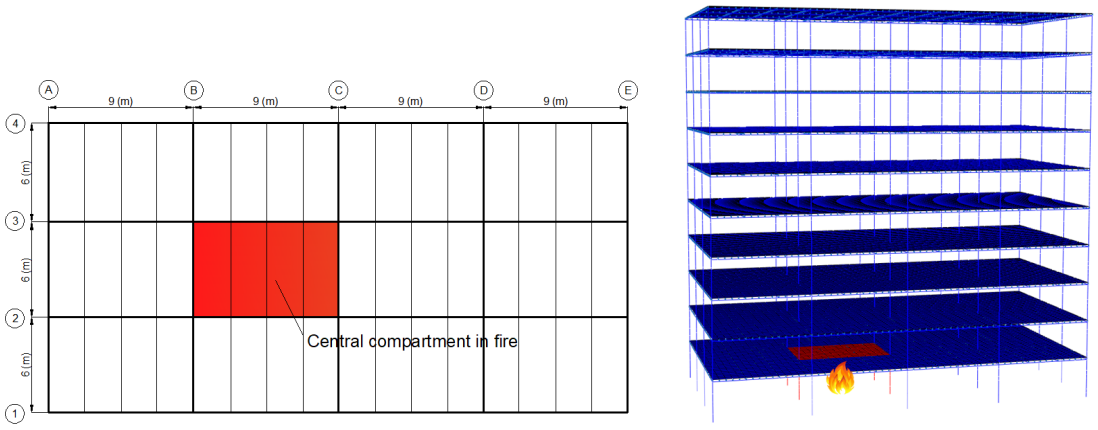

(a) (b)

Fig. 5.38 Location of the central compartment fire on the ground floor

by the neighbouring columns. The deflection of the slab increases significantly due to the loss of the vertical support provided by columns. The structure remains stable while the deflection increases. The maximum vertical displacement of the slab system predicted by the EC3 model is 800 *mm* at the end of 2-hour fire duration, suggesting that the building withstands the internal compartment fire. On the other hand, in the damage model prediction substantial deterioration is predicted in the beams and due to loss of flexural capacity the beams would require large displacements to develop catenary action to resist the loads. The vertical deformation exceeds 1/10 of the span after 104 minutes of fire in the damage model prediction and as a result the stability of the building system is endangered.

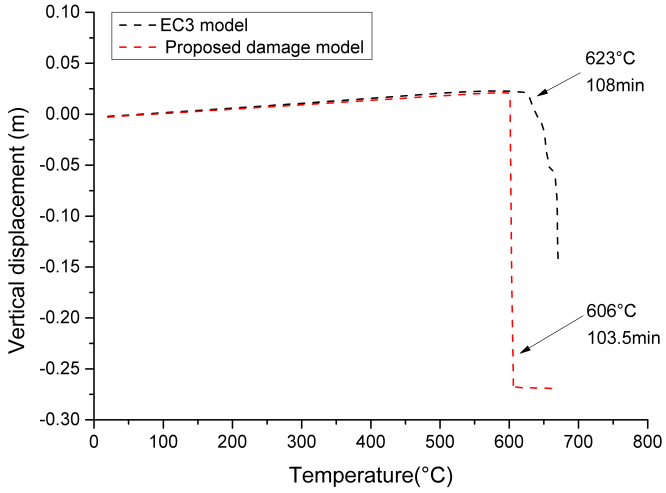

Fig. 5.39 Vertical displacement of the heated interior column B2

The building subjected to an internal fire switches the collapse mechanism to beam failure, which is more ductile than typical column failure. Compared to the corner fire scenario, the internal compartment fire scenario shows more robust collapse resistance due to a more uniform load redistribution and larger restraint on the fire compartment.

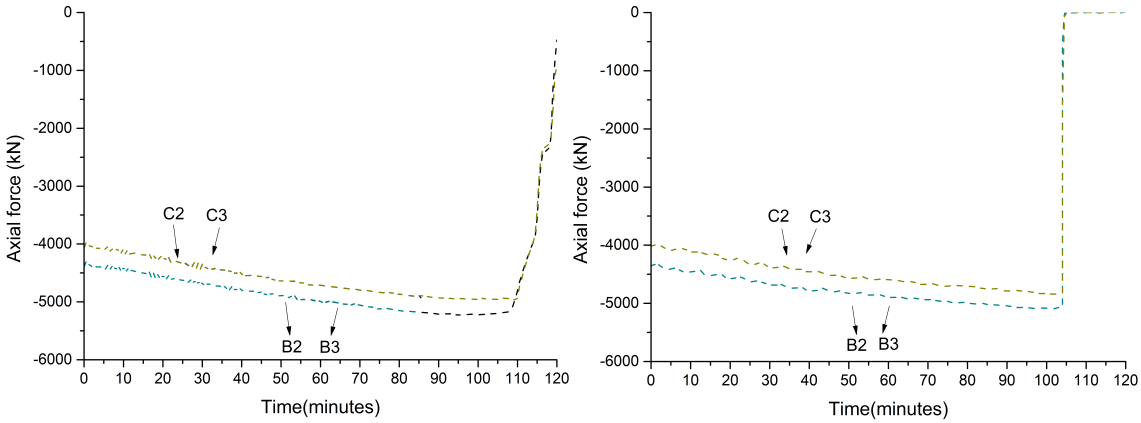

(a) EC3 model (b) Proposed damage model

Fig. 5.40 Axial forces in columns during fire event

There is significant formation of catenary action in primary beams and tensile membrane action in the slabs, which is facilitated by sufficient support provided by the surrounding cool slabs.

3. Corner compartment fire on the fifth floor.

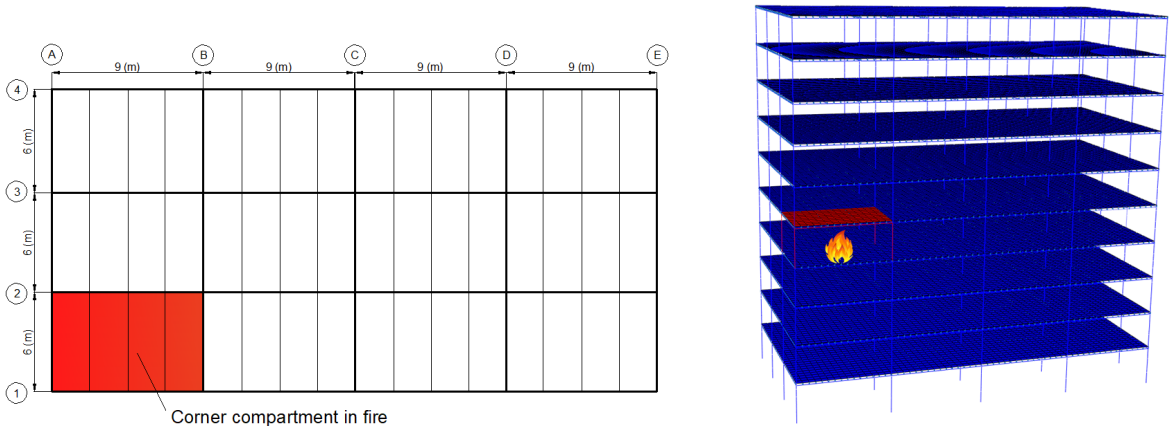

(a) (b)

Fig. 5.41 Location of the corner compartment fire at the mid-height of the building

The above conclusions are based on the triggering loads occurring on the ground floor. Progressive collapse is likely to have a higher risk to be initiated when the triggering loads occur on the upper floors because of the weaker collapse resistance provided by the smaller sections of steel members in the upper floors. In this case, the corner compartment on the fifth floor is heated as shown in Figure 5.41.

Compared to the ground floor fire scenarios, a drastic decrease is observed in the ultimate failure time of buildings as shown in Figure 5.42. A global downward collapse triggered by column failures occurs at 64 minutes and 77 minutes with and without considering damage, respectively. Axial load values in the heated columns of the fire compartment

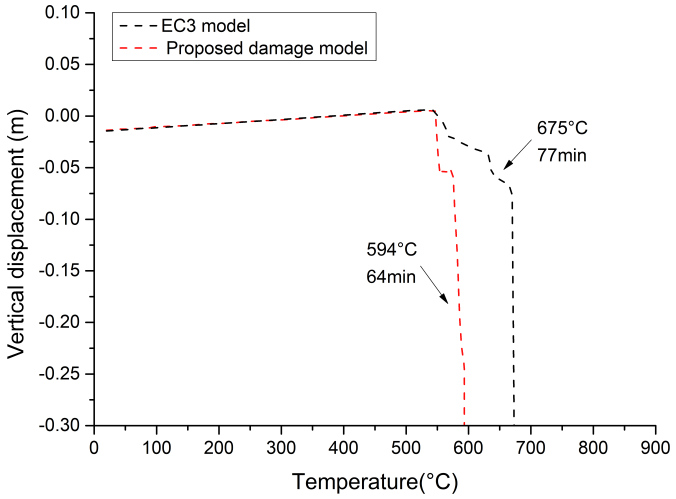

Fig. 5.42 Vertical displacement of the heated interior column B2

are plotted against time in Figure 5.43. After buckling of interior column B2, the vertical loads on the buckled columns are transferred to the adjacent columns and the structure remains stable for another 20 minutes in the EC3 model prediction and for only 7 minutes in the damage model prediction before inducing sequential buckling as well as the eventual collapse. This again shows the coupled effect of thermo-mechanical damage on structural fire resistance.

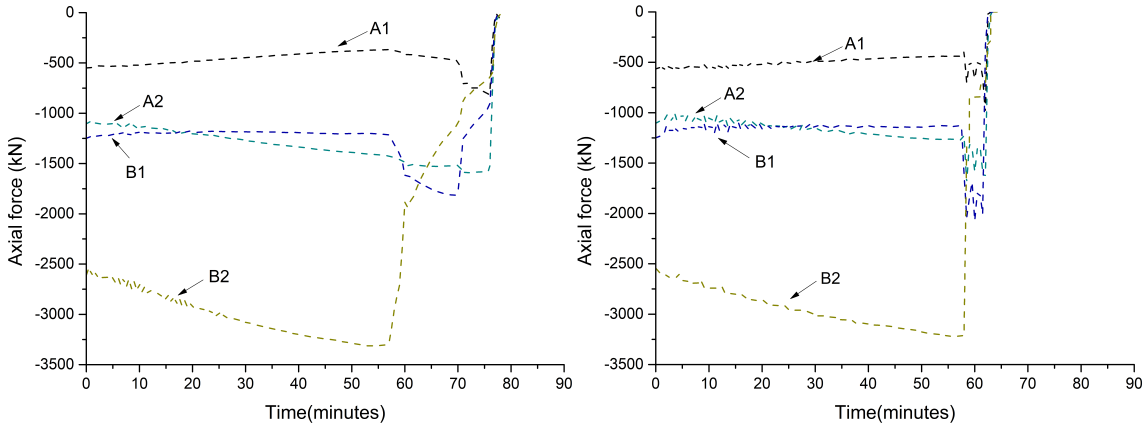

(a) EC3 model (b) Proposed damage model

Fig. 5.43 Axial forces in columns during fire event

4. Central compartment fire on the fifth floor.

Figure 5.44 shows the fire occurrence in the central compartment fire on the fifth floor. The vertical displacement of the heated interior column B2 is plotted in Figure 5.45 and the axial load values in the heated columns of the fire compartment are plotted against time in Figure 5.46. A sudden drop in the vertical displacement of column B2 occurs upon column buckling. However, the fall is resisted as fire progresses because the loads

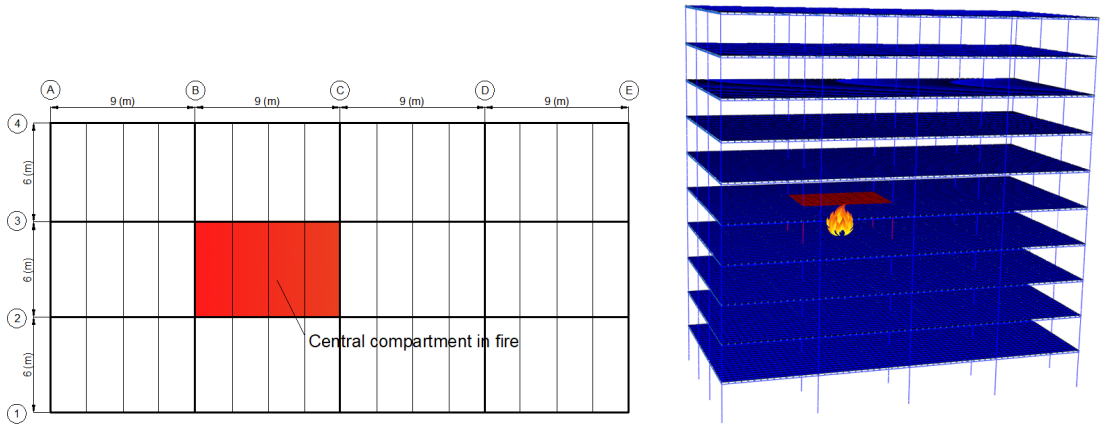

(a) (b)

Fig. 5.44 Location of the central compartment fire at the mid-height of the building

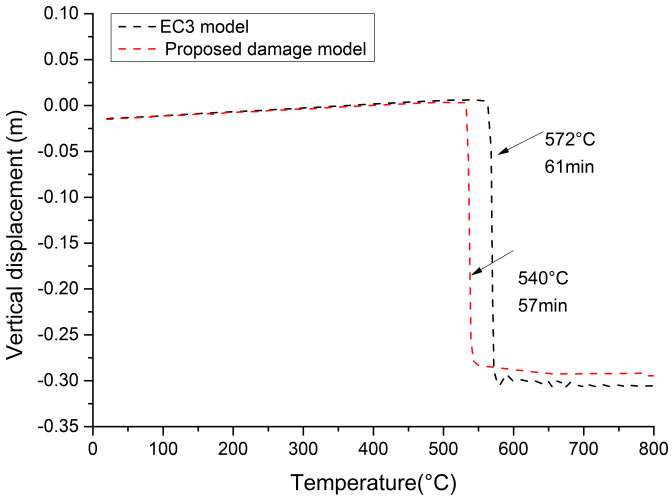

Fig. 5.45 Vertical displacement of the heated interior column B2

originally carried by the failed column are redistributed to the adjacent columns and no further buckling occurs.

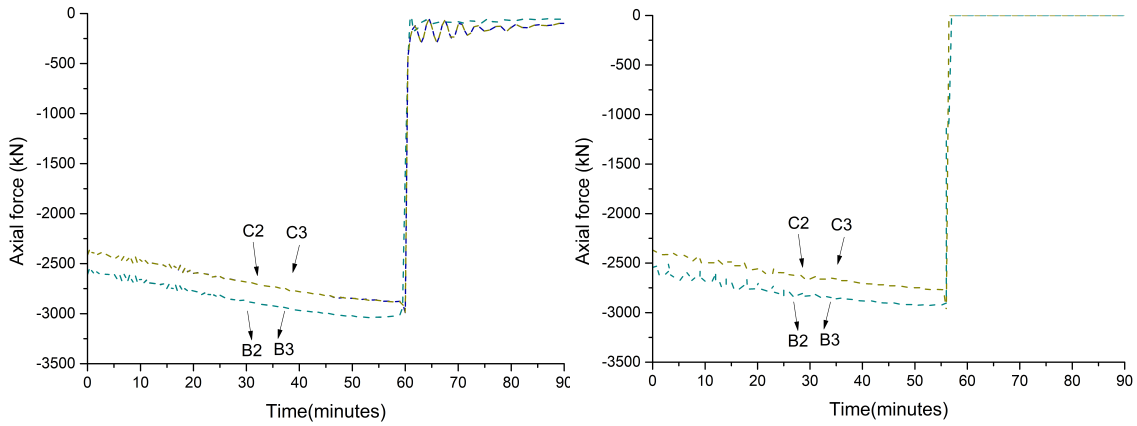

(a) EC3 model (b) Proposed damage model

Fig. 5.46 Axial forces in columns during fire event

Similar to the ground floor central fire scenario, the stability of the building system is maintained as a result of the uniform load redistribution mechanism. The maximum vertical displacement of slab system exceeds 1/10 of the span at 107 minutes of fire in EC3 model prediction and at 93 minutes of fire in the damage model prediction, signalling the initiation of collapse caused by excessive deflection. The fire resistance of the building achieved is significantly longer than that of individual members because the extra redundancy inherent in the structure is capable of providing alternate load paths after local failure occurs. The incorporation of the damage model provides a more realistic assessment of the structural fire resistance which is 13.08% lower than that of the EC3 model.

5. Corner compartment fire on the tenth floor.

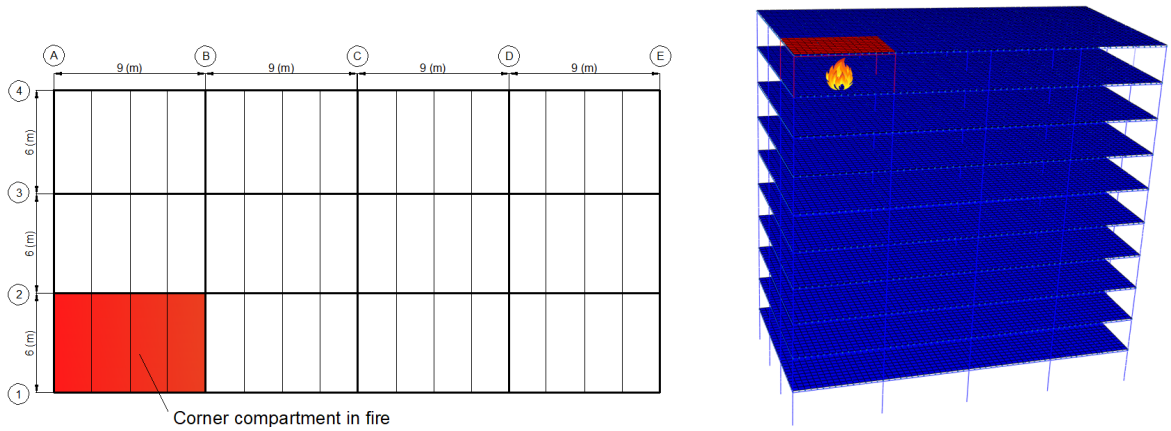

(a) (b)

Fig. 5.47 Location of the corner compartment fire on the top floor

Figure 5.47 shows the corner compartment fire on the top floor. Results show that progressive collapse occurs at 107 minutes in EC3 model prediction and at 85 minutes in damage model prediction. The vertical displacement of the heated interior column B2 is plotted in Figure 5.48 and the axial load values in the heated columns are plotted in Figure 5.49.

Similar to the analysis of the five-storey building, a gradual decrease is observed in the axial force values of column B2 as fire progresses. At the time of column failure, EC3 model results suggest that the redistributed loads are safely carried by the neighbouring columns for another 12 minutes before the failure of other columns and the eventual global collapse. By contrast, the column failure creates a chain reaction by bringing immediate failure to the adjacent columns and initiates progressive collapse of the whole building in the damage model prediction. Again this difference is attributed to the inability of the surrounding columns to support this load due to severely damaged load-carrying capacities. It can be concluded that the incorporation of damage model results in a significant decrease of 20.56% in fire resistance.

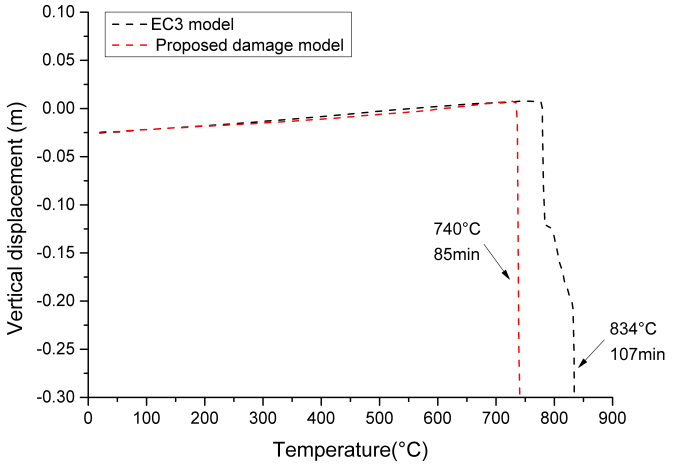

Fig. 5.48 Vertical displacement of the heated interior column B2

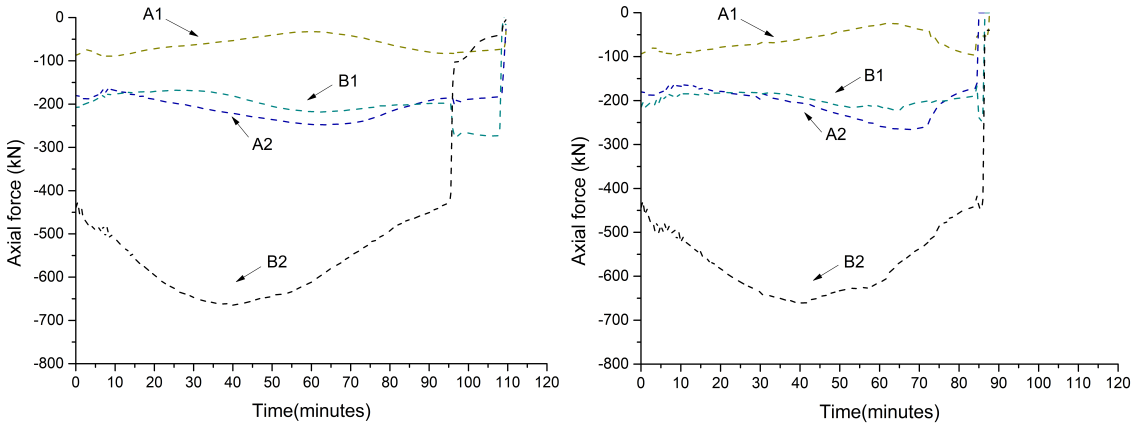

(a) EC3 model (b) Proposed damage model

Fig. 5.49 Axial forces in columns during fire event

6. Central compartment fire on the tenth floor.

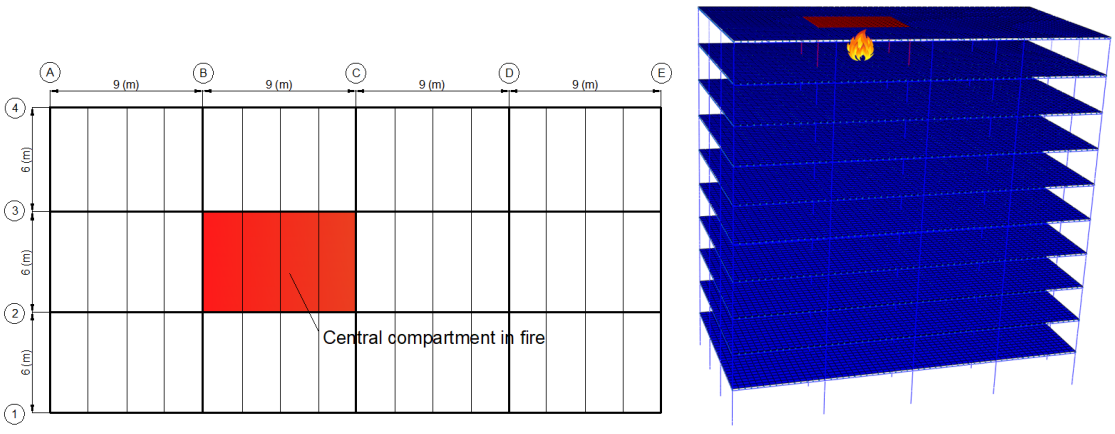

(a) (b)

Fig. 5.50 Location of the central compartment fire on the top floor

The location of the central compartment fire on the top floor of the ten-storey building is shown in Figure 5.50. The vertical displacement of the heated interior column B2 is plotted in Figure 5.51. The axial load values in the heated columns are plotted in Figure 5.52. Progressive collapse is triggered by simultaneous buckling of the heated columns, occurring at 97 minutes in EC3 model prediction and at 89 minutes in damage model prediction. A decrease of 8.25% is observed in the fire resistance as a result of considering the coupled effects of coupled thermo-mechanical damage propagation.

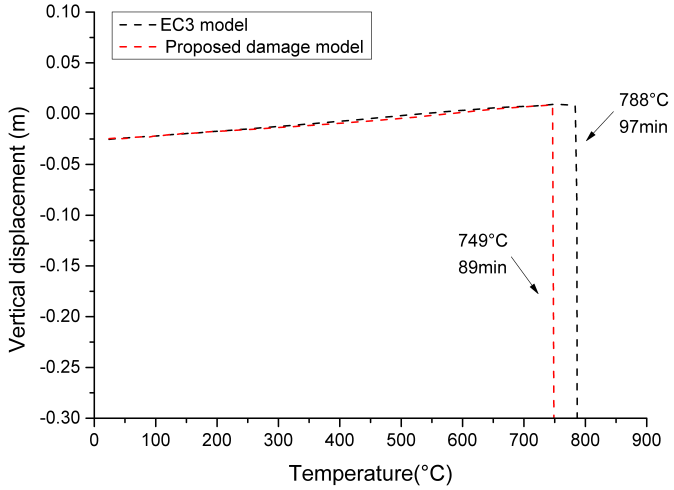

Fig. 5.51 Vertical displacement of the heated interior column B2

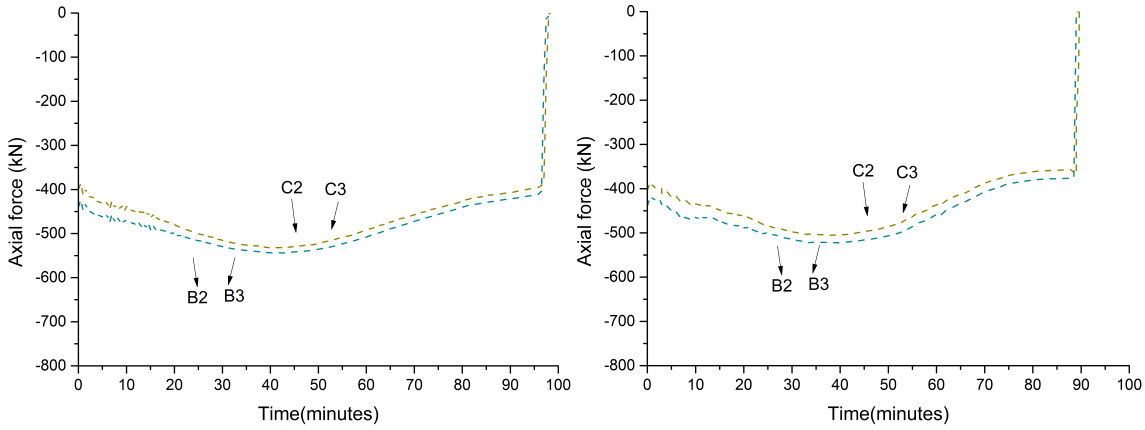

(a) EC3 model (b) Proposed damage model

Fig. 5.52 Axial forces in columns during fire event

5.7.2 Post-blast fire analysis

The previous section has studied the progressive collapse potential of steel structures under fire. The response of structures under the combined actions of explosion and fire is also a major concern in advanced structural fire engineering. Though this field has

received increasing attention after September 11th incident, limited studies have been done on structural robustness under the combined actions of blast and subsequent fire. This section provides an assessment of the fire resistance of steel buildings with initial structural damage, aiming to demonstrate the influences of blast-induced damage on the collapse initiation time. The detrimental effects from the blast loading will be discussed and the fire resistance of the damaged building will be re-assessed.

After the blast-induced response of the steel frame stabilises, the fire action is applied subsequently in order to evaluate the progressive collapse potential of the damaged frame. As damage on the fire insulation caused by blast load or fragmentation impact is very difficult to assess quantitatively, the insulation material is assumed to remain intact on member surfaces though this might not be a realistic assumption for the majority types of fire resistant materials. It is further assumed that the fire would not spread and the temperature histories of the structural members are identical to the fire only cases. It is anticipated that the steel frames in this scenario are likely to have lower failure temperatures.

5.7.2.1 Five-storey office building

1. Corner compartment post-blast fire on the ground floor.

The response of the structure can be divided into two stages: blast-induced and fire-dominant. The deformed shape of the building at the end of blast analysis is displayed in Figures 5.53. Due to its lower moment capacity, a maximum lateral deflection of 200 *mm* occurs in column A1 on the ground floor. This causes some loads to be transferred to the neighbouring column A2 which has a maximum lateral deflection of 48 *mm*. The floor system is blown upward by the blast pressure for 265 *mm* at the centre of the slab system. Despite these permanent deformations, the blast loading imposes no threat to the overall structural stability.

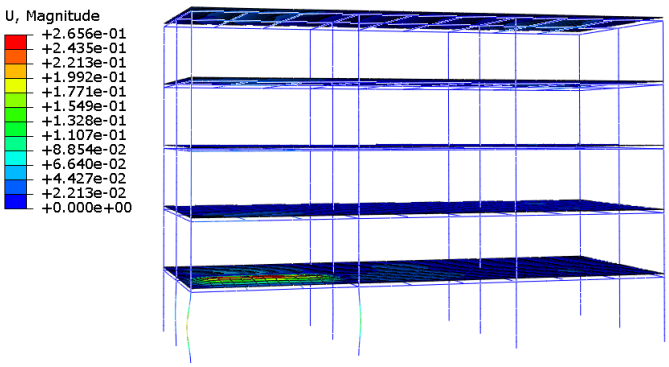

Fig. 5.53 Blast induced deformation after the blast analysis in the corner compartment on the ground floor

The vertical displacement of the heated interior column B2 in the subsequent fire analysis is plotted in Figure 5.54. Compared with fire only case at the same location, the collapse time in this combined hazard scenario is earlier due to the initial blast-induced damage in the structural system. The critical temperature of column B2 is 622°C in EC3 model prediction decreasing from 670°C in the fire only scenario, whereas the critical temperature in the damage model prediction is 576°C which is reduce by 32°C compared to the fire only scenario.

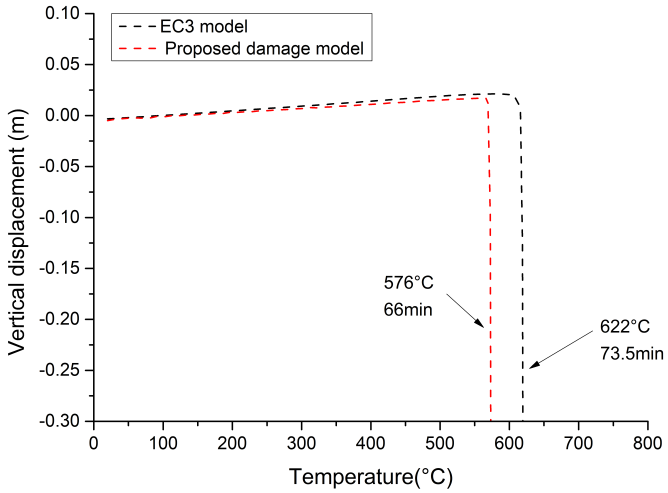

Fig. 5.54 Vertical displacement of the heated interior column B2

The development of axial force values in four heated columns is shown in Figure 5.55. The initial axial force in column A1 is smaller than in the fire only case, because the blast-induced displacement causes the load to be redistributed to the neighbouring column A2. The combined effects of increased axial forces and the load-displacement effect cause column failure to occur earlier compared to under fire attack only. And the failure of columns is identified as the trigger of the global collapse in both cases.

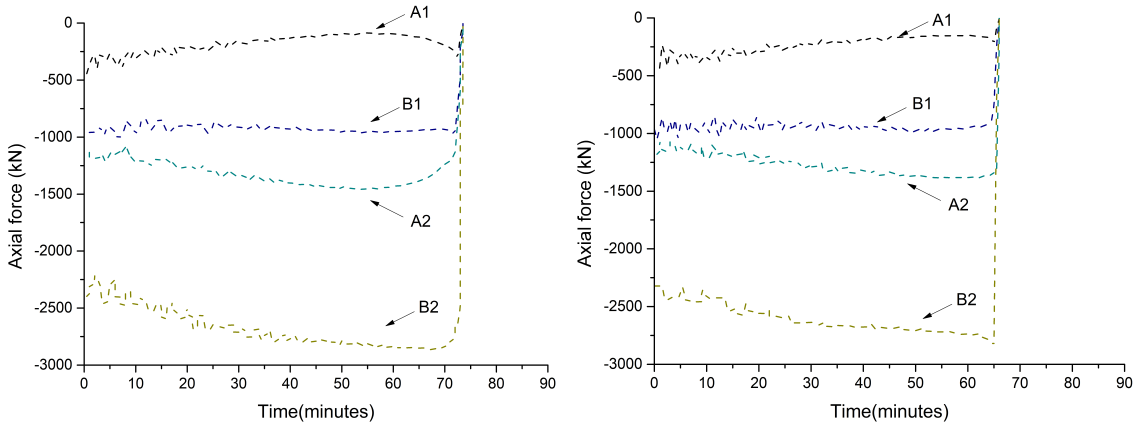

(a) EC3 model (b) Proposed damage model

Fig. 5.55 Axial forces in columns during fire event

It should be emphasized that in the case of integrated blast and fire analysis, the damage model has demonstrated the capability of capturing blast-induced mechanical damage. A comparison of the temperature development and evolution of damage in the element of the top of blast-damaged columns as predicted by the damage model is provided in Figure 5.56. Two stages of damage development, sudden blast-induced damage growth (denoted by red circles) and gradual coupled thermo-mechanical damage propagation under the subsequent fire loading, are evident in Figure 5.56 (b). All of this leads to considerable deterioration in the load carrying capacity of the columns and thereby reducing the fire resistance of the building system. By comparing the models with and without damage, it may be concluded that the incorporation of damage model in integrated blast and fire analysis decreases the fire resisting time of the building by 7.5 minutes (10.20%) or the fire resisting temperature by 46°C (7.40%).

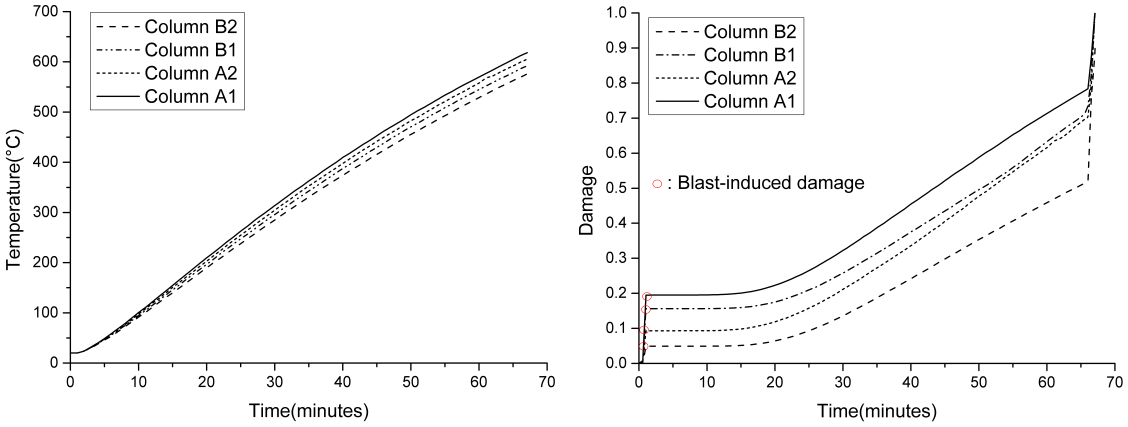

(a) Temperature development (b) Damage development

Fig. 5.56 Damage development in the top of columns subjected to blast and fire

2. Central compartment post-blast fire on the ground floor.

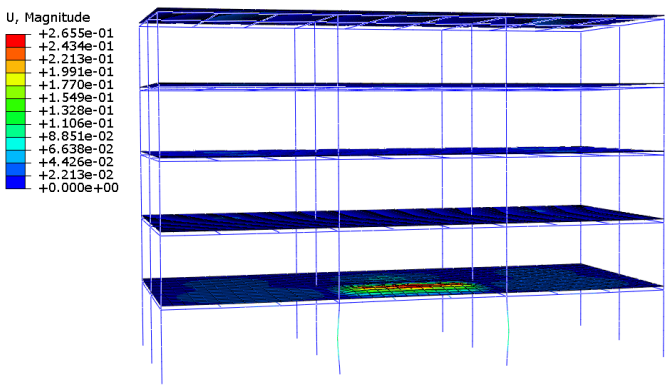

Fig. 5.57 Blast induced deformation after the blast analysis in the central compartment on the ground floor

In this case, a maximum lateral deflection of 113 *mm* occurs in the middle of column B1 and C1 on ground floor due to their lower moment capacity as shown in Figure 5.57.

Because of the uplift pressures, the slab system is blown upward for about 265 *mm* at the centre of the slab. Again, no threat is imposed to the structural stability by blast loads alone. Figure 5.58 shows the vertical displacement of the heated interior column B2 in the subsequent fire analysis, suggesting that fire-induced progressive collapse occurs at 65.5 minutes and 73.5 minutes with and without incorporating damage model, respectively. Again the fire resistance of the blast-damage structure decreases compared to that of fire only scenario.

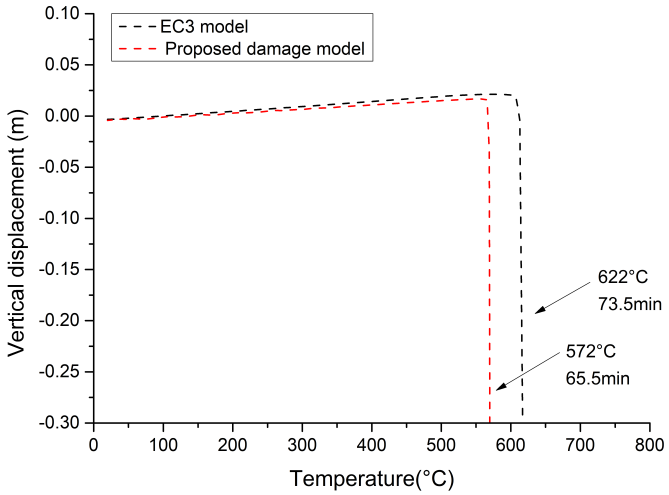

Fig. 5.58 Vertical displacement of the heated interior column B2

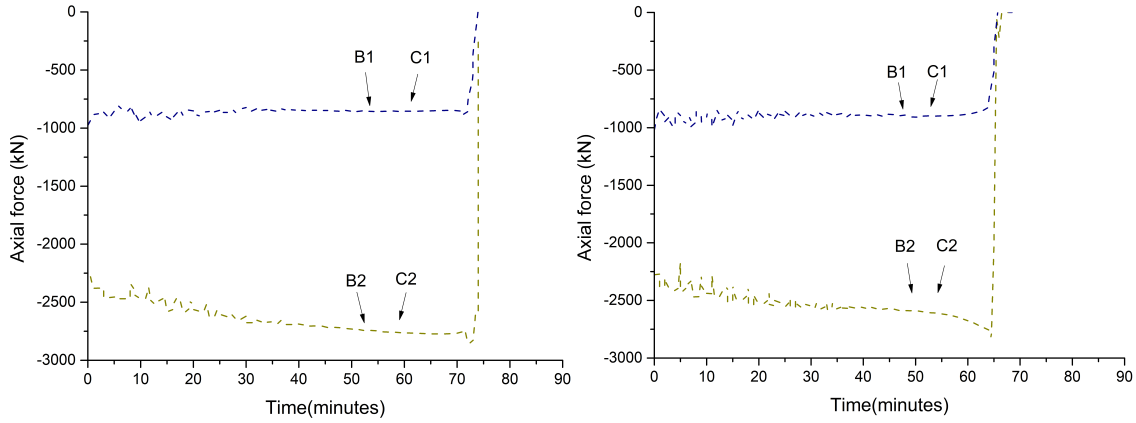

(a) EC3 model (b) Proposed damage model

Fig. 5.59 Axial forces in columns during fire event

In contrast with the fire only scenario at the same location, perimeter column B1 and column C1 with obvious permanent deformations caused by blast loads buckle earlier than the interior columns with the highest utilization ratios. This is followed by a brief load redistribution process, as observed in the axial force values of column B2 and column C2 in Figure 5.59. Progressive collapse occurs shortly afterwards due to the inability of the surrounding columns to sustain the loads shed by the failed columns. This

observation suggests a contradictory collapse initiation mechanism to that of fire only scenario, in which the highest utilization ratio of interior columns is a deciding factor in structural fire resistance. Results show that perimeter columns have a high potential to cause collapse of structures in fire due to a higher level of lateral deflection induced by blast loads.

3. Corner compartment post-blast fire on the third floor.

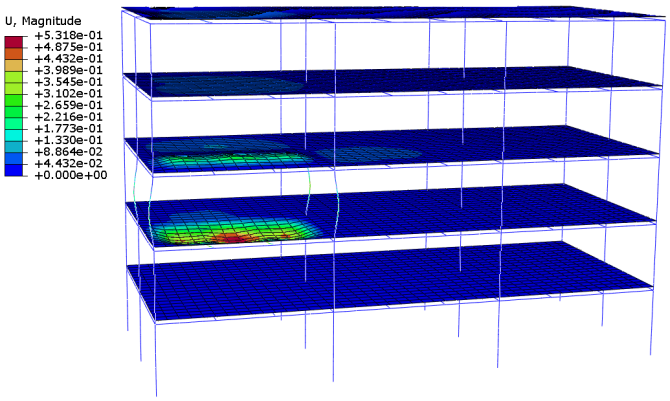

Fig. 5.60 Blast induced deformation after the blast analysis in the corner compartment on the third floor

On examining the post-blast fire occurrences on upper floor, note that because of both the uplift and downward blast pressures working on the slabs, the floor system above is blown upward for 258 *mm* and the floor system below is blown downward for 530 *mm* at the slab centre. This is within the maximum allowable deflection limit and therefore no failure is triggered in slab systems. Figure 5.60 shows that blast loads induce substantial lateral deflection in columns, being 222 *mm* in column A1, 216 *mm* in column A2 and column B1, and 250 *mm* in column B2. This large lateral deflection in combination with high utilization ratios cause some loads in column A2 and column B2 be transferred to the adjacent columns. No risks of collapse are detected at this stage.

This is followed by subsequent fire analysis and the global downward collapse is triggered by column failures as fire progresses. The fire resistance of the damaged building is observed to decrease drastically compared to fire only scenario as shown in Figure 5.61. In the EC3 model prediction, the fire resisting time is 62.5 minutes, decreasing from 76 minutes in fire only scenario, with the critical temperature of column B2 decreasing from 680°C to 594°C. Whereas in the damage model, the fire resisting time is 51.5 minutes, decreasing from 63 minutes in fire only scenario, with the critical temperature of column B2 decreasing from 600°C to 514°C. This suggests that the time realistically available for evacuation before progressive collapse occurs does not meet the required fire resistance of 1 hour, imposing significant threat to the safety of occupants in the building.

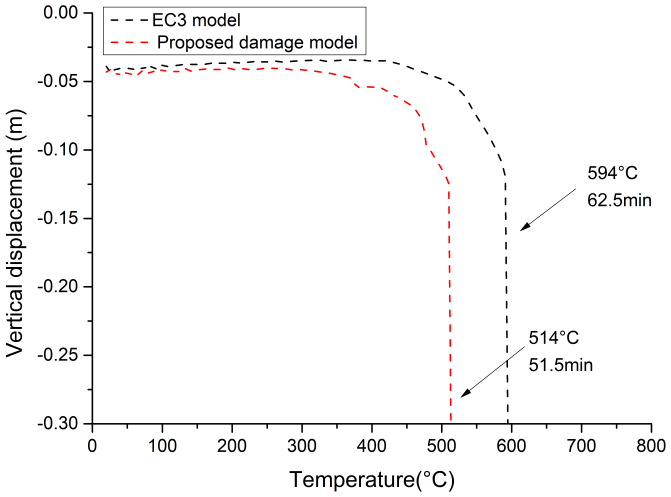

Fig. 5.61 Vertical displacement of the heated interior column B2

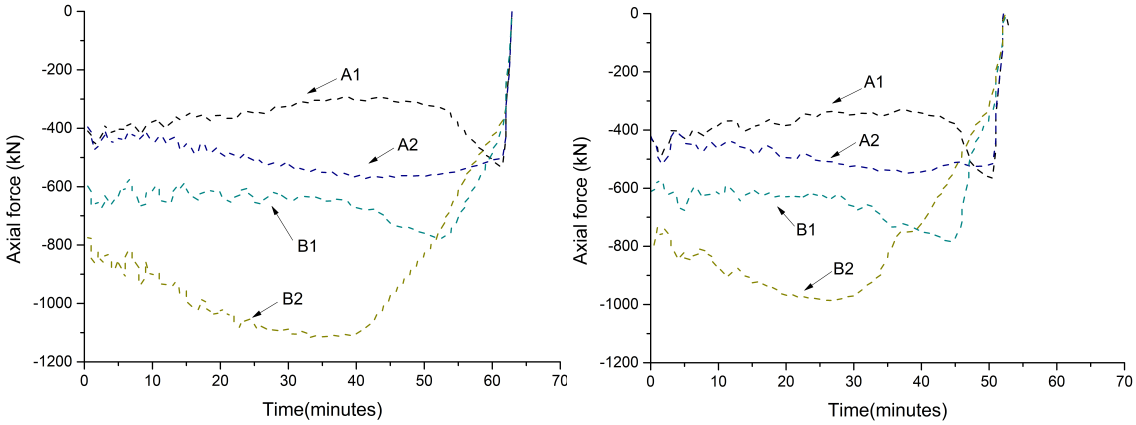

(a) EC3 model (b) Proposed damage model

Fig. 5.62 Axial forces in columns during fire event

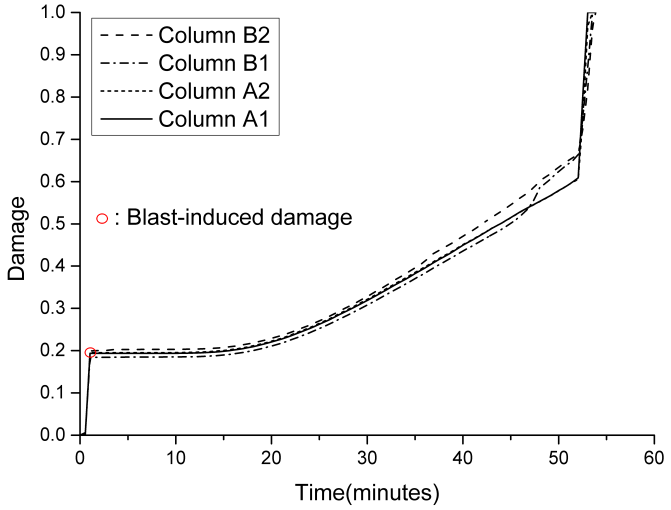

Fig. 5.63 Damage development in the top of blast-damaged columns

Figure 5.62 shows the axial forces of the heated columns. During the initial heating phase, additional compression force is developed in column B2 due to thermal expansion and consequent restraint forces. Afterwards a gradual decrease is observed in axial force values of column B2 as a result of excessive bending. The damage development pattern in the top of blast-damage columns is plotted in Figure 5.63. The contribution of the blast-induced damage in the subsequent coupled damage propagation is evident. It is clear that fire following an extreme event could impose significant threat to structural safety and the importance of adopting damage model approach in the integrated blast and fire analysis is highlighted.

4. Central compartment post-blast fire on the third floor.

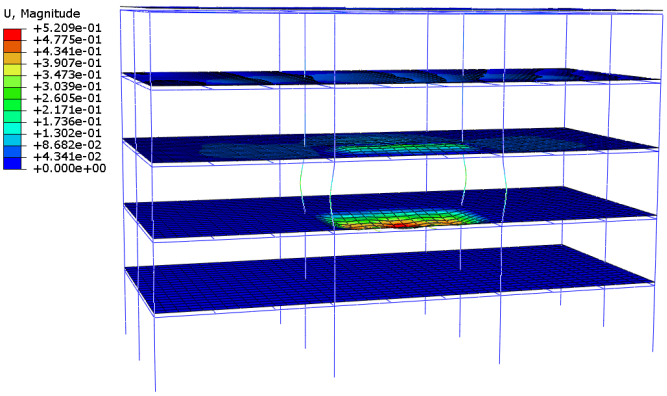

Fig. 5.64 Blast induced deformation after the blast analysis in the central compartment on the third floor

As the study moves to central compartment on the third floor, the deformed shape of the building at the end of blast analysis is shown in Figure 5.64. The floor system above is blown upward for 273 *mm* and the floor system below is blown downward for 520 *mm* at the slab centre. The lateral deflection induced by blast is 222 *mm* in column B1 and column C1, and 269 *mm* in column B2 and column C2. This large lateral deflection in column B2 and column C2 causes some loads to be transferred to the adjacent columns.

Under the subsequent fire action, the building remains stable until a global downward collapse is triggered by buckling of interior columns. The fire resistance of the building is severely deteriorated as a result of the blast impact, with the vertical displacement of interior column shown in Figure 5.65 and the axial force values of heated columns shown in Figure 5.66. Due to the damage from the blast effect, the limiting temperature decreases from 656°C to 533°C without considering damage, and from 585°C to 448°C by incorporating damage model. Accordingly, the fire resistance of the building is also reduced from 72 minutes to 51.5 minutes in EC3 model prediction, and from 61 minutes to 41.5 minutes in damage model prediction. It should be noted that the fire resistance predicted by both models is lower than the predefined 1-hour fire resistance rating of the building, suggesting that this type of scenario imposes huge threat to structural safety.

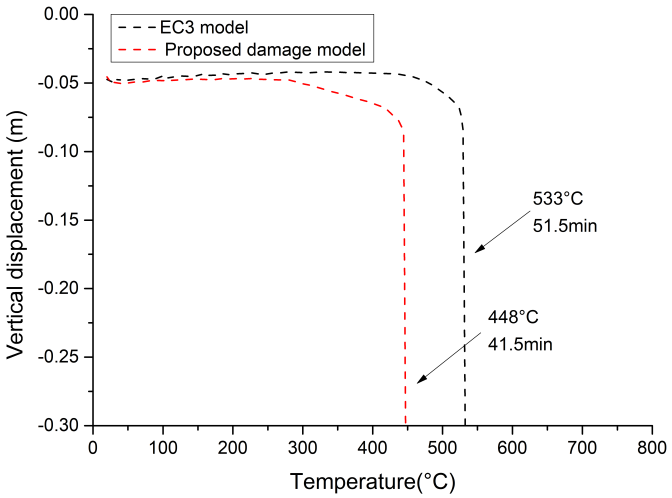

Fig. 5.65 Vertical displacement of the heated interior column B2

Comparison of results with and without damage incorporated in Figure 5.66 shows a noticeable difference in the axial force values development as a result of substantial deterioration of column strength predicted by the damage model.

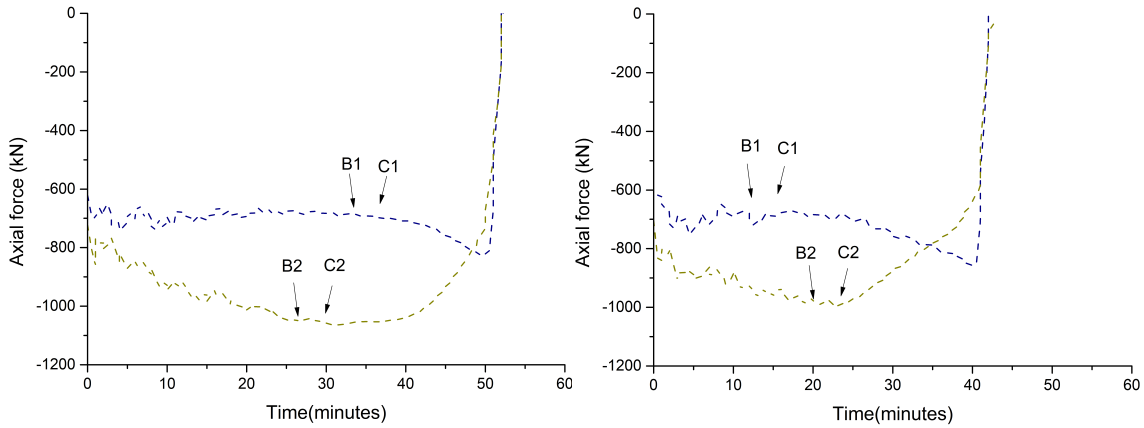

(a) EC3 model (b) Proposed damage model

Fig. 5.66 Axial forces in columns during fire event

5. Corner compartment post-blast fire on the fifth floor.

The deformed shape of the building when the blast loads act inside the corner compartment of the top floor is shown in Figure 5.67, with the maximum upward deflection of slab system being 265 *mm* and the maximum downward deflection of the floor system below being 538 *mm*. The lateral deflection induced by blast is 255 *mm* in column A1, 214 *mm* in column A2, 234 *mm* in column B1, and 210 *mm* in column B2. The effects of large lateral deflection in combination with high utilization ratios cause some loads in column A2 and column B2 be transferred to the adjacent columns.

A significant reduction in the fire resistance of the building is observed due to the blast impact. Progressive collapse occurs due to column failure and the inability of the

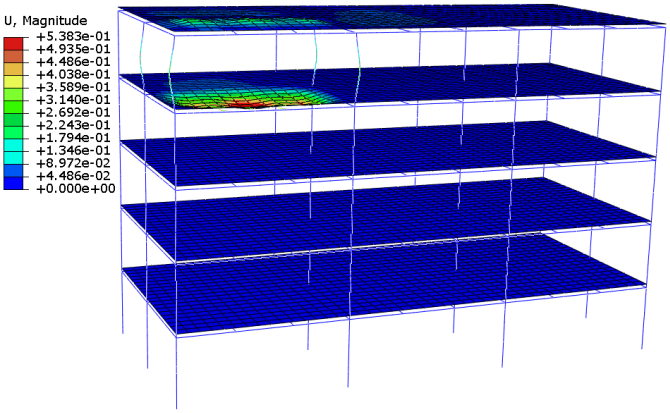

Fig. 5.67 Blast induced deformation after the blast analysis in the corner compartment on the top floor

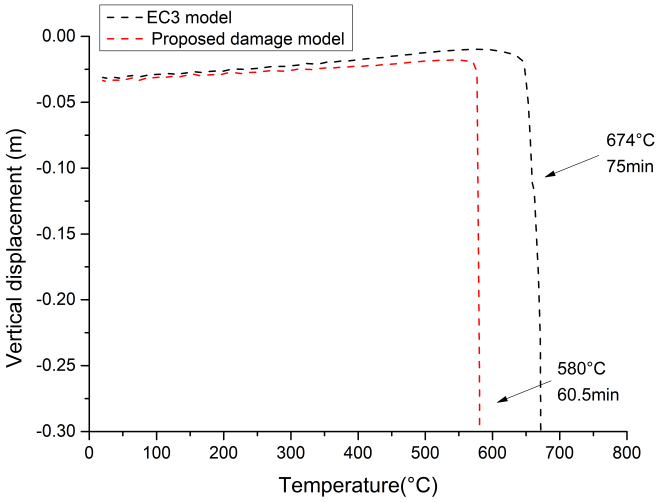

Fig. 5.68 Vertical displacement of the heated interior column B2

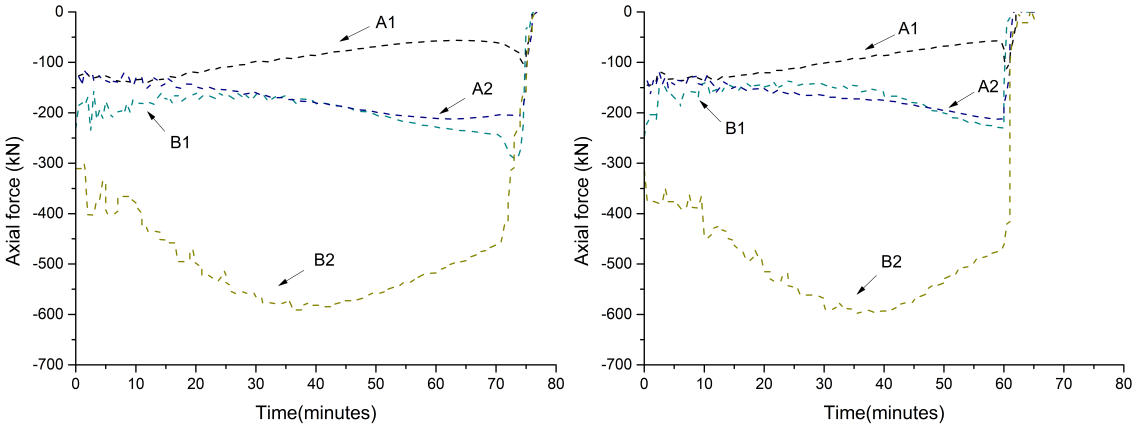

(a) EC3 model (b) Proposed damage model

Fig. 5.69 Axial forces in columns during fire event

structure to redistribute the loads away from the failed members. Compared to fire only scenario, the fire resistance of the building is reduced from 97 minutes to 75 minutes

without considering damage, and from 81 minutes to 60.5 minutes by incorporating the damage model. Correspondingly, the limiting temperature of interior column B2 decreases from 822°C to 674°C without considering damage, and from 712°C to 580°C by incorporating the damage model. Comparison of models with and without damage incorporated shown in Figure 5.68 and Figure 5.69 indicates a substantial deterioration of 19.33% in fire resistance due to the effects of taking into account coupled damage propagation.

6. Central compartment post-blast fire on the fifth floor.

As shown in Figure 5.70, because of the uplift and downward blast pressure, the floor system above is blown upward for 289 *mm* and the floor system below is blown downward for 523 *mm* at the slab centre. The lateral deflection induced by blast is 231 *mm* in column B1 and column C1, and 213 *mm* in column B2 and column C2. This large lateral deflection combined with high utilization ratios in column B2 and column C2 causes some loads to be transferred to the adjacent columns.

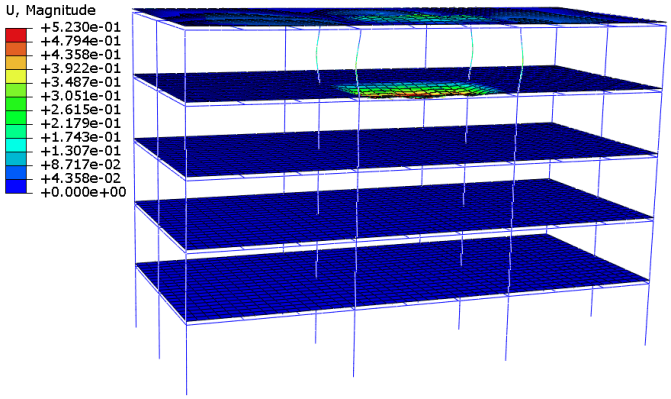

Fig. 5.70 Blast induced deformation after the blast analysis in the central compartment on the top floor

The vertical displacement of the heated interior column B2 is shown in Figure 5.71 and the axial force values of heated columns are shown in Figure 5.72. A typical collapse mechanism of column failure is also observed here. Again the fire resistance of the building is severely deteriorated by the blast impact, with the limiting temperature decreasing from 786°C to 675°C without considering damage, and from 727°C to 611°C with damage model. The fire resisting time of the building is also reduced from 97 minutes to 72 minutes without considering damage, and from 84 minutes to 62 minutes with damage model.

Thus far, in all cases the progressive collapse time in post-blast fire scenario is earlier than fire only scenario due to the blast-induced damage. The results clearly show the detrimental impact of the blast-induced damage and moreover the effects of incorporating

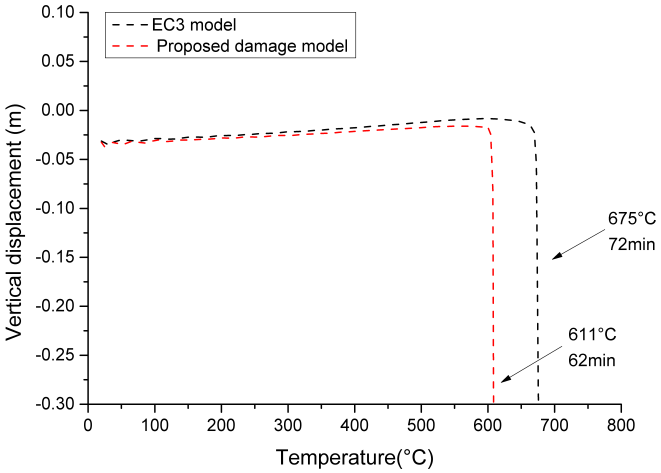

Fig. 5.71 Vertical displacement of the heated interior column

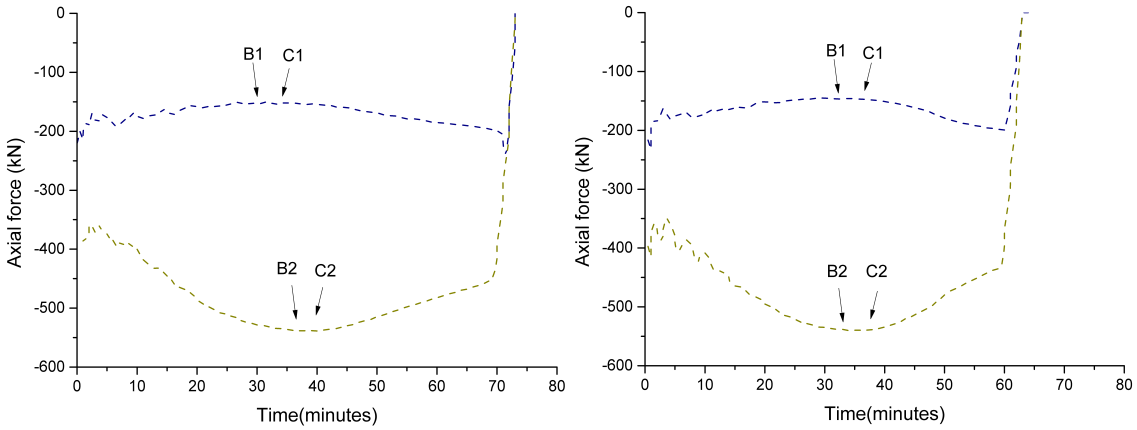

(a) EC3 model (b) Proposed damage model

Fig. 5.72 Axial forces in columns during fire event

the damage model in simulations by capturing the coupled thermo-mechanical damage growth.

5.7.2.2 Ten-storey office building

The behaviour and limit-states of the ten-storey steel-framed building subjected to post-blast fire scenarios are investigated in this section.

1. Corner compartment post-blast fire on the ground floor.

The deformed shape of the ten-storey building at the end of blast analysis is displayed in Figure 5.73. The blast pressure induces a maximum upward deflection of 234 *mm* in the slab centre, whereas the lateral deflections in steel columns are negligible owing to the high moment capacities associated with the robust sections on the ground floor, being 15 *mm* in column A1, 6 *mm* in column A2 and column B1, and 1 *mm* in column B2. Thus, it

is not surprising that the reduction in the fire resistance induced by blast loads is only 1.5 minutes with the same collapse mechanism compared to fire only scenario at the same location. The fire resisting time with and without considering damage is 88 minutes and 107 minutes, respectively.

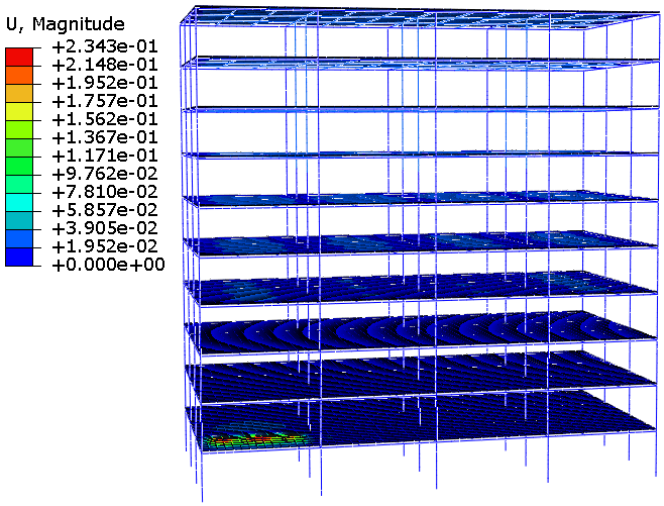

Fig. 5.73 Blast induced deformation after the blast analysis in the central compartment on the ground floor

2. Central compartment post-blast fire on the ground floor.

Similar to the previous case, negligible deformation is induced in steel columns by the blast loads. The building remains safe through the 2-hour fire in EC3 model prediction, while the fire resisting time with considering damage is 103 minutes. By comparing to fire only scenario at the same location, the fire resisting time is the same in EC3 model prediction, whereas a reduction of 1 minute is observed in the damage model prediction while the same collapse mechanism is obtained.

3. Corner compartment post-blast fire on the fifth floor.

In contrast with ground floor accidental scenarios, considerable lateral deformations are induced in columns when triggering loads occur on upper floors as the section sizes of columns are reduced. Because of the uplift and downward blast pressures working on the slabs, a maximum upward displacement of 232 *mm* and a maximum downward displacement of 468 *mm* are observed in the floor systems above and below, respectively. No failure is induced in the slab systems and the deformed shape of the building at the end of the blast analysis is shown in Figure 5.74. On the other hand, the lateral deflection induced by blast is 222 *mm* in column A1, 167 *mm* in column B1, 75 *mm* in column A2, and 80 *mm* in column B2. It should be noted that the extent of blast-induced permanent deformation is reflected in the damage development plots in Figure 5.77 which is denoted by red circles. The large lateral deflection in combination with high utilization ratios

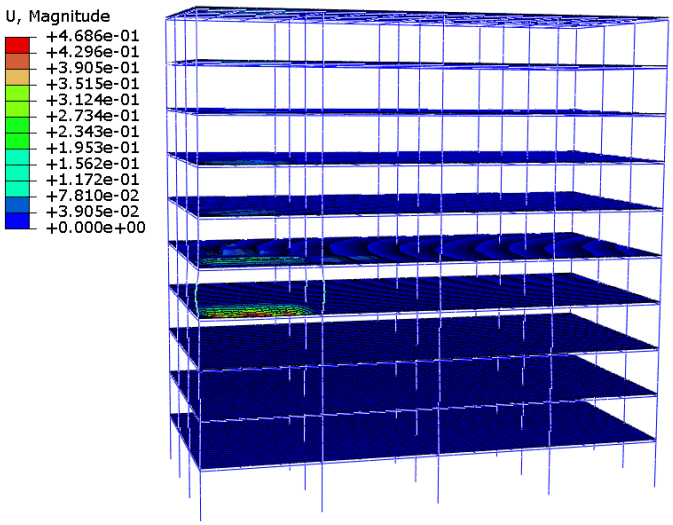

Fig. 5.74 Blast-induced deformation after the blast analysis in the corner compartment on the fifth floor

cause some loads in column B1 and column B2 be transferred to the adjacent columns. The axial load values of the columns in fire compartment are plotted in Figure 5.76. No risks of collapse are detected at this stage.

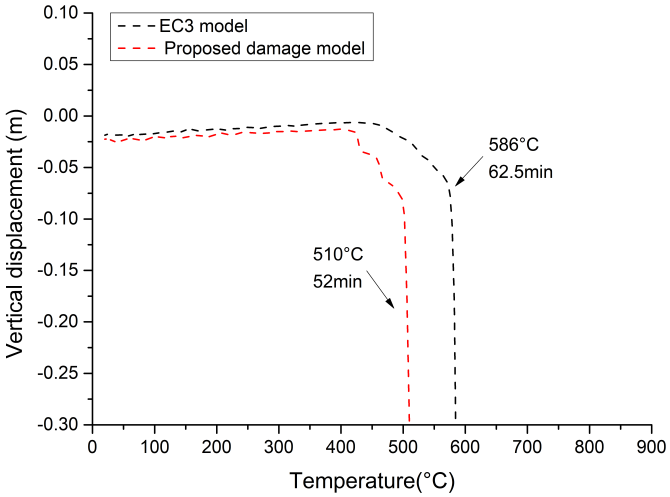

Fig. 5.75 Vertical displacement of the heated interior column B2

This is followed by subsequent fire analysis and progressive collapse is triggered by sequential column buckling which initiates from failure of column B2. The vertical displacement of interior column B2 is shown in Figure 5.75. Compared to fire only scenario, the EC3 model results indicate that the fire resisting time of the damaged building decreases from 77 minutes to 62.5 minutes, with the critical temperature of column B2 decreasing from 675°C to 586°C. Whereas in the damage model prediction, the fire resisting time decreases from 64 minutes to 52 minutes, with the critical temperature of column B2 decreasing from 594°C to 510°C.

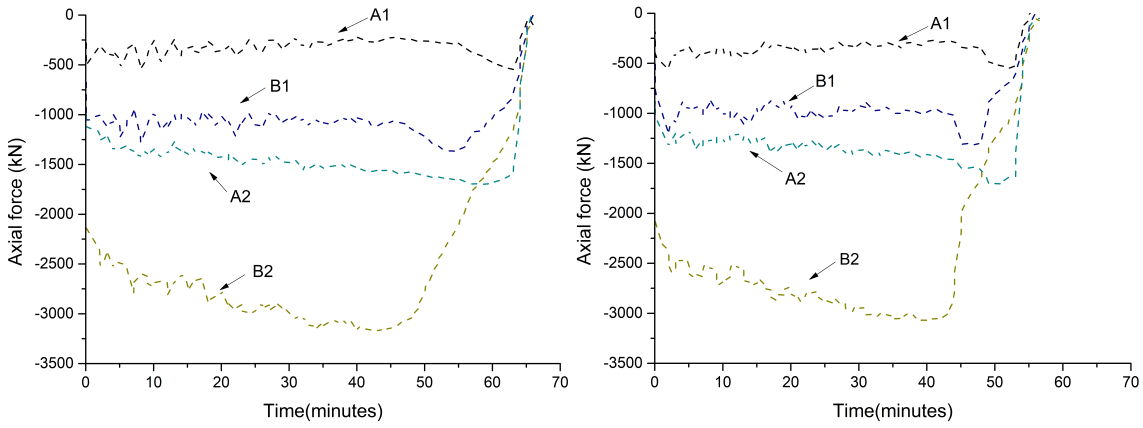

(a) EC3 model (b) Proposed damage model

Fig. 5.76 Axial forces in columns during fire event

It should be pointed out that the fire resistance predicted by the damage model is 52 minutes, which is lower than the predefined 1-hour fire resistance rating of the building. By contrast, the EC model prediction of 62.5 minutes suggests that the structure achieves the level of safety required and might lead to non-conservative design decisions. Again the importance of adopting damage model approach in the simulation is fully demonstrated in this study.

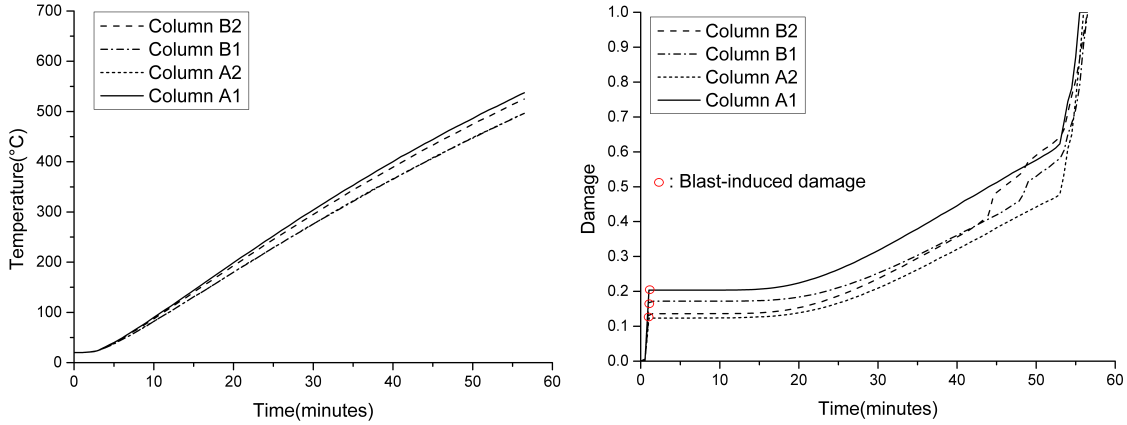

(a) Temperature development (b) Damage development

Fig. 5.77 Damage development in the top of columns subjected to blast and fire

4. Central compartment post-blast fire on the fifth floor.

A central compartment blast induces a maximum upward deflection of 162 *mm* and downward deflection of 370 *mm* in the floor systems, as shown in Figure 5.78. The lateral deflection induced by blast is 86 *mm* in column B2 and column B3, and 112 *mm* in column C2 and column C3. In the subsequent fire analysis, the vertical displacement of interior column B2 is shown in Figure 5.79 and the axial force values of heated columns are shown in Figure 5.80. Again, the buckling of heated columns occur earlier compared

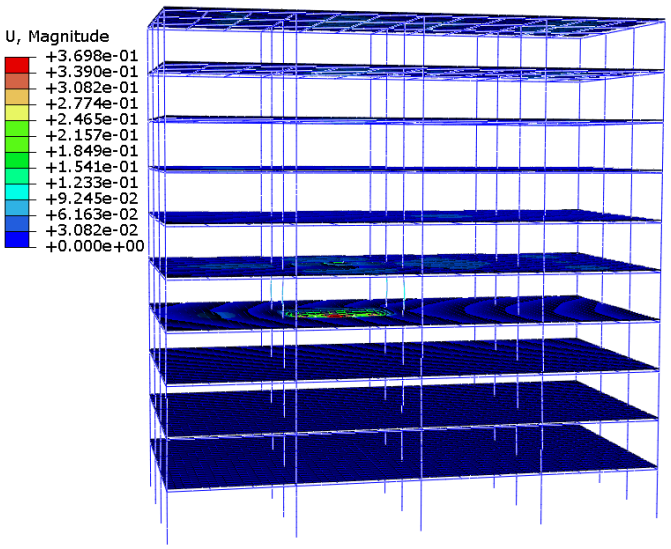

Fig. 5.78 Blast induced deformation after the blast analysis in the central compartment on the fifth floor

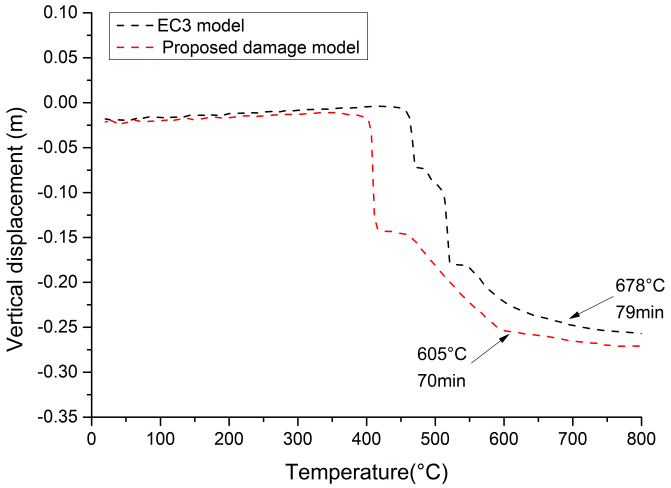

Fig. 5.79 Vertical displacement of the heated interior column B2

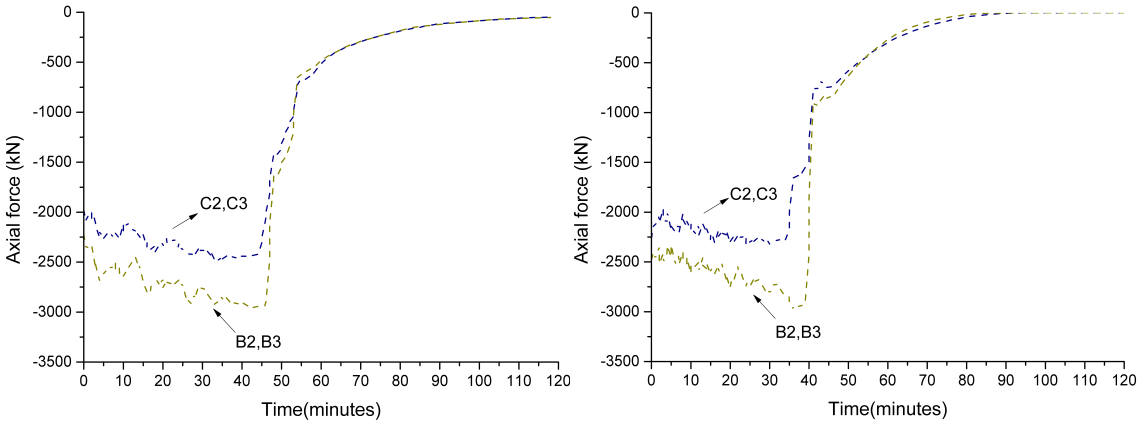

(a) EC3 model (b) Proposed damage model

Fig. 5.80 Axial forces in columns during fire event

to that of the same building when it is under fire attack only. Afterwards the loads of the failed columns are safely carried by the surrounding columns without further propagation of column failures, which is consistent with the observations from fire only scenario. Progressive collapse occurs at 106.5 minutes of fire in EC3 model prediction and at 81.5 minutes of fire in damage model prediction when the maximum allowable deflection limit is exceeded. A substantial decrease of 23.47% is observed in fire resistance as a result of incorporating the damage model in the integrated blast and fire analysis.

5. Corner compartment post-blast fire on the tenth floor.

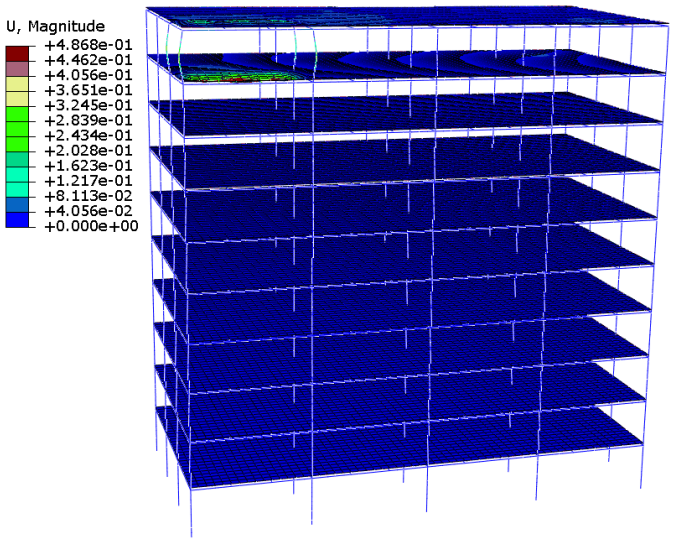

Fig. 5.81 Blast induced deformation after the blast analysis in the corner compartment on the top floor

When the blast loads occur inside the corner compartment on the top floor, the floor system above is blown upward for 217 *mm* and the floor system below is blown downward for 487 *mm* at the slab centre. As shown in Figure 5.81, the lateral deflection induced by blast is 263 *mm* in column A1, 217 *mm* in column A2, 228 *mm* in column B1, and 195 *mm* in column B2. This causes some loads in column A2 and column B2 be transferred to the adjacent columns. As fire progresses, comparison of models with and without damage incorporated shown in Figure 5.82 and Figure 5.83 indicates that progressive buckling is induced by failure of interior column B2 in both models.

Compared to under fire attack only, the fire resisting time decreases from 107 minutes to 79 minutes in the EC3 model prediction, with the critical temperature of column B2 decreasing from 834°C to 699°C. Whereas in the damage model prediction, the fire resisting time decreases from 85 minutes to 63.5 minutes, with the critical temperature of column B2 decreasing from 740°C to 605°C. By taking into account the coupled thermo-mechanical damage growth, the predicted fire resistance of the office building deteriorates by 19.62%.

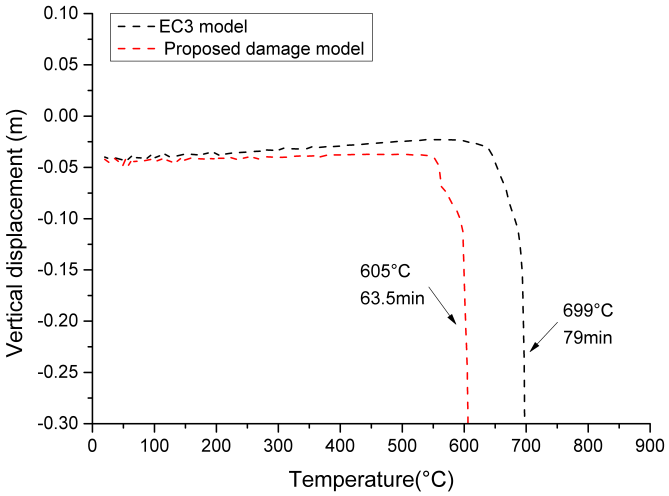

Fig. 5.82 Vertical displacement of the heated interior column B2

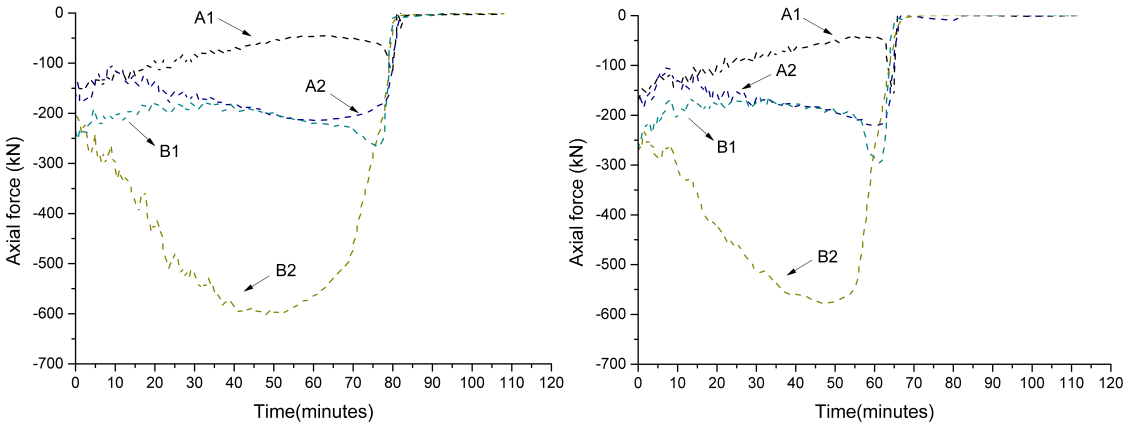

(a) EC3 model (b) Proposed damage model

Fig. 5.83 Axial forces in columns during fire event

6. Central compartment post-blast fire on the tenth floor.

Moving to the scenario of central compartment on the top floor, the floor system above is blown upward for 159 *mm* and the floor system below is blown downward for 373 *mm* at the slab centre. As shown in Figure 5.84, the lateral deflection induced by blast is 200 *mm* in column B2 and column B3, and 198 *mm* in column C2 and column C3, causing some loads in the heated columns be transferred to the adjacent cool columns.

As fire progresses in the subsequent fire analysis, it is the simultaneous buckling of the heated columns that triggers the onset of progressive collapse. The vertical displacement of interior column B2 is shown in Figure 5.85 and the axial force values of heated columns are shown in Figure 5.86. In the EC3 model, the fire resisting time decreases from 97 minutes to 72.5 minutes, with the critical temperature of column B2 decreasing from 788°C to 659°C. Whereas in the damage model, the fire resisting time decreases from 89 minutes to 60 minutes, with the critical temperature of column B2 decreasing

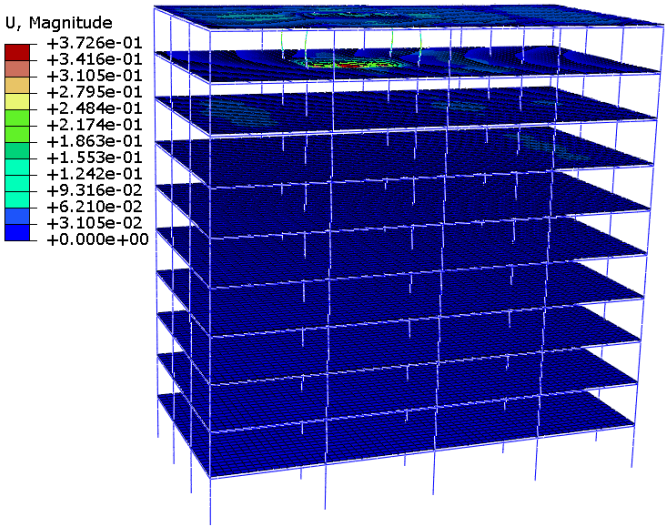

Fig. 5.84 Blast induced deformation after the blast analysis in the central compartment on the top floor

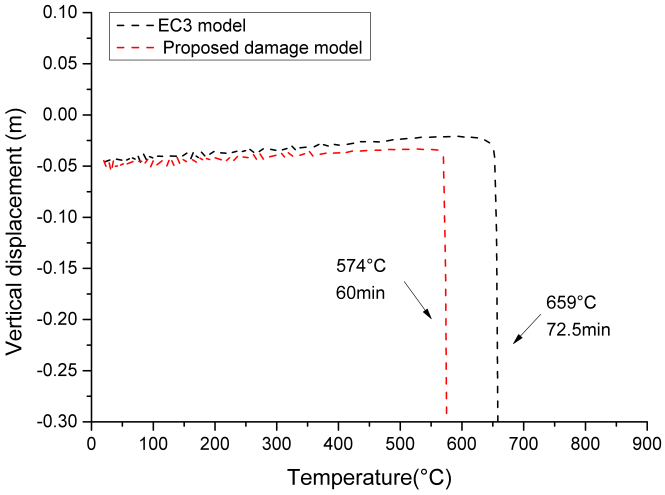

Fig. 5.85 Vertical displacement of the heated interior column B2

from 749°C to 574°C. The decrease in the fire resisting time by incorporating the damage model is 17.24%. The results clearly show the detrimental impact of the blast-induced damage on structural fire resistance and moreover the effects of incorporating the damage model in simulations by capturing the coupled thermo-mechanical damage growth.

5.7.3 Fire-triggered explosion analysis

The study above has shown that the collapse initiation time could be significantly affected by the initial blast-induced damage. An explosion could also be triggered at any time during a fire event, which is likely to have a more detrimental impact on the fire resistance of the buildings. In order to throw light on understanding the impacts of the accidental loads sequence on structural failures, this study examines the fire resistance of the office

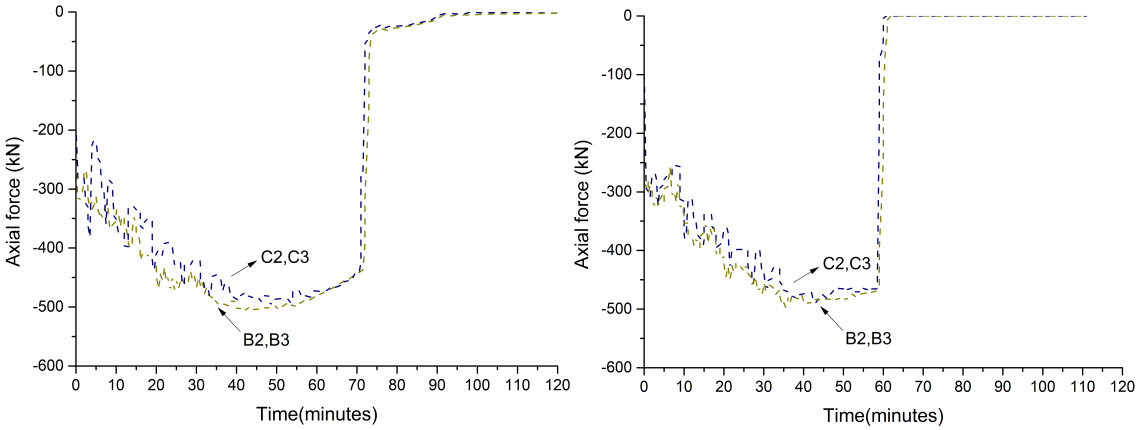

(a) EC3 model (b) Proposed damage model

Fig. 5.86 Axial forces in columns during fire event

buildings assuming that the explosion acts inside the corner fire compartment on ground floor after 30 minutes of fire.

5.7.3.1 Five-storey office building

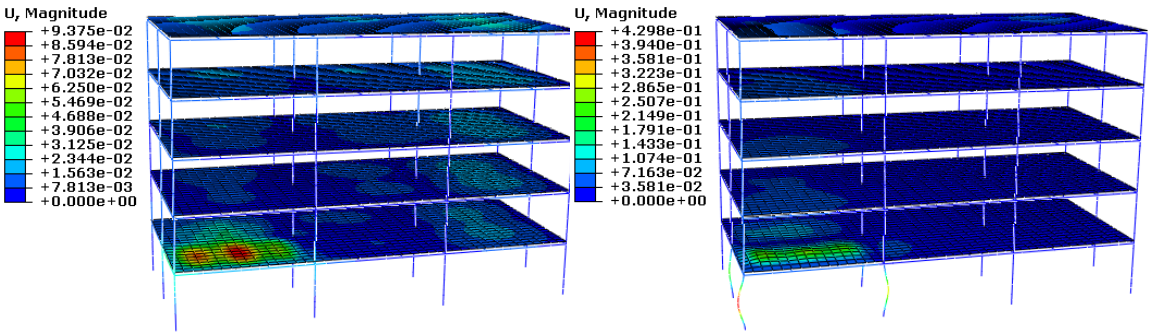

(a) Deformation at 30 minutes of fire (b) Deformation after fire-triggered explosion

Fig. 5.87 Deformation before and after fire-triggered explosion occurence

An explosion is assumed to occur inside the corner fire compartment on the ground floor of five-storey building after 30 minutes of fire. A comparison of the structural deformation prior to and after explosion occurrence is shown in Figure 5.87. The floor system is blown upward for 258 *mm* at the slab centre. The lateral deflection induced by blast is 428 *mm* in column A1, 225 *mm* in column A2, 316 *mm* in column B1 and 104 *mm* in column B2. The deformation-based member failure criterion (Ding et al., 2017), which is based on the horizontal displacement of the SDOF system (TM5-1300, 1990), is adopted to determine whether the column loses its load-carrying capacity under blast loading. The lateral deformation of blast-affected columns is checked against the

following acceptance criterion to evaluate the failure of columns against blast:

$$b_{mem} = \theta_u(\frac{H}{2}) \tag{5.3}$$

where H is the column height, θ_u is the maximum rotation at column support and $\theta_u = 12^\circ$ (TM5-1300, 1990).

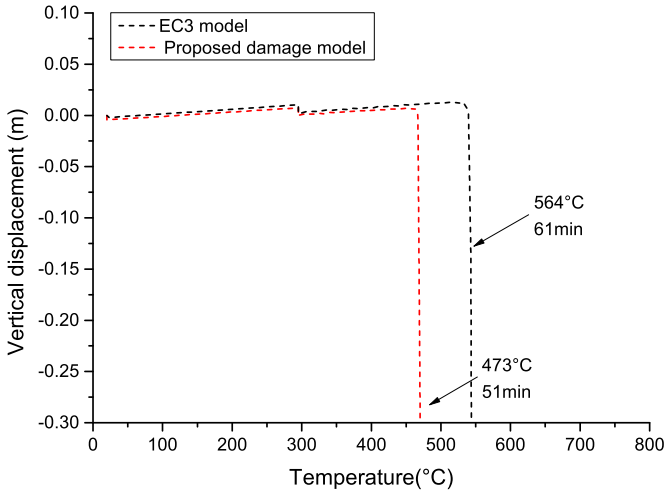

Fig. 5.88 Vertical displacement of the heated interior column B2

Following the deformation rule, the lateral deflection in column A1 has exceeded the acceptable limit and this is considered to equate to loss of the column under blast loads. This alone does not signify systematic failure of the building as long as the surrounding members are capable of redistributing forces away from the failed column. It can be seen from Figure 5.88 that a slight drop occurs in the vertical displacement of the heated interior column B2 as a result of blast-induced lateral deflection. A brief instability is also observed in the axial force values of the columns as shown in Figure 5.89. Column A1 loses its load-carrying capacity upon the action of explosion, and the redistributed forces are safely carried by the adjacent columns. With continuing heating, progressive collapse is triggered by simultaneous buckling of the remaining heated columns. The eventual collapse occurs at 61 minutes in the EC3 model prediction, which is reduced from 81.5 minutes in fire only scenario, with the critical temperature of column B2 decreasing from 670°C to 564°C. Whereas in the damage model, the fire resisting time reduces from 71 minutes to 51 minutes, with the critical temperature of column B2 decreasing from 608°C to 473°C.

Taking a close look at the damage development in the top of the blast-damaged columns in Figure 5.90 would help to understand the effects of the sequential accidental loads on structural members. A marked increase of damage is noticed upon the occurrence of blast loads at 30 minutes of fire, which confirms the effectiveness of the proposed damage model in representing the coupled thermo-mechanical damage propagation in

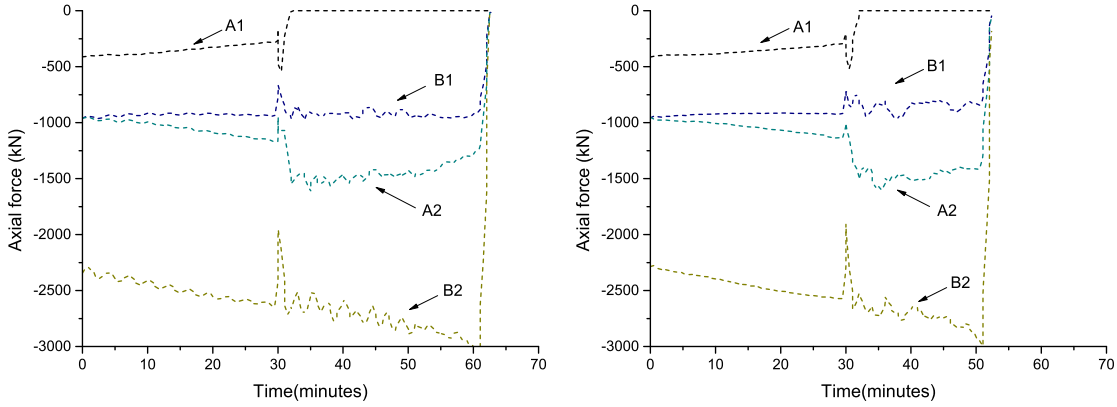

(a) EC3 model (b) Proposed damage model

Fig. 5.89 Axial forces in columns during fire event

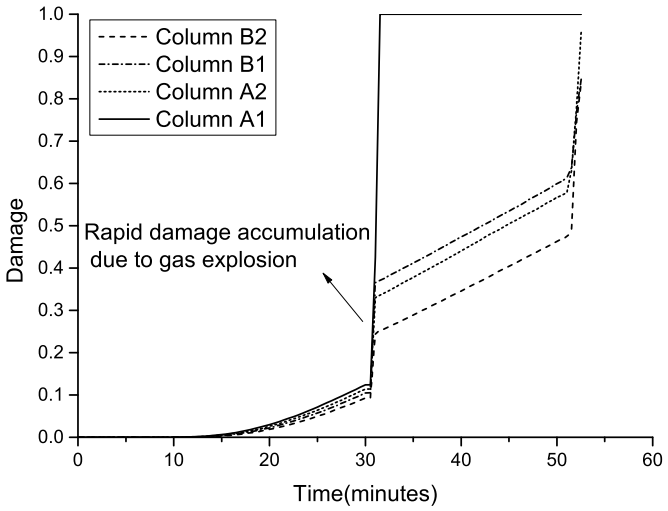

Fig. 5.90 Damage development in the top of blast-damaged columns

fire-triggered explosion analysis. The detrimental impact of the explosion on the heated structural members is highlighted in the graph, which explains the fact that the building in this scenario has lower fire resistance as compared to both fire only scenario and post-blast scenario. Note that the fire resistance predicted by the damage model is lower than the required 1-hour fire rating. This suggests that if the structure is not designed to resist such combined actions of abnormal loads, there is a danger of collapse before the safe evacuation of the occupants. Thus, comparison of the models with and without damage incorporated indicates that the fire resistance predicted by the damage model is 16.39% lower than EC3 model prediction. This substantial difference demonstrates the importance of incorporating the propose damage model in assessing the susceptibility of structures in another extreme case of multi-hazards.

5.7.3.2 Ten-storey office building

Moving now to apply the explosion loading in the corner compartment on the ground floor of the ten-storey building after 30 minutes of fire. The structural deformation prior to and after explosion is shown in Figure 5.91. It can be seen from the graph that the permanent deformation induced by explosion is small compared to the previous case of the five-storey building. This can be explained by the robust sections in the ten-storey building design and the relatively low temperatures achieved after 30 minutes of fire. Therefore, the occurrence of fire-triggered explosion only causes slight deterioration in the structural fire resistance.

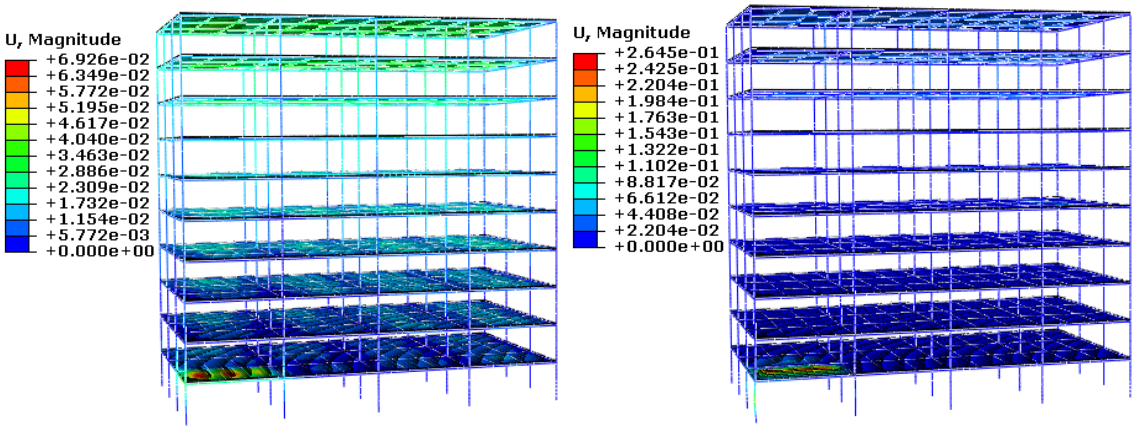

(a) Deformation at 30 minutes of fire (b) Deformation after fire-triggered explosion

Fig. 5.91 Deformation before and after fire-triggered explosion occurence

The vertical displacement of the interior column B2 is plotted in Figure 5.92. Results with the EC3 model indicate that the fire resisting time reduces from 108.5 minutes to 105 minutes compared to under fire attack only, with the critical temperature of column B2 decreasing from 625°C to 610°C. Whereas in the damage model prediction, the fire resisting time reduces from 89.5 minutes to 87 minutes, with the critical temperature of column B2 decreasing from 550°C to 535.5°C.

The development of axial force values in the heated columns are very similar to that of the fire only scenario, except that a brief instability is observed in the plots upon the explosion occurrence, as shown in Figure 5.93. By evaluating the damage development in the top of the blast-damaged columns, it can be observed from Figure 5.94 that the action of explosion at 30 minutes of fire does not produce a high level of damage, which again confirms the mild impact of fire-trigged explosion on the collapse resistance in this scenario.

Thus, this study has attempted to give insights into the structural collapse mechanism in fire and gas explosion scenario which has not been fully examined in the past research. It may therefore be concluded that fire-triggered explosion hazard has a more detrimental

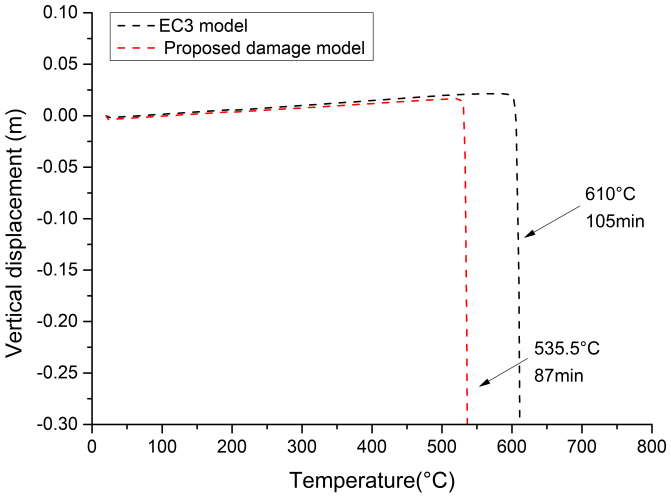

Fig. 5.92 Vertical displacement of the heated interior column B2

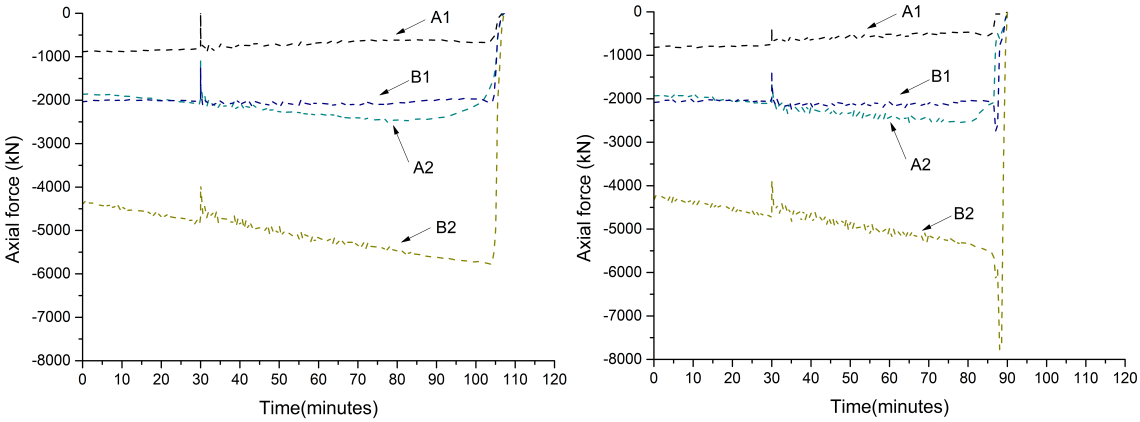

(a) EC3 model (b) Proposed damage model

Fig. 5.93 Axial forces in columns during fire event

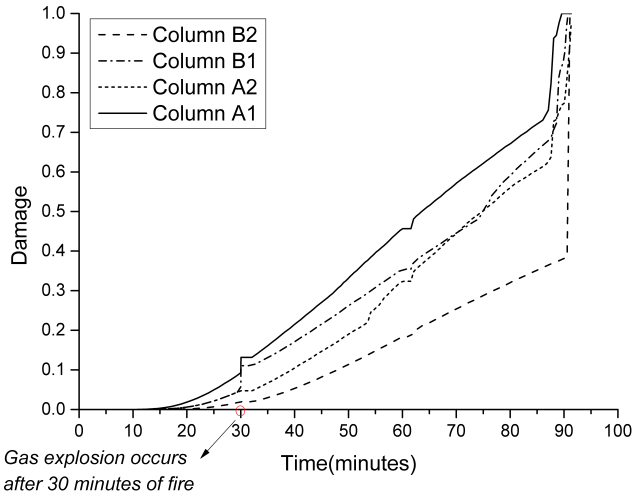

Fig. 5.94 Damage development in the top of blast-damaged columns

impact on the fire resistance of buildings than both fire only scenario and post-blast fire scenario. The capability of the proposed damage model approach in producing

safe and conservative predictions is also highlighted. The assessment of this type of scenario is based on a limited case study example and further studies are recommended to determine the correlation between the initiation time/location of fire-triggered explosion and structural fire resistance. The proposed modelling techniques in combination with the coupled damage model are suggested as the preferable means to conduct such studies.

5.8 Discussions

A summary of the collapse initiation time in all the studied cases is provided in Table 5.6, which can be utilized as a useful tool in helping designers to determine how much time is realistically available for evacuation before progressive collapse occurs in this type of building. Overall, it can be seen from Table 5.6 that the damage model approach produces more conservative results while the EC3 model has the potential risks of overestimating the structural fire resistance as it can not reasonably capture the potential deterioration induced by coupled thermo-mechanical propagation. This serves to illustrate that the damage model does significantly impact the limit state of steel buildings under fire, and especially under combined actions of blast and fire. An 8.25% $\sim$ 23.47% decrease is observed in the fire resisting time by incorporating the damage model. Results show that buildings achieve the level of safety required (1-hour fire resistance) in almost all cases when analysed using EC3 model. By contrast, in several scenarios a high potential of progressive collapse occurs during the required fire resisting time when analysed using the proposed damage model approach.

The simulation results of fire only scenarios show that overall the buildings under investigation demonstrate good inherent fire resistance, which is consistent with findings from Cardington fire tests and past fires. On the other hand, the buildings that fully survive the fire events are found to be more vulnerable to the combined hazards of blast and fire and have a higher potential to collapse. The two extreme scenarios presented in this study could be used as a guideline in performance based design to resist progressive collapse in multi-hazard scenarios.

When the blast loads precede the fire analysis, the five-storey building remains stable for a duration of approximately 41.5 minutes to more than 1 hour and the ten-storey building withstands the fire from 52 minutes to nearly 2 hours depending on the fire location. The blast-induced damage is found to result in considerable deterioration in structural fire resistance, thus it is clear that fire following an extreme event represents a significant threat to stability of the structure. The impacts of the accidental loads sequence on structural failures are examined in another extreme case of fire-triggered explosion multi-hazards. Owing to the fact that the structure is weakened due to heating

Table 5.6 Summary of the collapse initiation time in all analysed cases

Type of building	Fire location	Type of scenario	Time of global collapse (min)		
			EC3 model	Damage model	Difference(%)
Five-storey	1st floor corner fire	Fire only	81.5	71	12.88
		Post-blast fire	73.5	66	10.20
		Fire-triggerd explosion	61	51	16.39
	1st floor central fire	Fire only	80	71	11.25
		Post-blast fire	73.5	65.5	10.88
	3rd floor corner fire	Fire only	76	63	17.11
		Post-blast fire	62.5	51.5	17.60
	3rd floor central fire	Fire only	72	61	15.28
		Post-blast fire	51.5	41.5	19.42
	5th floor corner fire	Fire only	97	81	16.49
		Post-blast fire	75	60.5	19.33
	5th floor central fire	Fire only	97	84	13.40
		Post-blast fire	72	62	13.89
Ten-storey	1st floor corner fire	Fire only	108.5	89.5	17.51
		Post-blast fire	107	88	17.76
		Fire-triggered explosion	105	87	17.14
	1st floor central fire	Fire only	Safe	104	N/A
		Post-blast fire	Safe	103	N/A
	5th floor corner fire	Fire only	77	64	16.88
		Post-blast fire	62.5	52	16.80
	5th floor central fire	Fire only	107	93	13.08
		Post-blast fire	106.5	81.5	23.47
	10th floor corner fire	Fire only	107	85	20.56
		Post-blast fire	79	63.5	19.62
	10th floor central fire	Fire only	97	89	8.25
		Post-blast fire	72.5	60	17.24

at the time of explosion occurrence, it is not surprising that fire-triggered explosion hazard has a more detrimental impact on the fire resistance of buildings compared to both fire only scenario and post-blast fire scenario. As the purpose of the study here is to examine the nature of structural behaviour in this type of scenario, the assessment of the critical mechanism is based on a limited case study example which serves to demonstrate the effect of fire-triggered explosion on structural fire resistance in fire events.

Two types of collapse mechanisms can be observed depending on fire locations: column buckling failure mode and large deformation failure mode. Simulation results indicate that the dominant failure mechanism is column failure. The difference of the collapse initiation time between EC3 model results and damage model results can be largely attributed to the fact that the coupled thermo-mechanical damage causes column buckling to occur earlier than in EC3 model. The buckling of heated interior columns is a critical mechanism due to the highest utilization ratio. In addition, the analyses conducted with

the damage model incorporated shows that perimeter columns also have the potential to initiate sequential buckling, particularly when perimeter columns undergo large blast-induced lateral deflection in integrated blast and fire analysis. It is found that damage could accumulate steeply under the coupled effects of thermo-mechanical loading and then all of a sudden the material fails due to a mixture of thermal degradation and mechanical damage. Therefore, adequate insulation is essential on both interior columns and perimeter columns in order to avoid collapse during fires.

When local failure of column occurs, the load transfer mechanism plays an important role in the collapse resistance of building system. The survival of the buildings in fire is often dependent on the utilization of the inherent structural redundancy, which is another major contributor to the differences in structural responses obtained by EC3 model and by the damage model. A key finding from this study is that the alternative load paths in building systems may be unachievable due to the effect of coupled thermo-mechanical damage propagation which is generally neglected in conventional numerical approaches. The residual load bearing capacity of the surrounding columns is a crucial factor in determining their capability to provide an alternative load-carrying path. As can be seen in most of the analysed cases for both types of buildings, the deterioration in the member capacity predicted by the damage model is more severe compare to that of EC3 model. As a result, the realistic capability of the surrounding columns in sustaining the increased loads that are transferred from the failed columns is compromised and a change of load redistribution path is observed. To a large extent it is the inability of the building to redistribute the loads away from the failed columns that leads to an earlier progressive collapse compared to that of EC3 model.

If the surrounding structure of the column is strong enough to provide an alternative load-carrying path, the structure withstands the heating without further propagation of column failures and the fire resistance of the structure achieved is significantly longer than that of individual members. As the temperature increases further, the large deformation failure mode tends to occur due to the loss of the flexural capacity and the floor system transitions from a flexural load-carrying mechanism to a catenary mechanism by deflection more. By accepting large deformation during fires, the ten-story building could survive a prolonged fire event that is significantly longer than the designed 1-hour fire resistant rating. The cut-off point is that the large deflection becomes unacceptable when the vertical displacement of the slab system exceeds 1/10 of the span. This type of failure mechanism is observed when the initial load ratio is low or the network of columns has sufficient strength to carry the loads despite the extremely high temperature. The results clearly show the effects of incorporating the damage model in assessing this type of beam failure mode. Due to severe deterioration in the bending moment capacity induced by the coupled thermo-mechanical damage propagation, the beams would require excessive displacements in order to develop catenary action to resist the loads. Increasing the fire

insulation on beams would be beneficial for structural survivability as the deflection of floor system would be reduced. However this enhancing measure will be unnecessary for these types of buildings as the fire resistance achieved under the large deformation failure mode has adequately met the design needs.

The time of collapse occurrence seems to be largely affected by fire locations. Results indicate that the internal compartment fire scenario shows robust collapse resistance due to a more uniform load redistribution and larger restraint on the fire compartment. By contrast, the peripheral compartment fire and corner compartment fire have similar collapse initiation time, which are both characterized by weak boundary restrain conditions of the floor and limited load redistribution paths. It is interesting to note that for both types of buildings the most vulnerable compartment exposed to threat is at the mid-height of the building, being the third floor peripheral compartment for the five-storey building and the fifth floor corner compartment for the ten-storey building. This observation will help the designers to identify the critical structural components that have a high potential to trigger progressive collapse under extreme hazard loading in this type of moment-resisting office buildings.

The findings illustrate again that the structure does not necessarily suffer from progressive collapse upon local failure. The structural performance is considered satisfactory if the area at risk of collapse is deemed acceptable. This permits the use of less restrictive acceptance criteria compared to prescriptive fire codes which are normally based on strength requirements or critical temperature of structural members. A key aspect of this lies in transforming fire safety objectives in terms of safe evacuation within a specified time into quantifiable performance criteria that evaluate the performance of structural system as a whole. It is established that the building exhibits a high potential for progressive collapse when the first buckling of adjacent cool columns occurs or the vertical displacement of the slab system exceeds 1/10 of the span. This is because the first buckling of adjacent cool columns would normally induce sequential buckling of other columns. It is unlikely that the structure is capable of effectively redistributing loads thereafter, suggesting that global collapse is imminent. The vertical deflection in excess of the aforementioned limit is another indicator of high potential for global collapse. The largely deformed slabs may fall down in reality due to connections fracture and cause threats to structural integrity, triggering progressive collapse. If the analysis results show that the structural performance is in compliance with the established criteria, the building is considered to exhibit a low potential for progressive collapse and require no further progressive collapse considerations. Without resulting in an extremely high level of safety, the performance criteria used here are effective in identifying the conditions that are threatening to a building, and can provide a good estimate of the stability of multi-storey buildings under fire or combined blast and fire. The established criteria are therefore suggested for use in determining whether a fire safety design meets the level of

safety required for these types of buildings. Based on the recommendation as well as the building characteristics and the fire protection features, the fire safety engineers can make a judgement on what to use that best suit their needs in reliable analysis procedures, allowing for more flexible solutions and more cost-efficient designs.

It should be mentioned here that the above findings are based on a number of assumptions made in the simulations and care must be exercised in extrapolating the results to predict structural performances under different sets of conditions. For instance, by assuming no damage to fire protection, the obtained blast-affected structural fire resisting time might be longer than realistically possible, as the insulation materials are easily damaged by blast loads. Note that the impact of blast on walls is also neglected in this study. Whereas in reality fire compartment walls might be damaged by blast, which would lead to increase in the fire compartment size and possibly more severe fire development with disastrous consequences. The use of moment resisting joints with infinite axial rigidity in this study is another simplified modelling assumption. Taking into consideration the realistic joint behaviour may achieve a more conservative limit state of the structural performance in fire, which is beyond the scope of the present study.

5.9 Summary

This chapter has presented the design of a low-rise and a mid-rise steel-framed buildings with office occupancy and identified typical accidental scenarios for robustness assessments. The progressive collapse mechanism of steel frames in single-compartment fire scenario is first studied, which represents one of the most typical fire events that might occur during the service life of office buildings. This is followed by assessing the vulnerability of steel frames subjected to combined hazards of internal blast and subsequent fire in order to determine the detrimental effects of internal blast loads on structural fire resistance. As an extension to this case, behaviour of the buildings exposed to fire-triggered explosion is also studied as another extreme case of multi-hazard scenario. The severity of various fire locations (corner compartment, central compartment) at different floor levels is investigated in order to determine the most vulnerable location for the building system.

Simulations are carried out on three-dimensional finite element models of the steel-framed buildings in ABAQUS. For the purpose of emphasizing the role of damage modelling in collapse assessment, the proposed damage model is adopted in numerical simulations. Parallel analyses are also carried out using stress-strain relationships of steel from Eurocode 3 for comparison. Results provide a check of the office buildings for satisfying robustness requirements under accidental loading and give substantial

insight into the reasons that cause structural collapse. The proposed computational framework has demonstrated robustness in simulating the structural response of steel buildings including the coupled thermo-mechanical damage propagation. Compared with conventional numerical model, the proposed damage modelling framework provides a more conservative prediction of the failure probability of structure during fire event or under combined hazards of blast and fire, and has the potential to be utilized as a useful tool in helping designers to determine how much time is realistically available for evacuation before progressive collapse occurs in this type of building. The main findings and general conclusions obtained from this study are presented in the next chapter.

Chapter 6

Conclusions

6.1 Major findings and conclusions

The aim of this study is to propose a new methodology that fills the gap in sophisticated modelling of steel deterioration behaviour in support of evaluating steel buildings' vulnerability subjected to fire, or combination of blast and fire loads. To achieve this aim, a coupled thermo-mechanical damage model is developed in an attempt to capture the steel deterioration under combined actions of mechanical loading and fire loading. The proposed damage model is successfully implemented in FE software ABAQUS and validated against a comprehensive set of experimental results and established numerical results, ranging from a single beam test to multi-story steel frames subjected to severe fire or combined hazards of blast and fire. The consistent and accurate predictive capabilities of the proposed damage model is demonstrated.

Having verified its effectiveness and the applicability, the proposed damage model with carefully calibrated parameters is applied in collapse assessment of a low-rise and a mid-rise office building under fire as well as under combined hazards of blast and fire. The severity of various fire locations (corner compartment, central compartment) at different floor levels has been investigated in order to determine the most vulnerable location for the building system. Results provide a check of the office buildings for satisfying robustness requirements under accidental loading and offer substantial insight on the structural response of steel buildings including collapse mechanism and behaviour of structural members during fire events.

The main findings and general conclusions obtained from this research are summarized in the following key points:

- The proposed damage model provides a more conservative prediction of structural collapse resistance under fire, and especially under combined actions of blast and fire. Whereas EC3 model has the potential risks of overestimating fire resistance due to the fact that it can not reasonably capture the potential deterioration induced by coupled thermo-mechanical propagation. An 8.25% $\sim$ 23.47% decrease is observed in the fire resisting time by incorporating the damage model.

- Though the moment-resisting steel-framed office buildings designed in accordance with the current building codes in this study are found not vulnerable to severe fire loading alone, they are more vulnerable to the combined hazards of blast and fire as the blast-induced damage results in considerable deterioration in structural fire resistance.

- The impact of the accidental loads sequence on structural failures is highlighted in this study. Of all sequences examined, fire-triggered explosion hazard is shown to have the most detrimental impact on the fire resistance of buildings owing to the fact that the structure is weakened as a result of heating at the time of explosion occurrence.

- The dominant failure mechanism, buckling of heated interior columns, is identified in this study. By incorporating the damage model, perimeter columns are also found to have the potential to initiate sequential buckling due to the coupled effects of thermal degradation and mechanical damage, particularly when perimeter columns undergo large blast-induced lateral deflection in integrated blast and fire analysis. Therefore, adequate insulation is essential on both interior columns and perimeter columns in order to avoid collapse during fires.

- The alternative load path in building systems, which is a crucial factor in deciding the survival of buildings upon local column failure, may be severely compromised due to the coupled thermo-mechanical damage propagation in surrounding columns which is neglected in EC3 model.

- The proposed damage model also provides a more accurate prediction of beam deflections due to material softening, which might cause threats to structural integrity when the deflection becomes excessive. In some cases beams remain safe until the end of 2-hour fire duration when analysed with EC3 model, whereas the maximum allowable deflection limit is exceeded due to substantial damage accumulation in beams by incorporating the proposed damage model.

- Analyses with both EC3 model and the proposed damage model show that the time of collapse occurrence is largely affected by fire locations and the most vulnerable location is at the mid-height of the buildings. While almost all the cases analysed using EC3 model suggest that buildings survive 1-hour fire, the proposed damage

model could effectively identify the fire locations which have a high potential to trigger progressive collapse and result in buildings failing to achieve the level of safety required.

- This study provides estimation of ultimate failure time by incorporating damage model with the suggested damage parameter set and has the potential to be utilized as a useful tool in helping designers to determine how much time is realistically available for evacuation before progressive collapse occurs in this type of building. The damage parameter set adopted is recommended for this type of analysis on steel-framed buildings provided that adequate fire insulation is in place.

In conclusion, the proposed damage modelling approach sheds light on issues related to fire-induced progressive collapse of steel framed-buildings, one of the most challenging fields in structural engineering. The potential for further improvement of design and research are studied in the following sections.

6.2 Recommendations for design

The implications of the new understanding gained in this study are considerable. Traditional performance based design relies on EC3 material model. However, the modelling attempts in this study demonstrate that the collapse resistance of representative steel-framed office buildings is significantly different from that predicted by EC3 model. When determining the potential of fire-induced collapse, the designer is interested to know whether the amount of time realistically available for evacuation before progressive collapse occurs achieves the level of safety required. Compared with the EC3 model, the proposed damage modelling framework manages to provide a more conservative prediction of the failure probability of a structure during fire event or under combined hazards of blast and fire, thus yielding important design implications.

A check of collapse initiation time provided in this study allows designers to take full advantage of the demonstrated collapse resistance of the investigated buildings. Results suggest that when the five-storey building and ten-storey building are protected with 1-hour fire resistant rating, the buildings withstand the fire event during the required fire resisting time and therefore achieve a satisfying level of structural safety. This indicates that this type of five-storey office building designed in accordance with the current building codes is not vulnerable to severe fire loading alone and therefore requires no further consideration to prevent progressive collapse due to fire action only. The same conclusion cannot be made about the ten-storey building as its minimum period of fire resistance is 2 hours (Approved document B, 2006).

The two extreme scenarios presented in this thesis could be used as a guideline in performance based design to resist progressive collapse in multi-hazard scenarios. The buildings that fully survive the fire events are found to be more vulnerable to the combined hazards of blast and fire and have a higher collapse potential. Based on the understanding developed, the dominant failure mechanism is column failure. Therefore, increasing the fire insulation of the critical columns can improve the collapse resistance of the steel frame and delay the initiation of progressive collapse. It should be noted that the fire insulation might be damaged by blast loads or fragmentation impact. The extent of damage is very difficult to assess quantitatively and therefore the insulation material is assumed to remain intact on the surfaces of protected members in this study. Whereas in reality the insulation material might come off due to the impact of blast loads and leave the structural components unprotected, leading to very early global collapse owing to the rapid temperature rise. The alternative fire protection option is encasing the critical columns in concrete or using fire-resistant steels which are superior to conventional steels in terms of high-temperature yield strength. This option could maintain the effectiveness of fire protection to a larger extent after the impact of blast loads, but inevitably involves higher construction costs at the same time.

The multi-hazard study conducted in this thesis suggests that if the structure is not designed to resist such combined actions of abnormal loads, there is a danger of collapse before the safe evacuation of the occupants. A key aspect of performance-based design lies in identifying the critical buildings that exhibit a hight potential for progressive collapse under abnormal loading and applying reliable analysis procedures to redesign the critical structural components with the intention of preventing progressive collapse. In order to ensure that the level of safety required is met in the rare extreme multi-hazard event, it is recommended that the designers apply the proposed damage modelling framework when performing the analysis procedures to mitigate the potential for progressive collapse. The damage model parameter set adopted in the case study of this thesis is recommended for conducting such analysis provided that steel members are adequately insulated. The incorporation of the damage model will provide for a much more robust steel-framed structure and increase the probability of achieving a low potential for progressive collapse in design methods.

Adoption of the above recommendations are mainly concerned with the control of progressive collapse and should provide a building with a satisfying level of robustness. That being said, the analyses conducted that allow for utilizing structural robustness to meet performance requirements are based on confined compartment fires. This suggests the needs for effective control of fire spread in order for the buildings to localise failure without disproportionate collapse. It is thus recommended that care should be taken in terms of constructional aspects to ensure the integrity of the compartment, thereby preventing progressive collapse of the structure triggered by uncontrollable fire spread.

6.3 Recommendations for future research

This study has successfully developed and implemented coupled thermo-mechanical damage modelling in collapse assessment of steel buildings during fire events or under combined hazards of blast and fire. It is the author's view that this study provides a number of opportunities for future research, which could be categorized into the following three aspects.

6.3.1 Recommendations for damage model enhancement

The application of the proposed damage model in this study indicates a number of characteristics of the current model that can be enhanced to improve the predictive capability, which has been largely limited by the currently available experimental studies. Thus, the areas in need of experimental studies are also identified, which will benefit the model development and validation.

One of the deficiencies of the current model is that it is developed on the simplified assumption that the triaxiliaty function is constant during loading. The effect of triaxiliaty is not accounted for in the current study because there is insufficient experimental data to address the effects of triaxiality. More experiments are required to support incorporation of the effect of triaxiality and validation of the damage model over a wide range of triaxiality.

In the aspect of modelling damage in integrated blast and fire analysis, the proposed damage model shows its potential in dealing with blast-induced damage while refraining from the complexity and uncertainty of explicitly addressing stages of dynamic damage development. In this study, the blast-induced damage is calculated based on the permanent structural deformation after the blast loading ceases. The incorporation of dynamic damage development during the blast analysis in the current damage coupling model is yet to be explored. This motivates further modification of the damage equation to account for the complex material damage processes induced by the combined effects of high strain rate loading and elevated temperature to enhance the predictability of the proposed damage model in these regions of loading.

Another drawback is the lack of a unified procedure for calibration. Although the calibration of the damage model parameters has been successfully carried out and validated using an inverse type of calibration procedure, it is strongly recommended that more tests be conducted to establish a proper and unified calibration procedure for determining damage parameters in support of modelling steel deterioration behaviour under different loading conditions.

6.3.2 Recommendations for analysis scenarios

Owing to the excessive computational effort associated with the simulations, a limited number of fire scenarios have been evaluated in this study. Future work needs to include the examination of additional analysis scenarios that are sufficient in number so that progressive collapse is fully understood and documented. It is recommended that the developed damage model is used as a tool in future investigations to ensure accurate prediction of the progressive collapse potential.

- *Type of framing system*

  The observations made in this study are based on structural response of a generic five-storey and ten-storey moment resisting steel frames with a simple, uniform and repetitive layout. It is of interest to investigate the response of structures with substantially different layouts. The differences could include, but are not limited to, atypical structural configurations, different types of connections, and different bay spans. All these differences that potentially affect the collapse resistance of buildings could help develop effective strategies to protect different types of structural systems against extreme attacks.

- *Model travelling fire*

  This study assumes the fire to be compartmentalized and does not account for multi-compartment fire in which the fire spreads horizontally or vertically beyond the fire initiation compartment. Investigation of multi-compartment fire would be a recommended extension of the study because it represents a more onerous scenario which might result in short failure times of steel frames.

- *Model fire event using parametric fire*

  The fire event is modelled with standard ISO834 fire heating curve. Using a parametric fire curve including both heating phase and cooling phase of fire, which takes into account the compartment size, fuel load, and ventilation conditions (defined by opening factor), is recommended in future work. A series of parametric studies could be performed to identify the correlation between opening factors and the vulnerability of structures.

- *Fire insulation*

  In this study, the building is protected for 1-hour fire resistant rating. While this allows a check of the office buildings for satisfying robustness requirements during the specified fire resisting period, it is of interest to investigate the survivability of the building with different fire resistant rating. For example, protecting the building with 2-hour fire resistance or leaving the beams unprotected would make

an interesting research topic. On the other hand, this study assumes that the insulation materials remain intact under blast loads. The vulnerability of the framing system should be further studied assuming the insulation materials are partially or completely damaged by blast pressure in order to eliminate overestimation of fire resistance.

- *Multi-hazards*

  It is clear, based on this study, that combined hazard of blast and fire represents a significant threat to stability of the structure. Further studies are recommended to determine the correlation between fire intensity, passive fire protection rating, blast load levels and collapse time, which have the potential as a useful tool in performance-based fire resistant design of structures. In addition, from a multi-hazard view, it is also of interest to assess the post-earthquake fire resistance of steel-framed buildings using the propose damage model, where the mechanical damage induced by earthquake is likely to have a crucial role in the survivability of the damaged buildings.

6.3.3 Recommendations for FE modelling techniques

The techniques of FE modelling that are recommended for future analysis are:

- *Refined shell element models*

  The advantage of using beam elements in modelling steel members lies in the computational efficiency and reasonable accuracy. However, beam elements are not capable of capturing some behaviour aspects including local buckling and lateral torsional buckling of steel members. More accurate simulation results could be achieved if shell elements are used for modelling steel members in further studies.

- *Connection behaviour*

  The damage-coupled numerical simulations presented in this thesis have concentrated on global behaviour of the structure and therefore neglected the modelling of actual connections behaviour. It is important to note that there have been important developments in the area of connection behaviour modelling (Burgess et al., 2012), and the accurate representation of connection behaviour should be incorporated in performing further damage-coupled numerical simulations.

- *Failure criteria*

  There are questions as to when a structure should be considered to have failed, since different criteria can be used. The criterion used here allows the analysis

results to be judged with a satisfying level of precision. When evaluating the susceptibility of buildings to progressive collapse in future research, researchers and designers will need to set measurable performance criteria according to the variations in initial assumptions and the specific needs of the building owners.

References

Agarwal, A. and Varma, A. H. (2014). Fire induced progressive collapse of steel building structures: The role of interior gravity columns. *Engineering Structures*, 58:129–140.

Alashker, Y. and El-Tawil, S. (2011). A design-oriented model for the collapse resistance of composite floors subjected to column loss. *Journal of Constructional Steel Research*, 67(1):84–92.

Ali, H. M., Senseny, P. E., and Alpert, R. L. (2004). Lateral displacement and collapse of single-story steel frames in uncontrolled fires. *Engineering Structures*, 26(5):593–607.

Arrhenius, S. (1889). Über die dissociationswärme und den einfluss der temperatur auf den dissociationsgrad der elektrolyte. *Zeitschrift für physikalische Chemie*, 4(1):96–116.

ASCE (1992). *Structural fire protection*. ASCE Manuals and Reports on Engineering, No. 78, American Society of Civil Engineers.

ASCE (2005). *Minimum design loads for buildings and other structures*. ASCE/SEI Standard 7-05, American Society of Civil Engineers, Reston, VA.

Bailey, C. and Moore, D. (2000a). The structural behaviour of steel frames with composite floor slabs subject to fire: Part 1: Theory. *Structural Engineer*, 78(11):19–27.

Bailey, C. and Moore, D. (2000b). The structural behaviour of steel frames with composite floor slabs subject to fire: Part 2: Design. *Structural Engineer*, 78(11):28–33.

Benallal, A., Billardon, R., and Doghri, I. (1988). An integration algorithm and the corresponding consistent tangent operator for fully coupled elastoplastic and damage equations. *International Journal for Numerical Methods in Biomedical Engineering*, 4(6):731–740.

Block, F. M., Burgess, I. W., Davison, J. B., and Plank, R. J. (2007). The development of a component-based connection element for endplate connections in fire. *Fire Safety Journal*, 42(6-7):498–506.

Bodner, S. R. and Symonds, P. S. (1960). Plastic deformations in impact and impulsive loading of beams. In *Plasticity*, pages 488–500. Elsevier.

Bonora, N. (1997). A nonlinear cdm model for ductile failure. *Engineering fracture mechanics*, 58(1-2):11–28.

Bonora, N., Gentile, D., and Pirondi, A. (2004). Identification of the parameters of a non-linear continuum damage mechanics model for ductile failure in metals. *The Journal of Strain Analysis for Engineering Design*, 39(6):639–651.

Bonora, N. and Milella, P. P. (2001). Constitutive modeling for ductile metals behavior incorporating strain rate, temperature and damage mechanics. *International Journal of Impact Engineering*, 26(1-10):53–64.

Børvik, T., Hopperstad, O., Berstad, T., and Langseth, M. (2001). A computational model of viscoplasticity and ductile damage for impact and penetration. *European Journal of Mechanics-A/Solids*, 20(5):685–712.

Bouchard, P.-O., Bourgeon, L., Fayolle, S., and Mocellin, K. (2011). An enhanced lemaitre model formulation for materials processing damage computation. *International Journal of Material Forming*, 4(3):299–315.

British steel (1999). The behaviour of multi-storey steel framed buildings in fire. Technical report, Swinden Technology Center, UK.

Buchanan, A. H. and Abu, A. K. (2017). *Structural design for fire safety*. John Wiley & Sons.

Building Regulations (2004). *Approved Document A (structure)*. Department for Communities and Local Government.

Building Regulations (2006). *Approved Document B (Fire safety, Volume 2 – Buildings other than Dwellinghouses), 2006 Edition incorporating 2007, 2010 and 2013 amendments)*. Department for Communities and Local Government.

Burgess, I., Davison, J. B., Dong, G., and Huang, S.-S. (2012). The role of connections in the response of steel frames to fire. *Structural Engineering International*, 22(4):449–461.

Byfield, M., Mudalige, W., Morison, C., and Stoddart, E. (2014). A review of progressive collapse research and regulations. *Proceedings of the ICE-Structures and Buildings*, 167(8):447–456.

Chaboche, J.-L. (1988). Continuum damage mechanics: Part ii damage growth, crack initiation, and crack growth. *Journal of applied mechanics*, 55(1):65–72.

Chaboche, J.-L. (1997). Thermodynamic formulation of constitutive equations and application to the viscoplasticity and viscoelasticity of metals and polymers. *International Journal of Solids and Structures*, 34(18):2239–2254.

Chandrakanth, S. and Pandey, P. (1993). A new ductile damage evolution model. *International Journal of Fracture*, 60(4):R73–R76.

Chen, H. and Liew, J. (2005). Explosion and fire analysis of steel frames using mixed element approach. *Journal of Engineering Mechanics*, 131(6):606–616.

Chen, J., Young, B., and Uy, B. (2006). Behavior of high strength structural steel at elevated temperatures. *Journal of structural engineering*, 132(12):1948–1954.

Chow, C. and Wang, J. (1987). An anisotropic theory of continuum damage mechanics for ductile fracture. *Engineering Fracture Mechanics*, 27(5):547–558.

Cooke, G. M. (1988). An introduction to the mechanical properties of structural steel at elevated temperatures. *Fire safety journal*, 13(1):45–54.

Cottrell, A. H. (1981). *The mechanical properties of matter*. Krieger Publishing.

de Souza Neto, E. A., Peric, D., and Owen, D. R. (2011). *Computational methods for plasticity: theory and applications*. John Wiley & Sons.

Dharma, R. B. and Tan, K.-H. (2007). Rotational capacity of steel i-beams under fire conditions part i: Experimental study. *Engineering structures*, 29(9):2391–2402.

Ding, Y., Chen, Y., and Shi, Y. (2016). Progressive collapse analysis of a steel frame subjected to confined explosion and post-explosion fire. *Advances in Structural Engineering*, 19(11):1780–1796.

Ding, Y., Song, X., and Zhu, H.-T. (2017). Probabilistic progressive collapse analysis of steel frame structures against blast loads. *Engineering Structures*, 147:679–691.

DoD (United States Department of Defense) (2009). *Unified facilities criteria: design of buildings to resist progressive collapse*. UFC 4-023-03.

Dong, G., Burgess, I., and Davison, J. (2011). Component-based element for endplate connections in fire. *Proc. ASFE*, pages 195–200.

Dowling, A. and Harding, J. (1967). Tensile properties of mild steel under high strain rates. In *Proceedings of the 1st HERF Conf.*

Egner, W. and Egner, H. (2016). Thermo-mechanical coupling in constitutive modeling of dissipative materials. *International Journal of Solids and Structures*, 91:78–88.

Elghazouli, A., Izzuddin, B., and Richardson, A. (2000). Numerical modelling of the structural fire behaviour of composite buildings. *Fire Safety Journal*, 35(4):279–297.

Ellingwood, B. R., Smilowitz, R., Dusenberry, D. O., Duthinh, D., Lew, H. S., and Carino, N. J. (2007). Best practices for reducing the potential for progressive collapse in buildings. *NIST Interagency/Internal Report (NISTIR)-7396*.

EN 1991-1-7 (2006). *Eurocode 1 - Actions on structures, Part 1-7: General actions - Accidental actions*. European Committee for Standardization, Brussels, Belgium.

EN 1993-1-1 (2005). *Eurocode 3: Design of Steel Structures, Part 1-1: General rules and rules for buildings*. European Committee for Standardization, Brussels, Belgium.

EN 1993-1-2 (2005). *Eurocode 3: Design of Steel Structures, Part 1-2: General Rules – Structural Fire Design*. European Committee for Standardization, Brussels, Belgium.

EN 1994-1-2 (2005). *Eurocode 4: Design of Composite Steel and Concrete Structures, Part 1-2: General Rules – Structural Fire Design*. European Committee for Standardization, Brussels, Belgium.

Forni, D., Chiaia, B., and Cadoni, E. (2017). Blast effects on steel columns under fire conditions. *Journal of Constructional Steel Research*, 136:1–10.

Foster, S., Chladná, M., Hsieh, C., Burgess, I., and Plank, R. (2007). Thermal and structural behaviour of a full-scale composite building subject to a severe compartment fire. *Fire Safety Journal*, 42(3):183–199.

Fu, Q. N., Tan, K. H., Zhou, X. H., and Yang, B. (2017). Numerical simulations on three-dimensional composite structural systems against progressive collapse. *Journal of Constructional Steel Research*, 135:125–136.

Gilsanz, R., DePaola, E., Christopher, M., and Harold, N. (2002). *World Trade Center Building performance study: Chapter 5 WTC7*. Federal Emergency Management Agency.

GSA (General Services Administration) (2003). *Progressive collapse analysis and design guidelines for new federal office buildings and major modernization projects*. Washington, DC.

GSA (General Services Administration) (2013). *Alternate path analysis & design guidelines for progressive collapse resistance*. GSA Washington, DC.

Hendry, A. (1979). Summary of research and design philosophy for bearing wall structures. In *Journal Proceedings*, volume 76, pages 723–738.

Hu, Y., Davison, B., Burgess, I., and Plank, R. (2009). Component modelling of flexible end-plate connections in fire. *International Journal of Steel Structures*, 9(1):1–15.

Huang, Y. (2009). *Simulating the inelastic seismic behavior of steel braced frames including the effects of low-cycle fatigue*. PhD thesis, University of California, Berkeley.

Izzuddin, B. and Fang, Q. (1997). Rate-sensitive analysis of framed structures part i: model formulation and verification. *Structural Engineering and Mechanics*, 5(3):221–237.

Izzuddin, B., Song, L., Elnashai, A., and Dowling, P. (2000). An integrated adaptive environment for fire and explosion analysis of steel frames —-part ii: verification and application. *Journal of Constructional Steel Research*, 53(1):87–111.

Izzuddin, B., Vlassis, A., Elghazouli, A., and Nethercot, D. (2008). Progressive collapse of multi-storey buildings due to sudden column loss—part i: Simplified assessment framework. *Engineering structures*, 30(5):1308–1318.

Jiang, J. and Li, G.-Q. (2016). Progressive collapse analysis of 3D steel frames with concrete slabs exposed to localized fire. *Engineering Structures*, 149:21–34.

Jiang, J. and Li, G.-Q. (2017). Disproportionate collapse of 3D steel-framed structures exposed to various compartment fires. *Journal of Constructional Steel Research*, 138:594–607.

Jiang, J., Li, G.-Q., and Usmani, A. (2014). Progressive collapse mechanisms of steel frames exposed to fire. *Advances in Structural Engineering*, 17(3):381–398.

Johnson, G. R. and Cook, W. H. (1985). Fracture characteristics of three metals subjected to various strains, strain rates, temperatures and pressures. *Engineering fracture mechanics*, 21(1):31–48.

Kachanov, L. (1958). On rupture time under condition of creep. *Izvestia Akademi Nauk USSR, Otd. Techn. Nauk, Moskwa*, 8:26–31.

Kim, J. and Kim, T. (2009). Assessment of progressive collapse-resisting capacity of steel moment frames. *Journal of Constructional Steel Research*, 65(1):169–179.

Kirby, B. (1983). The behaviour of structural steels manufactured by bsc under stress controlled anisothermal creep conditions. Technical report, Report SH/RS/3664/4/83/B, BSC Sheffield Laboratories.

Kirby, B. and Preston, R. (1988). High temperature properties of hot-rolled, structural steels for use in fire engineering design studies. *Fire safety journal*, 13(1):27–37.

Kodur, V., Dwaikat, M., and Fike, R. (2010). High-temperature properties of steel for fire resistance modeling of structures. *Journal of Materials in Civil Engineering*, 22(5):423–434.

Kodur, V., Garlock, M., and Iwankiw, N. (2012). Structures in fire: state-of-the-art, research and training needs. *Fire Technology*, 48(4):825–839.

Lamont, S., Gillie, M., and Usmani, A. (2007). Composite steel-framed structures in fire with protected and unprotected edge beams. *Journal of Constructional Steel Research*, 63(8):1138–1150.

Lamont, S., Usmani, A., and Gillie, M. (2004). Behaviour of a small composite steel frame structure in a "long-cool" and a "short-hot" fire. *Fire safety journal*, 39(5):327–357.

Lange, D., Röben, C., and Usmani, A. (2012). Tall building collapse mechanisms initiated by fire: Mechanisms and design methodology. *Engineering Structures*, 36:90–103.

Lee, W.-S. and Liu, C.-Y. (2006). The effects of temperature and strain rate on the dynamic flow behaviour of different steels. *Materials Science and Engineering: A*, 426(1-2):101–113.

Lemaitre, J. (1985). A continuous damage mechanics model for ductile fracture. *Transactions of the ASME. Journal of Engineering Materials and Technology*, 107(1):83–89.

Lemaitre, J. and Chaboche, J.-L. (1994). *Mechanics of solid materials*. Cambridge university press.

Lennon, T. (2003). Results and observations from full scale fire test at bre cardington. Technical report, Building Research Establishment (215).

Leston-Jones, L. C. (1997). *The influence of semi-rigid connections on the performance of steel framed structures in fire.* PhD thesis, University of Sheffield.

Lestriez, P., Saanouni, K., Mariage, J.-F., and Cherouat, A. (2004). Numerical prediction of ductile damage in metal forming processes including thermal effects. *International Journal of Damage Mechanics*, 13(1):59–80.

Li, H. and El-Tawil, S. (2013). Three-dimensional effects and collapse resistance mechanisms in steel frame buildings. *Journal of Structural Engineering*, 140(8):A4014017.

Li, Z., Jiang, F., and Tang, Y. (2012). Multi-scale analyses on seismic damage and progressive failure of steel structures. *Finite Elements in Analysis and Design*, 48(1):1358–1369.

Liew, J. R. (2008). Survivability of steel frame structures subject to blast and fire. *Journal of Constructional Steel Research*, 64(7):854–866.

Liew, J. R. and Chen, H. (2004). Explosion and fire analysis of steel frames using fiber element approach. *Journal of structural engineering*, 130(7):991–1000.

Liu, M., Zhao, J., and Jin, M. (2010). An experimental study of the mechanical behavior of steel planar tubular trusses in a fire. *Journal of Constructional Steel Research*, 66(4):504–511.

Longinow, A. and Ellingwood, B. (1998). The impact of the ronan point collapse–25 years after. *Structural Engineering World Wide*.

Luccioni, B., Figueroa, M., and Danesi, R. (2003). Thermo-mechanic model for concrete exposed to elevated temperatures. *Engineering Structures*, 25(6):729–742.

McAllister, T., MacNeill, R., Erbay, O., Sarawit, A., Zarghamee, M., Kirkpatrick, S., and Gross, J. (2011). Analysis of structural response of WTC 7 to fire and sequential failures leading to collapse. *Journal of Structural Engineering*, 138(1):109–117.

McClintock, F. A. (1968). A criterion for ductile fracture by the growth of holes. *ASME Journal of Applied Mechanics*, 35(2):363–371.

Mirmomeni, M., Heidarpour, A., Zhao, X.-L., Hutchinson, C. R., Packer, J. A., and Wu, C. (2015). Mechanical properties of partially damaged structural steel induced by high strain rate loading at elevated temperatures–an experimental investigation. *International Journal of Impact Engineering*, 76:178–188.

National Institute of Standards and Technology (2008). Final report on the collapse of the World Trade Center Building 7. Technical report, NIST NCSTAR 1A. Gaithersburg: National Institute of Standards and Technology (NIST).

Nechnech, W., Meftah, F., and Reynouard, J. (2002). An elasto-plastic damage model for plain concrete subjected to high temperatures. *Engineering structures*, 24(5):597–611.

Newman, G. M., Robinson, J. T., and Bailey, C. G. (2006). *Fire safe design: A new approach to multi-storey steel-framed buildings*. 2nd ed. SCI Publication P288, Steel Construction Institute.

O'Connor, M. (2003). Behaviour of a multi-storey composite steel framed building in fire. *Structural Engineer*, 81(2):27–36.

Outinen, J. and Mäkeläinen, P. (2004). Mechanical properties of structural steel at elevated temperatures and after cooling down. *Fire and materials*, 28(2-4):237–251.

Pauli, J., Somaini, D., Knobloch, M., and Fontana, M. (2012). Experiments on steel columns under fire conditions. Technical report, Institute of Structural Engineering (IBK), ETH Zürich, Switzerland.

Pearson, C. and Delatte, N. (2005). Ronan point apartment tower collapse and its effect on building codes. *Journal of Performance of Constructed Facilities*, 19(2):172–177.

Perzyna, P. (1966). Fundamental problems in viscoplasticity. *Advances in applied mechanics*, 9:243–377.

Poh, K. (2001). Stress-strain-temperature relationship for structural steel. *Journal of Materials in Civil Engineering*, 13(5):371–379.

Quiel, S. E. and Marjanishvili, S. M. (2011). Fire resistance of a damaged steel building frame designed to resist progressive collapse. *Journal of Performance of Constructed Facilities*, 26(4):402–409.

Razmi, J. (2012). *Thermo-mechanical fatigue of steel piles in integral abutment bridges*. PhD thesis, University of Maryland, College Park.

Rice, J. and Tracey, D. M. (1969). On the ductile enlargement of voids in triaxial stress fields. *Journal of the Mechanics and Physics of Solids*, 17(3):201–217.

Rubert, A. and Schaumann, P. (1986). Structural steel and plane frame assemblies under fire action. *Fire Safety Journal*, 10(3):173–184.

Saanouni, K., Lestriez, P., and Labergère, C. (2011). 2D adaptive FE simulations in finite thermo-elasto-viscoplasticity with ductile damage: application to orthogonal metal cutting by chip formation and breaking. *International Journal of Damage Mechanics*, 20(1):23–61.

Sakumoto, Y. (1999). Research on new fire-protection materials and fire-safe design. *Journal of Structural Engineering*, 125(12):1415–1422.

Sanad, A., Rotter, J., Usmani, A., and O'Connor, M. (2000). Composite beams in large buildings under fire—-numerical modelling and structural behaviour. *Fire Safety Journal*, 35(3):165–188.

Sarraj, M. (2007). *The behaviour of steel fin plate connections in fire*. PhD thesis, University of Sheffield.

Simo, J. and Ju, J. (1987). Stress and strain based continuum damage models, parts i and ii. *International Journal of Solids and Structures*, 23(7):841–869.

Skinner, D. (1973). Steel properties for prediction of structural performance during fires. In *Fourth Australasian conference on the mechanics of structures and materials: Proceedings*, pages 269–276.

Skrzypek, J. J. and Ganczarski, A. (2013). *Modeling of material damage and failure of structures: theory and applications*. Springer Science & Business Media.

Somes, N. F. (1973). *Abnormal loading on buildings and progressive collapse*. Office of Research and Technology, Department of Housing and Urban Development.

Stabler, J. and Baker, G. (2000). Fractional step methods for thermo-mechanical damage analyses at transient elevated temperatures. *International Journal for Numerical Methods in Engineering*, 48(5):761–785.

Sun, R., Huang, Z., and Burgess, I. W. (2012a). The collapse behaviour of braced steel frames exposed to fire. *Journal of Constructional Steel Research*, 72:130–142.

Sun, R., Huang, Z., and Burgess, I. W. (2012b). Progressive collapse analysis of steel structures under fire conditions. *Engineering Structures*, 34:400–413.

Sun, R. R. (2012). *Numerical modelling for progressive collapse of steel framed structures in fire*. PhD thesis, University of Sheffield.

Takagi, J. (2007). *Collapse performance assessment of steel-framed buildings under fires*. PhD thesis, Stanford University.

TM5-1300 (1990). *The design of structures to resist the effects of accidental explosions*. Technical Manual, US Department of the Army, Navy, and Air Force Washington DC.

Twilt, L. (1991). Stress-strain relationships of structural steel at elevated temperatures: Analysis of various options and european proposal. Technical report, Netherlands Organization for Applied Scientific Research, Van Mourik Broekmanweg 6, Delft, The Netherlands.

Uddin, T. and Culver, C. G. (1975). Effects of elevated temperature on structural members. *Journal of the Structural Division*, 101(7):1531–1549.

Velay, V., Bernhart, G., and Penazzi, L. (2006). Cyclic behavior modeling of a tempered martensitic hot work tool steel. *International Journal of Plasticity*, 22(3):459–496.

Wang, Y. (2000). An analysis of the global structural behaviour of the cardington steel-framed building during the two bre fire tests. *Engineering Structures*, 22(5):401–412.

Xi, F. (2016). Large deflection response of restrained steel beams under fire and explosion loads. *SpringerPlus*, 5(1):752.

Yandzio, E. and Gough, M. (1999). *Protection of buildings against explosions*. Steel Construction Institute UK.

Yu, H., Burgess, I., Davison, J., and Plank, R. (2010). Experimental and numerical investigations of the behavior of flush end plate connections at elevated temperatures. *Journal of Structural Engineering*, 137(1):80–87.

Appendix A

Mathematical function construction in damage model development

In choosing an appropriate form for representing the coupling function between the mechanical component and the thermal component, a number of coupling functions have been formulated in this study and the performances of them are compared in order to determine the versatile function to predict the coupled thermo-mechanical damage development of steel. The aim is to construct a coupling function which is a convenient, phenomenological formulation featuring mutual strain and temperature effects on damage growth with only a limited number of parameters.

A review of the constructed mathematical functions that have achieved relatively good performance is presented below. The constructed functions have a common characteristic of incorporating mutual mechanical and thermal effects by introducing coefficients that account for the experimentally observed phenomenon of accelerated growth of damage.

The developed mathematic functions are fitted to experimental data of tensile coupon tests by Pauli et al. (2012) (test data presented in Chapter 3) with the method of least squares and a summary of the fitting results is provided in Table A.1. Adjusted R-Square and Residual Sum of Squares are chosen as the measure of the goodness of fit. It can be seen from the table that Function 1 has the best fit to the series of test data points and effectively captures aspects of thermo-mechanical damage interaction in a smoothed manner. The couple thermo-mechanical damage formulation in the form of Function 1 is therefore proposed in this thesis, which allows an accurate prediction of coupled damage growth with the ease in fitting to the data.

Function 1:

$$D = \frac{{\sigma_s}^2}{2ES}(p-p_D)^{(1-r-T_1^m)}H(p-p_D) + ae^{\frac{b}{T+c}}e^{k(p-p_D)H(p-p_D)} \tag{A.1}$$

Function 2:

$$D = \frac{{\sigma_s}^2}{2ES}(p-p_D)^{(1-r-T_1^m)}H(p-p_D) + (ae^{\frac{b}{T+c}})^{[1-(p-p_D)H(p-p_D)]} \tag{A.2}$$

Function 3:

$$D = \frac{{\sigma_s}^2}{2ES}(p-p_D)^{(1-r-T_1^m)}H(p-p_D) + ae^{\frac{b}{T+c}}e^{(p-p_D)^k H(p-p_D)} \tag{A.3}$$

Function 4:

$$D = \frac{{\sigma_s}^2}{2ES(1+mT_1)}(p-p_D)^{(1-r)}H(p-p_D) + ae^{\frac{b}{T+c}}e^{k(p-p_D)H(p-p_D)} \tag{A.4}$$

Function 5:

$$D = \frac{{\sigma_s}^2}{2ES}(p-p_D)^{(1-r+mT_1)}H(p-p_D) + ae^{\frac{b}{T+c}}e^{k(p-p_D)H(p-p_D)} \tag{A.5}$$

Function 6:

$$D = \frac{{\sigma_s}^2}{2ES}[p-(1+mT_1)p_D]^{(1-r)}H(p-p_D) + ae^{\frac{b}{T+c}}e^{k(p-p_D)H(p-p_D)} \tag{A.6}$$

Function 7:

$$D = \frac{{\sigma_s}^2}{2ES}(p-p_D)^{(1-r)}(1+mT_1)H(p-p_D) + ae^{\frac{b}{T+c}}e^{k(p-p_D)H(p-p_D)} \tag{A.7}$$

Function 8:

$$D = \frac{{\sigma_s}^2}{2ES}(p-p_D)^{(1-r+T_1^m)}H(p-p_D) + ae^{\frac{b}{T+c}}e^{k(p-p_D)H(p-p_D)} \tag{A.8}$$

Function 9:

$$D = \frac{{\sigma_s}^2}{2ES}(p-p_D)^{(1-r-T_1^m)}H(p-p_D) + ae^{\frac{b}{T+c}}[1+k(p-p_D)H(p-p_D)] \tag{A.9}$$

Table A.1 Summary of the performances of the constructed mathematical functions in fitting to experimental data

Function	Test series M7		Test series M8		Test series M9	
	Adj. R-Square	Residual Sum of Squares	Adj. R-Square	Residual Sum of Squares	Adj. R-Square	Residual Sum of Squares
1	0.99718	0.00205	0.97426	0.01312	0.97088	0.01728
2	0.9959	0.0027	0.959	0.0174	0.92545	0.03686
3	0.99758	0.00161	0.97095	0.01234	0.96667	0.01648
4	0.99323	0.00492	0.96634	0.01572	0.96754	0.01765
5	0.99691	0.00206	0.97112	0.01227	0.97073	0.01447
6	0.99448	0.00367	-0.40199	0.59536	-0.10313	0.54538
7	0.99635	0.00265	0.95965	0.01885	0.96309	0.02007
8	0.96937	0.02225	0.95055	0.0231	0.95238	0.0259
9	0.99692	0.00205	0.97112	0.01227	0.95238	0.0259